UNIVERSITÀ DEGLI STUDI DI MESSINA

DIPARTIMENTO DI SCIENZE CHIMICHE, BIOLOGICHE, FARMACEUTICHE ED AMBIENTALI

DOCTOR OF PHILOSOPHY IN CHEMICAL SCIENCES

Use of advanced sample preparation and multidimensional gas chromatography-mass spectrometry methods within the context of food and biological sample analyses

PhD Thesis of:
Micaela Galletta

Tutor:
Chiar.mo Prof. Peter Q. Tranchida

Coordinator:
Chiar.ma Prof.ssa Concetta De Stefano

CICLO XXXVI – A.A. 2022/2023 – SSD CHIM/10

TABLE OF CONTENTS

Chapter 1
General scope and introduction

The main aim of the research, described in the present Ph.D. thesis, is based on the development of advanced gas chromatography-mass spectrometry methods and sample preparation protocols for the characterization and investigation of complex biological and food samples.

Currently, one-dimensional (1D) gas chromatography (GC) is widely exploited and is a powerful separation technique for the separation of volatile and semi-volatile compounds. However, sample complexity can often exceed the capacity of the separation system. In fact, considering that one 1D GC separations often rely on a single separation criterion, such as the different volatility of the analytes, if the vapour pressure of several analytes in a mixture are not sufficiently different, then coelution(s) will occur. In such a respect, the application of multidimensional analytical methods is a suitable alternative in cases of high sample complexity.

Comprehensive 2D GC (GC×GC) was first described in 1991 [1], when Liu and Phillips employed dual-stage thermal modulation to achieve a GC×GC separation. The introduction of GC ×GC, can be considered as one of the most important evolutions in the field of GC. Since its appearance, many developments have been made in this field in terms of hardware, software, and practical/theoretical studies.

In terms of published research, the use of GC was exploited for the analysis of fatty acids in dietary supplements and blood samples. In detail, a robotic preparative station enabled automatic derivatization in a fully automatic manner. Fatty acid derivatization was performed by using a direct derivatization protocol. The separation was achieved by using a medium-polarity ionic liquid column and dual detection was carried out to obtain quali-quantitative results in a single run [2].

A further study was focused on the use of GC×GC combined with time-of-flight mass spectrometry (ToFMS) to characterize geographical-based differences in the volatilome of five white "Grillo" wines (of Sicilian origin), forming five sample classes. The technique generates a high quantity of data that should be transformed into useful information after data processing with chemometric approaches. Specifically, Fisher ratio analysis (F-ratio analysis) was applied to find the class-distinguishing analyte features, followed by the use of Principal Component Analysis as a tool to visualize the success of the F-ratio analysis [3].

In another research, hydrogen was evaluated as a more sustainable alternative to helium, within the context of fast flow modulation (FM) GC×GC-ToFMS. In such a respect, a comparison was made between the two mobile phases in terms of speed and overall chromatography performance (efficiency, resolution). Finally, mass spectral profiles obtained analyzing pesticides and fatty acid methyl esters using the two mobile phases were compared [4].

In addition, a greener and more sustainable methodology was developed for Capsicum volatilome investigation by means of headspace solid-phase microextraction (HS SPME) coupled with FM GC×GC-ToFMS using hydrogen as carrier agas. A tile-based Fisher-ratio software was used to easily determine compounds that varied the most within the same variety of Capsicum samples. Particular emphasis was also devoted to the aroma profile of the thirty most sample-distinguishing compounds [5].

In a later period of the PhD course, focus was devoted to the targeted determination of chiral lactones, along with the untargeted characterization of the volatile fraction of Marsala wines through HS SPME combined with FM GC×GC-ToFMS (enantioselective column×polar column), using hydrogen as carrier gas. Lactones are important constituents of food and beverage aromas and are markers of alcoholic beverages aged in wood barrels. In such a respect, and considering important aspects related to food authenticity, their determination can provide information on such aging processes.

During the Ph.D. course, I spent six months at ESPCI Paris (École Supérieure de Physique et de Chimie Industrielles) under the supervision of Prof. Valérie Pichon to develop solid supports functionalized with target-specific oligonucleotides, commonly known as aptamers, for the selective extraction of mycotoxins present in biological samples.

References

[1] Z. Liu, and J.B. Phillips, Comprehensive Two-Dimensional Gas Chromatography using an On-Column Thermal Modulator Interface, J. Chromatogr. Sci. 29 (1991) 227, doi: 10.1093/chromsci/29.6.227.

[2] A. Ferracane, I. Aloisi, M. Galletta, M. Zoccali, P.Q. Tranchida, G. Micalizzi, L. Mondello, Automated sample preparation and fast GC–MS determination of fatty acids in blood samples and dietary supplements, Anal. Bioanal. Chem. 414 (2022) 8423-8435, doi: 10.1007/s00216-022-04379-8.

[3] P.E. Sudol, M. Galletta, P.Q. Tranchida, M. Zoccali, L. Mondello, R.E. Synovec, Untargeted profiling and differentiation of geographical variants of wine samples using headspace solid-phase microextraction flow-modulated comprehensive two-dimensional gas chromatography with the support of tile-based Fisher ratio analysis. J. Chromatogr. A 1662 (2022) 462735, doi: 10.1016/j.chroma.2021.462735.

[4] M. Galletta, M. Zoccali, N. Jones, L. Mondello, P.Q. Tranchida, Flow-modulated comprehensive two-dimensional gas chromatography combined with time-of-flight mass spectrometry: use of hydrogen as a more sustainable alternative to helium, Anal. Bioanal. Chem. 414 (2022) 6371-6378, doi: 10.1007/s00216-022-04086-4.

[5] M. Galletta, M. Zoccali, D. Creti, L. Mondello, P.Q. Tranchida, A green and sustainable method for Capsicum volatilome investigation by means of headspace solid-phase microextraction combined with flow-modulated two-dimensional gas chromatography-mass spectrometry using hydrogen as carrier gas, Green Analytical Chemistry 4 (2023) 100050, doi: 10.1016/j.greeac.2023.100050.

Chapter 2
Sample preparation: an analytical perspective

2.1 Sample preparation

Sample preparation is a fundamental step of the analytical process. Appropriate use of sample preparation techniques contributes to the success of the analysis, both in terms of the reliability of the result and in terms of optimising the time and cost of the overall process. Sample preparation aims to isolate and pre-concentrate the analytes, while reducing the co-extraction of unwanted components from the sample to achieve adequate sensitivity and enable reliable quantification [1]. The compounds of interest and the instrumental technique used for the final analytical determination are the most important factors in selecting the most appropriate sample preparation technique.

Liquid–liquid extraction (LLE) and solid-phase extraction (SPE), traditionally-used techniques, have several disadvantages, including long times, high costs and the consumption of solvents and reagents, with negative consequences for operator health and the environment. For this reason, research is increasingly focusing on the development and use of innovative techniques - solventless or solvent-minimized, miniaturisation of the sample preparation devices, automation, green chemistry - to improve performance in terms of accuracy and robustness of the method. In recent years, several miniaturised techniques have been introduced, including solid-phase microextraction (SPME), which follows the principles of green chemistry and is therefore one of the most widely used [2]. In such a respect, green analytical chemistry (GAC), promotes the reduction of toxic chemicals/reagents, the use of energy-efficient equipment and the minimisation of waste [3]. In 1998 Anastas and Warner [4] formulated the 12 principles of GAC, that are a basic guideline for inducing greenness in the analytical procedures and are as follows:

1. direct analytical techniques should be applied to avoid sample treatment;

2. minimal sample amount and minimal number of samples are goals;

3. in situ measurements should be performed;

4. integration of analytical processes and operations saves energy and reduces the use of reagents;

5. automated and miniaturized methods should be selected;

6. derivatization should be avoided;

7. generation of a large volume of analytical waste should be avoided and proper management of analytical waste should be provided;

8. multi-analyte or multi-parameter methods are preferred versus methods using one analyte at a time;

9. the use of energy should be minimized;

10. reagents obtained from renewable source should be preferred;

11. toxic reagents should be eliminated or replaced;

12. the safety of the operator should be increased.

Several metrics have been developed to assess the greenness of analytical methods, such as Analytical Greenness Calculator (AGREE), where each of the 12 input variables is transformed into a common scale in 0−1 range [5]. The output is a clock-like graph, with the overall score and colour representation in the middle (Figure 2.1).
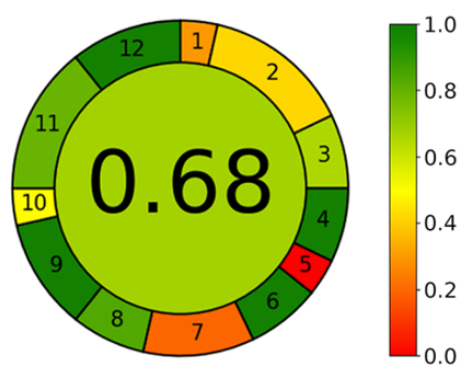
Figure 2.1. *Generic result of assessment (left) and the corresponding colour scale for reference (right).*

The performance of the procedure in each principle is reflected with the intuitive red-yellow-green colour scale, while the weight of each principle is reflected with the width of its corresponding segment.

2.2 Solid-phase extraction

Solid-phase extraction is a common sample preparation technique used for pharmaceutical, environmental, forensics and food safety applications, among others [6,7]. It is a method used for the isolation and concentration of analytes from a gas, or liquid sample stream by their transfer to and interaction (adsorption) on a solid phase. Specifically, the extraction procedure is based on the interaction of the analytes to be extracted, dissolved in a liquid (or sometimes gaseous) phase, with a solid phase (adsorbent). After preliminary conditioning of the adsorbent, the extraction process generally involves a liquid sample loading phase (or gaseous sample passage) and retention of the analytes, followed by an elution phase with a suitable solvent [8]. In the case of gaseous samples (*i.e.* in the analysis of volatile substances), desorption can also be performed thermally. SPE was initially developed as a complement or replacement for liquid-liquid extraction (LLE) and presents numerous advantages: low cost and solvent consumption, shorter and simpler processing procedures. In addition, SPE methods are easier to automate increasing productivity because multiple simultaneous extractions can be accomplished [9,10]. SPE provides higher concentration factors than LLE and can be used to store analytes in a sorbed state or as a vehicle for chemical derivatization. Due to its many advantages over other traditional methods, SPE was applied for the first time during the 1940s and quickly expanded in many applications during the 1970s involving the use of laboratory-prepared packed columns [11]. The first application of SPE described the isolation of histamine from wine samples by using an octadecylsilane (C18) phase [12].

2.3 SPE configurations

SPE is a versatile technology for the purification, separation, and concentration of analytes from a sample solution matrix using a sorbent bed by flow-through equilibrium. The selectivity of extraction depends on three factors: the sorbent, chemical structure of the analytes and the chemical composition of the sample matrix. Maximum selectivity is achieved by choosing a sorbent able to interact with the functional groups of the target molecules and rather than with the other

compounds present in the sample. A wide range of SPE extraction configurations, including SPE cartridges, discs, multi-well SPE are designed [7,13].

2.4 SPE cartridges

Cartridges constitute a traditional SPE configuration. A typical SPE disposable cartridge is shown in Figure 2.2; they are small polypropylene or glass open-ended syringe barrels filled by different amounts of the sorbent bed between two frits. Standard cartridges are also available with reservoir volumes of 0.5-60 mL with packing weights of 35 mg -2 g [10]. The liquid phase can be passed through the column by gravitational force or using positive pressure using syringes, air or nitrogen lines, a vacuum flask, or a centrifuge (dynamic method). SPE can retain approximately 5% of its sorbent mass without significant breakthrough. In general, SPE cartridges packed with bonded silica or sorbent packings are relatively inexpensive [14]. They are generally used a single time and discarded because of the potential of sample cross-contamination.
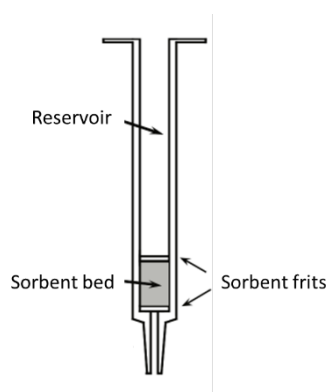
Figure 2.2. SPE cartridge.

2.5 Sorbents

Appropriate SPE sorbent selection is critical to obtain efficient SPE recovery and minimise interferences without affecting the sensitivity of the method. It depends on several factors: nature of the analytes (functional groups, polarity, ionic properties) and sample matrix. Many different sorbents are available for the SPE procedure. Generally, sorbents for SPE can be divided according to the nature of the material (inorganic oxide-based, polymeric, carbon-based) or to the interactions they can give rise to (polar, non-polar, ionic adsorbents, restricted access, immunosorbents, oligosorbents, molecular imprinted polymers) [7,15]. In addition, the sorbent mass

should be selected according to the sample concentration and the analytical method used. The capacity of a sorbent is defined as the total mass of strongly retained analyte that can be retained by a given sorbent mass under optimum conditions. Typically, non-polar and polar SPE sorbents have a capacity of between 1 and 5% of the sorbent mass (*i.e.*, 100 mg of sorbent can retain up to 5 mg of strongly retained analyte under optimum conditions) [1].

2.5.1 Polar sorbents

The most common polar sorbents are silica (SiO_2), alumina (Al_2O_3), magnesium silicate ($MgSiO_3$), and the bonded silica sorbents with highly polar functional groups such as aminopropyl, cyanopropyl and diol-modified silica sorbents. Due to its high polarity, non-modified silica can cause problems with irreversible adsorption of water; therefore, to ensure reproducible results, it should be kept away from humidity and not mixed with highly polar solvents. Functionalized silica with polar groups (cyano, diol, and amino) exhibit hydrophilic interaction with the solute based on charge-based interactions, hydrogen bonding, π–π, and dipole–dipole interactions. For example, the diol phase does not absorb water and other highly polar compounds; moreover, like silica, it tends to form hydrogen bonds. While amino phases show high polarity and capable of non-polar and anionic exchange interactions.

2.5.2 Non-polar sorbents

The most commonly used non-polar adsorbent is the octadecylsilane (C18) phase, which is generally classified as non-specific for its ability to retain many types of analytes. The C18 phase exhibits some residual polarity due to the free silanols in the silica substrate; the residual polarity varies depending on the carbon loading and possible derivatization of the residual silanols. Extremely apolar (high PM) compounds are sometimes eluted difficultly with a C18 phase, which is advantageously replaced with a octyl phase (C8) which are more affected by interactions due to residual silanols. Also, cyclohexyl and phenyl phases have similar polarity to C8, cyanopropyl (CN) phase is a very versatile medium-polarity sorbent,

used for molecules that can be retained too strongly by more apolar (C8 or C18) or more polar (silica or diol) sorbents.

2.5.3 Aptamer-modified sorbents

Molecular recognition processes became popular in the early 1980s and are highly specific. Such sorbents include immunosorbents, molecularly-imprinted materials, and aptamer-functionalized sorbents called oligosorbents (OS) (Figure 2.3).
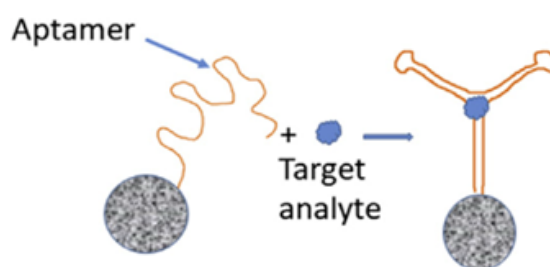
Figure 2.3. *Representation of the specific entrapment of a compound by an oligosorbents.*

Aptamers are single-stranded DNA or RNA molecules with a short length (20–60 nucleotides) first discovered in 1990 by Ellingto [16] *et al*. and Tuerk & Gold [17]. They are generated by in-vitro combinatorial selection method called *Systematic Evolution of Ligands by Exponential enrichment* (SELEX) [18,19]. As shown in Figure 2.4, through an iterative process (typically 7 to 15 repeated steps) a synthetic random DNA or RNA oligonucleotide library consisting of a multitude of single-stranded DNA/RNA fragments with different sequences is used directly for the selection of DNA/ RNA aptamers. The procedure is then characterised by repetition of three steps including of selection (binding, partitioning, and elution), amplification, and conditioning. The library and the target molecules are incubated for binding during the first SELEX round. Unbound oligonucleotides are removed by washing of the binding complexes in several stringent steps. The target-bound oligonucleotides are eluted and then amplified by PCR or reverse transcription PCR generating a new enriched pool of selected oligonucleotides that is then used for the next selection round [20]. Aptamers are continuously developed through this on-going process and must be characterized. Aptamers can fold into a unique three-dimensional conformation capable of binding with high specificity and affinity target

molecules. Considering their large surface area, the interactions between aptamers and target strengthens, preventing binding even in the most negligible possible differences. Recognition arises from interactions such as stacking interactions, hydrogen bonding, dipole and van der Waals forces. Most of isolated sequence are directed against large molecules such as peptides, proteins, or nucleic acids. Nevertheless, a notable selection of aptamers targeting small molecules are developed [21-22]. Furthermore, aptamers have many advantages over the use of an antibody, including an equal or superior affinity and specificity to the target, a smaller size, easier modification and immobilization, better stability at ambient as well as high temperatures, and higher reproducibility.
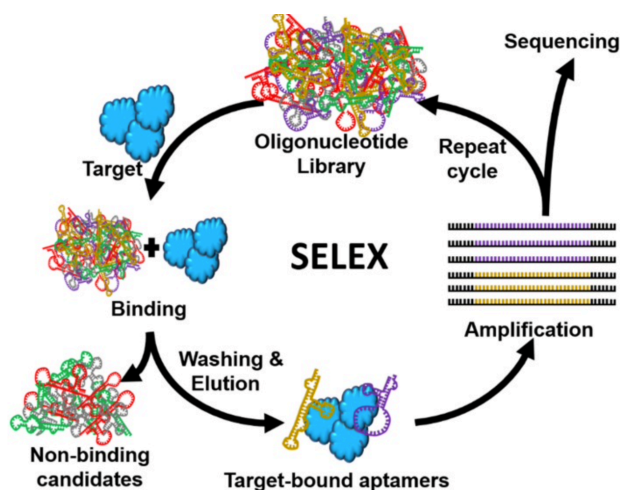
Figure 2.4. Scheme of the SELEX process. The procedure involves repeated cycles of: 1. Incubation of the high complexity library with the targets (binding); 2. Removal of unbound sequences and recovery of the bound oligonucleotides (partitioning); 3. Amplification of the bound sequences by PCR (for DNA library) or RT-PCR and transcription (for RNA library).

Finally, the aptamer immobilization on a solid support is a crucial step for the design of the OSs. The supports must possess a chemical and biochemical inertness, good mechanical stability, and homogeneity in terms of particle size or surface area. Furthermore, the sorbent should be easily activated to allow attachment of aptamers and should be hydrophilic to avoid any nonspecific interactions. Finally, the immobilization procedure must preserve the affinity of aptamers toward their target analyte [21]. Aptamer chemical synthesis allows to introduce modifications at the 5'

or 3' end of the oligonucleotide sequence to facilitate their immobilization, that are chosen according to the nature of the bonding. The binding properties of the aptamer can be maintained by adding a spacer arm when it is attached to a surface and it be an n-alkyl chain in C6 or C12, an ethylene glycol derivative [23-26]. Covalent immobilization of aptamers is facilitated by the possibility of introducing different functional groups (amino, thiol, carbonyl groups, etc.) into the aptamer sequence during its preparation, which facilitates the binding of aptamers to various types of activated sorbents. Some sorbents, such as CNBr-activated Sepharose [23-26,27] and N-hydroxysuccinimide-activated Sepharose [28], which are frequently employed for the covalent binding of antibodies and have been used for the immobilization of aptamers. These sorbents, which are packed between two frits in disposable cartridges or columns, are especially suitable to the extraction process. After the binding of aptamers with a solid support, oligosorbents are generally packed between two frits into disposable cartridges or columns as a conventional sorbent for the SPE procedure. The three steps of an oligoextraction procedure (Figure 2.5), which are very similar to those of a conventional SPE sequence, are:

1. sample percolation after a conditioning step;
2. washing of the oligosorbent;
3. elution of the target analyte(s).
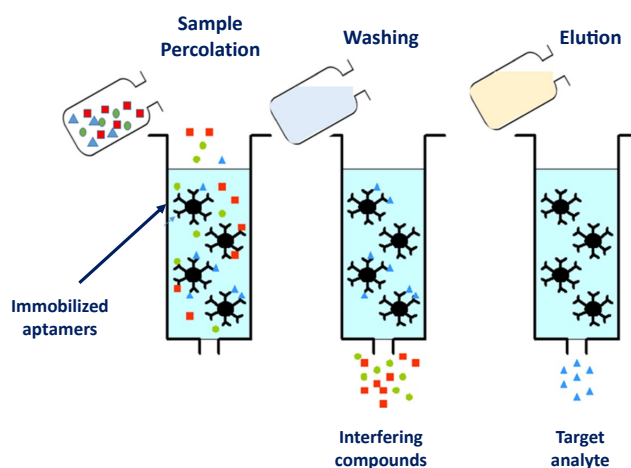
Figure 2.5. *Principle of oligoextraction on immobilized aptamers packed in a disposable extraction cartridge.*

A buffer solution with a similar composition to the binding buffer (BB), employed during the selection procedure, is used to preserve the oligosorbent at 4 °C when not in use. The percolation conditions are analogous to the composition of the buffer used during the aptamer selection to favour the interaction between both entities. Different parameters such as temperature, ionic strength, and pH influence the conformation of the aptamers and thus must be controlled and adapted to ensure high extraction recoveries or to promote the elution [29,30].

2.6 Analyte-sorbent interactions

The choice of SPE sorbent is determined by the functional groups of the analyte and the polarity. The interactions most frequently exploited in SPE are based on van der Waals forces (non-polar interactions), hydrogen bonds, dipole-dipole forces (polar interactions) and anion or cation exchange interactions (ionic interactions) [31].

2.6.1 Non-polar interactions

Non-polar interactions occur between the C-H bonds of the adsorbent functional groups and the C-H bonds present in the analyte molecule and are exploited for reversed phase (RP)-SPE [32]. All RP sorbents contain non-polar functional groups such as C18, C8, C6, C4, C2, phenyl, cyclohexyl, and cyanopropyl and are used for the extraction of molecules containing non-polar functional groups from predominantly polar matrices. The interaction between the analyte and the sorbent is facilitated by polar solvents, which repel the analyte from the solution phase and more strongly onto the sorbent surface. The interactions between the analyte and SPE functional groups must then be disrupted to elute analytes from sorbent surface. This can be achieved by employing solvents with some non-polar character.

2.6.2 Polar interactions

Normal phase (NP)-SPE is characterised by a more polar sorbent phase than the sample. Specifically, the sorbent presents polar functional groups such as diol, aminopropyl, cyanopropyl, unbonded silica, alumina. Analytes containing polar functional groups can interact and, therefore, be retained on the sorbent surface via dipole–dipole or hydrogen bonding interactions [10]. To maximize analyte–sorbent

interactions, non-polar solvents should be used, and to disrupt these interactions a solvent with some polar character should be used.

2.6.3 Ion exchange

For ion exchange, the isolation mechanism is based on the high-energy electrostatic interaction between the charged functional groups of analytes and sorbent [14]. Thus, the sorbent selection depends on the analyte charge, and it can be divided into two classes:

- anion-exchange resins: they have cationic functional groups, such as primary, secondary, tertiary, and quaternary amines, as well as inorganic cations, such as Ca^{2+}, Na^+ and Mg^{2+}, which interact with analytes characterised by acidic (negatively charged) groups and inorganic anions;

- cation exchange resins: they have anionic functional groups, such as carboxylic and sulphonic acids, phosphates and sulphonic acids, phosphates, and similar groups, which react with analytes characterised by basic (positively charged) groups and inorganic cations.

There are three mechanisms for disrupting analyte or sorbent interactions: use of a high ionic strength buffer or buffers containing counterions that have a high affinity for the sorbent surface, or alteration of the pH through the addition of an acid or base.

2.7 Theoretical aspects

Analyte concentrations are generally low, and the amount of analyte isolated, is determined by the breakthrough volume of the sampling device. The breakthrough volume is one of the most important factors to determine the capacity of a sampling device to isolate target analytes [33]. This parameter defines the sample volume that can be loaded onto the solid sorbent without analyte loss. V_B (breakthrough volume) depends on the concentration of analytes in the solution loaded onto the sorbent, the temperature, the flow rate, and the number of theoretical plates. It is determined by the breakthrough curve (Figure 2.6), showing dependence between the concentration

of the analyte in the effluent and the volume of the sample passed through the sorbent [34].
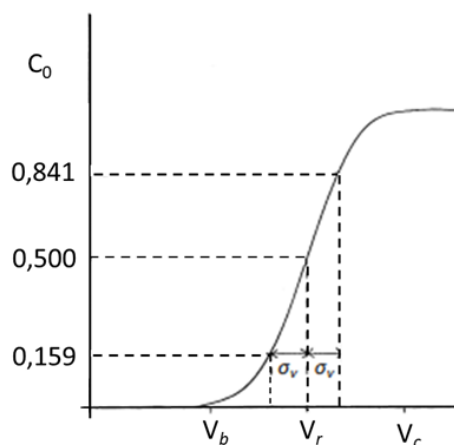
Figure 2.6. *Breakthrough curve.*

In the initial sampling phase, the analytes are quantitatively retained by the sorbent up to the point that the sample volume exceeds the retention capacity of the sorbent. Further sample passing through the sorbent bed is not quantitatively retained by the sorbent, and eventually the analyte concentration entering and exiting the sampling device become analogous. The point on the curve at which some arbitrary amount of sample is identified at the outlet of the sampling device, typically 1%, 5%, or 10%, is defined as the breakthrough volume (V_B). Usually, a value of 1% is chosen in keeping with the desire to define a maximum sample volume that can be processed with a minimum (acceptable) analyte loss. A second point of the curve (V_C) corresponds to the sample volume at which the retention capacity of the sorbent is saturated and the concentration of analyte exiting the sampling device is the same as that entering the sampling device. This value corresponds to the volume of sample that will result in the isolation of the maximum amount of analyte but with a lower overall recovery, because a fraction of the sample is lost during the sorption process. The inflection point for the breakthrough curve corresponds to the chromatographic retention volume (V_R), provided that the plate number for the sampling device is not too small. A relationship between V_B and V_R can be derived from the general theory of frontal chromatography:

$$V_B = V_R - 2.3\sigma_V \qquad\qquad (2.1)$$

where σ_V is the standard deviation depending on the axial dispersion of the analyte along the sorbent bed, and is evaluated through:

$$\sigma_V = \frac{V_M}{\sqrt{N}} (1 + k) \tag{2.2}$$

where V_M is the interparticle volume of the sorbent bed, k the retention factor, and N the plate number for the sorbent bed calculated by the following equation:

$$N = \frac{V_R(V_R - \sigma_V)}{\sigma_V^2} \tag{2.3}$$

It should be possible to calculate V_B from these equations by determining V_M and N for the sampling device and measuring V_R for the analytes of interest. Equations 2.1 and 2.3 are applicable for a sorbent bed with a large N. Instead, for sorbent beds with a low N, the above equations can result in a poor estimate of breakthrough volumes. Lovkist and Jonsson [35] proposed a model described by Equation 2.4:

$$V_B = \left(\alpha_0 + \frac{\alpha_1}{N} + \frac{\alpha_2}{N}\right)^{-1/2} (1 + k)V_M \tag{2.4}$$

and the coefficients α_0, α_1, α_2, are summarized in Table 2.1.

Table 2.1. Coefficients for the Lovkist and Jonsson model.

Breakthrough level (%)	Coefficients		
	α_0	α_1	α_2
0.1	0.998	29.12	57.54
0.5	0.990	17.92	26.74
1.0	0.980	13.59	176.60
5.0	0.903	5.36	4.60
10.0	0.810	2.88	1.94

2.8 Pratical aspects

Generally, SPE consists of four steps (Figure 2.7): conditioning, sample loading, washing, and elution. The first step removes any impurities that may have randomly been collected while the cartridge was exposed to the laboratory environment or present in the cartridge supplied by the manufacturer and activates the sorbent surface to promote analyte interaction [14].

During loading the sample, dissolved in a weak solvent, is added to the cartridge. The most important parameter is the linear velocity of the sample as it passes through the column, that depends on both flow rate and column.

The washing step has the scope of removing undesirable contaminants and interferents not retained by the adsorbent. The solvent used for washing steps has a higher elution strength than the sample solvent but is weaker than the elution solvent to ensure that analytes are not eluted, which would lead to low recovery. Usually, the compounds of interest are retained on the sorbent while interferences are washed away.

The last step provides for elution and collection of the analyte fraction in as small a volume as possible.

Each of the protocol steps must be optimized during method development. Sometimes pre-treatment is required to make the sample compatible with the SPE procedure and to optimize the sample chemistry to promote analyte retention. Specifically, the matrix must be liquid with sufficiently low viscosity and free of solid particles (which may be removed by centrifugation, filtration, etc.).
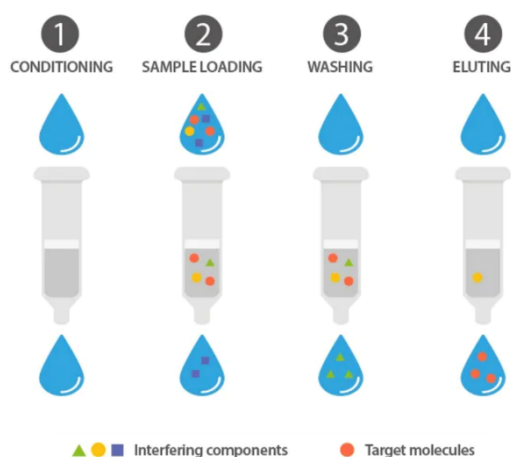
Figure 2.7. *Steps of SPE Process.*

2.9 SPME

SPME is a simple extraction technique that does not use solvents or complicated instrumentation. The technique, introduced by Prof. J. Pawlisyzn of the University of Waterloo (Canada) in 1989, integrates sampling, extraction, and concentration in a single step, followed by introduction of the sample for analysis [36]. SPME is based

on the principle of adsorption/desorption of analytes, using a fused silica fiber coated with a thin polymer film, and aims to concentrate volatile (and non-volatile) compounds from gaseous, liquid, or solid matrices. SPME has been applied to both gas chromatography (GC) and liquid chromatography (LC) separations, but its most successful application has been in GC. It has several advantages for the qualitative and quantitative analysis of even complex samples, such as: speed of sample preparation, small amount of sample required, minimal (or no) solvent consumption, possibility of automation, extraction from different types of matrices and high yields. An increasing number of studies describe diverse SPME workflows for novel investigations in a variety of fields, such as flavour and fragrance, environmental, and diverse bioanalytical applications [37-39].

2.10 Extraction devices

In SPME, the extraction phases are usually immobilized on supporting substrates (Figure 2.8) or prepared into monolithic fibers or thin films.
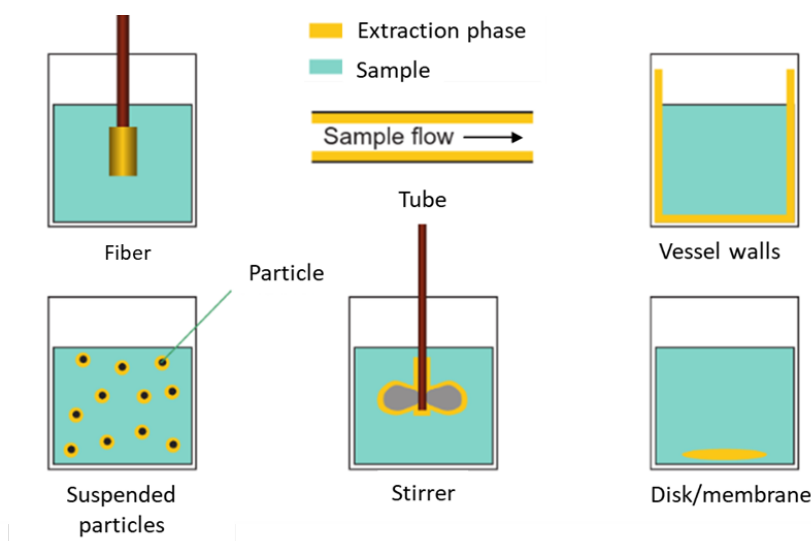
Figure 2.8. SPME configuration.

The traditional implementation approach of SPME involves the use of coated fibers and remains, to this date, the most used [40]. Specifically, the SPME technique requires a device such as a gas chromatography syringe, called a holder, consisting of a steel needle inside which the fused silica fiber (or stainless steel) is coated with a thin film (5-100 μm) of adsorbent polymer phase. When first used, the fiber must be conditioned according to the manufacturer's guidelines. For conditioning, the fiber is

exposed to a variable temperature and time, depending on the type of phase, under a constant gas flow (generally using the injector of a GC). Generally, one fiber can be used 50-100 times. Figure 2.9 shows both an external and internal view of the manual holder; in particular, on the left side the fiber is in the exposed position, and on the right side the fiber is retracted into the needle.
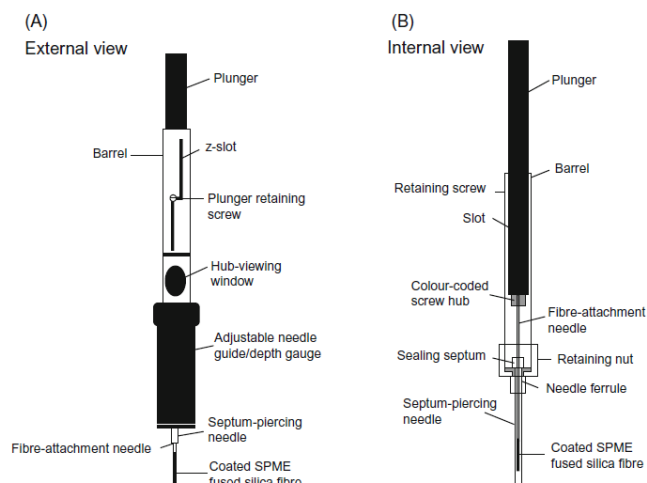
Figure 2.9. *Schematic view of SPME manual fiber assembly holder (external and internal view).*

The manual holder contains a needle guide depth gauge that can be screwed up or down to measure the needle's distance between the injection port and a vial. The manual holder has a z-slot that locks the fiber in the exposed position. When the plunger is unlocked, the fiber will retract into the needle if it is a manual assembly. SPME sorbents are most immobilized by coating onto the outside of fused silica fibers or on the internal surface of a capillary tube. The phases are not bonded to the silica fiber core, other coatings are cross-linked to improve stability in organic solvents. The most appropriate fiber for a specific application is selected considering the characteristics of interest analyte (weight, molecular size, volatility, and polarity), and the complexity of the matrix from which it must be extracted is considered. Coatings consisting of only one polymer, such as the non-polar polydimethylsiloxane (PDMS) are commercially available in film thickness of 7 (non-polar semi-volatile organic compounds), 30 (nonpolar semi-volatile organic compounds), 100 μm (for nonpolar semi volatile organic compounds) [41]. While coating more polar such as polyacrylate (PA) and Carobowax (CW) are suitable for the extraction of polar compounds. When using solid coating, in which the adsorption surface is limited, as

analyzed samples complexity increases, the high quantities of interfering compounds can compete with the target analytes. This reduces the linear dynamic range, and the amount of analyte extracted at equilibrium depends on its initial concentration and the presence of interferents. To resolve this problem, it is essential to reduce the extraction time to limit the phenomenon of analyte displacement by interferents (sampling under pre-equilibrium conditions). In this context multiphase fibers are used, as the divinylbenzene phase (DVB) increases the fiber capacity. Therefore, the fiber DVB-Carboxen-PDMS allows excellent performance over a wider concentration range than biphasic fibers, provided the extraction time remains relatively short.

The chemical nature and thickness of fiber coatings have a strong influence on the distribution of analytes between the sample matrix and the extraction phase, which affects the extraction efficiency, selectivity, and reproducibility of the analysis. SPME coatings can be classified into four categories based on: type of coating, coating thickness, polarity and whether the coating is an absorbent or an adsorbent. The type of phase determines the polarity of the fiber, and consequently its selectivity. All the SPME fibers are bipolar because they will extract both polar and non-polar analytes because porous adsorbents extract primarily by the size of the analyte. The thickness of the coating determines the analyte capacity of the fiber and the duration of the extraction time required to reach equilibrium. Specifically, it takes longer to reach equilibrium with a thicker coating compared to a thin coating [40]. Volatile analytes require a thick coating to retain them, whereas thin coatings are preferred for the extraction of high-molecular-weight analyte. Furthermore, the release of components (especially the higher boiling components) from the fiber is slower with greater thicknesses, so there is a risk that desorption will not be complete, and the fiber will remain dirty.

2.11 SPME theory and fundamentals

SPME can be performed in three different modes (Figure 2.10):

1. **direct extraction**, in which the coated fiber is inserted into the sample and analytes are transported directly from the sample matrix to the extracting phase (Figure 2.10A);

2. **head space (HS) configuration**, in which the fiber is exposed into the headspace of the solid or liquid sample (Figure 2.10B);

3. **membrane protection approach** (Figure 2.10C) results in better reproducibility and accuracy for samples containing both non-volatile target analytes and high molecular weight interfering compounds.
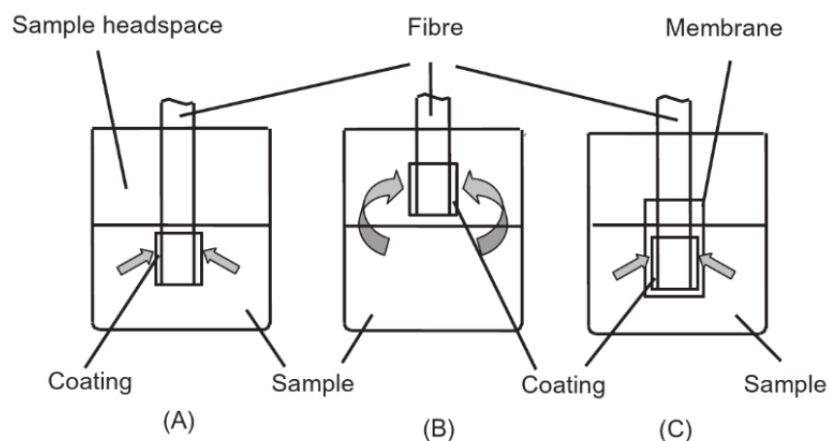
Figure 2.10. *Modes of SPME operation: (A) direct extraction; (B) headspace SPME; and (C) membrane-protected SPME.*

The theoretical principles behind SPME are based on the equilibrium [42] and interactions between analyte and fiber coating. The coated fiber is immersed directly in the sample or the headspace of the sample, where the analytes are concentrated. After equilibrium has been reached (from a few minutes to several hours depending on the properties of the analytes measured) or after a defined time, the fiber is withdrawn and transferred either to a GC injection port. The fiber is exposed, and the analyte is desorbed thermally in the hot GC injector port.

The extraction process is complete when the concentration of the analytes reaches equilibrium between the sample matrix and the fiber coating. When equilibrium conditions are reached, exposing the fiber for a longer time does not increase the extraction yield [40]. The equilibrium conditions can be described as follows:

$$C_0 V_s = C_f{}^\infty V_f + C_s{}^\infty V_s \tag{2.5}$$

where C_0 is the initial concentration of the analyte in the matrix; $C_f{}^\infty C_s{}^\infty$ are the equilibrium concentrations of the analyte in the coating, and the sample, respectively; V_f and V_s are the volumes of the coating, and the sample, respectively (Figure 2.11).
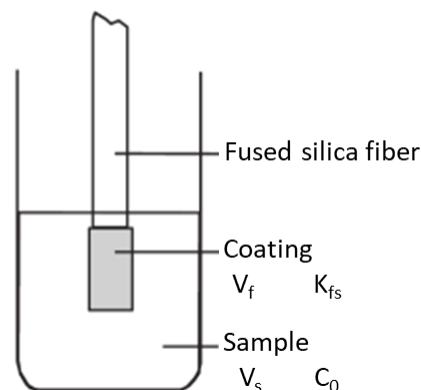
Figure 2.11. Sample preparation with SPME.

The coating/sample distribution constant is:

$$K_{fs} = C_f^{\infty} V_f / C_s^{\infty} V_s \tag{2.6}$$

The two equations can be combined and rearranged, resulting in:

$$C_f^{\infty} = C_0 \, (K_{f/s} V_s)/(K_{f/s} V_f + V_s) \tag{2.7}$$

Finally, the amount of analyte extracted by the fiber coating is calculated as:

$$n = C_f^{\infty} \, V_f = (K_{f/s} V_f V_s C_0)/(K_{f/s} V_f + V_s) \tag{2.8}$$

There is a direct proportional relationship between analyte concentration in the sample matrix and the amount of analyte extracted and it is the basis of analyte quantification for equilibrium SPME.

When the sample volume is very large, Eq. 2.8 can be simplified as follows:

$$n = K_{f/s} V_s C_0 \tag{2.9}$$

The equation highlights the usefulness of the technique even when the sample volume is unknown; this means that the fiber can be directly exposed to the ambient air, water, production stream, etc. The amount of extracted analyte corresponds directly to its concentration in the matrix, independent of the sample volume. The extraction system is complex, such as in a sample composing of an aqueous phase with suspended solid particles having various adsorption interactions with analytes, and a gaseous headspace. Sometimes specific factors must also be considered, such as analyte losses due to degradation or adsorption on the walls of the sample vial. In

such a context, only a three-stage system is considered: fiber coating, headspace, and homogenous sample. During extraction, the analytes migrate in all three phases until equilibrium is reached, the conditions are described by the following equation:

$$C_0 V_s = C_f^\infty V_f + C_s^\infty V_s + C_h^\infty V_h \qquad (2.10)$$

where C_0 is the initial concentration of the analyte in the sample; $C_f^\infty C_s^\infty C_h^\infty$ are the equilibrium concentrations of the analyte in the coating, the sample, and headspace respectively; V_f, V_s, V_h are the volumes of the coating, the sample, and headspace, respectively. Defining the coating/gas distribution constant and the gas/sample matrix distribution constant according to:

$$K_{f/h} = C_f^\infty / C_h^\infty \qquad (2.11)$$

$$K_{h/s} = C_f^\infty / C_h^\infty \qquad (2.12)$$

the mass of the analyte extracted by the coating $n = C_f^\infty V_f$, can be expressed as:

$$n = (K_{f/h} K_{h/s} V_f C_0 V_s) \, / \, (K_{f/h} K_{h/s} + K_{h/s} V_h + V_s) \qquad (2.13)$$

If the effect of moisture in the gaseous headspace can be neglected, $K_{f/h}$ can be approximated by the fiber/gas distribution constant ($K_{f/g}$), and $K_{h/s}$ can be approximated by the gas/sample distribution constant ($K_{g/s}$), thus:

$$K_{f/s} = K_{f/h} K_{h/s} = K_{f/g} K_{g/s} \qquad (2.14)$$

Therefore, Eq. 2.13 can be rewritten as:

$$n = (K_{f/s} V_f C_0 V_s) \, / \, (K_{f/s} V_f + K_{h/s} V_h + V_s) \qquad (2.15)$$

The equation demonstrates that the amount of analyte extracted is independent of the location of the fiber in the system. If the volume of the fiber, headspace and sample are kept constant, the fiber may be placed in the headspace or directly in the sample Assuming that the vial containing the sample is filled (no headspace), the term $K_{h/s}$ in the denominator, can be eliminated from equation 2.14. Furthermore, if $K_{h/s}$ is relatively small, as is the case for many analytes (e.g., 0.26 for benzene) or if $V_h \ll V_s$, the limit of determination becomes very similar to that obtained by direct immersion. For systems with n phases, $K_{f/s}$ is the product of the partition constants

between each phase; thus, the amount of analyte extracted is obtained from the equation:

$$n = (K_{f/s}V_e C_0 V_s) / (K_{e/s} V_e + \sum_{i+l}^{i=m} K_{i/s} V_i + V_s) \qquad (2.16)$$

From Eq. 2.16, it can be deduced that the fiber extraction capacity is mainly related to $K_{f/s}$, which is independent of the phase number present in the system, and the phase capacity present to retain the analyte. If this capacity is small (such as in the headspace), the total amount of analyte extracted will not be significantly affected.

After equilibrium is reached, the amount of analyte extracted is proportional to the initial analyte concentration in the sample. However, in SPME applications equilibrium is rarely reached and it can be demonstrated that the linear relationship between n and C_0 also exists before equilibrium is reached. In this case, the relationship is time-dependent, and it is therefore necessary to keep time constant so that the amount of analyte extracted is proportional to the amount present in the sample. The fundamental thermodynamic principle common to all extraction techniques involves distribution of the analyte between the sample matrix and extraction phase. When the liquid is used as extraction medium, the distribution constant (K_{es}) can be represented as follows:

$$K_{es} = \frac{\alpha_e}{\alpha_s} = \frac{C_e}{C_s} \qquad (2.17)$$

The equation defines the equilibrium conditions and enrichment factor achievable with this technique: α_e and α_s are the activities of analyte in the extraction phase and matrix, respectively, and can be approximated by the appropriate concentrations.

2.12 Effects of extraction parameters

Thermodynamic and kinetic theories predict the effects of extraction parameters on partitioning coefficients. Theory can be used to optimise the extraction conditions using minimum experiment numbers. Extraction conditions that affect K_{fs} include temperature, pH, salting, and organic solvent content in water.

The effect of temperature is represented by:

$$K_{f/s} = K_0 \exp\left[\frac{\Delta H}{R}\left(\frac{1}{T} - \frac{1}{T_0}\right)\right] \qquad (2.18)$$

where K_0 is the distribution constant at temperature T_0, ΔH is the molar change in enthalpy of the analyte when it transfers from the sample to the fiber coating, and R is the gas constant. When the K_{fs} value is greater than one, the analyte has a lower potential energy in the fiber coating than in the sample, so the analyte partitioning into the fiber is an exothermic process with ΔH greater than zero. Thus, a temperature raise causes an increase in the extraction rate, but simultaneously a decrease in the distribution constant. The choice of extraction temperature must also consider possible adverse reactions, such as the decomposition of thermolabile compounds and the formation of artefacts. To avoid this loss of sensitivity as the temperature increases, it is ideal to heat the sample and keep the fiber cold at the same time [43].

Two techniques used to enhance the extraction of organic compounds from aqueous solutions are salting and pH adjustment. The addition of salts can increase or decrease the amount extracted, depending on the salt concentration and compound. Generally, the salting effect increases as the polarity of the compound increases. However, if the salt concentration rises above a certain level, its ions can interact electrostatically with polar analytes, reducing the amount of analyte extracted from the fiber. For some compounds, the solubility does not change: the addition of salt, therefore, may cause a decrease in the amount extracted by reducing the activity coefficient of the compound that negatively affects the fiber-sample partition constant.

Solid-phase microextraction can only extract neutral species from sample matrices unless special coatings fiber are used. By adjusting the pH weak acids and bases can be converted to their neutral forms, so that they can be extracted by the SPME fiber. Specifically, for the basic analytes the pH should be two units greater than the pK_b, while for acidic compounds, the pH should be at least two units less than the pK_a of the analyte. In addition, it is advisable to use a buffer that allows more efficient pH control throughout the extraction process of the neutralised analyte. There are pH limits beyond which fibers are not stable: for example, PDMS fibers cannot be used at pH values below 2 or above 10. Therefore, when adjusting pH it is generally preferable to use headspace sampling, especially when working at pH values close to the limits of fiber use.

References

[1] S. Moret, G. Purcaro, L. S. Conte, Il campione per l'analisi chimica: Tecniche innovative e applicazioni nei settori agroalimentare e ambientale, Springer, 2014, doi:10.1007/978-88-470-5738-8.

[2] S. Mitra, Sample Preparation Techniques in Analytical Chemistry, John Wiley & Sons, Hoboken, NJ, USA (2003), doi:10.1002/0471457817.

[3] S. Armenta, S. Garrigues, M. de la Guardia, Green analytical chemistry, TrAC Trends Anal. Chem. 27 (2008) 497-511, doi: 10.1016/j.trac.2008.05.003.

[4] P.T. Anastas, J.C. Warner, Green Chemistry: Theory and Practice, Oxford University Press, Oxford (1998).

[5] F. Pena-Pereira, W. Wojnowski, M. Tobiszewski, AGREE-Analytical GREEnness Metric Approach and Software, Anal. Chem. 92 (2020) 10076–10082, doi: 10.1021/acs.analchem.0c01887.

[6] A. Żwir-Ferenc, M. Biziuk, Solid Phase Extraction Technique – Trends, Opportunities and Applications, Polish J. of Environ. Stud. 15 (2006), 677-690.

[7] C. F. Poole, New trends in solid-phase extraction, TrAC Trends in Analytical Chemistry 22 (2003) 362-373, doi: 10.1016/S0165-9936(03)00605-8.

[8] N.J.K. Simpson (Ed.), Solid-Phase Extraction: Principles, Strategies and Applications, Marcel Dekker, New York, USA, 2000.

[9] M. Faraji, Y. Yamini, M. Gholami, Recent Advances and Trends in Applications of Solid-Phase Extraction Techniques in Food and Environmental Analysis, Chromatographia 82 (2019) 1207–1249, doi: 10.1007/s10337-019-03726-9.

[10] V. Camel, Solid phase extraction of trace elements, Spectrochimica Acta Part B 58 (2003) 1177-1233, doi: 10.1016/s0584-8547(03)00072-7.

[11] I. Liška, Fifty years of solid-phase extraction in water analysis – historical development and overview, J. Chromatogr. A 885 (2000) 3–16, doi: 10.1016/S0021-9673(99)01144-9.

[12] R.E. Subden, R.G. Brown, A.C. Noble, Determination of histamines in wines and musts by reversed-phase high-performance liquid chromatography, J. Chromatogr. A166 (1978) 310–312, doi: 10.1016/s0021-9673(00)92280-5.

[13] C.F. Poole, Solid-phase extraction, Encyclopedia of Separation Science, Elsevier, 2000.

[14] M.E.I. Badawy, M.A.M. El-Nouby, P.K. Kimani, L.W. Lim, E.I. Rabea, A review of the modern principles and applications of solid-phase extraction techniques in chromatographic analysis, Analytical Sciences 38 (2022) 1457–1487, doi: 10.1007/s44211-022-00190-8.

[15] S. Mitra, Sample Preparation Techniques in Analytical Chemistry, Wiley-Interscience, 2003.

[16] A.D. Ellington, J.W. Szostak, In vitro selection of rna molecules that bind specific ligands, Nature 346 (1990) 818-822, doi: 10.1038/346818a0.

[17] C. Tuerk, L. Gold, Systematic evolution of ligands by exponential enrichment - Rna Ligands to Bacteriophage-T4 DNA-Polymerase, Science 249 (1990) 505-510, doi: 10.1126/science.2200121.

[18] R. Stoltenburg, C. Reinemann, B. Strehlitz, SELEX-A (r)evolutionary method to generate high-affinity nucleic acid ligands, Biomol. Eng. 24 (2007) 381-403, doi: 10.1016/j.bioeng.2007.06.001.

[19] M. Mascini, I. Palchetti, S. Tombelli, Nucleic acid and peptide aptamers: fundamentals and bioanalytical aspects, Angew. Chem. Int. Ed. Engl. 51 (2012) 1316-1332, doi: 10.1002/anie.201006630.

[20] V. Pichon, F. Brothier, A. Combès, Aptamer-based-sorbents for sample treatment-a review, Anal. Bioanal. Chem. 407 (2015) 681–698. doi: 10.1007/s00216-014-8129-5.

[21] E. Peyrin, Nucleic acid aptamer molecular recognition principles and application in liquid chromatography and capillary electrophoresis, J. Sep. Sci. 32 (2009) 1531–1536, doi: 10.1002/jssc.200900061.

[22] C.L.A. Hamula, J.W. Guthrie, H. Zhang, X.-F. Li, X.C. Le, Selection and analytical applications of aptamers, TrAC Trend Anal. Chem. 25 (2006) 681-691, doi: 10.1016/j.trac.2006.05.007.

[23] B. Madru, F. Chapuis-Hugon, E. Peyrin, V. Pichon, Determination of cocaine in human plasma by selective solid-phase extraction using an aptamer-based sorbent, Anal. Chem. 81 (2009) 7081– 7086, doi: 10.1021/ac9006667.

[24] B. Madru, F. Chapuis-Hugon, V. Pichon, Novel extraction supports based on immobilised aptamers: evaluation for the selective extraction of cocaine, Talanta 85 (2011) 616-624, doi: 10.1016/j.talanta.2011.04.016.

[25] F. Chapuis-Hugon, A. du Boisbaudry, B. Madru, V. Pichon, New extraction sorbent based on aptamers for the determination of ochratoxin A in red wine, Anal. Bioanal. Chem. 400 (2011) 1199–1207, doi: 10.1007/s00216-010-4574-y.

[26] W. Hadj Ali, V. Pichon, Characterization of oligosorbents and application to the purification of ochratoxin A from wheat extracts, Anal. Bioanal. Chem. 406 (2014) 1233-1240, doi: 10.1007/s00216-013-7509-6.

[27] S.N. Aslipashaki, T. Khayamian, Z. Hashemian, Aptamer based extraction followed by electrospray ionization-ion mobility spectrometry for analysis of tetracycline in biological fluids, J. Chromatogr. B Analyt. Technol. Biomed. Life Sci. 925 (2013) 26–32, doi: 10.1016/j.jchromb.2013.02.018.

[28] X. Yang, W. Kong, Y. Hu, M. Yang, L. Huang, M. Zhao, Z. Ouyang, Aptamer-affinity column cleanup coupled with ultra high performance liquid chromatography and fluorescence detection for the rapid determination of ochratoxin A in ginger powder, J. Sep. Sci. 37 (2014) 853–860, doi: 10.1002/jssc.201301136.

[29] Michaud M, Jourdan E, Villet A et al (2003) A DNA aptamer as a new target-specific chiral selector for HPLC. J Am Chem Soc 125: 8672–8679.

[30] Stead SL, Ashwin H, Johnston B et al (2010) An RNA-aptamer based assay for the detection and analysis of malachite green and leucomalachite green residues in fish tissue. Anal Chem 82:2652– 2660.

[31] M. Zief, R. Kiser, Solid Phase Extraction for Sample Preparation Manual, J.T. Baker, Phillipsburg, 1988.

[32] D.D. Blevins, M.F. Burke, T.J. Good, Sorbent extraction technology handbook, N. Simpson, K.C. Van Horne KC, 1993.

[33] C.W. Huck, G.K. Bonn, Recent developments in polymer-based sorbents for solid-phase extraction. J. Chromatogr. A, 885(2000) 51-72, doi: 10.1016/s0021-9673(00)00333-2

[34] C.F. Poole, A.D. Gunatilleka, R. Sethuraman, Contributions of theory to method development in solid-phase extraction, J. Chromatogr. A 885 (2000)17-39, doi: 10.1016/s0021-9673(00)00224-7.

[35] P. Lovkvist, J.A. Jonsson, Capacity of sampling and preconcentration columns with a low number of theoretical plates, Anal. Chem. 59 (1987) 818–821.

[36] Z. Zhang, J. Pawliszyn, Headspace Solid-Phase Microextraction, Anal. Chem. 65 (1993) 1843-1852.

[37] É.A. Souza-Silva, R. Jiang, A. Rodríguez-Lafuente, E. Gionfriddo, J. Pawliszyn, A critical review of the state of the art of solid-phase microextraction of complex matrices I. Environmental analysis, TrAC Trend Anal. Chem. 71 (2015) 224-235, doi: 10.1016/j.trac.2015.04.016.

[38] É.A. Souza-Silva, E. Gionfriddo, J. Pawliszyn, A critical review of the state of the art of solid-phase microextraction of complex matrices II. Food analysis, TrAC Trend Anal. Chem. 71 (2015) 236-248, doi: 10.1016/j.trac.2015.04.018.

[39] É.A. Souza-Silva, N. Reyes-Garcés, G.A. Gómez-Ríos, E. Boyacı, B. Bojko, J. Pawliszyn, A critical review of the state of the art of solid-phase microextraction of complex matrices III. Bioanalytical and clinical applications, TrAC Trend Anal. Chem. 71 (2015) 249-264, doi: 10.1016/j.trac.2015.04.017.

[40] J. Pawliszyn, Handbook of Solid Phase Microextraction, Elsevier, London, 2012.

[41] Solid-phase microextraction: a promising technique for sample preparation in environmental analysis, J. Chromatogr. A 889 (2000) 3-14, doi: 10.1016/s0021-9673(00)00453-2.

[42] I. Bruheim, X. Liu, J. Pawliszyn, Anal. Chem. 75 (2003) 1002-1010, doi: 10.1021/ac026162q.

[43] Z. Zhang, J. Pawliszyn, Quantitative Extraction Using an Internally Cooled Solid Phase Microextraction Device, Anal. Chem. 67 (1995) 34-43.

Chapter 3
Comprehensive two-dimensional gas chromatography: fundamentals and pratical aspects

3.1 Gas chromatography fundamentals

Gas chromatography (GC), with open tubular capillaries (OTC), is a physical separation technique suitable for the analysis of volatile and semi-volatile compounds. Gas chromatography was invented by Martin and James in 1952, with the separation of volatile fatty acids [1]. The principle of separation is based on the affinity of the components with the stationary phase, while the mobile phase (a gas) migrates them through the system. A schematic representation of a GC setup is shown in Figure 3.1. The column is at the central part of the system, in which the physicochemical process of the separation occurs. In fact, it contains the stationary phase, while the mobile phase, called carrier gas, flows through the column from a pressurized gas cylinder. The rate of mobile phase delivery is monitored by a pressure- and/or flow-regulating device. The sample is introduced through a device known as an injector. The sample is transferred from the injector to the column, with the sample components continuously redistributed between the mobile and stationary phases. The single components of the sample reach the column outlet at different times due to their different affinities for the stationary phase. The detector monitors individual components eluting from the separating column, and is connected to the analytical column. The GC system consists of three independently controlled thermal zones:

- injector zone, that ensures rapid volatilization of the introduced sample;
- oven temperature, which is controlled to optimize the separation process;
- detector zone, which must be at temperatures where the individual sample components are measured in the vapor phase.
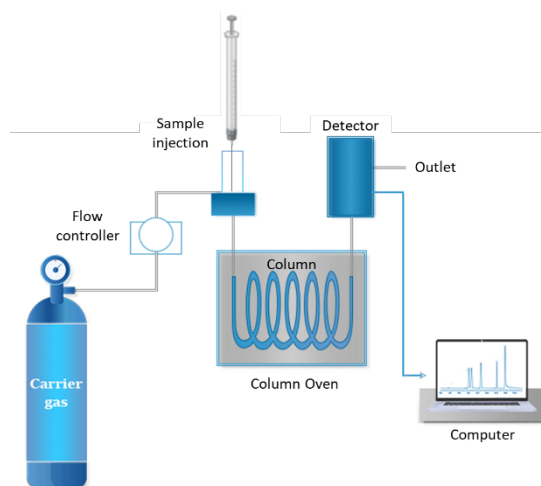
Figure 3.1. *The main components of a gas chromatograph.*

3.2 Chromatographic parameters

The most important chromatographic parameters will be described as follows.

Retention

It is related to the time the analyte spends between the injection and the maximum of a chromatographic peak. In order to evaluate retention properties, a suitable term is the retention factor, namely k':

$$k' = \frac{t_R - t_0}{t_0} \qquad (3.1)$$

where t_R is the retention time and t_0 is the void time (retention time of an unretained compound). The nominator value represents the time spent by an analyte in the stationary phase. Analytes with a small value of k' will have low affinity with the stationary phase, while analytes with a large k' will have high affinity for the stationary phase.

An important parameter to measure column selectivity is the separation factor (α), calculated as the ratio between the retention factors, for any two compounds, with the numerator always the more retained of the two compounds. If $\alpha \geq 1$ there is a good separation, otherwise co-elution at different degrees occur.

The capacity of a specific analyte to interact with the stationary phase is described with a thermodynamic parameter, called distribution constant (K_c):

$$K_c = \frac{C_s}{C_M} \tag{3.2}$$

where the terms C_s and C_M are equal to the solute concentration in the stationary and mobile phases, respectively.

The retention index assumes essential importance because it compares the retention time of a solute with respect to those of reference standard analytes, always employed as a homologous series. In the case of isothermal conditions, the retention index (I) can be calculated by using the following formula:

$$I = 100_z + 100\,\frac{logt_{r(x)} - logt_{r(z)}}{logt_{r(z+1)} - logt_{r(z)}} \tag{3.3}$$

where z corresponds to the number of carbon atoms related to the homologous series compound (*i.e.,* 600 for hexane, 700 for heptane, *etc.*), while x is related to the target component. The programmed-temperature retention index calculation is based on the following equation proposed by H. van den Dool and D. J. Kratz, which does not use the logarithmic form.

$$I = 100_z\,\frac{t_{r(x)} - t_{r(z)}}{t_{r(z+1)} - t_{r(z)}} \tag{3.4}$$

As previously cited, when the latter equation is applied for the calculation of indices, these are commonly denominated as linear retention indices (*LRI*).

Band broadening

The main aim of GC is to separate components in a mixture according to their different retention times. Analytes are detected following the GC separation exhibiting an approximately Gaussian concentration distribution defined by the retention time and the width at the base of each corresponding chromatographic peak. For this reason, band broadening must be reduced, and it is also suitable to measure the efficiency of the column, which is defined by the number of theoretical plates, N. The latter is calculated by:

$$N = \left(\frac{t_r}{\sigma}\right)^2 = 16\left(\frac{t_r}{w_b}\right)^2 = 5.54\left(\frac{t_r}{w_h}\right)^2 \tag{3.5}$$

where t_r, σ, w_b and w_h represent the retention time, standard deviation, peak width at base and mean height, respectively. An efficient column is indicated by a high value of N.

Another term related to the number of theoretical plates is the height equivalent to one theoretical plate, namely *H*:

$$H = \frac{L}{N} \qquad (3.6)$$

where *L* is the length of the chromatographic column. The definition of band broadening was provided by the van Deemter equation and was expressed in terms of *H*, with the following equation:

$$H = A + \frac{B}{\bar{u}} + C\bar{u} \qquad (3.7)$$

where the term *A* is Eddy diffusion and describes the chromatographic band dispersion due to the irregularities in pathways in packed columns; longitudinal molecular diffusion (term *B*) represents the peak dispersion due to the diffusion processes occurring longitudinally inside the column, while the mass transfer in the stationary liquid phase (term *C*) occurs in relation to radial diffusion of the analytes. When Golay introduced the theory of the open tubular capillary column, the *A* term becomes zero, and two *C* terms were introduced in the equation [2]; one for mass transfer in the stationary phase (C_s), and one for mass transfer in the mobile phase (C_M). Thus, the Golay equation is:

$$H = \frac{B}{\bar{u}} + (C_S + C_M)\bar{u} \qquad (3.8)$$

where the *B* term is the molecular diffusion, calculated by the following equation:

$$B = 2D_G \qquad (3.9)$$

where D_G is the diffusion coefficient of the analyte in the carrier gas. As visible from the Golay equation, this term is divided by the linear velocity ($\bar{u}$), thus a high velocity will reduce the contribution of the molecular diffusion to peak broadening, since the analyte will spend a reduced time in column. The C_s term is defined as:

$$C_S = \frac{2kd_f{}^2}{3 + (1+k)^2 D_s} \tag{3.10}$$

where d_f is the average film thickness of the liquid stationary phase and Ds is the diffusion coefficient of the solute in the stationary phase. To reduce peak broadening for this term, the film thickness should be small and the diffusion coefficient large. With regard to k, large values will be related to a high solubility in the stationary phase. Since a large value may involve long analysis times, little advantage is gained by k values larger than 20. The C_M term is defined as:

$$C_M = \frac{(1 + 6k + 11k^2)r_c{}^2}{24(1+k)^2 D_G} \tag{3.11}$$

where r_c is the radius of the column. The contributions of the two C terms in the Golay equation depends on the film thickness and the column radius. Considering thin films (< 0.2 μm), mass transfer in the mobile phase is dominant; for thick films (2-5 μm) mass transfer in the stationary phase is prevalent, while for intermediate films (0.2 to 2 μm) both factors need to be considered.

The efficiency of a separation system is also represented by its peak capacity, n_c, which represents the maximum number of solutes that can theoretically be resolved at the baseline on a given column. An estimate of a column peak capacity for a retention time window from time t_1 to t_2 is given by:

$$n_c = 1 + \frac{\sqrt{N}}{4R} \ln\left(\frac{t_2}{t_1}\right) = 1 + \frac{\sqrt{N}}{4} \ln(1 + k_{max}) = 1 + \frac{\sqrt{N}}{4} \ln\left(\frac{V_{max}}{V_{min}}\right) \tag{3.12}$$

where V_{min} and V_{max} are the initial and final (in terms of retention time) volumes of mobile phase. This estimation is valid for isocratic elution. The peak capacity in gradient elution is generally higher and can be calculated by:

$$n_c = \frac{\sqrt{N}}{4}\left(\frac{t_2}{t_1} - 1\right) + 1 \tag{3.13}$$

Resolution

A parameter related to column efficiency, selectivity and retention is resolution (R_s) which indicates the degree of resolution between two adjacent peaks, with retention factors k_1 and k_2:

$$R_s = \frac{\sqrt{N}}{4} \left(\frac{\alpha - 1}{\alpha} \right) \left(\frac{k_2}{k_2 + 1} \right) \qquad (3.14)$$

If the column length is doubled, resolution will increase by a factor of 1.414. Thus, a considerable increase in resolution can only be achieved by using very long columns but this can lead to very long analysis times. An increase of the retention factor (k) has a significant effect on R_s only for analytes with low k values (≤ 3). Finally, a more selective stationary phase involves an increase in the separation factor and the resolution will be greatly improved. Considering the three variables, selectivity has the greatest effect on resolution; in fact, it is fundamental to select the most appropriate and suitable stationary phase in relation to the specific sample. However, in the case of complex samples the use of a more selective stationary phase will result in a modified chromatography profile, but not in the separation of many more compounds.

3.3 Why comprehensive two-dimensional GC?

Currently, one-dimensional (1D GC) is the most widely applied method for the separation of volatile and semi-volatile compounds contained in real-world samples. However, a satisfactory separation of all the components of a complex sample is a challenge when using a single chromatography column, resulting in co-elutions that do not allow the correct identification of compounds and/or difficulties in quantification. Gas chromatography separations are related to analyte properties (*i.e.,* vapor pressure, polarity) and so the combined use of different stationary phases can be very useful to resolve cases of co-elution [3].

A chromatographic procedure relies on two primary factors: peak capacity and the selectivity of the stationary phase. The first parameter is influenced by various aspects, including column dimensions (such as length, internal diameter and stationary-phase thickness) and experimental conditions (*i.e.*, mobile phase flow rate,

type, temperature, outlet pressure, *etc.*). On the other hand, selectivity is predominantly influenced by the chemistry of the stationary phase, specifically the nature of interactions between the analyte and the stationary phase (*i.e.*, dispersion, dipole-dipole, electrostatic forces, *etc.*). The determination of 1D GC n_c can be easily estimated by dividing the retention time window (excluding the dead time) by the average peak width (4σ). When a conventional capillary column (30 m × 0.25 mm ID × 0.25 μm d_f) is used, the peak capacity typically falls within the range of 400 to 600. Theoretically, if a GC method yields a peak capacity of 600, it implies that 600 peaks could potentially be accommodated side by side within the one-dimensional separation space. Nevertheless, GC peaks elute in a random manner, resulting in crowded portions of the chromatogram while other areas remain less populated. The principal effect is that the n_c value must greatly exceed the number of volatile compounds present in the sample. Specifically, to achieve a 98% level of resolution, the method's peak capacity should exceed the number of constituents in the sample by a factor of 100 [7]. Consequently, to separate a sample containing 50 compounds a GC method should ideally generate a peak capacity of 5000. These figures emphasize that the separation capabilities of a conventional single GC column may prove insufficient in numerous applications involving complex samples. One approach to enhance the separation efficiency of one-dimensional GC is to employ different column geometries, such as utilizing longer columns. However, this also comes with the trade-off of increased analysis time.

When two or more GC column having different selectivities are combined, the analytical system can be recognized as a multidimensional GC system (MDGC). In this chapter, particular attention is directed to comprehensive two-dimensional gas chromatography (GC×GC).

3.4 Multidimensionality concept

The basic requirements for an MDGC separation were discussed by Giddings in 1987 [4]. Each MDGC system has to satisfy two main conditions:

1. sample components are subjected to two or more separation steps;
2. components that are resolved in the previous separation should remain separated until the total separation process is completed.

From the first rule, the concept of separation orthogonality was established. When two (or more) independent separations are performed, an equal number of parameters contribute to define analyte identity [5]. In a GC×GC analysis, each analyte is characterized by two different retention times instead of one as in 1D GC. The separation is defined "orthogonal" if the dimensions are based on different interaction mechanisms (*e.g.*, analyte volatility and polarity). Since volatility and polarity are uncoupled now, it results in independent separations in the two columns [6]. Figure 3.2 illustrates the orthogonality concept in three different degrees of correlation. In orthogonal separations the peaks are distributed across the entire plane (Figure 3.2a), in separations with correlation the distribution will be centered along the diagonal (Figure 3.2b), while when there is total correlation, the analytes have the same retention in two dimensions, leading to an equivalent 1D separation along the diagonal (Figure 3.2c). Dimension selectivity can be characterized by different types of interactions: π-aromaticity interaction, chirality, hydrogen bonds, size or shape of molecules, volatility/number of carbon atoms, etc.
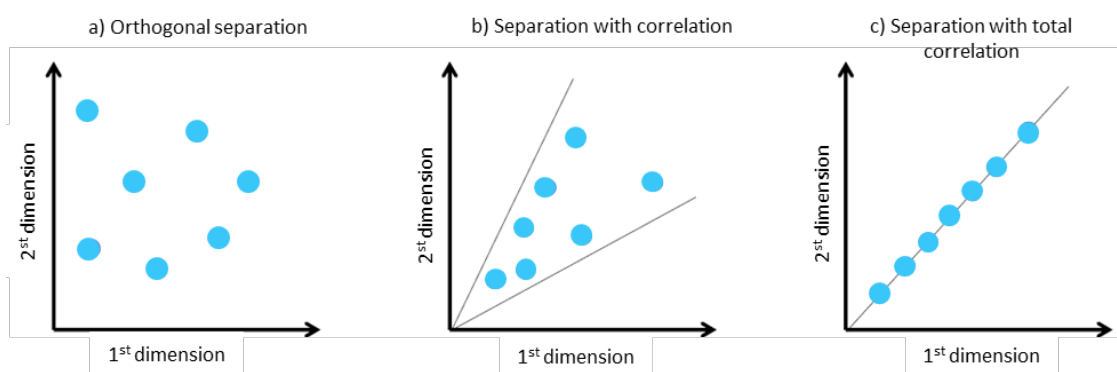
Figure 3.2. *Concept of orthogonality.*

In 1995 Giddings introduced the notion of sample dimensionality, defined as the number of independent variables describing sample compound properties [7]. Multidimensional separation techniques can be divided into two main approaches: heart-cutting (GC-GC) and comprehensive two-dimensional MDGC systems are equipped with two (or more) capillary GC columns coupled in series *via* a transfer device. Specifically, GC-GC allows the transfer of selected regions of eluate containing target compounds from the first (^{1}D) column to the second column (^{2}D);

while GC×GC applies the advantages of MDGC to the entirety of the separation of analytes injected on the ¹D column.

The usefulness of such a GC×GC system for the separation of a complex mixture is shown schematically in Figure 3.3. Considering a hypothetical sample constituted by components that differ in shape, colour and size, then following the dimensionality concept [7], a dimensionality of three will occur. With a 1D system, the separation can be achieved according to size, but then colour and shape will remain unresolved; or it can be carried out according to colour, but then the size and shape will remain unseparated; or at last, it can be performed according to shape, but without separation between size and colour. Thus, the only possibility for the separation of all constituents is an orthogonal 2D-separation system to use the entire separation space.
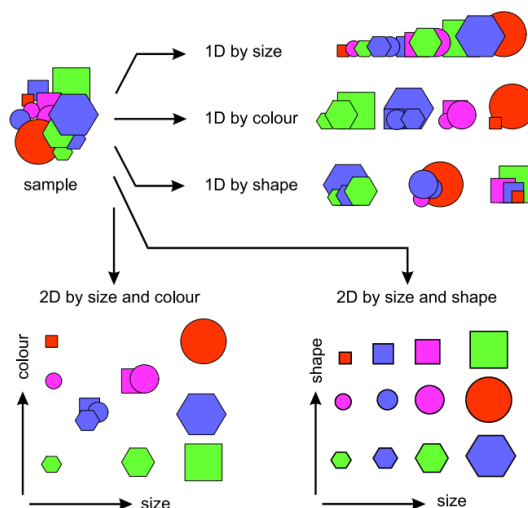
***Figure 3.3.** Match between separation and sample dimensionality in GC×GC.*

GC×GC systems offers different advantages over conventional 1D GC, including:

- enhanced separation power due to increased peak capacity compared to 1D analysis;

- enhanced sensitivity (the analyte band compression is accompanied by analyte re-concentration, especially when using cryogenic modulation);

- enhanced specificity (two stationary phases with different selectivity are employed);

- enhanced analysis speed due to the greater number of peaks resolved *per* unit of time;

- identification power due to the formation of highly organized chemical class patterns (*i.e.*, alkanes, fatty acid methyl esters, pyrazines, etc.) in the 2D chromatograms.

3.5 GC×GC instrumental setup

A scheme of a GC×GC system is shown in Figure 3.4, and it can be assembled using the same apparatus used for a conventional GC system (apart from the transfer device). In a typical GC×GC analysis, the sample is introduced by the injector (by different techniques, such as split, splitless, programmed temperature vaporization, solid-phase microextraction) onto the first conventional capillary column where it is subjected to the first separation; the eluate is then fractionated and re-injected onto the second column (coated with a different stationary phase) through the interface, namely modulator, for the further separation. In most cases, both columns are located within the same oven, but it is also possible to place the second column in a separate oven for greater flexibility in temperature control. During the entire duration of the analysis, the analytes are subjected to separation due to two different types of interaction. The columns used for the ^{2}D are very short, allowing rapid separations.
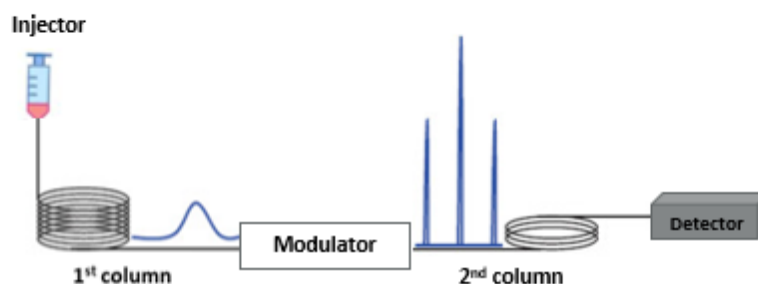
Figure 3.4. *Scheme of a GC×GC system.*

The critical component in a GC×GC system is therefore the modulator, which can be installed inside or outside any of the gas chromatograph. The modulator, which can be considered as an online injector within the system, is responsible for sampling and transferring the eluate from the first ^{1}D column to the ^{2}D column [5].

The modulator must be able to transfer the eluate quickly and consistently to the head of the second dimension, ensuring that the separation achieved in the first dimension is not destroyed. The transfer process is continuous throughout the entire duration of the chromatographic separation. The ^{1}D chromatogram is sliced by the

modulator, resulting in a two-dimensional separation and the generation of 2D contour plots (by using dedicated software). Ideally, the separation of analytes in the ^{2}D has to be completed before another pulse is injected, to avoid overlap of compounds deriving from different modulation cycles (an effect called "wraparound"). Wraparound occurs when the elution time of a specific analyte is greater than the modulation time. In terms of separation, wraparound does not generate new co-elutions, so it may not affect the chromatographic separation and there is no reason to spend time avoiding wraparound in a separation procedure. Moreover, dedicated software can easily re-establish a clear picture of the separation space [8].

3.5.1. Column combinations

Any existing column that can be used in GC can also be used in GC×GC, and column selection plays an important role in a successful GC×GC separation. Following Giddings's rules [7], a multidimensional separation is achieved by combining two columns capable of generating orthogonality. In GC×GC applications, polar-apolar or apolar-polar column combinations can be used. Usually, the ^{2}D column has a length ranging from 80 to 200 cm to maintain elution times shorter than the modulation period (1-10 s) for most analytes. A conventional capillary column, *i.e.* 30 m × 0.25 mm ID × 0.25 μm d_f is normally used in the first dimension. In fact, it is desirable to have rather large peak widths entering the modulator to ensure proper sampling of potentially co-eluting analytes prior to their separation in the ^{2}D. On the other hand, the ^{2}D column is shorter and has a smaller internal diameter than the ^{1}D column, allowing for fast ^{2}D analysis. The most frequently employed column setup (also named normal set) combines a non-polar ^{1}D stationary phase, such as dimethylpolysiloxane, with a more polar ^{2}D one, such as polyethylene glycol. In such a configuration, analytes are separated as a function of increasing boiling point on the ^{1}D, and on the basis of polarity on the ^{2}D. Structured elution pattern can be observed, where the non-polar compounds are located at the bottom of the chromatogram, while the more polar compounds are more retained in the second dimension and are thus present in the upper part (Figure 3.5).
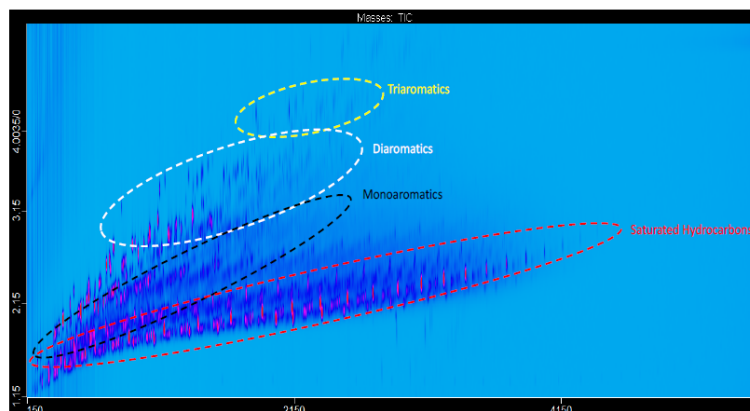
Figure 3.5. *GC×GC- high resolution time-of-flight mass spectrometry analysis of a diesel sample on a normal column configuration.*

In certain specialized applications, alternative column combinations (reverse set) may diverge from the typical non-polar/semipolar configuration [3,10].

3.5.2 Modulators: an overview

As the "heart" of the GC×GC system, the modulator is essential for sampling, focusing, and reinjecting analytes from the [1]D column to the [2]D column [10]. Since its invention in 1991, several modulators have been developed, utilizing various physical properties to achieve the modulation process. Modulators can be broadly divided into two main categories: ***thermal modulators*** and ***valve-base modulators*** or ***flow modulators***. The first class uses temperature control to trap analytes from the [1]D eluate and subsequently release these trapped analytes for a [2]D separation [12-15]. The second category uses a gas flow to control and isolate fractions of the [1]D eluate and redirect the isolated [1]D eluate through injection for [2]D separation [16-17]. The valve-based modulators are classified into two subcategories: ***differential flow modulators*** (including diaphragm valve-based), characterized by two independent carrier gas flows to achieve modulation, and ***diverting flow modulators*** (including Deans switching), which employ a valve (normally solenoid) to control gas pressure for eluate transfer from the [1]D column to the [2]D column. Modulators can be further categorized as "low duty cycle" (only small portions of the eluate from the [1]D is directed to the head of the [2]D column) and "high (or unit) duty cycle" (usually all the [1]D effluent is sampled) [11,18].

In order to preserve the separation performed in the first dimension, the ^{1}D eluate must be sampled many times to avoid coelution of already separated components [3]. Each chromatographic peak must be sampled three or four time to meet this requirement [19-20]. The modulation period (P_M) is related to the modulation ratio (M_R):

$$M_R = \frac{\omega_b}{P_M} \qquad (3.15)$$

where the peak width at the base (ω_b), defined as 4 times the ^{1}D column peak standard deviation (σ) or 1.6985 times the width at half height of the peak (ω_h), is divided by the modulation period (P_M) [20].

Furthermore, the *phase of modulation* is defined as the difference between the center of ^{1}D peak and the mean of the peak region sampled by the modulator. It influences the degree of resolution and the reconstructed peak width of the analyte eluting from the ^{1}D column [21]. There are two extreme situations (Figure 3.6):

1. *in-phase modulation*, when a symmetrical pulse sequence with a single maximum peak is observed;

2. *180 degrees out-of-phase modulation*, if the pulse sequence is still symmetric but has two (equal) maxima.

Unfortunately, due to the natural random distribution of analytes, it is not possible to predict the modulation phase, and there will be many different sampling scenarios in a single two-dimensional chromatographic run. For this reason, the sum of the areas of individual modulations should be used for quantitative analysis [22].
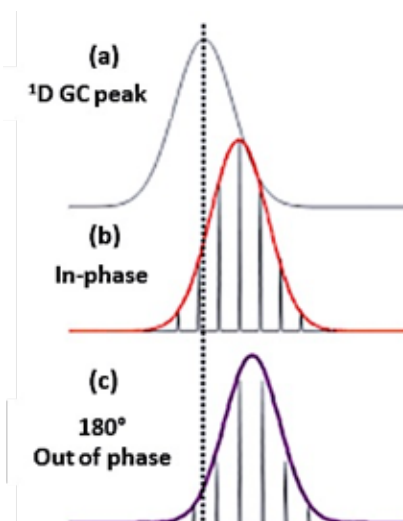
Figure 3.6. *Illustration of modulated peak patterns: (a) 1D peak, with (b) in-phase and (c) out-of-phase modulation.*

Finally, GC × GC relies on maximizing peak capacity and it is given by [23,24]:

$$n_{C,2D} = {}^1n_c \times {}^2n_c \tag{3.16}$$

where ${}^1n_c$ and ${}^2n_c$ are the ^{1}D and ^{2}D peak capacities, respectively. In order to enhance peak capacity, the GC × GC instrument must generate highly efficient separations, characterized by narrow peak widths in both dimensions.

3.5.2.1 Thermal modulation

Thermal modulation, introduced in 1991, uses a positive and/or negative temperature difference compared to the GC oven temperature [12]. The main advantage of thermal modulation over flow modulation is the focusing effect due to the re-concentration of the analyte bands during trapping, leading to an enhancement of the signal-to-noise (S/N) ratio.

In the pioneering GC×GC design, analytes eluting from the ^{1}D were transferred to the ^{2}D using a thermal modulator, namely a ***thermal desorption modulator*** (TDM). It was originally developed as a sample introduction device in multiplex and high-speed gas chromatography, and after exploited to perform the first dual-stage modulated GC×GC separation [26,27]. Modulation was achieved by alternating a trapping stage based on phase-ratio focusing and a re-injection one accomplished by thermal desorption. Specifically, the modulator was 15 cm long and was coated in

the initial part of the secondary column with a film of electrically conductive material (gold paint) and looped outside the GC oven, at room temperature. A TDM scheme is shown in Figure 3.7.
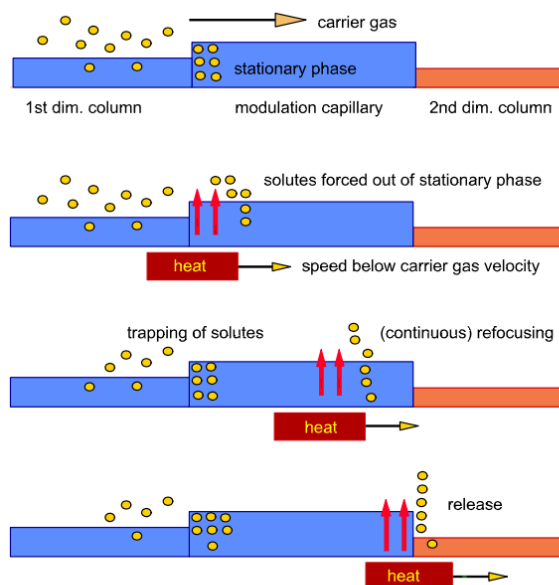
Figure 3.7. *Dual-stage thermal desorption modulation.*

The ***thermal sweeper modulator*** was described for the first time in 1996 [28], and was the first commercially available modulator (Zoex Corporation) in its final version in1999 [29]. The modulator, illustrated in Figure 3.8, is based on the use of a slotted heater, which rotates around a shaft, to heat the modulator capillary, thus remobilizing analytes at the head of the second dimension. This process must be sufficiently rapid to avoid *breakthrough* phenomena. In order to generate sufficiently narrow modulated peaks, the temperature difference between the heater and the modulator capillary should be at least 100 °C [30]. This can be considered as a limit, considering the maximum GC oven temperature and consequently also the volatility range of compounds that could be modulated.
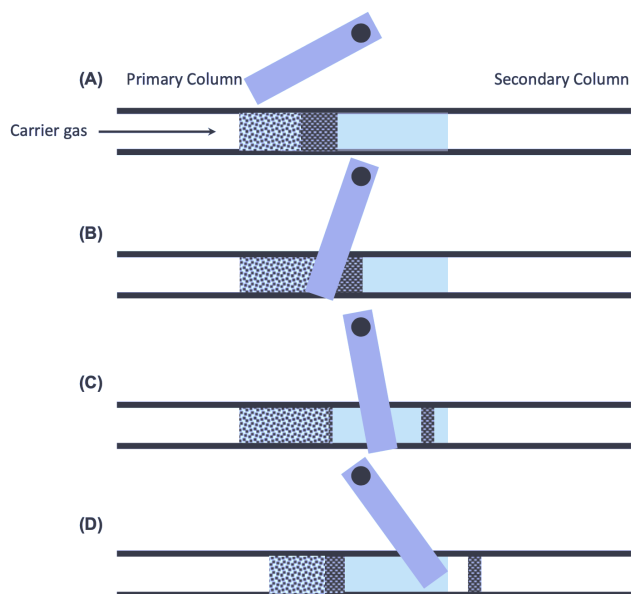
Figure 3.8. *Thermal sweeper modulation process.*

A further class of thermal modulators are known as cryogenic modulators. In this case, analyte focusing occurs using a cryogenic trap at a significantly lower temperature than the oven temperature. Although cryogenic modulation increases the overall consumable cost of the system, it provides the best performance, overcoming the previous temperature limitations of the heater designs. Among the cryogenic modulators available in the market are:

- ***Longitudinally modulated cryogenic system (LMCS)***: the LMCS was developed by Kinghorn and Marriott in 1997 [31]. The system consists of a cylindrical cryogenic trap that moves longitudinally and externally to the modulation capillary, enabling the double focusing of the analytes. However, desorption occurs due to the exposure to the oven temperature. Analyte re-mobilization could suffer at lower oven temperatures, especially when using a slow temperature program, and for high boiling analytes [32]. A diagram of an LMCS is reported in Figure 3.9.
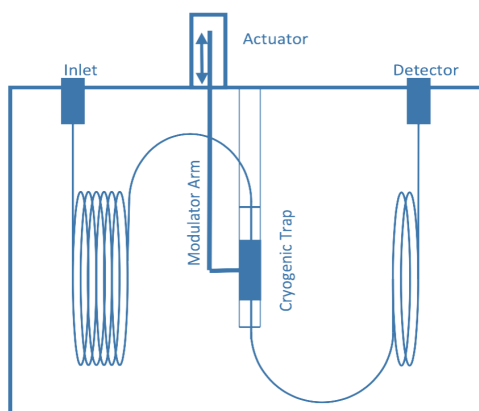
Figure 3.9. *Schematic diagram a GC×GC with an LMCS modulator.*

- ***Dual-stage jet modulator***: the system was introduced by Ledford in 2000 [33]. As can be observed in Figure 3.10, the mechanism was based on the use of two hot jets and two cold jets to provide dual-stage modulation. The jets were positioned to provide a transverse gas flow at the head of the ^{2}D column where the modulation occurred. Liquid nitrogen was used to cool the gas for the cold jets in a heat exchanger. On the other, the gas flowing to the hot jets was heated by an electric heater. This modulator is available in both a liquid nitrogen variant with a modulation range of C_4 to C_{40} and a consumable-free one, that uses a closed loop chiller instead of liquid nitrogen to cool the heat exchanger with a modulation range of C_8 to C_{40}.
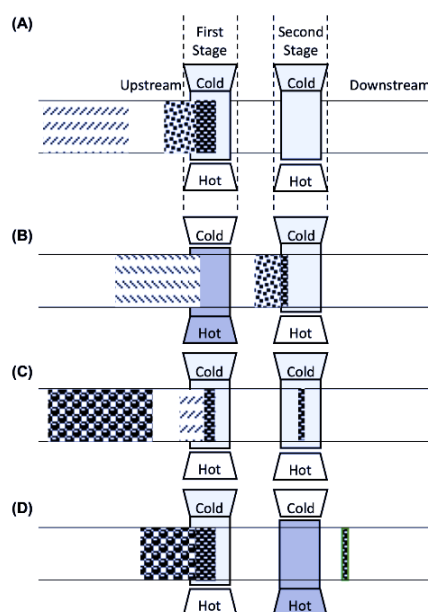
Figure 3.10. *Modulation process of the dual-stage, quad-jet thermal modulator.*

- ***Dual-jet loop modulator***: the system was proposed by Ledford *et al.*, and was characterized by a cold and a hot jet [34]. The two stages were created by looping a segment (1-1.5 m) of the capillary column (modulator tube) through the pathway of a cold jet of N_2 gas (Figure 3.11). The modulator tube can be generated by using the last part of the first dimension or the initial segment of the second. However, it is better to use an uncoated column, or a segment of stationary-phase coated capillary. The cold jet is directed vertically downward onto the modulator tube, generating two cold spots. Instead, the hot jet of nitrogen gas is activated periodically (*i.e.*, every 4-6 s, corresponding to the modulation period) for a brief period (*i.e.*, 300-375 ms) diverting the cold jet from the modulation tube. The hot jet is situated perpendicularly to the cold one, and rapidly heats the cold spots, remobilizing the entrapped analytes. This modulator works essentially in the same manner as the quad-jet modulator, and it is available in both a consumable-free variant and a liquid nitrogen one.
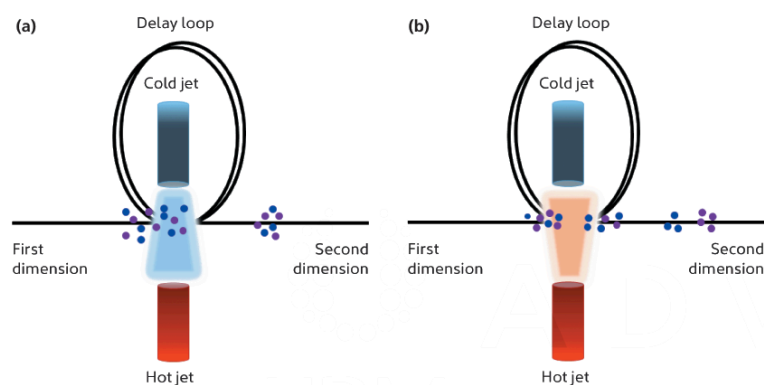
Figure 3.11. *Schematic of dual jet loop modulator: (a) the cold jet traps the analytes, and then (b) a hot jet re-injects the analyte onto the second dimension.*

3.5.2.1. Flow modulators

Flow modulators are characterized by an interface that involves an auxiliary carrier gas (the same carrier gas used at the injector) to control and isolate part of the ^1D eluate and re-inject the isolated ^1D eluate for the ^2D separation [17,35]. One classification was introduced by Tranchida *et al.* categorizing the modulators into two subcategories [36]: *in-line valve systems*, characterized by the presence of a

switching valve with a direct connection to the first and second analytical column; *out-of-line valve systems*, derived from the Deans switch principle, and thus based on the manipulation of the pressure between the two GC dimensions. Another classification, of flow modulators, as previously seen, was introduced by Synovec in 2019, dividing them into: *differential flow modulators* and *diverting flow modulators*. The main flow modulators available are:

- **Differential flow modulators**: a system appeared for the first time in the same year as the LMCS [37]. The modulator, presented by Bruckner *et al.*, involved the use of a six-port diaphragm valve (located in the GC oven) to generate a single stage flow modulation GC×GC analysis (Figure 3.12). Specifically, two valve ports were used to connect the first dimension, an apolar column with a poly(dimethylsiloxane) stationary phase measuring 4.9 m × 0.53 mm ID × 3.0 μm d_f, and the second dimension, consisting of a more polar polyethylene glycol stationary phase, measuring 0.85 m × 0.18 mm ID × 0.15 μm d_f. Additionally, a split line (0.5 m × 0.18 mm ID fused silica column) was used to reduce flows in the ^{2}D column. The other two valve ports were connected to an auxiliary pressure source and to a waste line.
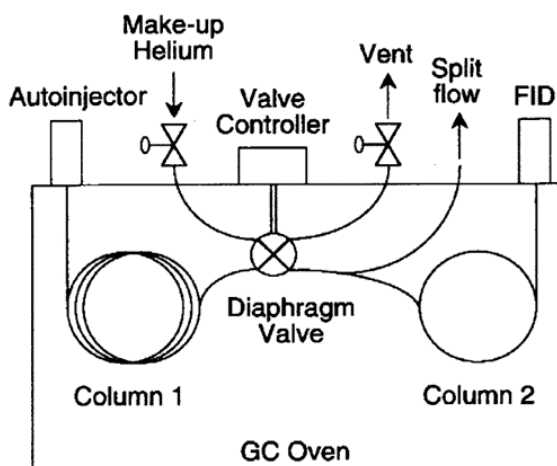
Figure 3.12. The first FM device (in the ''waste'' mode).

Modulation was carried out through control of the valve position, which connected the first dimension to the second or to the waste line, enabling the transfer of eluate to one of the two lines, in an alternate manner. The auxiliary pressure unit maintained gas flow in the second dimension, while the eluate was

directed to waste. In this specific research, the Authors used a P_M of 500 ms with a 50 ms period of re-injection (0.1 duty cycle). Apart issues related to sensitivity, due to the low duty cycle (95% of the ^{1}D column flow was directed to the waste), a major drawback was related to the restricted operational temperature of the valve, which could not be operated at a temperature above 175°C. An initial solution relative to the temperature limit concerns was obtained by placing the valve externally to the oven, extending the operating temperature range of the valve to 250°C [38].

- ***Loop flow modulator***: the system was developed by Seeley *et al.* to overcome the low duty cycle problem of the previous modulator [39]. The sampling loop can collect the ^{1}D eluate, allowing a much higher fraction of the ^{1}D column eluate to be transferred to the ^{2}D column, resulting in a significant improvement in detection sensitivity. The device included a six-port, two-position, diaphragm valve, equipped with a 20 µL stainless steel sampling loop, connected to a waste line and an additional pressure source (Figure 3.13). The part of the valve containing non-wetted components was located outside the oven and was maintained at 125°C by using an auxiliary heater.
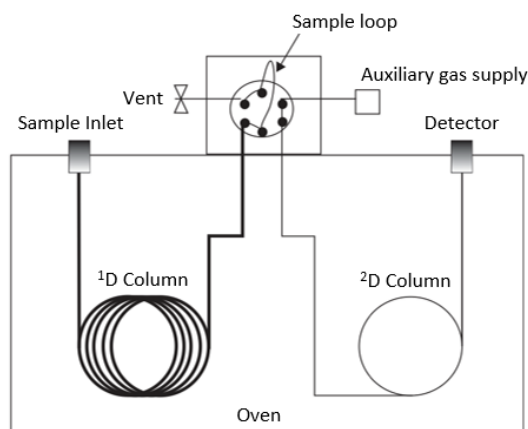
Figure 3.13. *The first FM GC×GC device equipped with a sampling loop.*

The GC×GC column set was: a 10 m × 0.25 mm ID × 1.4 µm d_f ^{1}D column with a 6% cyanopropylphenyl, 94% dimethylpolysiloxane stationary phase, and a 5 m × 0.25 mm ID × 0.25 µm d_f ^{2}D column with a polyethylene glycol stationary phase. In the original work, the valve was used in the accumulation and injection

states for 80% and 20% of the P_M, respectively. During the injection state, while the previously accumulated chromatography plug was launched onto the ^{2}D exploiting a high gas flow (15 mL min^{-1}), the ^{1}D column effluent (0.75 mL min^{-1}) was directed to waste. As in the case of the previously reported modulator, one of the issues is the restricted operating temperature, which did not allow the analysis of analytes requiring a temperature above 200 °C, as they would recondense in the valve at a lower temperature. Another disadvantage was related to the high ^{2}D column flows, which is an issue when using mass spectrometry. The problem was partially resolved in later studies by splitting the flow between two analytical capillaries [40,41].

- *Dual-stage flow modulator*: the system was introduced by Seeley *et al.* in 2006 [42]. It consisted of three deactivated fused silica columns, two micro-volume T-unions, and a two-way solenoid valve (located outside the GC oven) connected to an auxiliary pressure source (Figure 3.14). The output ports of the solenoid valve were connected to the unions by using two fused silica segments. One of the T-unions was linked to the ^{1}D column outlet, while the other directed the flow to the ^{2}D. Furthermore, a fused silica segment, linked between the two unions, acted as a sample loop with a volume of 24 μL.
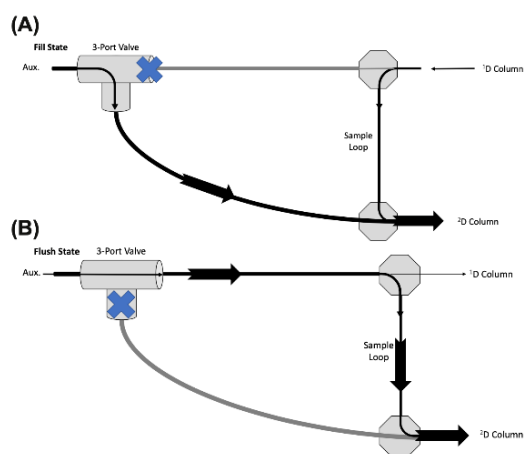
Figure 3.14. The schematic of the dual-stage flow modulators.

A non-polar 15 m × 0.25 mm ID × 0.50 μm d_f capillary was used in the ^{1}D (flow: 1.0 mL min^{-1}), while two polar 5 m × 0.25 mm ID columns were employed in the second dimension, one with a 0.25 μm polyethylene glycol film and the other with a 0.50 μm poly(methyltrifluoropropylsiloxane) one. The modulator operates

in two stages, *fill* and *flush*. When the modulator is in the *fill* stage, the auxiliary gas flow (20 mL min^{-1}) was directed to the ^{2}D and the primary column effluent flowed freely within the loop. Before the effluent reached the bottom union, the solenoid valve was switched to the *flush* state and the auxiliary flow flushed the content of the loop onto the head of ^{2}D column. The re-injection state is very fast (*e.g.*, 100 ms), whereas the accumulation state, which involves filling the loop, is in the order of seconds. Unlike the modulators previously described, this device was stable at high GC temperatures. Moreover, this modulator had a unit duty cycle. The main drawbacks were related to the complexity of method optimization, the rather high ^{2}D gas linear velocity, and the low P_M. Generally, during the accumulation/fill state, a specific time must not be exceeded to avoid loop breakthrough. In addition, during the re-injection state the time must be long enough to allow the complete emptying of the loop. In 2011, Tranchida *et al.* developed a differential flow modulator using a seven-port wafer chip with an external loop for effluent collection [43]. The interface, shown in Figure 3.15, comprises a metallic disc (2.5 cm diameter, 7 mm thickness), and internal rectangular channels (250 μm width/75 μm depth), connecting ports 1-2-3 and 4-5-6/7. A two-way electrovalve is located outside the GC oven and is connected to an advanced pressure control (APC) unit. Two metallic branches connect the valve to the interface in positions 2 and 5.
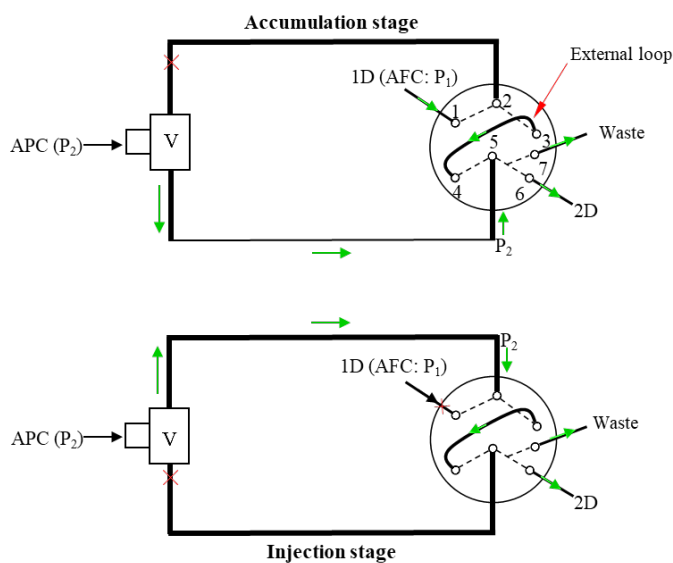
Figure 3.15. *Seven-port FM device in the accumulation and injection modes. Abbreviations: V: two-way solenoid valve; AFC: advanced flow controller.*

The first- and second-dimension columns are linked to positions 1 and 6, respectively. A 40 μL stainless- steel loop (20 cm × 0.71 mm OD × 0.51 mm ID) connects positions 3 and 4; the size of the loop is chosen considering the modulation period, first-column flow and second-column dimensions. It is noteworthy that the flow exiting the loop is divided between the channels linked to ports 6 and 7. Finally, a needle valve connected to a waste line at the head of the second column was employed to decrease the flow rate to ~2.5 mL min^{-1} leading to a low duty cycle of ~5.

- *Dynamic pressure gradient modulator*: the system was described at the beginning of 2020 by Synovec *et al.* [44]. The ^{1}D and ^{2}D columns of the GC×GC were connected to a 3-way T-union (Figure 3.16).
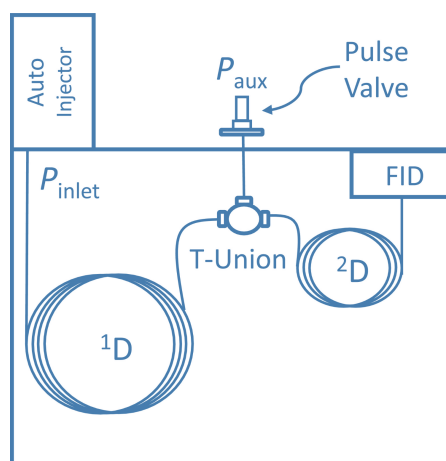
Figure 3.16. Scheme of the dynamic pressure gradient modulator.

The third port of the T-union was connected to a high-speed pulse valve. The ^{1}D eluate is confined at the T-junction, and introduced for ^{2}D separation with a cyclic rhythm, dependent upon the relationship of the P_M to the pulse width, defined as the time interval when the auxiliary gas flow at the T-junction is off. When the valve was closed a fraction of the ^{1}D effluent was transferred onto the ^{2}D, while when it was open, ^{1}D elution was interrupted (stop flow) and the ^{2}D separation proceeded. The entire ^{1}D column eluate is transferred to the ^{2}D column, providing a 100% duty cycle. A normal column set was used, consisting of a ^{1}D column with a non-polar stationary phase (10.0 m × 0.18 mm ID × 0.18 μm d_f) followed by a ^{2}D column with a polar stationary phase (1.0 m × 0.18 mm ID × 0.10 μm d_f). The P_M was only 750 ms, with a 60 ms valve close time. Peak

widths were narrow in time and variable, ranging from 20 to 180 ms. The applied P_{aux} generated a ^{2}D gas flow of 22.9 mL min^{-1} at the beginning of the analysis.

• *Multi-mode modulator (MMM)*: the system was introduced by Seeley *et al*. and it was based on the Deans switch principle [45]. The MMM device consisted of a three-port solenoid valve, a cross union, a T-union, and a metal joining capillary (Figure 3.17). The latter was connected, through the cross union, to the ^{1}D column and, through the T-union to the ^{2}D column, thus keeping the two columns near one other. The auxiliary carrier flow, known as the switching flow, entered through a two-way, three-port solenoid valve. The normally closed (NC) output port of the solenoid valve is connected to the cross and the normally opened (NO) output port is connected to the T-union. The fourth port of the cross union is connected to a flow restrictor.
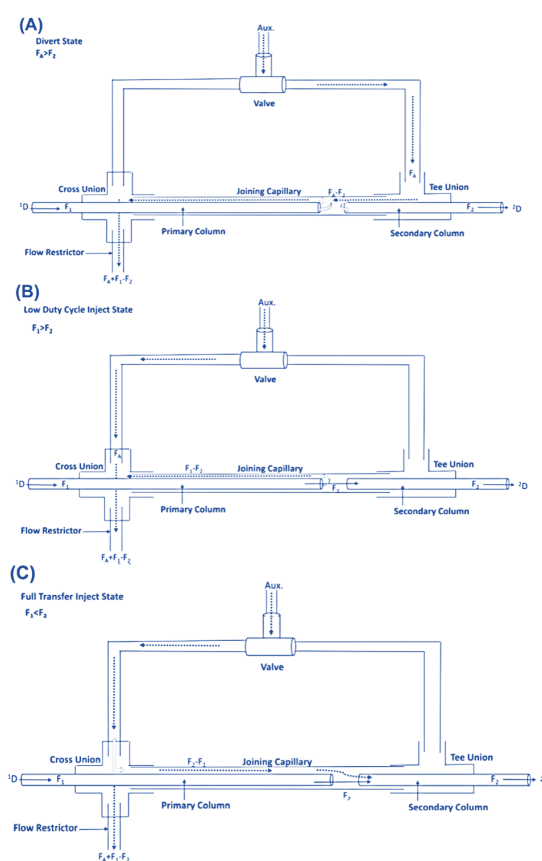
Figure 3.17. *Scheme of the multi-mode modulator. A) The divert state for both the low duty cycle and full transfer modes; B) the injection state for low duty GC×GC modulation mode; C) the injection state for the full transfer GC×GC modulation mode.*

There are two flows entering the modulator: the primary column flow (F_1) and the switching flow (F_S). Additionally, there were two flows exiting: restrictor flow (F_X) and the secondary column flow (F_2). When the valve is in the NO position, the ^{1}D flow is directed to the restrictor (low duty cycle) or stored in the joining capillary (high duty cycle); when the valve is in the normally closed (NC) position, the effluent from the ^{1}D column is directed to the second one. The MMM can operate as a low duty cycle modulator or a full transfer modulator depending on the gas flows involved, and on the proximity of the ^{1}D and ^{2}D column tips within the joining capillary. Specifically, when the F_1 is greater than the F_2 the device will operate as a low duty cycle modulator. While, if the F_1 is lower than the F_2, the device will perform as a full transfer modulator. When operated in the diverting mode, the modulator has several advantages such as lower column flow rates, eliminating the need for a splitter for MS coupling, and achieves narrower second dimension peak widths than differential flow modulation.

Based on the MMM, a diverting flow modulator (namely "FLUX" modulator) was developed and commercialized by LECO. A representation of the modulator is reported in Figure 3.18. The modulator operates in two different states by using an auxiliary gas flow: *divert mode* and *inject mode*. In the first case, the auxiliary gas flow opposes the effluent from the ^{1}D column, sending it to waste. The auxiliary gas flow rate is higher than the ^{1}D flow, and during the divert state it supplements the flow through the ^{2}D column, as well as forcing the entirety of the ^{1}D column flow to waste. When the modulator changes its position to the inject state, the majority of the auxiliary gas flow is directed to waste, thus enabling the transfer of the flow from the ^{1}D column to the ^{2}D one. The modulator is characterized by a cross fitting connected to the ^{1}D column, and a tee fitting from which the ^{2}D column exits. The cross and tee are connected by a length of tubing which is crimped in the center to set the columns at an appropriate distance from each other to ensure the optimal transfer of analytes between the dimensions. The switching valve is then connected to an auxiliary flow module for control of the switching gas (3.5 mL min^{-1}).
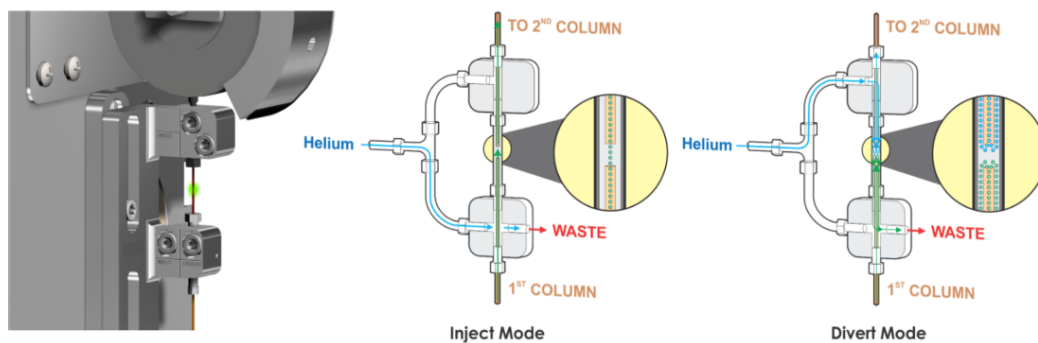
Figure 3.18. *The FLUX modulator in the inject and divert mode.*

3.5.3 Detectors

The column outlet is connected to a detector, which provides information regarding the distribution of individual peaks within a chromatogram and their relative amounts. Detectors are classified in universal and selective types.

Universal detectors allow the detection of all (or nearly all) the components present in a mixture, although their response to the same quantities of different compounds is not similar. Instead, selective detectors generate a response only to compounds that contain a unique structural feature in their molecular structure. For example, a gasoline sample contains a high number of compounds belonging to different chemical classes. A nitrogen selective detector (NPD) allows the qualitative and quantitative measurement of only nitrogen-containing compounds in gasoline, while the others mixture constituents are not detected.

In addition to the classic GC detector specifications, a GC×GC detector must provide rather high sampling rates, such as for high-speed GC to enable adequate peak reconstruction. In fact, typical GC×GC peak widths are in the range 100-600 ms. The rise time of the detector should therefore be short, and the sampling rate should be at least 100 Hz.

3.5.3.1 Flame ionization detector

The flame ionization detector (FID) is the most commonly used detection system in GC. It is classified as a universal type detector, and has an acquisition speed far above 100 Hz. It is characterized by high sensitivity (the minimum detectable amounts are in the order of 10^{-12} g s^{-1}), a wide dynamic range, and ease of operation.

Detection is based on the decomposition of the solute-neutral molecules, within a flame, into charged components and on the electrical measurement of the resultant changes of conductivity. The column outlet is directly connected to the FID, and the column effluent is introduced at the detector base in a continuous manner, where it is mixed with the combustion gas (H_2) and, if necessary, a make-up gas. This mixture is then combined with air and burnt through a metallic jet, which also serves as an anode (positive electrode), while the cathode (negative electrode) is positioned above the jet itself. Changes in conductivity between the electrodes are monitored, amplified by an electronical device, and recorded. Externally, the FID is composed of a metallic body maintained at a high temperature (250-300 °C) to prevent the gases produced by combustion from condensing inside the detector, potentially damaging it or reducing its performance. The main drawback of using an FID, is the lack of structural information.

3.5.3.2 Mass spectrometry

Mass spectrometry (MS) is a fundamental analytical technique, used to generate ions from either inorganic or organic compounds by any suitable method, which are then separated by their mass-to-charge ratio (*m/z*) and detected qualitatively and quantitatively. The analyte may be ionized thermally, by electric fields or by impacting energetic electrons, ions or photons. Ion separation is performed in a variety of manners, in the mass analyzer [47].

The coupling of GC×GC with various forms of MS forms a three-dimensional system, with the first work published in 1999 by Frysinger and Gaines [48]. The authors reported the use of single quadrupole mass spectrometry (QMS), using a system with a very low acquisition speed (2.43 scan s^{-1}). Since 1999, a great deal of evolution has occurred in the GC×GC-MS field (on both the GC and MS sides), with it being described in a series of review articles [49-51].

Generally, co-eluting analytes at the outlet of the ^{1}D column possess the same or similar vapour pressures (if a low polarity column is used); these overlapping analytes are subjected to a ^{2}D separation in which specific interactions with the stationary phase occur. If co-elution persists, the mass analyzer can perform a further separation based on *m/z* values. Therefore, GC×GC-MS can potentially create a

cubic separation space, providing four potential levels of identification: 1 and 2) retention times on the two GC columns; 3) the presence of chemical class patterns; 4) the mass spectral data.

The MS system (Figure 3.19) consists of a *sample inlet*, which operates under atmospheric pressure conditions, while the other components, *ion source*, *mass analyzer* and *detector* operate under high vacuum conditions. A vacuum system maintains a very low pressure in the mass spectrometer; the ion source region is usually maintained at a pressure between 10^{-4} and 10^{-8} torr; a somewhat lower pressure is required in the mass analyzer region (around 10^{-8} torr). An essential requirement is to maintain the integrity of the sample molecules during their transfer from atmospheric pressure (sample inlet) to the ion source (vacuum). When the mass spectrometer is used as a detector, the column (^{2}D column for a GC×GC system) is directly linked to the MS through a heated metal transfer line (the temperature must be high enough to avoid analyte condensation). The ion source (*usually electron ionization*) converts the neutral sample molecules into gas-phase ions, which are then separated, by the mass analyzer. The detector measures and amplifies the ion current of the mass-resolved ions. Finally, the data system records, processes, stores, and displays the data in the form of a mass spectrum.
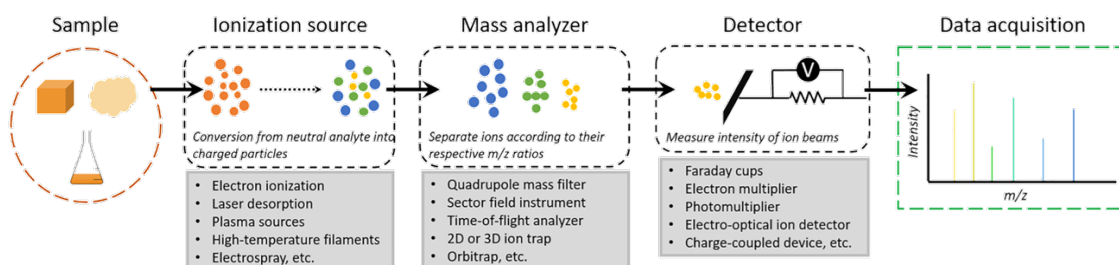
Figure 3.19. *Schematic representation of mass spectrometry*

The energy tranferred to the analytes during the ionization processes is varied, leading to the classification of the various ionization techniques based on their relative "hardness" or "softness". Volatile compounds are most commonly ionized by electron ionization (EI) sources. In this case, a high energy beam of electrons hits the neutral analyte forming a radical cation (M^{+} •), the molecular ion, which may itself fragment to produce a characteristic fragmentation pattern, creating a cascade of ion-forming reactions before leaving the ion source [52]. The ions are then focused into a beam, accelerated into the mass analyzer, and reach the detector. The

individual ion current intensities at each mass are sequentially recorded, generating a mass spectrum. The latter is a histogram of the relative abundance of the ions and their subsequent separation, based on their *m/z* values.

Mass spectrometers are classified according to the mass analyzer; QMS, triple quadrupole MS (QqQMS) and time-of -flight MS (ToFMS) are three of the main MS techniques coupled with gas chromatography.

- *Quadrupole mass spectrometry*: the approach was first described by Paul and Steinwegen in 1953 [53]. The mass analyzer comprises four parallel hyperbolic or cylindrical metal rods arranged in a square array (Figure 3.20); the rods vary in length from 15 to 25 cm and have a diameter of 10-20 mm. Each pair of opposing rods is held at the same potential (but opposite sign), which is composed of a direct current (DC) and an alternating current (AC) component. Mass separation is accomplished by the stable vibratory motion of ions in a high-frequency oscillating electric field and the voltage applied to the bars is between 102 and 103 V [54]. When ions enter in the space between the rods, they oscillate in the *x* and *y* directions, with the amplitude depending on the frequency of the potential applied and the masses of the ion. A positive ion will be attracted towards a negative rod and as the potential changes sign, the ion will change direction to avoid discharging itself onto the rod. For given DC and radio frequency values, only ions within a certain *m/z* range will have stable trajectories and reach the detector, while the others will be eliminated.
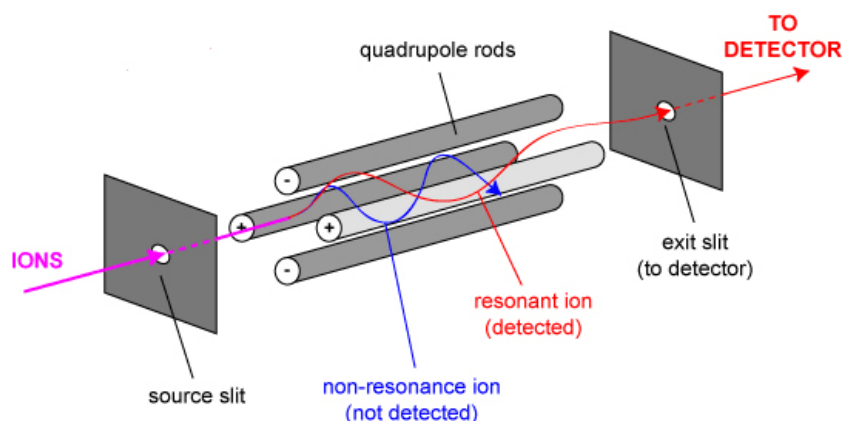
Figure 3.20. Schematic representation of a quadrupole mass analyzer.

The motion of an ion traveling through the quadrupole is described by the *Mathieu equation* [55], introduced in 1866. The QMS analyzers have two operating modes, the first, defined scan, in which all the ions within a mass range (set by the operator) are monitored. The scan mode allows for untargeted analysis and comparison of experimental mass spectra with those in MS databases, obtaining qualitative results with a reduced margin of identification error compared to other detectors. The second mode is selected ion monitoring (SIM), used for targeted analysis, where only one or a few ions are selected for detection, providing greater selectivity and sensitivity than the scan mode.

- *Triple quadrupole mass spectrometry*: in such systems there are two mass analyzers (quadrupoles Q1 and Q3), after the ionization source, which are arranged in series and separated by a collision cell (q). The quadrupoles Q1 and Q3 have exactly the same functions as seen for QMS and can operate independently in either the scan or SIM mode. The collision cell, instead, is an octapole or hexapole, and is gas-filled (helium or more commonly argon); within the cell, fragmentation occurs through collision-induced dissociation (CID). The collision of the gas in q increases the energy of the ion(s) filtered by Q1, which will in turn fragment. A schematic of a QqQMS system is shown in Figure 3.21.
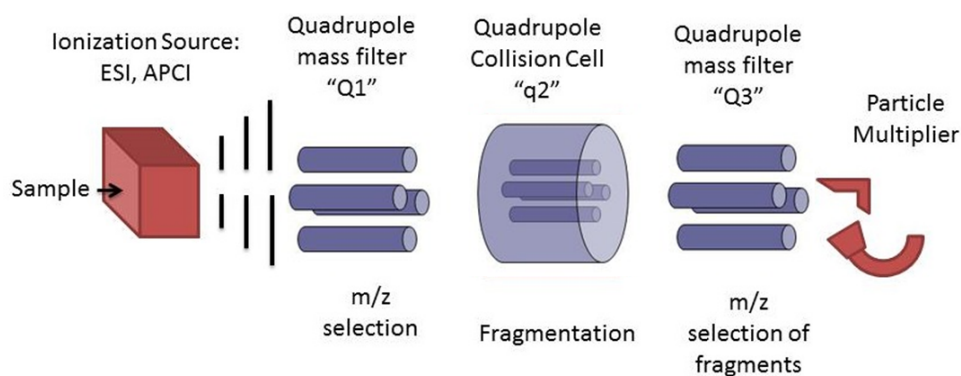
Figure 3.21. *Schematic representation of a triple quadrupole mass analyzer.*

There are five types of operational modes, used for both qualitative and quantitative applications, depending on the specific case and requirements (Figure 3.22).

- *Full scan*: can be performed using either Q1 or Q3, with the latter being the most widely used. In such a case, Q1 is not. Of course, the SIM mode can also be used.

- *Product ion scan*: Q1 is set to scan a given *m/z* value (precursor ion), while Q3 scans a range of *m/z* values.

- *Precursor ion scan*, is achieved by performing a scan in Q1, while a specific *m/z* value is monitored in Q3.

- *Neutral loss scan*: Q1 and Q3 operate in the scan mode. However, Q3 is shifted by a specific *m/z* value with respect to Q1. Only ions that lose a neutral mass, corresponding to the *m/z* difference between the two analyzers, can be detected.

- *Multiple/selected reaction monitoring*, where transitions from a specific *m/z* (precursor ion) to a product ion are monitored. Both Q1 and Q3 are set to monitor a specific *m/z* value.
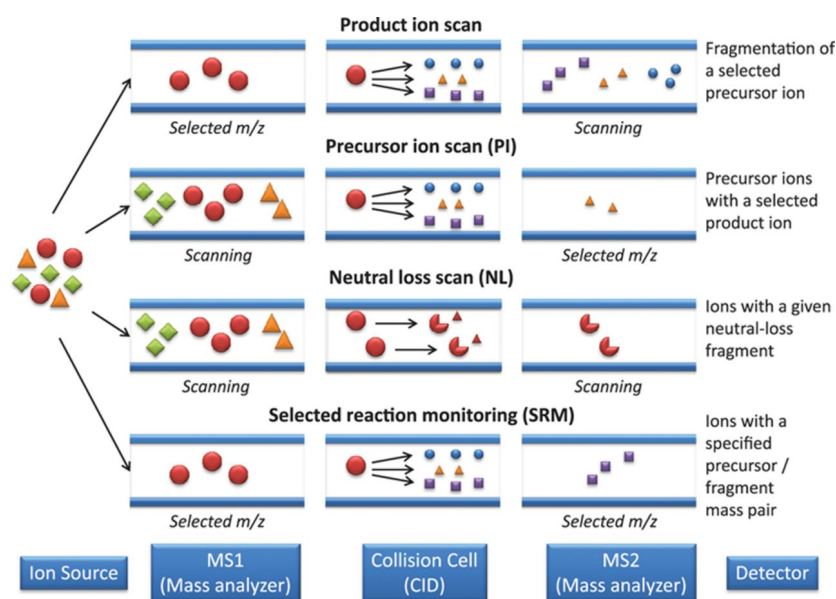
Figure 3.22. *Schematic overview of the different QqQMS operational modes.*

- ***Time-of-flight mass spectrometry***: the technique was introduced by Stephens in 1946 [56], but only in 1995 Wiley and McLaren published the design of a linear ToF mass spectrometer, which later became the first commercial instrument [57]. Such mass analyzers are field-free and allow ion separation on the basis of their

different velocities assumed inside the drift region. Heavier ions require more time to travel through the flight tube and reach the detector. After ion generation and acceleration, the ions arrive at the ToF interface as ion packages. They are advanced towards the flight tube through a potential difference between an electrode and the extraction grid. When they leave the acceleration zone, all ions with the same charge ideally have the same kinetic energy and enter a field-free zone. They then reach the detector at the opposite end of the flight tube at different velocities depending on their mass. Thus, all the ions start their journey at the same time, or at least within a sufficiently short time, with the lighter ions reaching the detector earlier than the heavier ones. Such an instrumental setup, where the ions travel in a straight line from the point of their generation to the detector, is called a linear ToF. The time difference between the start signal of the pulse and the time at which an ion hits the detector is the time of flight and can be expressed as:

$$t_{ToF} = \frac{L}{v} = L \sqrt{\frac{m}{2qU_a}} \propto \sqrt{m/z} \qquad (3.16)$$

where L is the length of the field-free region, v is the ion velocity after acceleration, m is the ion mass, q is the charge of the ion, U_a is the accelerating electric potential difference, and z the charge state.

All the mass range is analyzed simultaneously, in contrast to scanning analyzers where the ions are transmitted successively along a time scale, leading to higher sensitivity.

One of the main breakthroughs in the technological development of ToF analyzers arose from the design of the orthogonal acceleration ToF analyzer (oaToF). In an oaTof analyzer, ion pulses are extracted orthogonally from a continuous ion beam. Initially, the ions occupy the first stage of the ion accelerator, between the extraction plate and a grid. Subsequently, a pulsed electric field at a frequency of several kilohertz is applied and force the ions to take a direction orthogonal to their original trajectory, beginning their flight towards the analyzer.

Notably, the duty cycle of an oaToF is significantly less than 100%, usually lower than a conventional ToF analyzer. This is due to the time required for the ion beam to fill the orthogonal acceleration area, which is shorter than the time required for the sampled ions to reach the detector. Since new ions cannot be introduced until the previous ions have reached the detector, a portion of the ions produced in the source is lost in the initial stage of the orthogonal acceleration. The most important advantages of oaToF are: high mass resolving power and exceptional mass accuracies, 1 ppm or lower. Thus, oaToF instruments are currently widespread used in combination with GC, fast GC and GC×GC.

In 1994 the so-called *reflectron* was developed by Mamryn to improve the mass resolution [58]. The most basic form of reflectron, namely single-stage reflectron, comprises a sequence of uniformly spaced ring-shaped electrodes set at an increasing potential which focus ions having the same *m/z* value but different kinetic energies in time. Ions with higher kinetic energy, and thus greater velocity, penetrate the reflectron more deeply compared to the ions with lower kinetic energy. Consequently, the faster ions spend more time within the reflectron and reach the detector simultaneously with slower ions of the same *m/z* value. Despite the capability to extend the flight path without increasing the mass spectrometer dimensions, the beneficial enhancement in mass resolution comes at the cost of reduced sensitivity and a mass range limitation.

Finally, TOF analyzer are divided into two categories: low resolution systems (LR ToFMS) and high resolution systems (HR ToFMS). The former exhibits unit-mass resolution and operates at a high acquisition frequency (*i.e.*, 500 Hz). Its duty cycle is variable, approximately 30% [59], with a sensitivity higher compared to a scanning instrument. Deconvolution software enables the resolution of mass spectra for compounds that partially co-elute during the chromatographic run. To obtain optimal deconvolution, high spectral coherence is required, with an acquisition rate of about 20-30 spectra per peak. Quantification can be achieved through the extracted ion chromatogram (EIC) approach. In the field of GC×GC-MS, LR ToFMS systems are the most commonly-used.

On the other hand, the spectra produced by an HR ToFMS system have higher resolution and high mass accuracy, generating highly specific extracted ion chromatograms, facilitating a "pre-targeted" analysis. The acquisition of fragments with accurate mass values up to the fourth decimal place provides valuable information about molecular structures, thus reducing the possibility of incorrect   identification.

References

[1] A. T. James, A. J. P. Martin, Gas-liquid partition chromatography; the separation and micro-estimation of volatile fatty acids from formic acid to dodecanoic acid, Biochem. J. 50 (1952) 679, doi: 10.1042/bj0500679.

[2] L. S. Ettre, The Invention, Development and Triumph of the Flame Ionization Detector, LC-GC Europe 15 (2002) 364-373, doi: 10.1142/9781860949449_0023.

[3] Comprehensive Two Dimensional Gas Chromatography in: D. Barcelo (Ed.), Wilson and Wilson's Comprehensive Analytical Chemistry, Elsevier 2009).

[4] J. C. Giddings, Concepts and comparisons in multidimensional separation, J. High Resolut. Chromatogr. Commun. 10 (1987) 319, doi:10.1002/jhrc.1240100517.

[5] P.J. Schoenmakers, P. Marriott, J. Beens, Nomenclature and conventions in comprehensive multidimensional chromatography, LC-GC Eur. 16 (2003) 335.

[6] C.J. Venkatramani, J. Xu, J.B. Phillips, Separation orthogonality in temperature-programmed comprehensive two-dimensional gas chromatography, Anal. Chem. 68 (1996) 1486, doi: 10.1021/ac951048b.

[7] J.C. Giddings, Sample dimensionality: A predictor of order-disorder in component peak distribution in multidimensional separation, J. Chromatogr. A 703 (1995) 3, doi: 10.1016/0021-9673(95)00249-M.

[8] J.F. Focant, A. Sjödin, W.E. Turner D.G. Jr. Patterson, Measurement of selected poly- brominated diphenyl ethers, polybrominated and polychlorinated biphenyls, and organo-chlorine pesticides in human serum and milk using comprehensive two-dimensional gas chromatography isotope dilution time-of-flight mass spectrometry, Anal. Chem. 76 (2004) 6313-6320, doi: 10.1021/ac048959i.

[9] H. Daniel Bahaghighat, Chris E. Freye, Robert E. Synovec, Recent advances in modulator technology for comprehensive two dimensional gas chromatography, doi:

[10] J.M.D. Dimandja, G.C. Clouden, I. Colón, J.F. Focant, W.V. Cabey, R.C. Parry, Retention-time prediction in comprehensive two-dimensional gas chromatography to aid identification of unknown contaminants, J. Chromatogr. A. 1019 (2003) 261, doi: 10.1007/s00216-018-1415-x.

[11] H. Daniel Bahaghighat, Chris E. Freye, Robert E. Synovec, Recent advances in modulator technology for comprehensive two dimensional gas chromatography, TrAC Trends Anal. Chem. 113 (2019) 379-391 doi: 10.1016/j.trac.2018.04.016.

[12] Z. Liu, J.B. Phillips, Comprehensive two-dimensional gas chromatography using an on-column thermal modulator interface, J. Chromatogr. Sci., 29 (1991) 227-231, doi: 10.1093/chromsci/29.6.227.

[13] H.-J. de Geus, J. de Boer, U.A.T. Brinkman, Development of a thermal desorption modulator for gas chromatography, J. Chromatogr. A, 767 (1997) 137-151, doi: 10.1016/S0021-9673(97)00038-1.

[14] P.J. Marriott, R.M. Kinghorn, Longitudinally modulated cryogenic system. A generally applicable approach to solute trapping and mobilization in gas chromatography, Anal. Chem. 69 (1997)2582-2588, doi:10.1021/ac961310w.

[15] B.V. Burger, T. Snyman, W.J.G. Burger, W.F. van Rooyen, Thermal modulator array for analyte modulation and comprehensive two-dimensional gas chromatography J. Separ. Sci. 26 (2003) 123-128, doi: 10.1002/jssc.200390002.

[16] M. Edwards, A. Mostafa, T. Górecki, Modulation in comprehensive two-dimensional gas chromatography: 20 years of innovation, Anal. Bioanal. Chem. 401 (2011) 2335-2349, doi: 10.1007/s00216-011-5100-6.

[17] P.Q. Tranchida, G. Purcaro, P. Dugo, L. Mondello, Modulators for comprehensive two-dimensional gas chromatography, TrAC Trends Anal. Chem. 30 (2011) 1437-1461, doi: 10.1016/j.trac.2011.06.010.

[18] J.V. Seeley, N.J. Micyus, S.V. Bandurski, S.K. Seeley, J.D. McCurry, Microfluidic deans switch for comprehensive two-dimensional gas chromatography, Anal. Chem. 79 (2007) 1840-1847, doi: 10.1021/ac061881g.

[19] R.E. Murphy, M.R. Schure, J.P. Foley, Effect of sampling rate on resolution in comprehensive two-dimensional liquid chromatography, Anal. Chem. 70 (1998) 1585, doi: 10.1021/ac971184b.

Effect of Sampling Rate on Resolution in Comprehensive Two-Dimensional Liquid Chromatography, Anal. Chem. 70 (1998) 1585-1594, doi: 10.1021/ac971184b.

[20] W. Khummueng, J. Harynuk, P.J. Marriott, Modulation Ratio in Comprehensive Two-dimensional Gas Chromatography, Anal. Chem. 78 (2006) 4578-4587, doi: 10.1021/ac052270b.

[21] P. Marriott, R. Shellie, Principles and applications of comprehensive two-dimensional gas chromatography, TrAC Trends Anal. Chem. 21 (2002) 573-583, doi:1 0.1016/S0165-9936(02)00814-2.

[22] R.C.Y. Ong, P.J. Marriott, A Review of Basic Concepts in Comprehensive Two-Dimensional Gas Chromatography, J Chromatogr Sci. 40 (2002) 276–291, doi:10.1093/chromsci/40.5.276.

[23] J.M. Davis, J.C. Giddings, Statistical theory of component overlap in multicomponent chromatograms, Anal. Chem. 55 (1983) 418-424, doi: 10.1021/ac00254a003.

[24] J.M. Davis, J.C. Giddings, Statistical method for estimation of number of components from single complex chromatograms: theory, computer-based testing, and analysis of errors, Anal. Chem. 57 (1985), 2168-2177, doi:10.1021/ac00289a002.

[25] P.J. Marriott, S.-T. Chin, B. Maikhunthod, H.-G. Schmarr, S. Bieri. Multidimensional gas chromatography, TrAC Trends Anal. Chem. 34 (2012) 1-21, doi: 10.1016/j.trac.2011.10.013.

[26] Z. Liu, J.B. Phillips, High-speed gas chromatography using an on-column thermal desorption modulator, J. Microcolumn Sep. 1 (1989) 249–256, doi:10.1002/mcs.1220010508.

[27] Z. Liu, M. Zhang, J.B. Phillips, High-Speed Gas Chromatographic Analysis of a Simulated Process Stream using On-Column Thermal Desorption Modulation for Sample Preconcentration and Introduction, J Chromatogr Sci. 28 (1990) 567–571, doi: 10.1093/chromsci/28.11.567.

[28] J.B. Phillips, E.B. Ledford, Thermal modulation: A chemical instrumentation component of potential value in improving portability, Field Anal. Chem. Technol. 1

(1996) 23–29, doi: 10.1002/(SICI)1520-6521(1996)1:1<23::AID-FACT4>3.0.CO;2-F.

[29] J.B. Phillips, R.B. Gaines, J. Blomberg, F.W.M. van der Wielen, J.M.D. Dimandja, V. Green, J. Granger, D. Patterson, L. Racovalis, H.J. de Geus, J. de Boer, P. Haglund, J. Lipsky, V. Sinha, E.B. Ledford Jr., A robust thermal modulator for comprehensive two-dimensional gas chromatography, J. High Resolut. Chromatogr. 22 (1999) 3, doi: 10.1002/(SICI)1521-4168(19990101)22:1<3::AID-JHRC3>3.0.CO;2-U.

[30] J. Beens, H. Boelens, R. Tijssen, Quantitative aspects of comprehensive two-dimensional gas chromatography (GC× GC), J. High Resolut. Chromatogr. 21 (1998) 47, doi: 10.1002/(SICI)1521-4168(19980101)21:1<47::AID-JHRC47>3.0.CO;2-5.

[31] P.J. Marriott, R.M. Kinghorn, Longitudinally Modulated Cryogenic System. A Generally Applicable Approach to Solute Trapping and Mobilization in Gas Chromatography, Anal Chem. 69 (1997) 2582–2588. https://doi.org/10.1021/ac961310w.

[32] P. Haglund, M. Harju, C. Danielsson, P. Marriott, Effects of temperature and flow regulated carbon dioxide cooling in longitudinally modulated cryogenic systems for comprehensive two-dimensional gas chromatography, J. Chromatogr. A 962 (2002) 127, doi: 10.1016/s0021-9673(02)00433-8.

[33] E.B. Ledford, C. Billesbach, Jet-cooled thermal modulator for comprehensive multidimensional gas chromatography, HRC J High Resolut Chromatogr. 23 (2000) 202–204. https://doi.org/10.1002/(SICI)1521-4168(20000301)23:3<202::AID-JHRC202>3.0.CO;2-5.

[34] E.B. Ledford, C. Billesbach, J. Termaat, Pittcon 2002, 17–22 March 2002, New Orleans, LA, USA.

[35] J.V. Seeley, Recent advances in flow-controlled multidimensional gas chromatography, J. Chromatogr. A 1255 (2012) 24, doi: 10.1016/j.chroma.2012.01.027.

[36] P.Q. Tranchida, G. Purcaro, P. Dugo, L. Mondello, G. Purcaro, Modulators for comprehensive two-dimensional gas chromatography, TrAC Trends in Anal. Chem. 30 (2011) 1437–146, doi: 10.1016/j.trac.2011.06.010.

[37] C.A. Bruckner, B.J. Prazen, R.E. Synovec, Comprehensive Two-Dimensional High-Speed Gas Chromatography with Chemometric Analysis, Anal Chem. 70 (1998) 2796–2804, doi: 10.1021/ac980164m.

[38] A.E. Sinha, B.J. Prazen, C.G. Fraga, R.E. Synovec, Valve-based comprehensive two-dimensional gas chromatography with time-of-flight mass spectrometric detection: instrumentation and figures-of-merit, J Chromatogr A. 1019 (2003) 79–87, doi: 10.1016/j.chroma.2003.08.047.

[39] J.V. Seeley, F. Kramp, C.J. Hicks, Comprehensive Two-Dimensional Gas Chromatography via Differential Flow Modulation, Anal Chem. 72 (2000) 4346–4352, doi:10.1021/ac000249z.

[40] J.V. Seeley, F.J. Kramp, K.S. Sharpe, A dual-secondary column comprehensive two-dimensional gas chromatograph for the analysis of volatile organic compound mixtures, J. Sep. Sci. 24 (2001) 444, doi: 10.1002/1615-9314(20010601)24:6<444::AID-JSSC444>3.0.CO;2-5.

[41] J.V. Seeley, F.J. Kramp, K.S. Sharpe, Characterization of gaseous mixtures of organic compounds with dual-secondary column comprehensive two-dimensional gas chromatography (GC× 2 GC), J. Sep. Sci. 25 (2002) 53–59, doi: 10.1002/1615-9314(20020101)25:1/2<53::AID-JSSC53>3.0.CO;2-V.

[42] J.V. Seeley, Nicole J. Micyus, James D. McCurry, Stacy K. Seeley, Comprehensive two-dimensional gas chromatography with a simple fluidic modulator, Am. Lab. 38 (2006) 24–26.

[43] P.Q. Tranchida, G. Purcaro, A. Visco, L. Conte, P. Dugo, P. Dawes, L. Mondello, A flexible loop-type flow modulator for comprehensive two-dimensional gas chromatography, J Chromatogr A. 1218 (2011) 3140–3145, doi: 10.1016/j.chroma.2010.11.082.

[44] T.J. Trinklein, D. v. Gough, C.G. Warren, G.S. Ochoa, R.E. Synovec, Dynamic pressure gradient modulation for comprehensive two-dimensional gas chromatography, J Chromatogr A. 1609 (2020) 460488, doi: 10.1016/j.chroma.2019.460488.

[45] J.V. Seeley, N.E. Schimmel, S.K. Seeley, The multi-mode modulator: a versatile fluidic device for two-dimensional gas chromatography, J. Chromatogr. A 1536 (2018) 6, doi: 10.1016/j.chroma.2017.06.030.

[46] M. Adahchour, J. Beens, R.J.J. Vreuls, U.A.Th. Brinkman, Recent developments in comprehensive two-dimensional gas chromatography (GC×GC), TrAC Trends in Anal. Chem. 25 (2006) 438–454, doi:ttps:10.1016/j.trac.2006.03.002.

[47] K.H. Einführung, in: Massenspektrometrie, Weinheim, Verlag Chemie (1968).

[48] G.S. Frysinger, R.B. Gaines, Comprehensive two-dimensional gas chromatography with mass spectrometric detection (GC x GC/MS) applied to the analysis of petroleum, HRC J High Resolut Chromatogr. 22 (1999) 251–255, doi: 10.1002/(SICI)1521-4168(19990501)22:5<251::AID- JHRC251>3.0.CO;2-V .

[49] M. Adahchour, J. Beens, R.J.J. Vreuls, U.A.Th. Brinkman, Recent developments in comprehensive two-dimensional gas chromatography (GC × GC): II. Modulation and detection, TrAC Trends Anal. Chem. 25 (2006) 540-553, doi: 10.1016/j.trac.2006.04.004.

[50] M. Adahchour, J. Beens, U.A.Th. Brinkman, Recent developments in the application of comprehensive two-dimensional gas chromatography, J. Chromatogr. A 1186 (2008) 67-108, doi: 10.1016/j.chroma.2008.01.002.

[51] P.Q. Tranchida, F.A. Franchina, P. Dugo, L. Mondello, Comprehensive two-dimensional gas chromatography-mass spectrometry: Recent evolution and current trends, Mass Spectrom. Rev. 35 (2016) 524-534, doi: 10.1002/mas.21443.

[52] F. W. McLafferty, F. Tureček in: Interpretation of Mass Spectra. University Science Books, Mill Valley, (1993).

[53] W. Paul, H. Steinwedel, Notizen: Ein neues Massenspektrometer ohne Magnetfeld, Zeitschrift Für Naturforschung A. 8 (1953) 448–450, doi: 10.1515/zna-1953-0710.

[54] P.E. Miller, M.B. Denton, The quadrupole mass filter: Basic operating concepts, J Chem Educ. 63 (1986) 617, doi: 10.1021/ed063p617.

[55] D.W. McLachlan in: Theory and Applications of Mathieu Functions. Oxford, Clarendon Press (1947).

[56] W.E. Stephens, B. Serin, W.E. Meyerhof, A Method for Measuring Effective Contact e.m.f. between a metal and a semi-conductor. Phys. Rev. 69(1946), 42–43. doi:10.1103/physrev.69.42.2.

[57] W.C. Wiley, I.H. McLaren, Time-of-flight mass spectrometer with improved resolution, Rev. Sci. Instrum. 26 (1955) 1150-1157, doi: 10.1063/1.1715212.

[58] B.A. Mamyrin, Laser assisted reflectron time-of-flight mass spectrometry, Int. J. Mass Spectrom. Ion Proc. 131 (1994) 1-19, doi:10.1016/0168-1176(93)03891-O.

[59] E. de Hoffmann, V. Stroobant, in: Mass Spectrometry – Principles and Applications, John Wiley & Sons, Chichester, (2007).

Chapter 4
Evaluation of the fatty acid content in blood samples and dietary supplements by using a fully-automated robotic station and gas chromatography with mass spectrometry*

The present investigation is based on the optimization of an automatized sample preparation and fast gas chromatography–mass spectrometry (GC-MS) method for the analysis of fatty acid methyl esters (FAMEs) in blood samples and dietary supplements. The mass spectrometer was operated in the scan/selected ion monitoring (SIM) acquisition method, thus enabling the obtainment of qualitative and (highly sensitive) quantitative data. The separation of FAMEs was obtained in about 11 min by using a micro-bore column of dimensions 15 m × 0.10 mm ID × 0.10 μm d_f with a polyethylene glycol stationary phase. The novelty of the research involves reducing analysis time by using the novel fast GC–MS method with increased identification reliability and sensitivity in a single chromatographic run. About the figures of merit, linearity, accuracy, and limits of detection (LoD) and quantification (LoQ) were determined. Specifically, regression coefficients were between 0.9901 and 0.9996; the LoDs ranged from 0.05 to 1.02 μg g^{-1} for the blood analysis method, and from 0.05 to 0.26 mg g^{-1} in the case of the dietary supplement approach. With respect to LoQs, the values were in the ranges of 0.15–3.39 μg g^{-1} and 0.15–0.86 mg g^{-1} for blood and dietary supplements analysis methods, respectively. Accuracy was evaluated by analyzing certified reference materials (human plasma, fish oil).

4.1 Introduction

Several studies have demonstrated the importance of a correct balance of fatty acids (FAs) in the human organism [1–5]. The monitoring of FAs enables the establishment of possible FA dysregulation phenomena and, therefore, to intervene by using individual personalized treatments to restore a correct FA equilibrium. In this regard, long-chain $\omega 3$ polyunsaturated fatty acids (PUFAs) such as eicosapentaenoic acid (EPA, C20:5ω3) and docosahexaenoic acid (DHA, C22:6ω3) have shown to exhibit beneficial anti-inflammatory effects in multiple inflammatory diseases [6, 7]. Also, they contribute to maintain low levels of blood triglycerides and cholesterol esters [4, 8, 9]. The biological activity of FAs is dictated by the double bond location along the carbon chain; the importance of the $\omega 3$ family can be ascribed not only to EPA and DHA, but also to other PUFAs such as α-linolenic acid (ALA, C18:3ω3) particularly abundant in plant oils, stearidonic acid (SA, C18:4ω3), and docosapentaenoic acid (DPA, C22:5ω3). In relation to the emphasized health benefits of $\omega 3$ FAs, there has been a large increase in the retail market of fortified foods, as well as a variety of dietary supplements containing mainly EPA and DHA [9]. The total recommended daily intake of EPA and DHA is age-dependent: 1.5 g in the range 1–8 years old, 2.0 g in the range 9–13 years old, 2.5 g in the range 14–18 years old, and up to 3.0 g for adults [10]. Generally, an increase of the $\omega 3$ dietary intake corresponds to a proportional increase of the $\omega 3$ levels in human blood cells and this behavior typically determines a reduction of $\omega 6$ FAs, especially linoleic acid (LA, C18:2ω6) and arachidonic acid (AA, C20:4ω6). As reported in literature [11, 12], the incorporation of $\omega 3$ FAs into human immune cells reaches its peak within 4 weeks post initiation of dietary intake, and therefore, the lipid content of the cells is strongly influenced by the diet. However, despite the large consumption and consolidated beneficial effects of dietary supplements and fortified foods, several research studies have revealed that their labeling may not reflect the real $\omega 3$ FA content [13].

Lipid content can be evaluated by using different separative techniques such as high-performance liquid chromatography (HPLC) and gas chromatography (GC) coupled to mass spectrometry (MS), or shotgun approaches. Total lipid composition, in term of FAs, is commonly investigated by using GC techniques. In order to make the FAs

contained in lipids amenable to a GC separation, a derivatization procedure, following lipid extraction, is necessary [14]. Usually, methylation protocols are employed, leading to the formation of FA methyl esters (FAMEs). A series of derivatizing agents have been described in the literature for total blood FAME analysis [15–18]. In a previous study, it was demonstrated that a dual-stage direct derivatization procedure was suitable for the FA profiling of biological fluids such as whole blood, serum and plasma, collected on a dried blood spot (DBS) collection paper card [14]. The FAME GC separation was performed on a conventional 30 m column, with MS used for identification; quantification was carried out on another GC instrument, equipped with a flame ionization detector (FID). Even though the developed methodologies proved to be suitable for the investigation of FAs in biological samples, the entire analytical workflow resulted too slow in relation to the potentially high number of samples investigated in clinical laboratories. In direct relation with that research, the aim of the present work was the significant reduction of the analysis time and, hence, an enhanced sample throughput by the optimization of a fast GC–MS method operating in scan/ selected ion monitoring (SIM) acquisition mode for the elucidation of FAs in blood samples. Such an approach allowed the identification of the FA compounds using the mass spectra (scan acquisition) and the quantification of target compounds monitoring only specific fragment ions (SIM acquisition). The rapid separation of FAMEs (about 11 min) was performed on a 15 m polyethylene glycol micro-bore column, with a speed-gain factor of 6 with respect to the previous method. The novelty of the research involves reducing analysis time by using the novel fast GC–MS method with increased identification reliability and sensitivity in a single chromatographic run. The same analytical workflow was also used to verify the FA content in dietary supplements. Various figures of merit such as linearity, limits of detection (LoD) and quantification (LoQ), and accuracy were evaluated. The present research is focused on the development of an integrated bioanalytical platform for the identification and quantification of biomarkers, within the field of precision medicine. Within such a context, lipid analysis plays a fundamental role in providing information on the metabolic status of individuals.

4.2 Experimental

Standard and chemicals

The accuracy of the developed methodologies was deter- mined by using NIST certified reference materials (CRMs). In detail, NIST-1950 "*Metabolites in human plasma*" and *NIST-3275 "Omega-3 and Omega-6 Fatty Acids in Fish Oil*" (Part 3275–1, Part 3275–2, and Part 3275–3) were purchased from Merck Life Science (Darmstadt, Germany). All solvents, reagents, and standard materials were acquired from Merck Life Science. "Supelco 37 *Component* FAME Mix" standard, methyl miristate (C14:0, $\geq$ 99%), methyl palmitate (Me. C16:0, $\geq$ 99.0%), methyl stearate (Me. C18:0, 99.0%), methyl oleate (Me. C18:1ω9, 99.0%), methyl arachidonate (Me. C20:4ω6, $\geq$ 99.0%), methyl all-cis-5,8,11,14,17- eicosapentaenoate (Me. C20:5ω3, $\geq$ 98.5%), and all-cis- 4,7,10,13,16,19-methyl 4,7,10,13,16,19-docosahexaenoate (Me. C22:6ω3, $\geq$ 98.5%) were used for calibration curve construction. Isotope-labeled stearic acid-d35 (C18:0$_{d35}$ $\geq$ 98.0%) was used as internal standard (IS). For the derivatization procedure, boron trifluoride (BF_3) methanol solution (14%) and sodium methoxide (CH_3ONa, 0.5% w/v) were used. In order to extract the FAMEs, n-heptane (for HPLC $\geq$ 99%) was used. *903 Whatman Protein saver card* (Merck Life Science) was used as sampling support for blood drop collection. In our study, we used dried blood spot samples from nine informed donors, collecting a few drops of blood drawn by lancet from the finger of the donor. Blood samples were obtained from nine individuals (men and women) in an adult age range (30 to 60 years). Regarding dietary supplements, 11 samples were purchased from a local drugstore (Messina, Italy). Ten of the analyzed products declared on their labels fish oil origin (*i.e.*, anchovy, mackerel, sardine, tuna). One sample was marked as vegetable oil supplement. Dietary supplements were purchased in softgel ($n = 3$), capsule ($n = 6$), and liquid ($n = 2$) formulations.

Sample preparation for blood analysis

A certified analytical balance (AX204 Mettler Toledo, Milano, Italy; d = 0.1 mg) was used to prepare the standard solutions. Specifically, 10 mg of IS (C18:0$_{d35}$) was weighed and transferred into a 10 mL volumetric flask. *n*-heptane was utilized for the solubilization of the standard compound. 25 microliters of IS solution (1000 mg L^{-1})

was spotted on a DBS card containing 50 mg of blood. Dual-stage derivatization was carried out by adding 500 μL of CH_3ONa in methanol (0.5% w/v); the reaction mixture was heated for 15 min at 95 °C. After, 500 μL of BF_3 methanolic solution was added to the reaction mixture which was again heated for 15 min at 95 °C. Finally, 350 μL of *n*-heptane and 300 μL of NaCl aqueous solution were added to the reaction mixture; the sample was vortexed at 2000 rpm for 100 s. After gravitational separation (standby time 2 min), the upper heptanic layer containing the FAMEs was injected into the GC–MS instrumentation [14].

Calibration, quantification, and accuracy (blood analysis)

FAME quantification was performed by using the IS method. The "Supelco 37 Component FAME Mix" was used for the construction of calibration curves. For components not present in the "Supelco-37" standard mixture, the calibration curve of the chemically more similar compound was used. Calibration curves were constructed considering the absolute amount (μg) of each FAME reported in the certificate of analysis of CRM Supelco-37 divided by the quantity of blood (0.05 g). Twelve working mixtures at different concentration levels (five replicates were carried out at each level) were prepared by serial dilutions. Concentration levels ranged from a maximum value of 1800 μg g^{-1} for C16:0 FAME to a minimum value of 0.2 μg g^{-1} for C15:0 FAME. All calibration mixtures were spiked with a fixed volume (25 μL) of deuterated IS solution (1000 mg L^{-1}). Each working mixture was derivatized following the procedure above described. The LoD and LoQ were determined at the lowest concentration level, by performing 10 replicates and through the following equations:

$$LoD = 3 \times s'_o \qquad\qquad LoQ = 10 \times s'_o$$

where s'_o represents the ratio of the standard deviation of the replicate measurements and the square root of the number of measurements. The accuracy of the developed method was evaluated by analyzing the NIST-1950 "Metabolites in human plasma" and comparing the experimental results with certified (approximately 95% confidence) and reference (non-certified value that is the best estimate of the true value) values [19].

Sample preparation for dietary supplement analysis

For the quantification of FAs in dietary supplements, 100 mg of IS was weighed directly in a 10-mL volumetric flask and solubilized in *n*-heptane. Lipid derivatization was carried out as follows: 10 mg of dietary supplement was spiked with 50 μL of deuterated IS solution (C18:0$_{d35}$, 10,000 mg L^{-1}); 500 μL of CH$_3$ONa methanolic solution (0.5% w/v) and 500 μL of BF$_3$ in methanol (14%) were utilized as derivatizing agents. Both derivatization stages were carried out by heating the mixture at 95 °C for 15 min as above described. In order to extract the FAME derivatives, 500 μL of *n*-heptane was added to the mixture. Finally, 100 μL of NaCl aqueous solution was added to the mixture for phase separation; the mixture was vortexed at 2000 rpm for 100 s and left to stratify for 2 min. The *n*-heptane layer containing FAMEs was ready for fast GC–MS analysis.

Calibration, quantification, and accuracy (dietary supplement analysis)

Linearity of the method was evaluated by the construction of calibration curves. For the most abundant FAs in the dietary supplements, FAME standard solutions were prepared as follows: 100 mg of Me. C14:0, Me. C16:0, Me. C18:0, Me. C18:1ω9, Me. C20:4ω6, Me. C20:5ω3, and Me. C22:6ω3 was weighed using an analytical balance and diluted in a volumetric flask, by using 10 mL of *n*-heptane. For FAs at a lower concentration level, the Supelco 37 standard mixture was used. All working mixtures were spiked with a fixed volume (50 μL) of deuterated IS solution. LoD and LoQ parameters were determined as previously described for blood analysis. The accuracy of the analytical method (expressed in terms of recovery) was evaluated by analyzing the NIST-3275 "*Omega-3 and Omega-6 fatty acids in fish oil*" sample [20].

Automatic workstation for lipid derivatization

All the procedures so far described were performed using an AOC-6000 workstation (Shimadzu, Duisburg, Germany). In this respect, the preparation of calibration mixtures at different concentration levels, dual-stage derivatization procedure, and injection of the FAME layer were fully automated. The robotic platform used in this research work was equipped with an automatic tool exchange arm and two park

stations containing a total of 6 syringes for the adding of the IS solution (100 μL syringe), derivatizing agents (500 μL syringe), extraction solvent (500 μL syringe), and sample injection (10 μL syringe). In addition, the robotic preparative station was equipped with a vortex mixer and an oven. The AOC- 6000 parameter settings were managed by the GCMS Solution software (version 4.50, Shimadzu). All samples, including the working mixtures, were prepared in triplicate.

Instrumentation

The GC–MS analyses were performed on a system consisting of a GC-2030 NEXIS (Shimadzu) gas chromatograph coupled to a triple quadrupole mass spectrometer (TQ8050 NX, Shimadzu). The instrument was equipped with a split/ splitless injector (280 °C) and an AOC-6000 multifunctional autosampler preparative station. The separation of the analytes was performed on a Supelcowax-10 (100% polyethylene glycol phase) 15 m × 0.10 mm ID × 0.10 μm d_f (Merck Life Science) capillary column. Temperature program: from 70 to 280 °C (0.5 min) at 20 °C min^{-1}. Helium was utilized as carrier gas at a constant linear velocity of 50 cm s^{-1} (initial pressure: 591.5 kPa). Injection volumes and split ratios were as follows: 0.5 μL split 1:10 for DBS samples and 0.2 μL split 1:800 for dietary supplements.

The triple quadrupole MS system was operated in the simultaneous scan/SIM mode (loop time 100 ms, dwell time 33 ms). Scan acquisition was performed monitoring all fragment ions within a mass range of 45–550 *m/z* (acquisition frequency: 10 Hz). On the other hand, SIM acquisition was carried out by selecting three diagnostic fragment ions for each FAME. The most intense ion (quantifier ion) was used for quantification, while the other two ions were utilized to confirm compound identity (qualifier ions). Interface and MS source temperatures were 250 °C and 220 °C, respectively. A dedicated mass spectra database, namely LIPIDS GC–MS Library (version 1.0, Shimadzu), was utilized for the scan spectral similarity process. In the case of undistinguishable mass spectra such as isomer compounds (configurational or positional isomers), peak assignment was achieved through the injection of pure analytical standards.

4.3 Results and discussion

Fast GC–MS analysis for blood FA elucidation

As aforementioned, an automated sample preparation procedure was applied to the analysis of DBS samples. The time required for the preparation of a single sample was about 35 min. In previous research [14], the FAME GC run time, using a narrow-bore column (30 m × 0.25 mm ID × 0.20 μm d_f) is about 60 min; however, sample preparation can occur simultaneously with the GC run, thus "eliminating" the time of sample preparation in the case of multiple analyses. With the scope of reducing the analysis time, a scan/ SIM fast GC–MS method based on the use of a micro-bore column (15 m × 0.10 mm ID × 0.10 μm d_f), an accelerated temperature program, and a rather high gas linear velocity was developed. The relationship between gas linear velocity and column efficiency was defined through the construction of a Golay curve, reported in Figure 4.1, by analyzing myristoleic acid (C14:1ω5) at a temperature of 160 °C, and at gas linear velocities within the range of 20–60 cm s^{-1} (at intervals of 5 cm s^{-1}). The minimum height equivalent to a theoretical plate (HETP min = 0.108 mm) was obtained at a carrier gas velocity of 35 cm s^{-1}, providing a column efficiency of approx. 140,500 theoretical plates (N). In the present study a gas linear velocity of 50 cm s^{-1} was used, providing about 70% of the maximum column efficiency (approx. 98,000 N) and ensuring the sufficient separation of the target compounds. A temperature gradient of 20 °C min^{-1}, equivalent to 10 °C/void time [21], was applied.
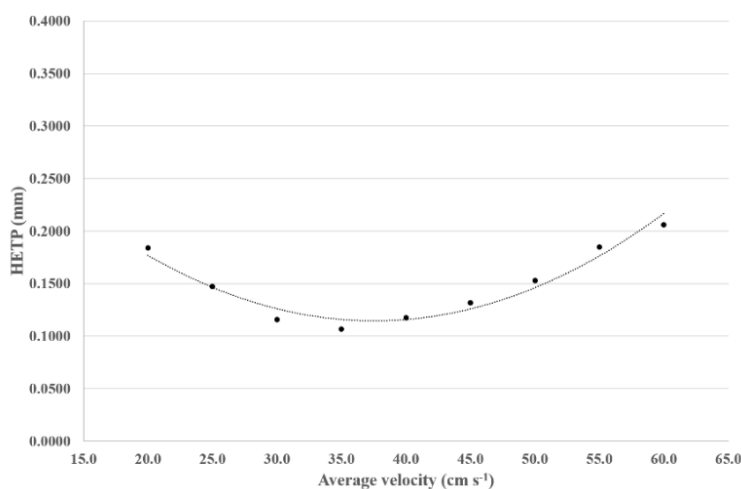
Figure 4.1. *Golay curve constructed by analyzing C14:1ω5 FAME on a 15 m × 0.10 mm ID × 0.10 μm d_f column at 160°C.*

The fast GC–MS chromatogram of the certified human plasma sample is shown in Fig. 4.2: the chromatography separation, achieved in about 11 min, can be considered as satisfactory. The average peak base width was about 2 s; the acquisition frequencies (10 Hz for the scan mode and 20 Hz for the SIM mode) of the developed method were more than sufficient for the scopes of identification and quantification, considering that at least 10 data points per peak are required for an adequate peak reconstruction [22].
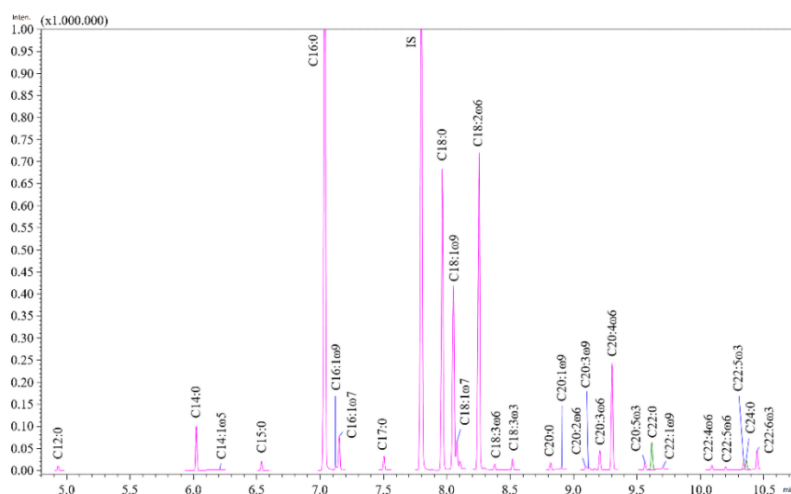
Figure 4.2. *Fast SIM GC–MS chromatogram of FAMEs relative to a certified human plasma sample. Peak signal was obtained monitoring quantifier (Q) ions.*

The scan/SIM method obviously enabled the attainment of both full spectral information and highly sensitive specific ion responses. In the case of trace-amount FAMEs, characterized by low signal-to-noise ratios and poor-quality full spectra (in any case, only mass spectral similarities $\geq 85\%$ were considered), the SIM data can be helpful also for the purpose of peak assignment. Such a factor is of utility using a micro-bore column because of the reduced sample capacity [23]. With respect to method figures of merit, the range of calibration and coefficients of determination (R^2), reported in Table 4.1, were derived for each FAME, contained in the human plasma sample. All calibration curves were characterized by satisfactory linearity with R^2 values ranging from 0.9901 for C18:2ω6 to 0.9993 for C14:1ω5. The LoDs and LoQs (Table 4.1) showed lower values for saturated fatty acids (SFAs), such as C16:0 (LoD: 0.05 µg g^{-1}, LoQ: 0.15 µg g^{-1}). Higher LoDs and LoQs were observed for monosaturated fatty acids (MUFAs) and PUFAs. In general, the LoDs ranged from 0.05 to 1.02 µg g^{-1}, while the LoQs ranged from 0.15 to 3.39 µg g^{-1}.

Table 4.1. *List of FAMEs detected in the NIST-1950 certified human plasma sample, quantifier (Q) and qualifier (q1 and q2) ions, and coefficient of determination (R^2). Calibration range, LoD, and LoQ values are expressed in µg g^{-1}.*

FAME	Q	q1	q2	R^2	Linearity range	LoD	LoQ
Lauric acid (C12:0)	74	87	55	0.9983	40 - 0.4	0.12	0.41
Myristic acid (C14:0)	74	87	55	0.9952	80 - 0.8	0.08	0.28
Myristoleic acid (C14:1ω5)	55	74	69	0.9993	40 - 2	0.42	1.40
Pentadecanoic acid (C15:0)	74	87	55	0.9975	20 - 0.2	0.08	0.26
Palmitic acid (C16:0)	74	87	55	0.9929	1800 - 300	0.05	0.15
Palmitoleinic acid (C16:1ω9)	55	69	74	0.9951	40 - 2	0.65	2.17
Palmitoleic acid (C16:1ω7)	55	69	74	0.9965	200 - 10	0.65	2.17
Heptadecanoic acid (C17:0)	74	87	55	0.9983	20 - 0.4	0.13	0.44
Stearic acid (C18:0)	74	87	55	0.9970	600 - 40	0.05	0.16
Oleic acid (C18:1ω9)	55	69	83	0.9979	900 - 60	0.12	0.40
cis-Vaccenic acid (C18:1ω7)	55	69	83	0.9922	120 - 1	0.12	0.40
Linoleic acid (C18:2ω6)	67	81	95	0.9901	1200 - 200	0.80	2.66
γ-Linolenic acid (C18:3ω6)	79	67	80	0.9972	40 – 2	0.86	2.87
α-Linolenic acid (C18:3ω3)	79	67	93	0.9953	40 - 2	0.63	2.11
Arachidic acid (C20:0)	74	87	55	0.9974	40 - 0.4	0.10	0.35
Gondoic acid (C20:1ω9)	55	69	97	0.9947	40 - 2	0.63	2.10
homo-γ-Linolenic acid (C20:2ω6)	67	81	95	0.9958	40 - 2	0.70	2.35
Mead acid (C20:3ω9)	79	67	80	0.9973	40 - 2	0.62	2.07
dihomo-γ-Linolenic acid (C20:3ω6)	79	67	80	0.9960	300 - 20	0.62	2.07
Arachidonic acid (C20:4ω6)	79	91	80	0.9985	400 - 40	0.72	2.38
Eicosapentaenoic acid (C20:5ω3)	79	91	67	0.9931	40 - 2	1.02	3.39
Behenic acid (C22:0)	74	87	55	0.9979	80 - 2	0.44	1.46
Erucic acid (C22:1ω9)	55	69	83	0.9972	40 - 2	0.56	1.87
Adrenic acid (C22:4ω6)	79	91	67	0.9970	100 - 2	0.59	1.97
Docosapentaenoic acid (C22:5ω6)	79	91	67	0.9970	100 - 2	0.59	1.97
Docosapentaenoic acid (C22:5ω3)	79	91	67	0.9970	100 - 2	0.59	1.97
Lignoceric acid (C24:0)	74	87	55	0.9979	40 - 0.8	0.44	1.45
Docosahexaenoic acid (C22:6ω3)	79	91	67	0.9970	100 - 2	0.59	1.97

The accuracy results expressed in terms of recovery percentage (%) are summarized in Table 4.2. Except for C17:0 and C18:3ω6, all FAME derivatives ranged from a minimum value of recovery of 76.6% (C20:0) to a maximum value of 119.7% (C22:5ω3). Additionally, the recovery values of C17:0 (128.9%) and C18:3ω6

(141.0%) were too high to be considered acceptable. With respect to C18:3ω6, Benner et al. reported concentration levels like those obtained in the present research [24, 25]. However, concentration value for C17:0 was not reported; thus, a comparison with other analytical studies was not possible. Finally, a blank automated sample was subjected to derivatization and fast GC–MS analysis. As reported in a previous manuscript [14], the analysis revealed the presence of low levels of C14:0, C16:0, C16:1ω9, C18:0, C18:1ω9, and C18:2ω6 that did not affect the recovery values.

Table 4.2. *Accuracy assessment expressed in terms of recovery percentage (%).*
Certified, reference, and undeclared values are expressed in µg g^{-1}.

FAME	Experimental	NIST	Recovery %
Certified Values			
C12:0	1.67 ± 0.2	1.86 ± 0.11	89.5
C16:0	589.59 ± 29.0	594 ± 19	99.3
C16:1ω7	60.93 ± 4.8	53.5 ± 6.4	113.9
C18:0	197.38 ± 13.5	179 ± 12	110.3
C18:1ω9	495.17 ± 22.8	447 ± 43	110.8
C18:2ω6	774.25 ± 28.2	780 ± 39	99.3
C18:3ω3	17.23 ± 1.2	14.9 ± 1	115.6
C22:0	16.95 ± 1.5	15.9 ± 1.5	106.6
Reference Values			
C14:0	18.33 ± 1.5	17.9 ± 3.8	102.4
C14:1ω5	1.27 ± 0.3	1.57 ± 0.03	81.0
C15:0	1.02 ± 0.5	1.08 ± 0.01	94.4
C17:0	6.06 ± 0.5	4.7 ± 0.2	128.9
C18:1ω7	36.96 ± 1.4	37.70 ± 0.90	98.0
C18:3ω6	15.36 ± 0.8	10.9 ± 2.3	141.0
C20:0	4.22 ± 0.6	5.5 ± 0.2	76.6
C20:1ω9	3.92 ± 0.2	3.5 ± 0.1	111.9
C20:2ω6	5.90 ± 0.9	5.7 ± 0.2	103.5
C20:3ω6	47.88 ± 3.3	41.80±1.1	114.5
C20:4ω6	312.29 ± 17.7	293 ± 54	106.6
C20:5ω3	12.17 ± 1.2	11.4 ± 0.1	106.8
C22:1ω9	1.28 ± 0.1	1.10 ± 0.40	116.1
C22:4ω6	6.79 ± 1.7	8.3 ± 0.2	81.9
C22:5ω6	5.79 ± 1.1	6.3 ± 0.1	91.9
C22:5ω3	14.96 ± 0.4	12.5 ± 0.2	119.7
C24:0	13.36 ± 0.5	16.8 ± 0.9	79.5
C22:6ω3	41.78 ± 3.5	37.9 ± 6.8	110.2
Undeclared Values			
C16:1ω9	7.42 ± 0.1	-	-
C20:3ω9	9.36 ± 1.3	-	-

Impact of dietary supplements on blood FA composition

A series of health benefits are ascribed to the consumption of ω3 FAs, in relation to the heart and blood circulation [10]. Consequently, one of the objectives of the present research was to use the fast GC–MS method to investigate the effects of ω3 FA dietary supplements on the FA blood composition of patients, after short and long periods of consumption. Within such a context, DBS samples from volunteer patients, who declared to consume ω3 FA dietary supplements, were analyzed. In detail, three different patient groups were subjected to attention: no intake and 1 month and 4 months of ω3 FA intake. The FA profile of the 9 analyzed samples, expressed in terms of relative percentage (%), FA families (SFA, MUFA, PUFA, ω6, and ω3), and specific FA ratios, are illustrated in Table 4.3. Such percentage values were extrapolated by considering the absolute quantitative values expressed in $\mu g\ g^{-1}$ obtained using the IS method. As expected, relevant differences between the three patient groups were observed. In fact, ω3 FA levels were much higher after 1 and 4 months of supplementation, ranging from 5.71 to 9.28% with an average value of 6.51 ± 1.37%. In the case of the no-intake patient group, the content of ω3 FAs was significantly lower (2.77–3.67%), registering an average value of 3.12 ± 0.48%. As reported by Calder, the incorporation of ω3 FAs in human blood cells was evident after 1 month of dietary intake [11]. On the other hand, the ω3 FA levels in no-intake patients were not in compliance with the cardioprotective target levels suggested by W.S. Harris in 2007 [4]. It is worth mentioning that the ω3 FA intake also influenced the ω6/ω3 ratio: the presence of values higher than the optimal range indicates a proinflammatory condition [26]. With respect to optimal ranges, all patients with personalized treatments revealed ω6/ω3 ratios in accordance with the indicated values (3.50–5.50). Higher ratio values (8.62–9.59) were observed in patients without ω3 FA supplementation. Other considerations can be made on the mead acid (C20:3ω9) contents, which resulted low in patients with personalized treatments. The accumulation of mead acid in the blood indicates an essential fatty acid (EFA) deficiency, and it is utilized as an indicator of PUFA deficiency [27]. Under normal conditions, the enzymatic processes of desaturation and elongation convert linoleic and α-linolenic acids to other long-chain FAs. In the case of EFA deficiency, the desaturase and elongase enzymes act on oleic acid resulting in the production of

another ω9 FA, such as mead acid. Based on such a consideration, the intake of ω3 FA dietary supplements allowed the increase of EFA levels in blood. Finally, the C20:4ω6/ C20:5ω3 ratio, indicated by Barry Sears as a gold standard test for monitoring eicosanoid levels [28], undergoes a relevant improvement in patients assuming ω3 FA dietary supplements, especially after 4 months of dietary intake. In fact, their C20:4ω6/C20:5ω3 ratios indicated that eicosanoid levels were in balance and, consequently, the patients were in the Omega Rx Zone of Wellness.

Table 4.3. *FAME levels in patients characterized by no intake and 1 month and 4 months of ω3 FA dietary supplement intake.*

FAME	No intake			1 month intake			4 months intake		
	DBS 1	DBS 2	DBS 3	DBS 4	DBS 5	DBS 6	DBS 7	DBS 8	DBS 9
C12:0	0.09	0.11	0.09	0.07	0.10	0.10	0.08	0.10	0.08
C14:0	0.46	0.86	0.29	0.23	0.30	0.37	0.23	0.31	0.29
C14:1ω5	0.09	0.14	0.10	0.12	0.12	0.13	0.10	0.12	0.09
C15:0	0.15	0.21	0.17	0.07	0.11	0.15	0.17	0.11	0.14
C16:0	24.63	24.27	26.61	24.05	23.70	25.61	26.01	25.21	22.69
C16:1ω9	0.76	0.82	0.83	0.37	0.57	0.51	0.64	0.46	0.51
C16:1ω7	0.84	2.03	0.95	1.20	0.81	0.54	0.66	1.03	0.86
C17:0	0.29	0.34	0.34	0.21	0.32	0.37	0.40	0.36	0.30
C18:0	13.40	10.92	10.53	12.15	15.08	13.49	12.33	13.22	10.79
C18:1ω9	21.95	27.77	26.90	24.05	24.45	21.15	27.12	23.78	22.86
C18:1ω7	0.97	1.21	2.76	2.63	2.28	2.04	2.08	1.82	2.21
C18:2ω6	21.85	18.37	19.72	19.01	16.35	19.21	17.40	19.40	20.17
C18:3ω6	0.19	0.39	0.22	0.20	0.08	0.15	0.16	0.20	0.21
C18:3ω3	0.19	0.27	0.16	0.17	0.21	0.21	0.14	0.13	0.21
C20:0	0.09	0.07	0.13	0.09	0.17	0.10	0.14	0.15	0.10
C20:1ω9	0.19	0.31	0.37	0.18	0.23	0.21	0.24	0.28	0.21
C20:2ω6	0.21	0.11	0.21	0.07	0.14	0.10	0.10	0.12	0.12
C20:3ω9	0.12	0.19	0.07	0.06	0.09	0.07	0.05	0.07	0.05
C20:3ω6	1.38	1.68	1.00	0.52	0.61	0.68	0.48	0.51	0.62
C20:4ω6	7.10	5.95	4.69	7.65	6.62	7.43	4.56	4.68	7.19
C20:5ω3	0.32	0.29	0.35	0.63	1.43	1.19	1.23	1.37	2.60
C22:0	0.26	0.23	0.22	0.33	0.39	0.35	0.32	0.53	0.34

C22:1ω9	0.19	0.20	0.15	0.16	0.21	0.19	0.17	0.17	0.15
C22:4ω6	0.52	0.37	0.37	0.35	0.34	0.42	0.29	0.53	0.24
C22:5ω6	0.40	0.36	0.36	0.32	0.33	0.39	0.32	0.45	0.22
C22:5ω3	1.48	1.11	0.99	1.74	1.86	1.78	2.34	2.15	2.82
C24:0	0.18	0.16	0.14	0.19	0.31	0.30	0.15	0.37	0.27
C22:6ω3	1.67	1.26	1.27	3.17	2.80	2.77	2.08	2.38	3.65
SFAs 36.52-41.90 [16]	39.55	37.16	38.52	37.39	40.48	40.83	39.83	40.36	35.00
MUFAs 24.62-31.22 [16]	25.01	32.48	32.07	28.72	28.67	24.76	31.01	27.65	26.89
PUFAs 29.29-36.45 [16]	35.45	30.36	29.42	33.88	30.85	34.40	29.16	31.99	38.11
ω6 25.73-32.63 [16]	31.66	27.24	26.58	28.12	24.46	28.38	23.32	25.89	28.78
ω3 <4 *undesirable [4]* 4-8 *intermediate [4]* >8 *desirable [4]*	3.67	2.93	2.77	5.71	6.30	5.95	5.79	6.03	9.28
ω6/ω3 3.5-5.5 [26]	8.62	9.29	9.59	4.93	3.88	4.77	4.03	4.30	3.10
C18:0/C18:1ω9 <0.7 *hyperactivity* [26] > 1.3 *hypoacitvity* [26]	0.61	0.39	0.39	0.51	0.62	0.64	0.45	0.56	0.47
C16:0/C16:1ω7 < 45 *hyperactivity* [26] > 132 *hypoacitvity* [26]	29.19	11.98	27.88	20.05	29.16	47.63	39.61	24.52	26.34
C18:2ω6/C20:3ω6	15.87	10.96	19.64	36.34	26.91	28.05	36.21	37.95	32.42
C20:4ω6/C20:3ω6	5.16	3.55	4.67	14.62	10.89	10.85	9.49	9.15	11.56
C20:4ω6/C20:5ω3	21.94	20.54	13.32	12.18	4.62	6.25	3.71	3.42	2.77

Scan/SIM fast GC–MS analysis of dietary supplements

The growing consumption of ω3 FA dietary supplements has acted as a stimulant for various analysts to verify that labeling reflects the real content. For example, Chee *et al.* found that two of the nine analyzed marine oil capsules had EPA and DHA contents lower than 80% of the declared values [29]. Additionally, Srigley et al. evaluated 46 commercially available marine supplements and the contents of EPA and DHA were within ± 20% of their label declarations in more than 80% of the products examined, while the remaining quote did not reflect label declarations [13]. Such studies clearly indicate that FA monitoring of dietary supplements is necessary.

In 1997, the Food and Drug Administration (FDA) agency established safety recommendations on the intake of EPA and DHA. In particular, the total daily intake of EPA plus DHA from conventional food and dietary supplement sources was not to exceed 3 g/day because greater amounts might lengthen bleeding time, increase low-density lipoprotein cholesterol, and adversely affect glycemic control in people with type 2 diabetes [13]. However, such recommendations were reviewed in 2014 by the FDA establishing that the ingestion of less than or equal to 5 g/day of EPA and DHA from dietary supplements did not increase the potential for adverse effects when used according to the product labeling [30]. Such a factor means that the monitoring of the actual content of EPA and DHA in dietary supplements has become more relevant in relation to the FDA suggestions.

In view of the above considerations, it was decided to extend the sample preparation procedure and the scan/SIM fast GC–MS method to dietary supplements. With respect to the sample preparation step, minor modifications were made compared to the DBS samples. In detail, the volume of *n*-heptane was increased to 500 μL to better extract and solubilize the higher amount of FAME derivatives. After, since the maximum volume of the autosampler vial used for the automated derivatization procedure was 2 mL, the saturated NaCl solution volume was reduced to 100 μL. This change did not affect the gravitational separation of the biphasic system (methanol and heptane), probably due to lower complexity of dietary supplements with respect to whole blood. From the GC–MS side and considering the sample-to-sample concentration variability of dietary supplements, two calibration ranges (low and high) were used for some FAs, as reported in Table 4.4. The quantifier and qualifier ions are listed in Table 4.4.

For the more abundant compounds, linearity was evaluated by using pure standard FAMEs. Regarding the less abundant components, calibration curves were constructed by diluting the standard mixture used for blood FA calibration. The lowest concentration level was used to determine LoD and LoQ values (Table 4.4). With respect to the determination of accuracy, certified fish oil samples were utilized. Three SIM fast GC–MS chromatograms are illustrated in Figure 4.3

Table 4.4. *List of FAMEs detected in the NIST-3275 fish oils, quantifier (Q) and qualifier (q1 and q2) ions, and coefficient of determination (R²). Calibration range, LoD, and LoQ values are expressed in mg g⁻¹.*

FAME	Q	q1	q2	R^2	Linearity Range	LoD	LoQ
C12:0	74	87	55	0.9931	20.0 - 0.5	0.06	0.21
C14:0	74	87	55	0.9969	(low) 20.0 - 1.0	0.06	0.19
				0.9961	(high) 350 - 20		
C14:1ω5	55	74	69	0.9932	10.0 - 0.25	0.12	0.42
C15:0	74	87	55	0.9987	10.0 - 0.25	0.04	0.13
C16:0	74	87	55	0.9995	(low) 30.0 - 1.50	0.05	0.18
				0.9976	(high) 310 - 15.5		
C16:1ω7	55	69	74	0.9996	10.0 - 0.50	0.11	0.37
C16:2ω4	67	81	95	0.9997	20.0 - 1.0	0.07	0.22
C17:0	74	87	55	0.9996	10.0 - 0.25	0.05	0.17
C16:3ω4	79	67	93	0.9987	10.0 - 0.25	0.10	0.34
C18:0	74	87	55	0.9996	(low) 20.0 - 1.0	0.05	0.15
				0.9993	(high) 300 - 15.0		
C18:1ω9	55	69	83	0.9999	(low) 30.0 - 1.50	0.12	0.41
				0.9961	(high) 300.0 - 15.0		
C18:1ω7	55	69	83	0.9999	(low) 30.0 - 1.50	0.12	0.41
				0.9961	(high) 300.0 - 15.0		
C18:2ω6	67	81	95	0.9997	20.0 - 1.0	0.07	0.22
C18:3ω6	79	67	80	0.9987	10.0 - 0.25	0.07	0.22
C18:3ω3	79	67	93	0.9990	10.0 - 0.50	0.08	0.28
C18:4ω3	79	67	93	0.9990	10.0 - 0.50	0.08	0.28
C18:4ω1	79	67	93	0.9990	10.0 - 0.50	0.08	0.28
C20:0	74	87	55	0.9975	20.0 - 0.5	0.05	0.17
C20:1ω11	55	69	97	0.9992	10.0 - 0.25	0.10	0.35
C20:1ω9	55	69	97	0.9992	10.0 - 0.25	0.10	0.35

C20:1ω7	55	69	97	0.9992	10.0 - 0.25	0.10	0.35
C20:2ω6	67	81	95	0.9992	10.0 - 0.50	0.13	0.42
C20:3ω6	79	67	80	0.9980	10.0 - 0.50	0.26	0.86
C20:4ω6	79	91	80	0.9969	20.0 - 0.5	0.17	0.56
C20:4ω3	79	91	80	0.9969	20.0 - 0.5	0.17	0.56
C20:5ω3	79	91	67	0.9963	430 - 20	0.25	0.84
C22:0	74	87	55	0.9970	20.0 - 0.5	0.05	0.18
C22:1ω11	55	69	83	0.9943	10.0 - 0.50	0.09	0.30
C22:1n9	55	69	83	0.9943	10.0 - 0.50	0.09	0.30
C22:1ω7	55	69	83	0.9943	10.0 - 0.50	0.09	0.30
C21:5ω3	79	91	67	0.9973 0.9963	(low) 8.5 - 0.40 (high) 430 - 20	0.25	0.84
C22:4ω6	79	91	67	0.9993	10.0 - 0.50	0.16	0.53
C22:5ω6	79	91	67	0.9993	10.0 - 0.50	0.16	0.53
C22:4ω3	79	91	67	0.9993	10.0 - 0.50	0.16	0.53
C22:5ω3	79	91	67	0.9957	430 - 20	0.16	0.53
C24:0	74	87	55	0.9966	20.0 - 0.5	0.06	0.19
C22:6ω3	79	91	67	0.9957	430 - 20	0.16	0.53

The list of detected FAs is reported in Table 4.5, along with the relative experimental and certified values. Palmitic and stearic acids were the most abundant in the SFA family, with recovery values ranging from 81.1 to 102.4% in the three certified fish oils. Regarding the most abundant MUFAs, the recoveries of oleic and *cis*-vaccenic (C18:1ω7) acids were within the range of 80 to 120% (min. 92.9% and max. 108.8%). In the case of palmitoleic acid (C16:1ω7), recovery values were of 103.7%, 102.5%, and 75.5% in part 1, part 2, and part 3, respectively. About ω6 PUFAs, scan/SIM fast GC–MS analyses indicated that the values of linoleic and arachidonic acids were all within the range of mass fraction values covered by the expanded uncertainty, with recoveries ranging from 98.0 to 106.0%. Higher recovery values were obtained for γ-linolenic acid (C18:3ω6) (min. 113.8% and max. 138.4%).
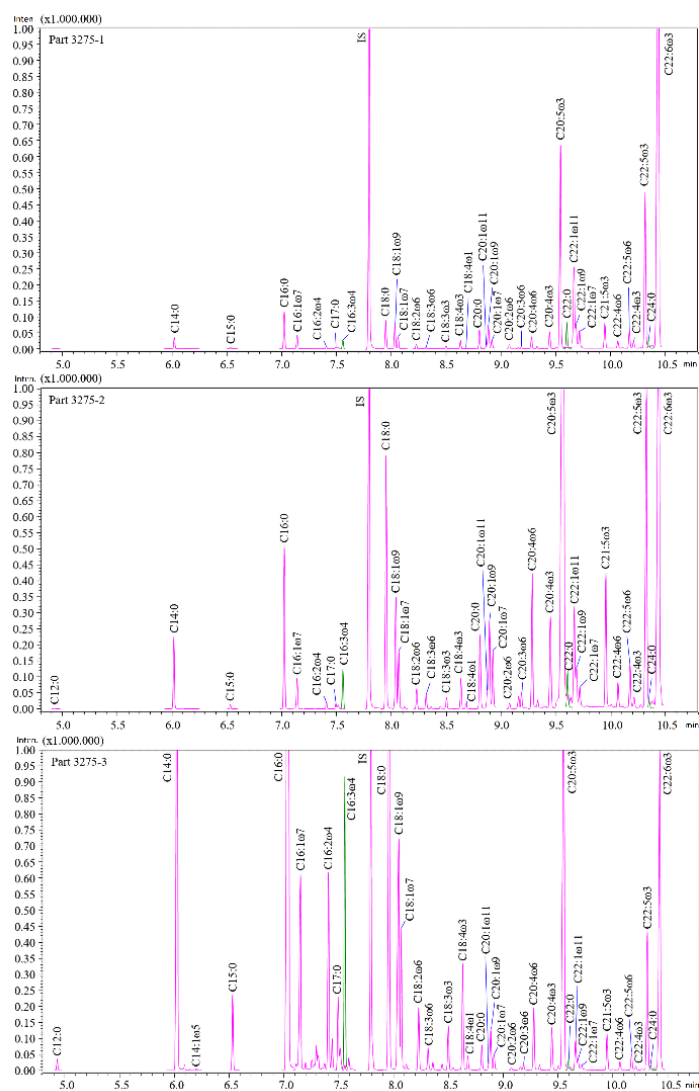
Figure 4.3. *SIM fast GC–MS chromatograms of FAMEs in certified NIST-3275 fish oils. From top to bottom: part 3275-1, part 3275-2, and part 3275-3 samples. Peak signal was obtained monitoring quantifier (Q) ion.*

Finally, the quantification data relative to ω3 FAs, such as EPA and DHA, were consistent with those certified: recovery values ranged from 105.4 to 116.9% and from 87.7 to 115.7%, respectively. In the case of nearly all other FAME derivatives, the entire analytical process showed its suitability for the qualitative and quantitative profiling of FAs in dietary supplements. Even so, there was a clear discrepancy regarding arachidic (C20:0) and gondoic (C20:1ω9) acids. Their recoveries (excessively high) could indicate the presence of interfering compounds, even though the SIM signals excluded this hypothesis confirming the absence of possible

coelutions. Similar results were also obtained by Srigle *et al.* [13]. The developed analytical protocol was utilized to evaluate the FA profile in some commercially available dietary supplements and to verify that the real content of FAs, such as EPA and DHA, met their label declarations (Fig. 4.4). It was found that nine of the analyzed products had an EPA content that was within the 80–120% range of their label declarations (Fig. 4.4). However, the EPA content of two samples was found to be 54% and 40% higher than their labeling. In the case of DHA content, all supplements analyzed in this research study matched the quantities declared on the labels. The obtained results were in accordance with those in published researches, in which more than 80% of ω3 FA dietary supplements had EPA and DHA quantities that were within ± 20% of their values reported on the labels [13, 31]. The monitoring was also extended to the ω3 PUFA family when the concentration was certified. Also, in these cases, the analyses revealed that ω3 FA total contents were in accordance with those declared. In detail, three of the analyzed samples registered a total content of ω3 FAs within ± 10% of their declared values (min. 91%–max. 105%), while other three samples were within ± 20% (min. 86%–max. 111%).
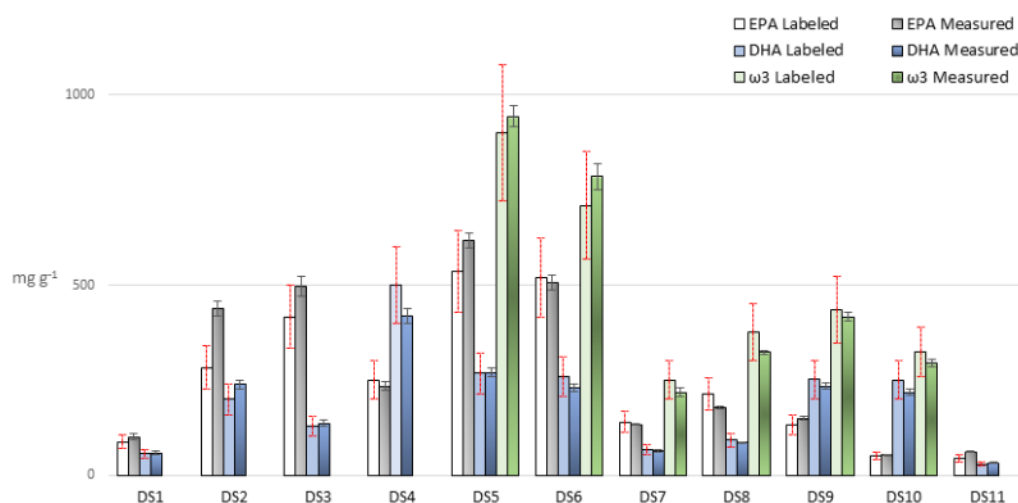
Figure 4.4. *EPA, DHA, and ω3 contents (mg g⁻¹) in analyzed dietary supplements (DS). Measured data are represented as mean ± standard deviation (n = 3). Labeled quantities include an error of ± 20% of the values declared.*

Table 4.5. *Accuracy assessment expressed in terms of recovery percentage (%). Experimental and NIST values are expressed in mg g^{-1}.*

FAME	Part 3275-1			Part 3275-2			Part 3275-3		
	Experimental	NIST	Recovery %	Experimental	NIST	Recovery %	Experimental	NIST	Recovery %
C12:0	< LoD	-	-	0.25 ± 0.0	-	-	0.91 ± 0.1	0.95 ± 0.12[A]	96.3
C14:0	1.77 ± 0.1	1.094 ± 0.053 [A]	161.8	3.60 ± 0.3	3.45 ± 0.40 [A]	104.3	57.31 ± 1.7	67.9 ± 1.5 [A]	84.4
C14:1ω5	< LoD	-	-	< LoD	-	-	0.59 ± 1.1	0.964 ± 0.043	60.3
C15:0	0.21 ± 0.0	-	-	0.25 ± 0.0	-	-	4.55 ± 0.3	-	-
C16:0	5.24 ± 0.2	5.25 ± 0.35 [A]	99.8	8.04 ± 0.3	8.01 ± 0.44 [A]	100.4	151.62 ± 3.8	186.9 ± 9.4 [A]	81.1
C16:1ω7	7.71 ± 0.3	7.43 ± 0.24 [A]	103.7	5.97 ± 0.5	5.83 ± 0.45 [A]	102.5	64.67 ± 3.5	85.7 ± 3.1 [A]	75.5
C16:2ω4	0.96 ± 0.1	-	-	1.24 ± 0.1	-	-	11.47 ± 0.7	-	-
C17:0	0.25 ± 0.0	-	-	0.29 ± 0.0	-	-	4.48 ± 0.2	-	-
C16:3ω4	1.22 ± 0.1	-	-	2.06 ± 0.2	-	-	14.95 ± 0.7	-	-
C18:0	3.99 ± 0.2	4.22 ± 0.13 [A]	94.6	13.25 ± 1.1	12.94 ± 0.62 [A]	102.4	33.22 ± 0.7	38.0 ± 5.7 [A]	87.4
C18:1ω9	12.04 ± 0.1	11.25 ± 0.93 [A]	107.0	21.89 ± 0.8	22.1 ± 1.6 [A]	99.1	104.27 ± 1.1	112.3 ± 2.6 [A]	92.9
C18:1ω7	5.80 ± 0.3	5.33 ± 0.35 [A]	108.8	9.36 ± 1.1	9.24 ± 0.77 [A]	101.3	37.02 ± 0.7	38.5 ± 2.2 [A]	96.2
C18:2ω6	2.39 ± 0.2	2.31 ± 0.19 [A]	103.5	2.94 ± 0.7	3.00 ± 0.42 [A]	98.0	13.27 ± 0.5	13.49 ± 0.45 [A]	98.4
C18:3ω6	0.41 ± 0.0	0.344 ± 0.025 [B]	118.2	0.58 ± 0.1	0.507 ± 0.043 [B]	113.8	2.63 ± 0.2	1.771 ± 0.099 [B]	148.7
C18:3ω3	1.30 ± 0.2	1.21 ± 0.05 [B]	107.7	1.44 ± 0.4	1.42 ± 0.12 [B]	101.6	9.15 ± 0.6	6.61 ± 0.31 [B]	138.4
C18:4ω3	4.30 ± 0.1	-	-	5.04 ± 0.4	-	-	22.47 ± 0.9	-	-
C18:4ω1	0.52 ± 0.0	-	-	0.78 ± 0.2	-	-	2.91 ± 0.4	-	-
C20:0	2.83 ± 0.1	1.910 ± 0.071	148.2	3.53 ± 0.4	0.357 ± 0.027	989.5	1.55 ± 0.1	1.14 ± 0.26 [A]	135.8

		B			A				
C20:1ω11	1.14 ± 0.1	-	-	3.56 ± 0.3	-	-	0.99 ± 0.1	-	-
C20:1ω9	10.49 ± 0.2	-	-	15.27 ± 1.4	6.66 ± 0.69 [A]	229.1	8.67 ± 0.6	2.92 ± 0.14 [A]	296.9
C20:1ω7	4.13 ± 0.3	-	-	9.69 ± 1.1	-	-	3.48 ± 0.1	-	-
C20:2ω6	2.30 ± 0.2	-	-	3.16 ± 0.4	-	-	1.48 ± 0.1	-	-
C20:3ω6	1.89 ± 0.1	-	-	3.93 ± 0.6	-	-	1.97 ± 0.3	-	-
C20:4ω6	6.03 ± 0.4	5.69 ± 0.19 [B]	106.0	23.54 ± 0.9	22.9 ± 1.0 [B]	102.8	13.87 ± 0.8	-	-
C20:4ω3	8.31 ± 0.2	-	-	18.22 ± 1.5	-	-	9.67 ± 0.8	-	-
C20:5ω3	119.10 ± 7.0	113 ± 12 [A]	105.4	428.81 ± 23.4	394 ± 17 [B]	108.8	180.04 ± 7.6	154 ± 9 [B]	116.9
C22:0	4.47 ± 0.1	4.02 ± 0.24 [A]	111.2	1.41 ± 0.4	1.396 ± 0.046 [A]	100.9	0.75 ± 0.1	0.502 ± 0.047 [A]	148.5
C22:1ω11	44.28 ± 1.5	-	-	19.53 ± 1.5	-	-	6.87 ± 0.4	-	-
C22:1ω9	9.81 ± 0.6	4.76 ± 0.22 [B]	206.0	5.89 ± 0.3	3.43 ± 0.32 [A]	171.7	2.24 ± 0.4	1.61 ± 0.11 [B]	139.1
C22:1ω7	10.98 ± 0.4	-	-	2.89 ± 0.9	-	-	0.87 ± 0.2	-	-
C21:5ω3	16.69 ± 0.8	-	-	15.28 ± 1.2	-	-	10.21 ± 0.4	-	-
C22:4ω6	6.15 ± 0.2	-	-	5.46 ± 1.3	-	-	2.74 ± 0.3	-	-
C22:5ω6	14.65 ± 0.7	-	-	10.82 ± 1.2	-	-	6.44 ± 0.8	-	-
C22:4ω3	6.65 ± 0.4	-	-	3.20 ± 0.5	-	-	1.58 ± 0.3	-	-
C22:5ω3	94.24 ± 2.0	70.2 ± 1.1 [B]	134.3	87.27 ± 2.6	67.6 ± 2.3 [B]	129.1	29.67 ± 2.3	27.0 ± 1.1 [B]	109.9
C24:0	1.47 ± 0.1	-	-	0.58 ± 0.1	0.618±0.028 [B]	93.9	0.36 ± 0.1	0.441 ± 0.013 [B]	81.6
C22:6ω3	376.44 ± 21.9	429 ± 15 [B]	87.7	192.56 ± 16.7	187 ± 8 [B]	103.0	120.30 ± 3.7	104 ± 5 [B]	115.7

4.4 Conclusions

A rapid and reliable methodology was developed providing its suitability for the qualitative and quantitative screening of FAs in DBS samples. The analytical strategy included the use of a robotic workstation that, in a fully automatic manner, allowed the derivatization, extraction of FAME derivatives, and injection into a GC–MS system. The signal acquisition was performed in the simultaneous scan/SIM mode. The fast GC–MS method here described improved significantly the laboratory throughput allowing not only a marked improvement in terms of time required to obtain the analytical results, but also a reduction of the cost per analysis. The analytical workflow, with minor modifications, proved to be suitable also for the establishing of the composition of ω3 FA dietary supplements. The analyses showed that more than 80% of the commercially available ω3 dietary supplements had EPA contents within ± 20% of their label declarations, while in the case of DHA, all supplements analyzed matched the quantities declared on the labels.

References

[1] R.C. Block, W.S. Harris, K.J. Reid, S.A. Sands, J.A. Spertus, EPA and DHA in blood cell membranes from acute coronary syndrome patients and controls, Atherosclerosis 197 (2008) 821–828, doi:1 0.1016/j.atherosclerosis.2007.07.042

[2] R.C. Block, W.S. Harris, K.J. Reid, J.A. Spertus, Omega-6 and trans fatty acids in blood cell membranes: a risk factor for acute coronary syndromes?, Am Heart J. 156 (2008) 1117–1123, doi: 10.1016/j.ahj.2008.07.014.

[3] W.S Harris, The omega-6/omega-3 ratio and cardiovascular disease risk: uses and abuses, Curr Atheroscler Rep. 8 (2008) 453-459, doi:1 0.1007/s11883-006-0019-7.

[4] Harris WS. Omega-3 fatty acids and cardiovascular disease: a case for omega-3 index as a new risk factor, Pharmacol. Res. 55 (2007) 217–223, doi: 10.1016/j.phrs.2007.01.013.

[5] N. Külzow N, A.V. Witte, L. Kerti, U. Grittner, J.P. Schuchardt, A. Hahn, A. Flöel, Impact of omega-3 fatty acid supplementation on memory functions in healthy older adults. J Alzheimers Dis. 51 (2016) 713–25, doi: 0.3233/JAD-150886.

[6] J.W. Sijben, P.C. Calder, Differential immunomodulation with long- chain n-3 PUFA in health and chronic disease, Proc. Nutr. Soc. 66 (2007) 237–259, doi: 10.1017/S0029665107005472.

[7] Chapkin RS, McMurray DN, Lupton JR, Colon cancer, fatty acids and anti-inflammatory compounds, Curr. Opin. Gastroenterol. 23 (2007) 48-54, doi: 10.1097/MOG.0b013e32801145d7.

[8] F. Rigano, P. Arena, D. Mangraviti, D. Donnarumma, P. Dugo, P. Donato P, L. Mondello, Identification of high-value generating molecules from the wastes of tuna fishery industry by liquid chromatography and gas chromatography hyphenated techniques with automated sample preparation, J. Sep. Sci. 44 (2021) 571–580, doi: 10.1002/jssc.202100108.

[9] F. Shahidi, Nutraceutical and specialty lipids and their co-products. 1st ed. Boca Raton, FL: CRC Press; 2006.

[10] F. Shahidi, Omega-3 fatty acids in health and disease. In: Hernan- dez EM, Hosokawa M, editors. Omega-3 oils - applications in functional foods. Urbana, Illinois: AOCS Press; 2011. p. 1–29.

[11] P.C. Calder, Immunomodulation by omega-3 fatty acids, Prostaglandins Leukot. Essent. Fat. Acids 77 (2007) 327–335, doi: 10.1016/j.plefa.2007.10.015.

[12] P. Yaqoob, H.S. Pala, M. Cortina-Borja, E.A. Newsholme, P.C. Calder, Encapsulated fish oil enriched in α-tocopherol alters plasma phospholipid and mononuclear cell fatty acid compositions but not mononuclear cell functions, Eur. J. Clin. Invest. 30 (2000) 260–274, doi: 10.1046/j.1365-2362.2000.00623.x.

[13] C.T. Srigley, J.I. Rader, Content and composition of fatty acids in marine oil omega-3 supplements, J. Agric. Food Chem. 62 (2014) 7268–7278, doi: 10.1021/jf5016973.

[14] G. Micalizzi, E. Ragosta, S. Farnetti, P. Dugo, P.Q. Tranchida, L. Mondello, F. Rigano, Rapid and miniaturized qualitative and quantitative gas chromatography profiling of human blood total fatty acids, Anal. Bioanal. Chem. 4124 (2020) 2327–2337, doi: 10.1007/s00216-020-02424-y.

[15] A.H. El-Hamdy, W. Christie, Preparation of methyl esters of fatty acids with trimethylsulphonium hydroxid an appraisal, J. Chromatogr A. 630 (1993) 438–441, doi: 10.1016/0021-9673(93)80484-P.

[16] C. Galli, P. Risé P, S. Ghezzi, F. Marangoni, Fast determination of fatty acids in whole blood collected from fingertips: application to the assessment of fatty acid patterns (and various indexes) in population studies, World Rev. Nutr. Diet. (2009) 35–45, doi: 10.1159/000235709.

[17] G. Lepage, C.C. Roy, Direct transesterification of all classes of lipids in a one-step reaction, J. Lipid Res. 27 (1986) 114–120, doi: 10.1016/S0022-2275(20)38861-1.

[18] A.M. Rizzo, G. Montorfano, M. Negroni, L. Adorni, P. Berselli, P. Corsetto, K. Wahle, B. Berra, A rapid method for determining arachidonic:eicosapentaenoic acid ratios in whole blood lipids: correlation with erythrocyte membrane ratios and

validation in a large Italian population of various ages and pathologies, Lipids Health Dis. 9 (2010) doi: 10.1186/1476-511X-9-7.

[19] Certificate of Analysis, Standard Reference Material 1950 metabolites in human plasma (accessed October 06, 2021). Available from: https://www-s.nist.gov/srmors/view_cert.cfm?srm=1950.

[20] Certificate of Analysis, Standard Reference Material 3275 Omega-3 and omega-6 fatty acids in fish oil (accessed October 06, 2021). Available from: https://www-s.nist.gov/srmors/quickSearch.cfm?srm=3275.

[21] L.M Blumberg, M.S. Klee, Optimal heating rate in gas chromatography. J. Microcolumn Sep. 12 (2000) 508-514, doi: 10.1002/1520-667X(2000)12:93.3.CO;2-P.

[22] P.A. Leclercq, J. Novak, Open tubular column. In: Quantitative analysis by gas chromatography, 2nd ed. Marcel Dekker Inc., New York; 1987. pp. 247–317.

[23] L. Mondello, P.Q. Tranchida, P. Dugo, G. Dugo, Rapid, micro-scale preparation and very fast gas chromatographic separation of cod liver oil fatty acid methyl esters, J. Pharm. Biomed. Anal. 41 (2006) 1566-1570, doi: 10.1016/j.jpba.2006.01.027.

[24] B.A. Benner Jr, M.M Schantz, C.D. Powers, R.L. Schleicher, J.E. Camara, K.E. Sharpless, J. H. Yen, L. T. Sniegoski, Standard reference material (SRM) 2378 fatty acids in frozen human serum. Certification of a clinical SRM based on endogenous supplementation of polyunsaturated fatty acids, Anal. Bioanal. Chem. 410 (2018) 2321-2329, doi: 10.1007/s00216-017-0841-5.

[25] M.M. Schantz, C.D. Powers, R.L. Schleicher, J.M. Betz, S.A. Wise, Interlaboratory analytical comparison of fatty acid concentrations in serum or plasma, Clin. Chim. Acta. 462 (2016) 148-152, doi: 10.1016/j.cca.2016.09.013.

[26] C.C. Ferreri, C. Chatgilialoglu, Membrane lipidomics for personalized health, 1st ed. Ltd: United Kingdom: John Wiley & Sons; 2015.

[27] H. Guillou, D. Zadravec, P.G.P. Martin, A. Jacobsson, The key roles of elongases and desaturases in mammalian fatty acid metabolism: Insights from

transgenic mice, Prog. Lipid Res. 49 (2010) 186–199, doi: 10.1016/j.plipres.2009.12.002.

[28] B. Sears, The Omega RX Zone: the miracle of the new high-dose fish oil. United Kingdom: Harper Collins Publishers Ltd.; 2003.

[29] K.M. Chee, J.X. Gong, D.M. Rees, M. Meydani, L. Ausman, J. Johnson, E.N. Siguel, E.J. Schaefer, Fatty acid content of marine oil capsules, Lipids 25 (1990) 523–528, doi: 10.1007/BF02537158.

[30] US Food and Drug Administration, Petition for a health claim for eicosapentaenoic acid and docosahexaenoic acid and reduction of blood pressure in the general population. 2019.

[31] R.G. Ackman, W.M.N. Ratnayake, E. J. Macpherson, EPA and DHA contents of encapsulated fish oil products, J. Am. Oil Chem. Soc. 66 (1989;)1162–1164.

Chapter 5
Untargeted profiling and differentiation of geographical variants of wine samples using headspace solid-phase microextraction flow-modulated comprehensive two-dimensional gas chromatography with the support of tile-based Fisher ratio analysis[*]

The characterization of the food volatilome is important to achieve desired flavor profiles in food production processes, or to differentiate different products, with winemaking being one popular area of interest. In the present research, headspace solid-phase microextraction coupled to flow-modulated comprehensive two-dimensional gas chromatography with time-of- flight mass spectrometry was used to characterize geographical-based differences in the volatilome of five white "Grillo" wines, comprising the five sample classes. Following, the instrumental software was exploited to identify class-distinguishing analytes in the dataset via tile-based Fisher ratio analysis. Off-line software was used to apply an ANOVA test. A p-value of 0.01 was applied to select the most important class-distinguishing analytes, which were input to principal component analysis (PCA). The PCA scores plot showed distinct clustering of the wines according to geographical origin, although the loadings revealed that only a few analytes were necessary to differentiate the wines.

5.1 Introduction

GC×GC combined with time-of-flight mass spectrometry (TOFMS) is used for the separation and detection of complex samples, generating a high quantity of data. The amount of data becomes extremely large when many samples, and replicates of each sample, are analyzed. For such a reason, GC×GC-TOFMS data handling has become very demanding, with related evolution occurring in recent years with the context of dedicated software [1-3]. The acquired data should be transformed into useful information after data processing; for such a purpose, chemometric methods can be exploited. In such a manner, different aims can be addressed, such as, sample characterization/differentiation, identification of key components, or to correlate chemical measurements to other properties of the samples [1]. By implementing an untargeted approach, several type of features can be investigated, such as tiles, datapoints, regions, and peak-regions [4]. Using either a supervised or unsupervised experimental design, GC×GC-TOFMS data collection followed by untargeted analysis is increasingly used for the analysis of a wide variety of chemical systems such as the volatile fraction of foods and beverages [5-13]. The distinction is that for a supervised experimental design sample class membership is known a priori, and a common data analysis method is to apply Fisher ratio analysis (F-ratio analysis), while for an unsupervised experimental design sample classes are not known, and the data can be examined by principal component analysis (PCA) to look for the presence of sample classes. We note that it is also common to apply F-ratio analysis, to find the class- distinguishing analyte features, then follow up with the use of PCA as a tool to visualize the success of the F-ratio analysis.

The study of wine aroma, which is the objective of this study, can be readily pursued using F-ratio analysis, since the aroma is extremely complex due to the presence of several classes of compounds. In fact, more than 1000 aroma constituents have been identified, covering a wide range of both polarities and volatilities [14]. The characteristic components of the wine aroma are commonly divided into three classes and relate to the geographical: grape (or varietal) aroma, fermentation aroma and aging aroma. However, these classes are not so clear-divided, most of them originate from grapes and are modified by the fermentation process or aging [15]. In the present research, headspace solid-phase microextraction (HS SPME) coupled to

flow-modulated comprehensive two-dimensional gas chromatography with time-of-flight mass spectrometry (FM GC×GC-TOFMS) was used to determine geographical-based differences in the volatilome of five "Grillo" wines (of Sicilian origin). The flow modulator used was a low duty cycle one, based on a concept introduced by Seeley et al. [16]. The new tile-based Fisher-ratio software released by the LECO corporation known as ChromaTOF Tile was applied to compare the acquired raw data. Briefly, the algorithm works by creating four grids composed of tiles, that are offset from each other, where each tile should be wide enough to embed the average analyte peak widths and retention time shift along both dimensions and sums all the signals at one or more m/z value. The four grids initially produce redundant hits, however, use of the tiling approach avoids the challenges of GC×GC chromatogram alignment and also provides an impressive signal-to-noise (S/N) enhancement for detection of low concentration chemical differences [17-22]. The redundant hits are readily removed via the pinning and clustering step of the software, leaving only the best hit for each analyte feature that is discovered. The hitlist of all analyte features obtained from ChromaTOF tile was subsequently subjected to an off-line one-way analysis of variance (ANOVA) to distinguish true and false positives, and the validity of this approach was assessed with a receiver operating characteristic (ROC) curve. Finally, PCA was performed to distinguish the wines using only the statistically significant chemical features identified via this ANOVA approach.

5.2 Experimental

Chemicals, samples, and sample preparation

Five commercial Grillo wines, from different geographical zones (in Sicily) and wineries, were analyzed. Specifically, Colosi wine was produced in "Petrosino" and "Segesta", Barone wine was produced in "Marsala", Capovero was produced in "Sambuca di Sicilia", Settesoli wine was produced in "Menfi", and FeudoArancio wine was produced in "Acate". All wines were obtained through the same winemaking process (Fig. 5.1). Three bottles of each of the five Grillo wines were utilized to study the reproducibility of the vinification procedure (15 total bottles of wine). Sodium chloride, ethanol, *n*-hexane and 3-octanol, used as internal standard

(IS), were purchased from Merck Life Science (Merck KGaA, Darmstad, Germany). The IS was solubilized in ethanol and was added to each sample at a concentration of 170 mg L^{-1}.
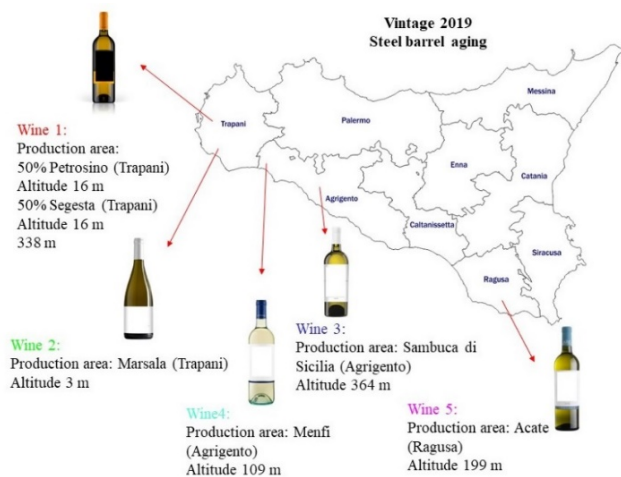
Figure 5.1. *Map displaying the regions of Sicily in which wines 1–5 were produced.*

Instrumentation

The extraction procedure was based on a previous report [8]. Headspace analysis was performed using a 50/30 μm divinylbenzene/carboxen/polydimethylsiloxane (DVB/CAR/PDMS) SPME fiber (Merck Life Science). Before the first use, the fiber was conditioned at 270 °C according to the conditioning guidelines. 5 mL of sample was introduced into a 20 mL headspace vial, along with 2 g of sodium chloride and 10 μL of IS. The samples were incubated for 5 min at 45 °C, followed by 30 min of extraction at the same temperature. The agitation speed was 250 rpm. Three HS SPME replicates were obtained for each bottle per Grillo wine, resulting in 45 total samples for GC×GC-TOFMS analysis (five wines, three bottles each, three replicates per bottle). Desorption was performed for 2 min at 260 °C in the split mode with a 10:1 split ratio. The HS SPME procedure was performed automatically by using an l-PAL3 GC Autosampler (LECO, Mönchengladbach, Germany). All FM GC×GC-TOFMS analyses were performed using a Pegasus GC-BT 4D system, equipped with a diverting flow modulator, called the FLUX modulator (LECO). The ^{1}D column was a Supelcowax 10 [polyethylene glycol] with dimensions 10 m × 0.25 mm ID × 0.25 μm d$_f$, while the ^{2}D column was an SLB-35 ms [silphenylene polymer with similar polarity to poly (35 % diphenyl/65 % dimethyl siloxane)] with dimensions 2

m × 0.10 mm ID × 0.10 μm d_f and with 0.3 m located inside the MS transfer line (280 °C). Both columns were supplied by Merck Life Science.

Helium was used as the carrier gas and was delivered at a constant flow of 1.9 ml min^{-1}. The main GC oven was held at 40 °C for 2 min, then ramped up to 280 °C at 20 °C min^{-1}, for a total analysis time of 14 min. The secondary oven offset was +20 °C. The modulation period (P_M) was set at 700 ms, with a re-injection period of 80 ms. The auxiliary pressure unit (EPC) provided a constant flow of 3.5 mL min^{-1} to the modulator. The MS parameters were as follows: acquisition delay 120 s, acquisition rate 150 spectra s^{-1}, electron ionization was performed at 70 eV, while mass spectra were acquired in the mass channel (*m/z*) range 35-360 amu.

Data analysis

Following data acquisition, the 45 raw .SMP files were transferred from the LECO ChromaTOF for BT software to LECO ChromaTOF Tile v.1.01 (LECO Corporation, St. Joseph, MI) for tile-based Fisher ratio analysis (ChromaTOF Tile). The sample files were labeled according to Grillo wine type, resulting in five classes for F-ratio analysis with nine replicates per class. One-point normalization was performed prior to data analysis using the 3-octanol IS peak signal (^1t_R = 375.783 s, ^2t_R = 0.644 s) at *m/z* 59. For the remainder of this report, with the term peak area, we will refer to the normalized peak area. No fluctuation in the mass spectral response was observed between replicate chromatograms, so a mass spectrum drift correction was deemed unnecessary. A tile size of 10 modulations (7 s) on ^{1}D and 45 spectra (300 ms) on ^{2}D was selected to encompass the average peak widths along both dimensions as well as modest retention time shifting of up to ~2 modulations on ^{1}D. Insignificant retention time shifting was observed on ^{2}D. A *S/N* threshold of 10 times the noise calculated on a per-tile basis for every m/z was applied to exclude low signal hits from the hitlist [17,23]. A minimum of 9 samples were required to exceed this *S/N* threshold, as this was the number of samples per F-ratio class. The hits were ranked in the hitlist according to their top F-ratio *m/z* to improve discoverability of true positive hits versus false positive hits [23]. No F-ratio threshold was set herein. The entire m/z range was included for tile-based F-ratio analysis. Following hitlist generation, analyte identification was performed using the mainlib (NIST) and the Flavors and

Fragrances of Natural and Synthetic Compounds [FFNSC version 4.0 (Chromaleont s.r.l., Messina, Italy)] library. Using the above mentioned parameters, ChromaTOF Tile produced an initial hitlist. Hits were excluded based on the following criteria: (1) artifact hits which streaked across multiple tile lengths, (2) hits which had noisy spectra, and (3) redundant analyte hits. Following this manual scrutinization, a final hitlist was generated and the ChromaTOF Tile-computed peak areas for these hits at their top F-ratio m/z were exported to MATLAB R2020a (The Mathworks Inc., Natick, MA, USA) for further data analysis. In order to ascertain the various contributions of chemical and non-chemical variation (*i.e.*, injection, sample preparation, etc.) to the overall variation in this dataset [24], the percent relative standard deviation (%RSD) in peak areas for each hit was calculated in four ways. First, the overall %RSD was calculated for each hit collectively for all the wines defined by Eq. 5.1:

$$\%RSD_{all\ wines} = \frac{[std.\,dev.\,(areas_{wine\ 1}, areas_{wine\ 2}, areas_{wine\ 3}, areas_{wine\ 4}, areas_{wine\ 5})] * 100}{mean\,(areas_{wine\ 1}, areas_{wine\ 2}, areas_{wine\ 3}, areas_{wine\ 4}, areas_{wine\ 5})}$$

Next, the %RSD was also calculated in Eq. 5.2 using the peak areas of the individual wines, one at a time, denoted as *n*,

$$\%RSD_{wine\ n} = \frac{[std.\,dev.\,(areas_{wine\ n})] * 100}{mean\,(areas_{wine\ n})}$$

Hence, Eq. 5.2 was repeated for each wines, resulting in five values of %RSD for each analyte hit. Futhermore, Eqs. 5.1 and 5.2 were applied both without averaging the SPME replicate areas (subscript 'all areas'), and then following averaging the SPME replicate areas for each bottle of wine (subscript 'ave areas'). These four %RSD calulation methods will be referred to as %RSD_all wines, all areas, %RSDall wines, ave areas, %RSD_wine n, all areas, and %RSD_wine n, ave areas. Examination of the %RSD distributions produced by collectively considering the %RSDs for all analyte hits informs us as to the major sources of variation in the experimental design and chemical measurements. Following examination of the %RSD distributions, a one-way analysis of variation (ANOVA) was performed using the average peak areas of the F-ratio hits (3 summed areas per wine, 15 areas total per hit). The one-way *ANOVA* enables calculation of a *p*-value across more than two sample classes, whereby the null hypothesis tested herein is that there is no statistically significant

difference in the mean peak areas of the different types of wine [25]. A one-way *ANOVA p*-value < 0.01 was used to distinguish true positives from false positives. These true positive and false positive labels were used to construct a receiver operating characteristic (ROC) curve, from which the area under the curve (AUC) was calculated. More specifically, a ROC curve is a plot of the true positive probability (TPP, *i.e.* sensitivity), versus the false positive probability (FPP *i.e.,* 1-specificity), which are calculated by calculating a running sum of the true and false positive instances divided by the total number of true and false positive instances, respectively [26]. This quantitative method has been widely used in the literature to evaluate the classifying capability of identified analytes, especially in biomarker research [17,26–28]. Finally, to highlight the class-distinguishing capability of the true positive F-ratio hits, the averaged peak areas were input to PCA. Mean centering was performed prior to PCA to ensure that analytes with the largest magnitude in peak areas did not unduly contribute to model performance [29,30]. The scores were used to classify respective "clusters" of the different wine samples, whereas the loadings were scrutinized to identify which analytes contributed most significantly to distinguishing the wines.

5.3 Results and discussion

A typical total ion current (TIC) chromatogram for each wine (wines 1-5 per Fig. 5.1) is provided in Fig. 5.2 A-E. Although the total run time was 14 min, minimal chemical information was present after a ^{1}D retention time (^1t_R) of 10 min, hence the ^{1}D axis of Fig. 5.2 A-E was adjusted accordingly. At this level, all of the wines appear to be dominated by just a few highly concentrated analytes, such as octanoic acid, ethyl ester (^1t_R = 6.6 min and ^2t_R = 300 ms), which is labeled with a star in Fig. 5.2 A-E. Thus, all of the wines at first glance appear chemically similar to each other, as the color scale is biased towards these highly concentrated analytes. However, closer examination of the chromatographic region centered around a ^1t_R of 6 min in Fig. 5.2 F-J for each wine, reveals a high level of chemical complexity within the wine samples. Six analytes (linalool ethyl ether, heptanoic acid ethyl ester, hex-(3E)-enyl-acetate, octanoic acid methyl ester, *n*-hexanol, and 3-octanol) within this separation window have been identified and labeled accordingly as analytes 1-6 in

Fig. 5.2 F-J, as the first five of these analytes exhibit noticeable concentration difference between these wines. For example, linalool ethyl ether (analyte 1) appears highly concentrated in wine 1 (Fig. 5.2 F), whereas it is much less concentrated in wines 2 and 3 (Fig. 5.2 G-H) and visually indistinguishable in wines 4 and 5 (Fig. 5.2 I-J). 3-octanol (analyte 6) is the internal standard, so it serves as a useful visual control to confirm that it is present at the same concentration in Fig. 5.2 F-J. This preliminary visual examination of the chromatograms serves to underscore the chemical complexity of the wines and highlights the likely benefit of applying chemometrics to elucidate their chemical differences.
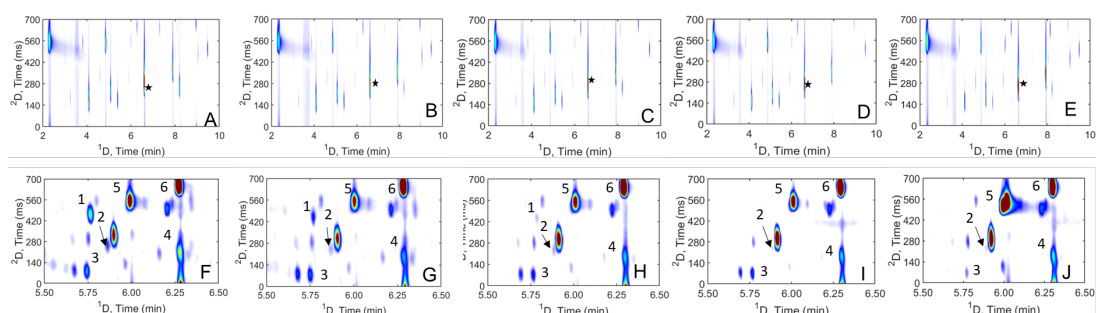
Figure 5.2. *Total ion current (TIC) GC×GC chromatograms from 2 to 10 min for (A) wine 1, (B) wine 2, (C) wine 3, (D) wine 4, and (E) wine 5. A zoom-in region from 5.5 to 6.5 min is included to highlight the high peak capacity/chemical complexity of the separations for (F) wine 1, (G) wine 2, (H) wine 3, (I) wine 4, and (J) wine 5.*

Although chemometric software tools such as ChromaTOF Tile are invaluable in extracting information from large GC×GC-TOFMS datasets, successful implementation requires a sound experimental design, particularly regarding the GC×GC separation conditions. For example, GC×GC chromatograms with minimal orthogonality, low sensitivity, wide ^{1}D and ^{2}D peak widths-at-base (^1w_b and ^2w_b), and/ or peak overlap and "wraparound" on ^{2}D can hamper extracting chemical information [2,3]. Herein, a relatively short 10 m ^{1}D column was utilized to produce narrow ^1w_b to maximize the ^{1}D peak capacity (^1n_c) and the resulting 2D peak capacity ($n_{c,2D}$) [31]. Additionally, the FLUX modulator was operated using a fast P_M of 700 ms and a long re-injection period of 80 ms (*i.e.*, the longest allowed by the instrument given the P_M) to modulate the narrow ^{1}D peaks with an appropriate sampling density (p_s) of 2-4 while simultaneously maximizing the modulator duty cycle, the latter of which is critical for improving detection sensitivity and *S/N*. The

resulting chromatograms shown in Fig. 5.2 exhibit minimal wraparound on ^{2}D that minimizes analyte co-elutions, which suggests the appropriateness of the modulation period selected. The impressive sensitivity afforded by the FLUX modulator can be indicated by the abundance of compounds observed in the zoom-ins provided in Fig. 5.2 F-J. Additionally, one of the most highly concentrated analytes in the wine samples, namely octanoic acid, ethyl ester has an approximate ^1w_b of 3.6 s and ^2w_b of 240 ms, which equates to $n_{c,2D}$ of ~ 680, or a peak capacity production of ~ 50 peaks/min [32,33]. Thus, the experimental design from the instrumentation perspective was optimized to maximize the chemical information available for chemometric analysis. It is instructive to initially apply PCA to all of the data to emphasize the need to apply ChromaTOF Tile for supervised feature selection to discover the analytes that best distinguish the five wines. The PCA scores plot of the 45 unfolded, normalized GC×GC-TOFMS chromatograms is provided in Fig. 5.3. It is important to note that only 58.43% of the variation within the dataset is captured in this PCA model (36.07% on PC1 and 22.36% on PC2), which suggests that potential class-distinguishing information is being buried by spurious chemical signal and noise. This is confirmed by the lack of clustering by wine type in the scores plot, as we would expect to see five distinct sample clusters if the wines were being properly classified by PCA at this stage (Fig. 5.3).
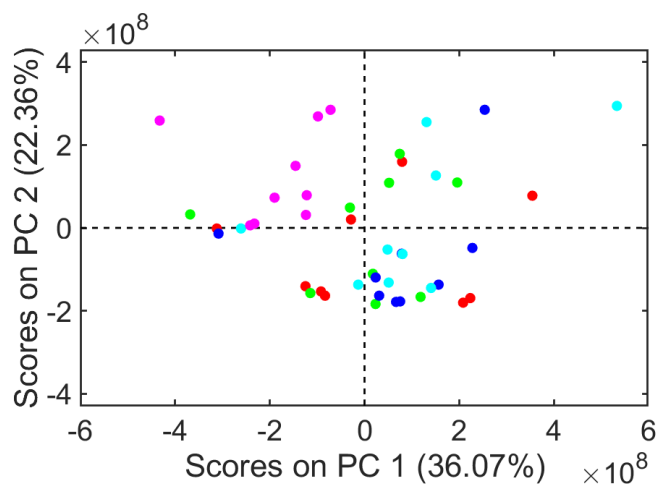

Figure 5.3. *PCA scores plot of unfolded chromatograms using all the m/z, normalized to the IS.*

Since PCA is an unsupervised chemometric tool, its ability to distinguish samples is hampered if spurious chemical signal and noise dominates the dataset input to PCA,

which is the case prior to applying ChromaTOF Tile. Based on a preliminary examination of the TIC chromatograms in Fig. 5.2, these wines do have low concentration differences for a given analyte peak from one wine chromatogram to another, but rigorous examination of the entire chromatogram dataset would be laborious and highly prone to error. Thus, a supervised cheometric tool such as ChromaTOF Tile is necessary and ideally suited to elucidate the extent of chemical differences between these wines. Arguably, the most critical input parameter to tile-based F-ratio analysis is the tile size. In this work, a ^{1}D tile dimension of 7 s (10 modulations) and a ^{2}D tile dimension of 300 ms were selected. The typical analyte linalool ethyl ether (analyte 1 in Fig. 5.2 F-J), in terms of ^1w_b and ^2w_b, is examined in greater detail in Fig. 5.4 to illustrate the justification behind this choice. The summed ^{1}D and ^{2}D peaks for linalool ethyl ether are provided in Fig. 5.4 A-B, respectively, with the same color coding by wine as was used in Fig. 5.3. The x-axes in Fig. 5.4 A-B are equivalent in length to the respective tile dimensions. Using the replicates for wine 1 (red), linalool ethyl ether has an approximate $^1w_b = 2.6$ s and $^2w_b = 130$ ms. Retention time shifting of up to 1.4 s (2 modulations) on ^{1}D is observed in Fig. 5.4 A, whereas insignificant retention time shifting on ^{2}D is seen in Fig. 5.4 B. An especially large ^{1}D tile dimension of 7 s can be justified to correct for the ^{1}D run-to-run shifting, whereas the 300 ms ^{2}D tile dimension is appropriate, given that the maximum ^2w_b observed for other analytes is 300 ms with essentially no ^{2}D shifting (see discussion of octanoic acid, ethyl ester with Fig. 5.2). Thus, this tile size is suitable for capturing the full range of ^1w_b and ^2w_b observed. Upon running the ChromaTOF Tile software using this tile size, an initial hitlist containing 899 hits was produced; 780/899 hits were assigned a *p*-value < 0.05 by the software, so these 780 hits were subjected to further examination. Following manual artifact and redundant hit removal, the initial hitlist was reduced to a final hitlist of 220 hits. The F-ratio distribution for these 220 final F-ratio hits is provided in Fig. 5.4 C, with the location of the analyte linalool ethyl ether indicated. Linalool ethyl ether is found at the top of the hitlist (hit 8) but is important to reiterate that the F-ratio magnitude of 1217 and hitlist ranking of linalool ethyl ether would be compromised had an inappropriate tile size been used, even though linalool ethyl ether is clearly class-distinguishing (Fig. 5.4 A-B). Furthermore, approximately 77% of the F-ratio

distribution shown in Fig. 5.4C falls below an F-ratio of 200 (170/220 hits), beyond which the frequency of hits levels off (frequency less than 10). Thus, it appears that most of the hits in the hitlist are compounded by complex sources of background variation (sample preparation, injection variation, sensitivity, etc.) in addition to chemical variation, which requires further investigation to ascertain statistical significance in distinguishing the wines.
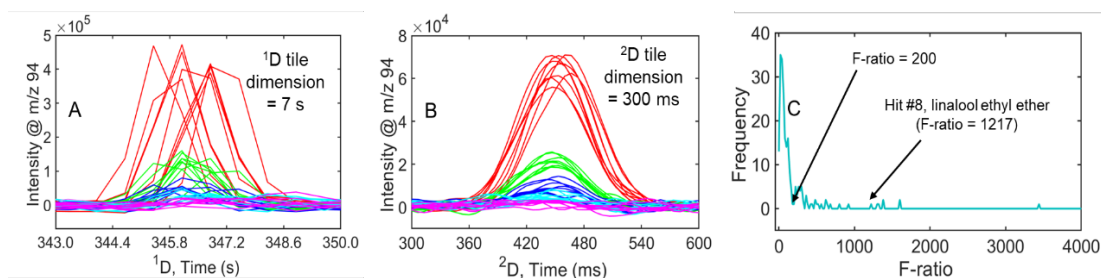

Figure 5.4. Background-corrected summed ^1D (A) and ^2D (B) peaks for linalool ethyl ether at m/z 94. The summed ^1D peaks were prepared by summing away the ^2D modulations, while the summed ^2D peaks were prepared by summing away the ^1D separation. The F-ratio distribution (bin size = 20) for the hitlist of 220 hits is provided in (C), with the F-ratio of linalool ethyl ether (1217) indicated accordingly.

Bar plots displaying the peak areas of linalool ethyl ether in all 45 chromatograms are provided in Fig. 5.4 A, with the same color coding previously applied to distinguish wines 1-5. The peak area differences observed in Fig. 5.4 A coincide with the peak profiles provided in Fig. 5.4 A-B, with wine 1 and wine 2 having the highest and second highest concentrations of linalool ethyl ether, respectively, and wines 3, 4, and 5 having successively lower concentrations. Note that three bottles of each wine were analyzed, with three SPME replicates collected per bottle. For each of the wines in Fig. 5.5 A, the bars are ordered by injection replicate for each consecutive bottle (*i.e.*, bottle 1 replicate 1, bottle 1 replicate 2, bottle 1 replicate 3, bottle 2 replicate 1, etc.). Visual inspection suggests that the injection replicates (recall a replicate refers to a separate wine aliquot with a separate SPME injection from the same bottle) are only marginally contributing to the overall variation in peak areas for a given analyte hit. Thus, averaging the replicates was performed. The resulting bar plot for linalool ethyl ether is shown in Fig. 5.5 B, where now only three bars per wine are provided to represent the summed peak areas per bottle. Note that the averaged bars in Fig. 5.5 B exhibit the same trends in peak areas between bottles of a

given wine as were observed in Fig. 5.5 A, which suggests that summing the replicates does not remove and/or add a significant portion of the total variation associated with the linalool ethyl ether hit. Indeed, for wine 2, the %RSD between peak areas in Fig. 5.5 A is approximately 13.9% and only slightly rises to 14.4% in Fig. 5.5 B after averaging the injection replicates, which indicates that the variation due to injection only amounts to 0.5% RSD and is thus negligible relative to the ~14% RSD due to bottle-based differences. However, this conclusion that the injection replicates contribute a neglibile amount of variation can not necessarily be extraploated to the remaining 219 hits in the hitlist, which necessitates a comprehensive assessment of %RSD in the peak areas. Using Eq. 5.1 and Eq. 5.2, four %RSD distributions in peak areas were generated, which are provided in Fig. 5.5 C: $RSD_{all\ wines,\ all\ areas}$ (gold solid line), $\%RSD_{all\ wines,\ ave\ areas}$ (gold dashed line), $\%RSD_{wine\ n,\ all\ areas}$ (purple solid line), and $\%RSD_{wine\ n,\ ave\ areas}$ (purple dashed line). The $\%RSD_{wine\ n,\ all\ areas}$ and $\%RSD_{wine\ n,\ ave\ areas}$ values were boxcar averaged from 1100 to 220 total %RSD values (boxcar size = 5) to facilite the comparison between all four RSD% distributions. Note that the $\%RSD_{all\ wines,\ all\ areas}$ and $\%RSD_{all\ wines,\ ave\ areas}$ distributions have a maximum frequency of occurence at %RSD of 48%, whereas the $\%RSD_{wine\ n,\ all\ areas}$ and $\%RSD_{wine\ n,\ ave\ areas}$ distributions are shifted to the left and have a maximum frequency of occurence at %RSD values of 12% and 8%, respectively. Thus, for most of the 220 total hits in the F-ratio hitlist, the %RSD in peak areas between wines 1-5 (wine-to-wine variation) is much is much larger than the %RSD in peak areas for a given wine (bottle-to-bottle variation), so it can be concluded that the wine-to-wine differences are the most significant source of variation in the dataset, rather than the bottle-to-bottle differences for a given wine (Fig. 5.5 C). Therefore, during the tile-based F-ratio analysis, the presence of only minor bottle-to-bottle variation should not signficantly hinder the discovery of chemically relavent differences between the wines. Furthermore, in comparing the $\%RSD_{all\ wines,\ all\ areas}$ and $\%RSD_{all\ wines,\ ave\ areas}$ distributions to each other, as well as the $\%RSD_{wine\ n,\ all\ areas}$ and $\%RSD_{wine\ n,\ ave\ areas}$ distributions to each other, they appear largely overlapped, with the %RSD distributions using the averaged areas slightly shifted to lower %RSD values relative to the distributions using all 45 original peak areas. What this reveals, is that injection/sample preparation-based variation is largely negligible in

the context of the chemically-based variation, as it amounts to an RSD% of ~ 5% when comparing the respective distributions. Thus averaging the peak areas of the injection replicates is justified and necessary prior to further statistical analysis, as this will simultaneously discount the influence of uninformative variables while reducing data density.
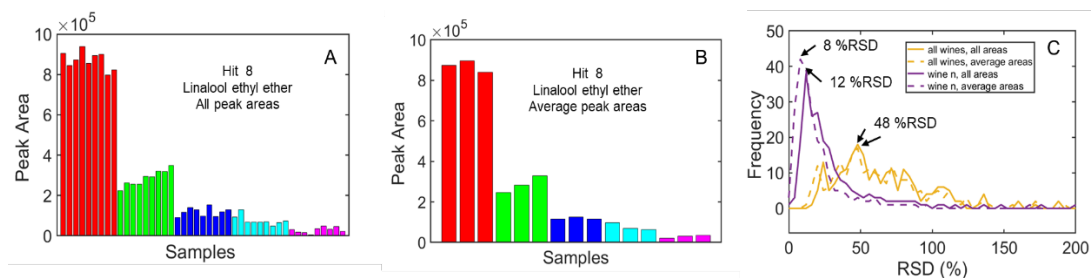
Figure 5.5. (A)All peak areas for linalool ethyl ether in wines 1-5, prior to averaging. (B) Averaged peak areas for linalool ethyl ether. (C) Overlaid RSD distributions for assessing the contributions of wine-to-wine variation, bottle-to-bottle variation, and replicate-to-replicate variation to the overall chemical variation provided by each hit.

The tentative identities of the top 30 hits in the F-ratio hitlist are provided in Table 5.1, along with their retention times on ^1D and ^2D, F-ratios, top F-ratio *m/z*, *p*-values from a one-way *ANOVA* test, the corresponding wine with the highest concentration, and abbreviated sensory information [34]. The entire hitlist for all 220 hits is provided in Table 5.2 with the corresponding concentration and detailed sensory information in Table 5.3. Note that 137/220 hits could be identified with a match value (MV) of at least 800 (1000 perfect match to library), while only 83 hits could not be identified. For the top 30 hits in Table 5.1, 23 have been identified in wines using 1D-GC-MS and GC×GC-MS in prior studies [14,15,40-46]. Interestingly, the advantage of using GC×GC relative to 1D-GC is underscored by examining just the top 30 hits in Table 5.1, with (1) geranyl isobutyrate and nerol oxide, and (2) myrcene and α-phellandrene, respectively, being overlapped on ^1D but having distinct ^2t_R. Further down the hitlist beyond hit 30, there are several other instances in which the benefits of using GC×GC relative to 1D-GC occur. Regarding the seven hits in the top 30 not previously identified in wine, five are structurally similar to other previously identified flavor volatiles in wine, so these compounds are shaded in blue in Table 5.1. The remaining two hits (shaded in orange in Table 5.1) are not

flavor volatiles, but artifacts of the vinification process. For example, phthalate esters such as di-isobutyl phthalate (hit #16) are common contaminants from plastics introduced during the winemaking process [42]. This information is still highly useful in the differentiation of the wines, as the vinification procedure for wine 1 appears to result in the highest concentration of di-isobutyl phthalate (Table 5.1).

Table 5.1. *Identities of the top 30 true positive hits identified following tile-based F-ratio analysis.*

Hit Number	^1t_R (min)	^2t_R (s)	F-ratio	Top m/z	Identity	p-value	Wine, highest concentration	Sensory profile
1	8.17	0.27	3434.2	152	ethyl trans-4-decenoate	2.9E-12	1	fatty
2	6.69	0.51	1608.4	87	cis-ocimenol	1.6E-12	1	unknown
3	8.24	0.01	1594.0	136	α-terpineol	6.9E-09	1	citrus
4	7.29	0.64	1385.7	72	linalool	1.9E-12	1	orange
5	7.07	0.35	1370.9	41	geranyl vinyl ether	9.7E-12	1	unknown
6	8.09	0.63	1323.6	174	diethyl succinate	5.9E-12	5	fruity
7	6.92	0.18	1301.6	55	ethyl 7-octenoate	9.4E-06	1	unknown
8	5.75	0.45	1217.2	94	linalool ethyl ether	6.4E-12	1	floral
9	7.47	0.59	917.3	70	isoamyl lactate	2.1E-11	5	fruity
10	6.86	0.35	806.6	93	geranyl isobutyrate	3.6E-10	1	sweet
11	5.96	0.52	689.6	75	ethyl lactate	1.1E-10	5	sweet
12	4.45	0.37	631.6	93	myrcene	1.1E-08	1	woody
13	5.21	0.32	623.0	93	3-carene	4.1E-07	1	citrus
14	7.68	0.61	610.4	71	2,6-dimethyl-3,7-octadiene-2,6-diol	2.2E-09	1	unknown
15	5.07	0.33	551.6	93	ethyl hexanoate	7.5E-07	1	sweet
16	12.95	0.07	529.2	149	di-isobutyl phthalate	9.3E-11	1	unknown
17	8.58	0.61	503.9	123	citronellol	1.2E-09	1	floral
18	4.45	0.54	475.1	93	α-phellandrene	2.4E-09	1	terpenic
19	9.26	0.47	472.4	91	benzyl alcohol	1.2E-10	3	chemical
20	9.35	0.04	442.9	129	ethyl isopentyl succinate	5.7E-10	5	unknown
21	6.83	0.19	412.7	68	nerol oxide	2.7E-10	1	green
22	4.76	0.52	373.0	92	limonene	2.8E-09	1	citrus
23	8.79	0.60	361.6	69	nerol	1.2E-09	1	lemon
24	9.42	0.44	353.7	70	isopentyl undecenoate	1.6E-07	1	floral
25	10.95	0.28	353.5	221	2,3-dihydro-1,1,3-trimethyl-3-phenyl-1H-indene	5.3E-09	2	unknown
26	6.09	0.60	318.6	99	allyl isothiocyanate	5.6E-07	1	mustard
27	5.56	0.37	317.1	70	3-methylbutyl pentanoate	3.3E-07	1	strawberry
28	3.02	0.13	305.2	55	isobutyl acetate	8.4E-08	1	sweet
29	9.04	0.59	301.0	68	geraniol	3.6E-06	1	floral
30	9.31	0.34	300.2	88	ethyl 10-undecenoate	1.2E-07	1	fatty

Future work could involve collecting additional replicate chromatograms of wine 1 to quantify the level of di-isobutyl phthalate contamination more accurately. Another non-flavor associated compound found in the top 30 hits is allyl isothiocyanate (hit #26), which has known antifungal properties and has been used widely in food preservation [48,49]. Thus, it appears that allyl isothiocyanate is used more widely as an antimicrobial agent in the north end of Trapani, where wine 1 is produced, as it has the highest concentration in wine 1. Interestingly, most of the flavor volatiles in the top 30 hits are also at their highest concentration in wine 1, with *p*-values four to ten orders of magnitude smaller than the typical *p*-value thresholds of 0.05 or 0.01 typically applied. Thus it appears that wine 1 may be the most "chemically unique" wine in this dataset.

Table 5.2. *220 hits which were manually selected from the ChromaTOF tile hitlist.*

Hit #	^1t_R (min)	^2t_R (s)	F-ratio	*m/z*	Identity	p-value
1	8.17	0.27	3434.2	152	ethyl trans-4-decenoate	2.9E-12
2	6.69	0.51	1608.4	87	cis-Ocimenol	1.6E-12
3	8.24	0.01	1594.0	136	α-Terpineol	6.9E-09
4	7.29	0.64	1385.7	72	Linalool	1.9E-12
5	7.07	0.35	1370.9	41	geranyl vinyl ether	9.7E-12
6	8.09	0.63	1323.6	174	Succinate <diethyl->	5.9E-12
7	6.92	0.18	1301.6	55	7-Octenoic acid, ethyl ester	9.4E-06
8	5.75	0.45	1217.2	94	linalool ethyl ether	6.4E-12
9	7.47	0.59	917.3	70	isoamyl lactate	2.1E-11
10	6.86	0.35	806.6	93	geranyl isobutyrate	3.6E-10
11	5.96	0.52	689.6	75	Lactate <ethyl->	1.1E-10
12	4.45	0.37	631.6	93	Myrcene	1.1E-08
13	5.21	0.32	623.0	93	Carene <delta-3->	4.1E-07
14	7.68	0.61	610.4	71	3,7-Octadiene-2,6-diol, 2,6-dimethyl-	2.2E-09
15	5.07	0.33	551.6	93	Hexanoic acid, ethyl ester	7.5E-07
16	12.95	0.07	529.2	149	Phthalate <di-isobutyl>	9.3E-11
17	8.58	0.61	503.9	123	Citronellol	1.2E-09
18	4.45	0.54	475.1	93	α-phellandrene	2.4E-09
19	9.26	0.47	472.4	91	benzyl alcohol	1.2E-10
20	9.35	0.04	442.9	129	Butanedioic acid, ethyl 3-methylbutyl ester	5.7E-10
21	6.83	0.19	412.7	68	nerol oxide	2.7E-10
22	4.76	0.52	373.0	92	limonene	2.8E-09
23	8.79	0.60	361.6	69	nerol	1.2E-09
24	9.42	0.44	353.7	70	Undecenoate <isopentyl->	1.6E-07
25	10.95	0.28	353.5	221	1H-Indene, 2,3-dihydro-1,1,3-trimethyl-3-phenyl-	5.3E-09
26	6.09	0.60	318.6	99	allyl isothiocyanate	5.6E-07
27	5.56	0.37	317.1	70	Pentanoic acid, 3-methylbutyl ester	3.3E-07
28	3.02	0.13	305.2	55	Acetate <isobutyl->	8.4E-08
29	9.04	0.59	301.0	68	Geraniol	3.6E-06
30	9.31	0.34	300.2	88	Undec-10-enoate <ethyl->	1.2E-07
31	7.14	0.45	294.8	136	2-carene	1.7E-06
32	9.55	0.24	292.2	183	methyl 2-oxooctadecanoate	5.0E-08
33	6.19	0.31	285.8	99	*unidentified 1*	2.1E-09
34	8.25	0.36	285.2	163	*unidentified 2*	1.5E-08
35	3.92	0.61	283.4	139	Bois de Rose oxide	2.2E-08
36	10.93	0.11	270.9	81	*unidentified 3*	5.7E-12
37	4.24	0.21	264.0	106	5-(1-methylethylidene)-1,3-cyclopentadiene	1.5E-11
38	8.93	0.68	258.8	106	phenethyl acetate	1.7E-08
39	4.33	0.53	257.4	56	butyl alcohol	5.7E-09
40	5.47	0.45	253.6	93	terpinolene	1.1E-06
41	8.69	0.67	250.0	143	diethyl glutarate	1.0E-07
42	3.61	0.15	247.3	73	butyl acetate	1.0E-08
43	8.43	0.37	240.2	163	*unidentified 4*	8.7E-09
44	9.02	0.44	231.5	63	ethyl dodecanoate	2.1E-07
45	8.98	0.13	220.0	122	(E)-β-damascenone	2.9E-07
46	9.21	0.09	215.0	123	butyl benzoate	4.0E-08
47	8.44	0.16	214.9	85	vinyl decanoate	2.3E-08
48	8.44	0.63	211.8	90	benzyl acetate	3.5E-08
49	6.37	0.15	211.0	95	*unidentified 5*	4.9E-07
50	6.86	0.51	203.2	96	furfural	6.7E-08
51	8.31	0.55	177.6	111	*unidentified 6*	4.1E-08
52	8.37	0.15	162.0	68	neryl phenylacetate	7.8E-04
53	6.96	0.42	161.1	93	trans-(-)-5-methyl-3-(1-methylethenyl)-cyclohexene	5.2E-07
54	10.86	0.51	153.0	135	4-vinyl guaiacol	3.5E-07
55	8.60	0.48	152.2	218	*unidentified 7*	3.3E-07
56	5.54	0.12	151.3	68	ethyl (3Z)-3-hexenoate	2.1E-05
57	7.24	0.47	145.0	151	1,1,4a-trimethyl-3,4,4a,5,6,7-hexahydro-2(1H)-naphthalenone	1.9E-07
58	3.42	0.25	144.7	57	ethyl 2-methylbutyrate	2.6E-07
59	8.00	0.21	143.6	123	citronellyl acetate	3.3E-07
60	4.59	0.52	141.4	121	*unidentified 8*	1.7E-07
61	3.56	0.24	141.3	85	ethyl isovalerate	5.2E-07
62	7.35	0.43	141.3	127	isobutyl octanoate	9.5E-06
63	7.72	0.41	140.7	127	butyl lactate	8.1E-08
64	9.23	0.34	138.9	71	2-methyl-1-(1,1-dimethylethyl)-2-methylpropanoic acid, 1,3-propanediyl ester	3.7E-05

65	5.86	0.25	133.6	113	ethyl heptanoate	1.8E-05
66	2.57	0.19	129.4	116	ethyl isobutyrate	8.1E-07
67	5.32	0.21	127.2	105	1-ethyl-3-methyl-benzene	1.7E-06
68	8.83	0.26	127.1	107	*unidentified 9*	5.2E-10
69	6.93	0.33	122.6	137	sulfur dioxide	2.3E-06
70	8.37	0.42	122.5	173	*unidentified 10*	7.1E-07
71	8.56	0.13	122.0	68	(R)-lavandulyl acetate	9.5E-06
72	6.26	0.21	121.5	129	methyl octanoate	7.7E-07
73	6.15	0.19	120.7	56	heptyl acetate	4.8E-07
74	7.67	0.69	120.3	132	7-methylbenzofuran	3.9E-06
75	5.48	0.22	119.0	106	mesitylene	8.8E-08
76	10.06	0.05	118.2	172	*unidentified 11*	6.6E-07
77	7.89	0.37	118.2	51	ethyl decanoate	2.2E-06
78	6.43	0.31	115.3	99	*unidentified 12*	4.5E-08
79	6.01	0.33	115.1	99	isobutyl hexanoate	2.3E-05
80	8.84	0.47	111.1	70	*unidentified 13*	2.9E-07
81	10.41	0.59	110.9	88	ethyl pentadecanoate	2.1E-06
82	7.15	0.17	106.3	113	*unidentified 14*	3.4E-06
83	8.86	0.60	106.2	55	9-decen-1-ol	7.0E-05
84	11.75	0.40	105.7	120	4-vinylphenol	7.2E-06
85	4.54	0.14	105.5	61	amyl acetate	3.9E-06
86	9.13	0.55	104.1	70	isoamyl decanoate	1.1E-05
87	5.01	0.24	101.5	105	2,4-nonadiyne	8.4E-06
88	9.93	0.23	101.2	157	*unidentified 15*	2.1E-06
89	8.52	0.39	99.9	68	*unidentified 16*	9.7E-04
90	6.20	0.50	99.5	45	*unidentified 17*	1.9E-07
91	4.06	0.19	99.4	101	isoamyl acetate	7.9E-07
92	8.55	0.49	96.2	155	isobutyl decanoate	1.3E-06
93	5.62	0.50	96.2	45	acetoin	3.9E-06
94	10.07	0.55	95.9	93	ethyl tetradecanoate	1.5E-05
95	9.38	0.49	92.7	88	ethyl tridecanoate	1.6E-04
96	5.67	0.24	89.4	125	*unidentified 18*	2.2E-07
97	10.75	0.43	87.5	107	*unidentified 19*	5.7E-08
98	10.03	0.08	87.3	67	nerolidol	2.4E-04
99	5.16	0.48	87.2	93	*unidentified 20*	1.8E-08
100	11.81	0.40	86.6	81	n-decanoic acid	5.9E-06
101	2.34	0.11	86.5	78	ethanol	8.4E-06
102	7.60	0.27	83.4	43	methyl decanoate	2.9E-04
103	6.76	0.47	82.9	45	*unidentified 21*	6.2E-06
104	7.21	0.09	81.7	43	methyl 2-oxononanoate	1.0E-06
105	5.72	0.09	81.7	68	(4Z)-4-hexenyl acetate	1.3E-05
106	8.51	0.19	80.2	57	*unidentified 22*	6.1E-06
107	11.02	0.21	78.6	183	guaiazulene	1.9E-06
108	7.58	0.54	76.6	109	*unidentified 23*	2.2E-06
109	10.22	0.57	76.1	101	methyl 2,8-dimethyl-undecanoate	1.5E-05
110	8.92	0.28	74.4	190	*unidentified 24*	6.3E-04
111	6.03	0.01	71.3	86	*unidentified 25*	5.8E-06
112	10.10	0.65	68.3	85	*unidentified 26*	1.4E-05
113	9.47	0.02	67.7	131	phenylethyl alcohol	2.6E-03
114	10.20	0.45	67.3	111	ethyl E-11-hexadecenoate	6.8E-06
115	8.00	0.45	66.7	101	isoamyl octanoate	3.5E-05
116	5.39	0.17	66.3	35	hexyl acetate	7.1E-06
117	9.61	0.03	65.9	163	*unidentified 27*	2.3E-05
118	5.93	0.19	65.5	105	*unidentified 28*	2.7E-05
119	10.67	0.52	63.7	85	*unidentified 29*	1.7E-05
120	4.66	0.17	63.2	106	methyl hexanoate	2.9E-04
121	10.44	0.69	63.2	126	*unidentified 30*	2.9E-05
122	5.30	0.05	62.6	104	styrene	3.6E-05
123	3.25	0.19	61.3	61	ethyl butyrate	5.5E-03
124	7.22	0.35	59.9	93	ethyl nonanoate	4.7E-06
125	6.69	0.44	59.9	174	α-ionene	1.8E-04
126	7.06	0.59	59.1	84	(S)-3-ethyl-4-methylpentanol	6.7E-06
127	5.93	0.53	59.0	159	*unidentified 31*	3.7E-05
128	6.53	0.47	58.9	174	*unidentified 32*	1.3E-03
129	7.46	0.67	57.2	61	ethyl 3-(methylthio)propionate	5.2E-06
130	10.17	0.66	57.0	70	*unidentified 33*	8.4E-05
131	13.44	0.49	56.1	82	2,6-bis(1,1-dimethylethyl)-1,4-benzenediol	3.7E-05
132	7.37	0.20	55.8	99	*unidentified 34*	1.7E-06
133	7.37	0.67	54.5	109	*unidentified 35*	6.6E-02
134	2.65	0.09	54.0	61	n-propyl acetate	1.6E-04

135	6.75	0.36	53.9	43	isopentyl hexanoate	2.5E-02
136	12.87	0.41	53.8	129	n-dodecanoic acid	1.2E-05
137	6.45	0.51	52.5	57	*unidentified 36*	8.2E-08
138	5.75	0.29	50.9	155	*unidentified 37*	1.0E-01
139	4.81	0.53	49.7	93	2-methyl-1-butanol	1.0E-03
140	9.20	0.49	49.3	101	*unidentified 38*	1.5E-04
141	8.56	0.27	48.8	155	dehydro-ar-ionene	6.8E-05
142	7.63	0.61	48.4	113	n-hexadecane	8.3E-05
143	6.33	0.53	47.2	127	tetradecane	1.4E-04
144	8.35	0.25	46.4	88	ethyl 9-decenoate	1.2E-04
145	4.74	0.05	46.4	68	*unidentified 39*	1.3E-05
146	5.95	0.12	45.9	99	ethyl hex-(2E)-enoate	5.6E-04
147	9.50	0.38	45.7	157	α-calacorene	7.0E-05
148	8.72	0.53	45.1	220	*unidentified 40*	2.4E-06
149	10.44	0.50	43.9	123	*unidentified 41*	2.8E-05
150	8.66	0.55	43.8	93	*unidentified 42*	5.0E-05
151	10.84	0.39	42.1	81	octanoic acid	2.0E-04
152	7.70	0.09	41.5	93	*unidentified 43*	1.2E-04
153	5.68	0.55	41.2	56	4-methyl-pentan-1-ol	1.0E-04
154	7.35	0.60	41.0	41	n-octyl acrylate	2.6E-04
155	3.81	0.55	40.7	74	2-methyl-1-propanol	5.7E-03
156	6.92	0.59	40.2	57	2-ethyl-1-hexanol	1.6E-04
157	5.86	0.07	39.6	67	(2Z)-2-hexenyl acetate	3.4E-06
158	6.32	0.23	38.9	84	*unidentified 44*	4.6E-04
159	6.69	0.15	38.4	91	*unidentified 45*	7.3E-04
160	5.83	0.49	38.3	43	*unidentified 46*	2.1E-03
161	5.16	0.27	38.2	109	1,2,3-trimethylbenzene	2.9E-02
162	9.42	0.16	38.1	205	butylated hydroxytoluene	9.8E-05
163	5.89	0.05	37.3	108	6-methyl-5-hepten-2-one	3.2E-05
164	10.63	0.23	36.6	197	*unidentified 47*	1.1E-03
165	11.24	0.56	36.3	91	*unidentified 48*	6.1E-05
166	7.42	0.22	35.3	68	*unidentified 49*	1.9E-05
167	8.38	0.49	35.1	59	3-(methylthio)-1-propanol	3.3E-02
168	6.03	0.23	33.9	119	*unidentified 50*	3.3E-04
169	11.06	0.25	33.7	197	*unidentified 51*	3.7E-04
170	3.16	0.46	33.0	151	*unidentified 52*	1.0E-02
171	12.49	0.67	31.7	111	*unidentified 53*	3.8E-04
172	7.14	0.32	31.5	61	propyl octanoate	1.1E-02
173	10.25	0.38	29.4	269	*unidentified 54*	3.6E-02
174	11.03	0.69	29.4	251	ethyl palmitate	8.8E-02
175	9.52	0.17	26.4	126	*unidentified 55*	2.8E-05
176	9.72	0.54	26.2	88	*unidentified 56*	2.1E-04
177	9.87	0.46	23.5	87	*unidentified 57*	5.1E-04
178	3.48	0.32	23.4	237	*unidentified 58*	2.4E-02
179	10.26	0.53	23.2	85	*unidentified 59*	4.8E-05
180	6.59	0.30	22.7	141	ethyl octanoate	1.2E-02
181	9.01	0.28	22.3	221	*unidentified 60*	6.7E-04
182	12.40	0.61	21.9	87	*unidentified 61*	1.2E-03
183	7.91	0.62	21.9	336	*unidentified 62*	9.1E-02
184	10.00	0.29	19.7	216	acetic acid	1.2E-03
185	7.10	0.65	19.5	45	2-nonanol	3.5E-02
186	5.40	0.48	19.3	78	phenacyl formate	6.7E-03
187	9.55	0.04	18.9	159	*unidentified 63*	3.8E-03
188	2.03	0.08	18.9	71	ethyl acetate	5.1E-04
189	7.80	0.57	18.1	140	ethyl 2-furoate	2.6E-03
190	10.81	0.64	17.1	88	*unidentified 64*	1.9E-04
191	7.31	0.19	17.0	146	2,3-dihydro-4,7-dimethyl-1H-indene	6.1E-06
192	3.58	0.48	15.9	40	*unidentified 65*	1.7E-02
193	7.66	0.19	15.6	71	*unidentified 66*	1.3E-05
194	3.01	0.43	15.3	248	(2-aziridinylethyl)amine	1.6E-01
195	11.92	0.02	15.1	101	ethyl stearate	6.4E-01
196	13.19	0.61	14.9	73	*unidentified 67*	6.4E-03
197	5.98	0.67	14.6	54	tetrahydro-3,6-dimethyl-2H-pyran-2-one	8.0E-06
198	6.71	0.13	14.1	134	cosmene	8.1E-02
199	13.75	0.56	14.0	89	metaldehyde isomer IV	1.9E-04
200	8.07	0.47	13.4	159	*unidentified 68*	8.7E-03
201	7.86	0.15	13.1	94	*unidentified 69*	1.8E-07
202	11.06	0.49	13.0	86	*unidentified 70*	6.6E-01
203	6.85	0.05	11.6	59	*unidentified 71*	3.6E-03
204	8.03	0.63	11.3	105	acetophenone	6.4E-02

205	6.27	0.52	11.2	121	*unidentified 72*	7.8E-02
206	9.11	0.15	10.7	43	neryl acetone	2.5E-01
207	12.83	0.15	10.6	245	*unidentified 73*	8.8E-02
208	5.76	0.17	9.7	59	*unidentified 74*	5.8E-03
209	5.96	0.41	9.6	334	*unidentified 75*	3.9E-01
210	5.19	0.45	7.8	85	*unidentified 76*	2.1E-02
211	13.90	0.19	7.3	89	metaldehyde isomer I	2.7E-01
212	11.98	0.56	6.8	157	*unidentified 77*	4.0E-01
213	12.73	0.01	6.0	89	metaldehyde isomer II	6.3E-03
214	13.12	0.53	6.0	121	*unidentified 78*	8.4E-02
215	13.03	0.53	5.9	121	*unidentified 79*	1.5E-01
216	10.41	0.11	5.6	217	*unidentified 80*	2.4E-01
217	4.53	0.41	5.1	343	*unidentified 81*	2.7E-01
218	11.54	0.69	4.9	73	*unidentified 82*	8.9E-01
219	4.87	0.09	4.6	67	isopentyl alcohol	1.2E-01
220	4.98	0.06	4.2	68	*unidentified 83*	5.1E-01

However, examination of Table 5.3 reveals that hits further down the hitlist are present at higher concentrations in wines 2-5. Thus, application of one-way *ANOVA* to all 220 hits is necessary to fully characterize the chemical differences between the wines, as trace level volatiles could be missed if one were just to rely on a subset of the top hits.

Table 5.3. *Sensory characteristics of 220 hits selected from ChromaTOF Tile. For analytes which could not be identified, the sensory profile is indicated as "n/a".*

Hit #	Identity	Wine, highest concentration	Sensory Profile
1	ethyl trans-4-decenoate	1	fatty, waxy, green, pineapple, pear
2	cis-Ocimenol	1	**unknown**
3	α-Terpineol	1	citrus, woody, lemon lie, soapy
4	Linalool	1	orange, lemon, floral, waxy, aldehydic, woody
5	geranyl vinyl ether	1	**unknown**
6	Succinate <diethyl->	5	fruity, tart, floral, tropical, passion fruit
7	7-Octenoic acid, ethyl ester	1	**unknown**
8	linalool ethyl ether	1	floral
9	isoamyl lactate	5	fruity, creamy, nutty
10	geranyl isobutyrate	1	sweet, floral, citrus, fruity
11	Lactate <ethyl->	5	sweet, fruity, creamy, pineapple, caramellic
12	Myrcene	1	woody, vegetable, citrus, fruity, tropical, minty
13	Carene <delta-3->	1	citrus, pine, terpenic, tropical, juniper, wasabi
14	3,7-Octadiene-2,6-diol, 2,6-dimethyl-	1	**unknown**
15	Hexanoic acid, ethyl ester	1	sweet, pineapple, fruity, waxy, banana, green
16	Phthalate <di-isobutyl>	1	**unknown**
17	Citronellol	1	floral, rose, sweet, green, fruity, citrus
18	α-phellandrene	1	terpenic, citrus, lime, fresh, green
19	benzyl alcohol	3	chemical, fruity, balsamic
20	Butanedioic acid, ethyl 3-methylbutyl ester	5	**unknown**
21	nerol oxide	1	green, vegetable, floral, waxy, herbal, minty
22	limonene	1	citrus, herbal, terpenic, camphoreous
23	nerol	1	lemon, bitter, green, fruity, terpenic
24	Undecenoate <isopentyl->	1	floral, rose, waxy
25	1H-Indene, 2,3-dihydro-1,1,3-trimethyl-3-phenyl-	2	**unknown**
26	allyl isothiocyanate	1	mustard, horseradish, wasabi
27	Pentanoic acid, 3-methylbutyl ester	1	strawberry
28	Acetate <isobutyl->	1	sweet, fruity, banana
29	Geraniol	1	floral, rose, waxy, fruity, peach
30	Undec-10-enoate <ethyl->	1	fatty, waxy, green, fruity
31	2-carene	1	**unknown**
32	methyl 2-oxooctadecanoate	5	**unknown**
33	*unidentified 1*	1	*n/a*
34	*unidentified 2*	5	*n/a*

35	Bois de Rose oxide	1	sweet, camphoreous, woody, cooling, floral
36	*unidentified 3*	5	*n/a*
37	5-(1-methylethylidene)-1,3-cyclopentadiene	1	**unknown**
38	phenethyl acetate	1	sweet, honey, floral, rose, green, fruity
39	butyl alcohol	2	banana, fusel
40	terpinolene	1	woody, terpenic, lemon, lime, herbal, floral
41	diethyl glutarate	5	**Unknown**
42	butyl acetate	2	sweet, ripe, banana, tropical, candy, green
43	*unidentified 4*	5	*n/a*
44	ethyl dodecanoate	5	waxy, soapy, floral, creamy, dairy, fruity
45	(E)-β-damascenone	2	apple, rose, honey, tobacco, sweet
46	butyl benzoate	1	amber, balsamic, fruity
47	vinyl decanoate	3	**unknown**
48	benzyl acetate	2	fruity, sweet, balsamic, jasmin, floral
49	*unidentified 5*	1	*n/a*
50	furfural	5	brown, sweet, woody, bready, nutty, burnt
51	*unidentified 6*	3	*n/a*
52	neryl phenylacetate	1	honey, rose, honeysuckle
53	trans-(-)-5-methyl-3-(1-methylethenyl)-cyclohexene	1	**unknown**
54	4-vinyl guaiacol	3	bacon, smoky, spicy, clove, phenolic, woody
55	*unidentified 7*	3	*n/a*
56	ethyl (3Z)-3-hexenoate	1	green, pear, apple, tropical
57	1,1,4a-trimethyl-3,4,4a,5,6,7-hexahydro-2(1H)-naphthalenone	3	**unknown**
58	ethyl 2-methylbutyrate	5	fruity, fresh, berry, grape, pineapple, mango
59	citronellyl acetate	2	floral, waxy, aldehydic, green, fruity, pear, apple
60	*unidentified 8*	1	*n/a*
61	ethyl isovalerate	5	sweet, fruity, spicy, metallic, green, pineapple
62	isobutyl octanoate	1	fruity, green, oily, floral
63	butyl lactate	2	dairy, creamy, milky, coconut, nutty
64	2-methyl-1-(1,1-dimethylethyl)-2-methylpropanoic acid, 1,3-propanediyl ester	1	**unknown**
65	ethyl heptanoate	1	fruity, pineapple, banana, strawberry, spicy, oily
66	ethyl isobutyrate	5	pungent, ethereal, fruity, alliaceous, egg nog
67	1-ethyl-3-methyl-benzene	1	**unknown**
68	*unidentified 9*	5	*n/a*
69	sulfur dioxide	1	**unknown**
70	*unidentified 10*	5	*n/a*
71	(R)-lavandulyl acetate	2	**unknown**
72	methyl octanoate	1	green, fruity, waxy, citrus, aldehydic, fatty
73	heptyl acetate	1	green, fatty, spicy, citrus, soapy, aldehydic, floral
74	7-methylbenzofuran	3	earthy, mushroom, hazelnut
75	mesitylene	1	**unknown**
76	*unidentified 11*	3	*n/a*
77	ethyl decanoate	5	waxy, fruity, sweet, apple
78	*unidentified 12*	2	*n/a*
79	isobutyl hexanoate	1	sweet, fruity, pineapple, green, tropical, estery
80	*unidentified 13*	1	*n/a*
81	ethyl pentadecanoate	1	honey, sweet
82	*unidentified 14*	1	*n/a*
83	9-decen-1-ol	1	fresh, waxy, metallic, cilantro, watery, oily, fatty
84	4-vinylphenol	1	phenolic, medicinal, spicy
85	amyl acetate	2	fruity, pear, banana, sweet
86	isoamyl decanoate	5	waxy, fruity, banana, green, creamy, cheesy, fatty
87	2,4-nonadiyne	1	**unknown**
88	*unidentified 15*	5	*n/a*
89	*unidentified 16*	1	*n/a*
90	*unidentified 17*	5	*n/a*
91	isoamyl acetate	2	sweet, fruity, banana, green, ripe
92	isobutyl decanoate	5	oily, sweet, brandy, apricot, fermented, cognac
93	acetoin	5	creamy, dairy, sweet, oily, buttery, yogurt
94	ethyl tetradecanoate	1	sweet, waxy, creamy
95	ethyl tridecanoate	1	**unknown**
96	*unidentified 18*	1	*n/a*
97	*unidentified 19*	4	*n/a*
98	nerolidol	1	green, floral, woody, fruity, citrus, melon
99	*unidentified 20*	1	*n/a*
100	n-decanoic acid	5	soapy, waxy, fruity
101	ethanol	4	alcoholic, ethereal, medicinal
102	methyl decanoate	1	fatty, oily, fruity
103	*unidentified 21*	5	*n/a*

104	methyl 2-oxononanoate	3	**unknown**
105	(4Z)-4-hexenyl acetate	2	**unknown**
106	*unidentified 22*	5	*n/a*
107	guaiazulene	2	**unknown**
108	*unidentified 23*	5	*n/a*
109	methyl 2,8-dimethyl-undecanoate	1	**unknown**
110	*unidentified 24*	2	*n/a*
111	*unidentified 25*	4	*n/a*
112	*unidentified 26*	1	*n/a*
113	phenylethyl alcohol	5	floral, sweet, rose, bready
114	ethyl E-11-hexadecenoate	1	**unknown**
115	isoamyl octanoate	5	sweet, fruity, waxy, pineapple, green, coconut
116	hexyl acetate	2	fruity, green, fresh, sweet, banana, apple, pear
117	*unidentified 27*	5	*n/a*
118	*unidentified 28*	1	*n/a*
119	*unidentified 29*	5	*n/a*
120	methyl hexanoate	1	fruity, fatty, banana, pineapple, apple, creamy
121	*unidentified 30*	3	*n/a*
122	styrene	2	sweet, balsamic, floral, plastic, almond
123	ethyl butyrate	4	fruity, sweet, apple, fresh, ethereal
124	ethyl nonanoate	3	waxy, soapy, cognac, estery, fruity, grape
125	α-ionene	3	**unknown**
126	(S)-3-ethyl-4-methylpentanol	1	**unknown**
127	*unidentified 31*	3	*n/a*
128	*unidentified 32*	3	*n/a*
129	ethyl 3-(methylthio)propionate	5	sulfurous, onion, garlic, pineapple, rummy
130	*unidentified 33*	2	*n/a*
131	2,6-bis(1,1-dimethylethyl)-1,4-benzenediol	1	**unknown**
132	*unidentified 34*	1	*n/a*
133	*unidentified 35*	3	*n/a*
134	n-propyl acetate	4	estery, fruity, ethereal, banana, honey
135	isopentyl hexanoate	1	fruity, green, pineapple, waxy
136	n-dodecanoic acid	2	fatty, coconut, bay
137	*unidentified 36*	5	*n/a*
138	*unidentified 37*	1	*n/a*
139	2-methyl-1-butanol	1	ethereal, alcoholic, fatty, cocoa, whiskey, leathery
140	*unidentified 38*	1	*n/a*
141	dehydro-ar-ionene	3	licorice
142	n-hexadecane	1	**unknown**
143	tetradecane	1	mild, waxy
144	ethyl 9-decenoate	1	fruity, fatty
145	*unidentified 39*	1	*n/a*
146	ethyl hex-(2E)-enoate	5	fruity, green, sweet, juicy
147	α-calacorene	1	woody
148	*unidentified 40*	3	*n/a*
149	*unidentified 41*	1	*n/a*
150	*unidentified 42*	5	*n/a*
151	octanoic acid	5	rancid, soapy, cheesy, fatty, brandy
152	*unidentified 43*	1	*n/a*
153	4-methyl-pentan-1-ol	5	nutty
154	n-octyl acrylate	1	**unknown**
155	2-methyl-1-propanol	1	ethereal, fusel, whiskey
156	2-ethyl-1-hexanol	3	sweet, fatty, fruity
157	(2Z)-2-hexenyl acetate	2	**unknown**
158	*unidentified 44*	1	*n/a*
159	*unidentified 45*	1	*n/a*
160	*unidentified 46*	5	*n/a*
161	1,2,3-trimethylbenzene	1	**unknown**
162	butylated hydroxytoluene	2	phenolic, camphoreous
163	6-methyl-5-hepten-2-one	3	green, vegetable, musty, apple, banana, bean
164	*unidentified 47*	2	*n/a*
165	*unidentified 48*	5	*n/a*
166	*unidentified 49*	1	*n/a*
167	3-(methylthio)-1-propanol	1	meaty, onion, garlic, bouillon, sweet, soup
168	*unidentified 50*	4	*n/a*
169	*unidentified 51*	2	*n/a*
170	*unidentified 52*	4	*n/a*
171	*unidentified 53*	5	*n/a*
172	propyl octanoate	5	coconut, cocoa, cognac, winey, fatty
173	*unidentified 54*	1	*n/a*

174	ethyl palmitate	1	waxy, fruity, creamy, fermented, vanilla
175	*unidentified 55*	5	*n/a*
176	*unidentified 56*	1	*n/a*
177	*unidentified 57*	1	*n/a*
178	*unidentified 58*	4	*n/a*
179	*unidentified 59*	1	*n/a*
180	ethyl octanoate	4	sweet, waxy, fruity, pineapple, creamy, fatty
181	*unidentified 60*	5	*n/a*
182	*unidentified 61*	2	*n/a*
183	*unidentified 62*	1	*n/a*
184	acetic acid	3	pungent, sour, overripe fruit, vinegar
185	2-nonanol	5	waxy, soapy, musty, green, fruity, dairy
186	phenacyl formate	5	**unknown**
187	*unidentified 63*	5	*n/a*
188	ethyl acetate	1	ethereal, fruity, sweet, grape, cherry
189	ethyl 2-furoate	3	burnt
190	*unidentified 64*	1	*n/a*
191	2,3-dihydro-4,7-dimethyl-1H-indene	3	**unknown**
192	*unidentified 65*	4	*n/a*
193	*unidentified 66*	1	*n/a*
194	(2-aziridinylethyl)amine	4	**unknown**
195	ethyl stearate	5	mild, waxy
196	*unidentified 67*	1	*n/a*
197	tetrahydro-3,6-dimethyl-2H-pyran-2-one	5	**unknown**
198	cosmene	1	**unknown**
199	metaldehyde isomer IV	1	**unknown**
200	*unidentified 68*	2	*n/a*
201	*unidentified 69*	5	*n/a*
202	*unidentified 70*	2	*n/a*
203	*unidentified 71*	1	*n/a*
204	acetophenone	3	powdery, bitter almond, cherry, coumarinic, fruity
205	*unidentified 72*	5	*n/a*
206	neryl acetone	3	fatty, metallic
207	*unidentified 73*	5	*n/a*
208	*unidentified 74*	4	*n/a*
209	*unidentified 75*	5	*n/a*
210	*unidentified 76*	4	*n/a*
211	metaldehyde isomer I	1	**unknown**
212	*unidentified 77*	5	*n/a*
213	metaldehyde isomer II	1	**unknown**
214	*unidentified 78*	1	*n/a*
215	*unidentified 79*	1	*n/a*
216	*unidentified 80*	5	*n/a*
217	*unidentified 81*	4	*n/a*
218	*unidentified 82*	1	*n/a*
219	isopentyl alcohol	4	fusel, fermented, fruity, banana, ethereal, cognac
220	*unidentified 83*	3	*n/a*

The results of the one-way *ANOVA* for all 220 hits in the F-ratio hitlist are provided as a scatterplot in Fig. 5.6 A, with *p*-value plotted versus hit number. A *p*-value threshold of 0.01 is shown with a dashed red line, whereby hits with a *p*-value < 0.01 indicate that the mean peak areas are significantly different and hits with a *p*-value ≥ 0.01 that the mean peak areas are not significantly different at the 99% confidence level. Since 220 hits were identified, the 99% confidence level equates to ~2 analyte hits erroneously exhibiting wine-to-wine concentration differences, whereas the 95% confidence level equates to 11 hits. Thus, the 99% confidence level was applied to avoid inclusion of false positives more robustly, while still including a substantial number of true positives. Indeed, 187 hits fall below a *p*-value < 0.01 in Fig. 5.6 A
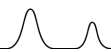
and can be deemed "true positive hits" (*i.e.*, class distinguishing), whereas the 33 hits which fall above the *p*-value cutoff can be considered "false positive hits" (*i.e.*, random noise and other background variation). Note that the first false positive (hit 133) occurs at an F-ratio of 55 and the last true positive (hit 213) occurs at an F-ratio of 6 (Fig. 5.6 A), so 54 true positives are intermingled with false positives at lower F-ratios. It is important to consider that the F-ratios in Table 5.1 and Table 5.2 were calculated using all 45 original peak areas in ChromaTOF Tile, whereby F-critical cutoffs at the 95% (*p*-value = 0.05) and 99% (*p*-value = 0.01) confidence levels equated to F-ratios of 2.6 and 3.8, respectively. Thus, simply applying either cut-off to the original ChromaTOF hitlist without off-line statistical analysis would have been problematic, as all 33 false positives would have been incorrectly deemed true positives. Using a large sample size of 45 samples, with 9 samples per class, led to an underestimation in *p*-values and a resulting overestimation in statistical significance, an effect that has been widely studied by statisticians and termed the "large sample size fallacy" in numerous research disciplines [50-53]. By applying an off-line *ANOVA* to the averaged peak areas, effectively reducing the total sample size from 45 to 15 peak areas for a given analyte hit, the F-values were recalculated and the new F-critical value of 6 at the 99% confidence level identified numerous false positives in the dataset. A receiver operating characteristic (ROC) curve using the true positive and false positive labels identified with off-line one-way *ANOVA* in Fig. 5.6 A is provided in Fig. 5.6 B, with the true positive rate (*i.e.*, sensitivity) plotted versus the false positive rate (*i.e.*, 1-specificity). The apparent "steps" in the ROC curve are indicative of intermingling of true and false positives, so the first false positive (hit 133) and last true positive (hit 213) are labeled accordingly. The area under the curve (AUC) was calculated to be 0.93. Note that AUC values range from 0.5 to 1, with an AUC of 1 indicating maximum classifying power for a given variable and an AUC of 0.5 (*i.e.*, a diagonal line with a slope of 1) equivalent to random chance decisions, meaning that a given variable has no classifying power. The AUC represents the probability of a given variable correctly distinguishing true and false positives [17, 26-28]. In this work, the variable being evaluated is a *p*-value threshold of 0.01. The large AUC of 0.93 indicates that a *p*-value threshold of 0.01 is highly accurate for distinguishing the statistically significant chemical differences

between the wines from superflous chemical signal, erroneous noise, and background variation. None the less, there is a 93% probability that the 33 hits with p-values $\geq$ 0.01 are false positives, so these hits should be excluded from further chemometric endeavors to distinguish these wines.
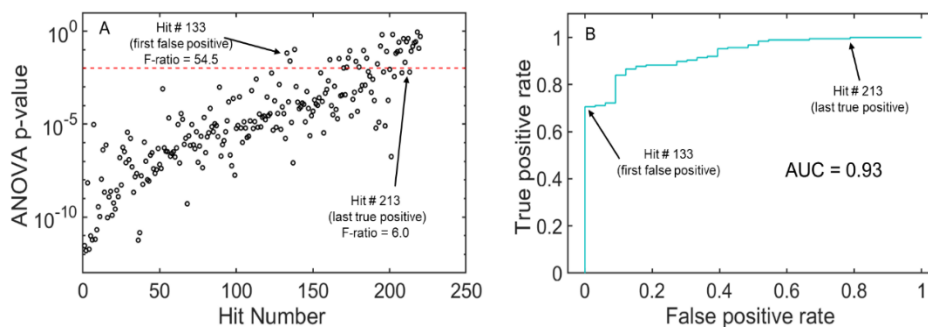
Figure 5.6. *(A) Results of an off-line one-way ANOVA applied to the averaged peak areas of the 220 hits identified via ChromaTOF tile analysis. (B) Receiver operating characteristic (ROC) curve prepared using the true and false positive labels obtained via one-way ANOVA in (A), with the first false positive (hit 133) and last true positive (hit 213) labeled.*

The resulting PCA scores plot using the average peak areas of the 187 true positive hits is provided in Fig. 5.7 A to serve as a visualization tool to highlight the performance of ChromaTOF Tile. It is important to note that 85.76% variance is captured along both PC axes, which is considerably greater than the 58.43% variance captured in the original PCA model using all 45 unfolded chromatograms. Furthermore, the averaged samples (3 per wine) now exhibit clustering by wine type in the PCA space, with minimal variation between the samples of a given wine cluster and no overlap between neighboring clusters (Fig. 5.7 A). Essentially, the workflow presented herein provides variable reduction; even though PCA itself is a dimensionality data reduction tool, variable reduction tools are often necessary to reduce noise and thus improve the discriminatory power of PCA models [54-56]. It is interesting to note that PC1 (64.50% variance) captures the chemical differences between wines 1 and the remaining wines 2-5, whereas PC2 (21.26% variance) captures the finer detail in the chemical differences between wines 2-5 themselves. The fact that PC1 accounts for ~ 40% more variance than PC2 reveals that, as was suggested by examining the top 30 hits in Table 5.1, wine 1 is highly "chemically unique" relative to the other wines.

Examination of the two-dimensional loadings plot in Fig. 5.7 B enables identification of which analyte peak areas contributed most significantly to the PCA model, wherein the blue circles represent the 187 true positive analyte hits. Since wine 1 is the only group with positive PC1 scores in Fig. 5.7 A, the five hits with highly positive PC1 loadings in Fig. 5.7 B (enclosed by the red circle) must be more highly concentrated in wine 1 relative to the other wines, effectively making these five hits signature compounds of wine 1. Similarly, based on their PC1 and PC2 loadings, hits 11 and 39 are signature compounds of wine 5 and wine 2, respectively. The fact that a large portion of the 187 hits, including hit 104, cluster around 0 in Fig. 5.7 B indicates that these hits contribute minimal variance to the PCA clustering of the wines. Thus, information about most of the analyte hits is not necessarily needed to quickly classify "unknown" samples of these wines, if such a need arose. However, the peak areas for all 187 hits have a *p*-value < 0.01, which indicates more subtle differences in concentration that are worth exploring for comprehensive fingerprinting purposes.
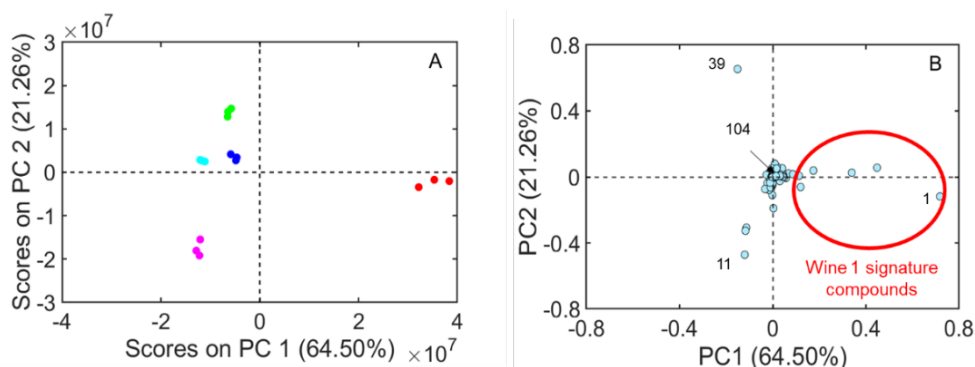
Figure 5.7. *Scores plot obtained from PCA of the peak areas of the 187 true positive hits. (B) Two-dimensional loadings plot.*

To explore this idea further, bar plots displaying the averaged peak areas of three highly loaded hits (hits 1, 11, and 39) and one lowly loaded hit (hit 104) are provided in Fig. 5.8, along with their chemical identities and one-way *ANOVA p*-values. Via examination of Fig. 5.8 A-C, it is obvious why ethyl trans-4-decenoate (hit 1), ethyl lactate (hit 11), and butyl alcohol (hit 39) have large loadings values in Fig. 5.7 B, as these compounds are highly concentrated in only one wine, namely wine 1, wine 5, and wine 2, respectively. Conversely, methyl 2-oxononanoate (Fig. 5.8 D) has a similar concentration in all of the wines, which is why it is lowly loaded on PC1 and

PC2 in Fig. 5.7 B. Thus, although methyl 2-oxononanoate is not one of the most notable signature volatiles in distinguishing the wines, its low *p*-value of 10^{-6} indicates that its higher concentration in wine 3 is indeed statistically significant (Fig. 5.8 D). These trace concentration differences are critically important to assess the overall chemical differences between the wines, such as their sensory profiles.
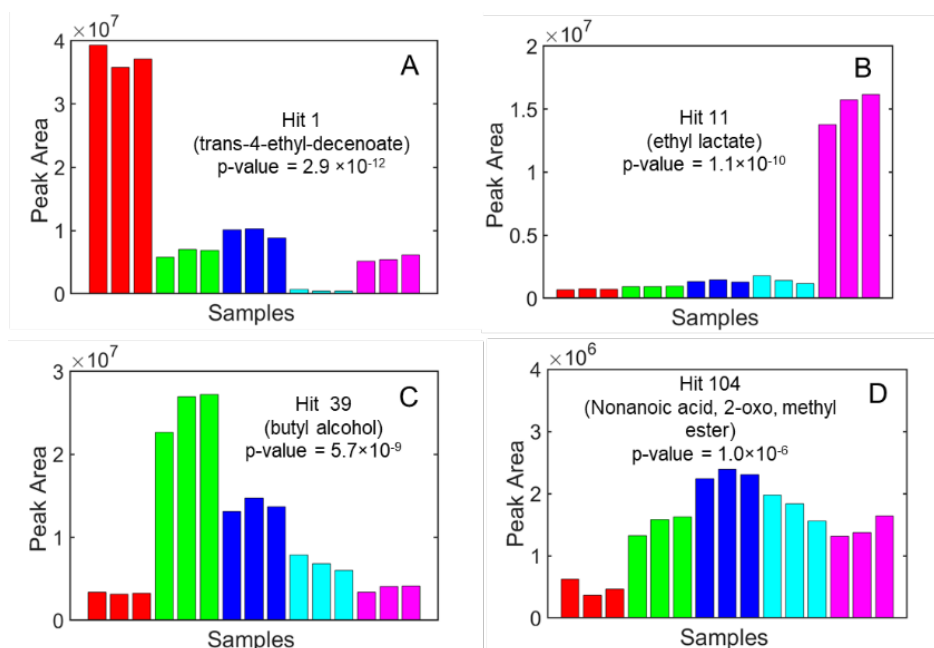
Figure 5.8. *Bar graphs displaying the averaged peak areas for (A) hit 1, (B) hit 11, ethyl lactate, (C) hit 39, and (D) hit 104.*

Of the 187 true positve hits identified herein, 90 analytes were the most highly concentrated (i.e., signature compounds) in wine 1; 24 analytes in wine 2; 21 analytes in wine 3; 7 analytes in wine 4; and 45 analytes in wine 5 (Table 5.2). Pie charts displaying the distributions of sensory descriptors for these signature compounds of each wine are provided in Fig. 5.9. It is important to note that Fig. 5.9 does not reflect quantitative concentrations of these signature compounds, but rather the relative proportions of signature compounds with certain flavor attributes. For example, of the 90 signature volatile compounds for wine 1, 19 compounds have been described as fruity; 14 as floral; and 14 as green, which is why these flavors are the largest "slices" for wine 1. Similarly, sweet (7/24), banana (5/24), and fruity (5/24) are the top flavor descriptors for wine 2; fruity (3/21) for wine 3; ethereal (3/7) and fruity (2/7) for wine 4; and fruity (12/45) and sweet (9/45) for wine 5. On a finer level, wine 3 is the only wine characterized by compounds with bacon flavor (4-

vinylguaiacol, hit 54 (Table 5.2)) and earthy/mushroom flavor (hit 74, 7-methylbenzofuran (Table 5.2)), while wine 5 has the highest proportion of compounds with creamy and related descriptions (i.e., cheesy, dairy, egg nog, etc.). Such a holistic assessment of the sensory characteristics of each wine is not possible using only the few highly loaded analytes identified with PCA in Fig. 5.7 B, which underscores the utility of the off-line one-way *ANOVA* performed herein. The combination of ChromaTOF Tile, followed by one-way *ANOVA* and PCA is a powerful workflow for enabling comprehensive fingerprinting and classification by wine type.
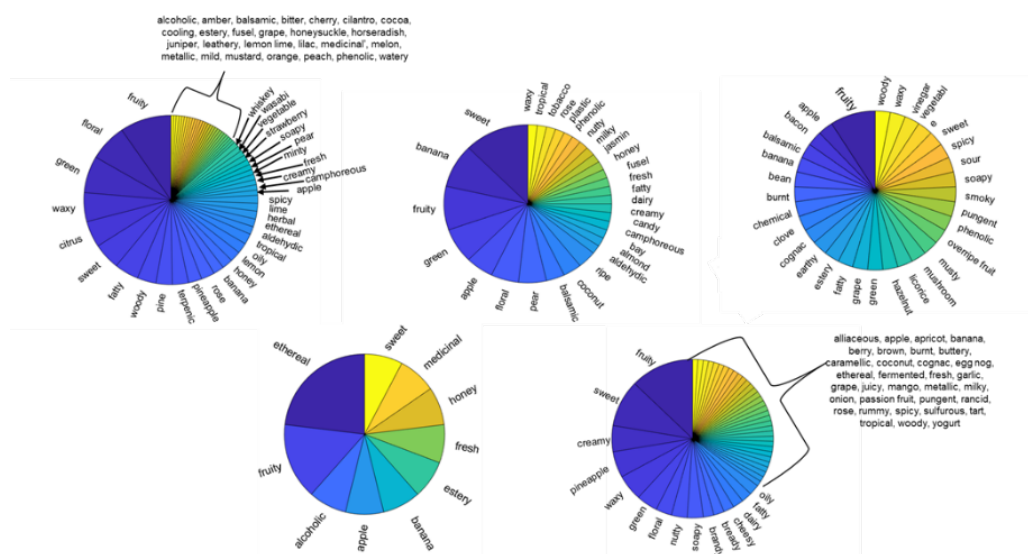
Figure 5.9. *Pie charts displaying the distribution of sensory descriptors for the analytes with the highest concentrations in Wines 1-5, with a p-value < 0.01 (wine 1, 90 analytes; wine 2, 24 analytes; wine 3, 21 analytes; wine 4, 7 analytes; wine 5, 45 analytes).*

5.4 Conclusions

Chromatographic fingerprinting through HS SPME coupled with FM GC×GC-TOFMS has demonstrated to be a valuable tool to characterize geographical-based differences in the volatilome of five white "Grillo" wines. A fast FM GC×GC approach was developed following, a supervised chemometric approach was carried out, exploiting the ChromaTOF Tile software, to elucidate the chemical differences between the wines. Of the 220 hits, 187 hits were discovered to be true positive, "class-distinguishing" hits via an off-line one-way ANOVA p-value threshold of

0.01, the validity of which was verified via a ROC curve. PCA using the average peak areas of the 187 true positive hits showed distinct clustering of the wines according to geographical origin in the scores plot, but only a handful of analytes were highly loaded and thus needed for classification purposes. The wines have distinct flavor profiles which would have been overlooked using only the most highly loaded analytes in PCA. Such sensory information may be critically important to winemakers looking to optimize their vinification process and/or experiment with new flavor profiles. Additional work to this end could include correlating geographical information (i.e., altitude, soil conditions, etc.) with GC×GC-TOFMS signatures, or even building complex neural networks to distinguish highly similar wines according to trace volatile concentrations. Thus, the work performed herein highlights the utility of the new ChromaTOF Tile software, both as a standalone supervised method and as a feature selection tool prior to additional chemometric/machine learning endeavors.

References

[1] S.E. Prebihalo, K.L. Berrier, C.E. Freye, H.D. Bahaghighat, N.R. Moore, D.K. Pinkerton, R.E. Synovec, Multidimensional Gas Chromatography: advances in

Instrumentation, Chemometrics, and Applications, Anal (2017), doi: 10.1021/ acs.analchem.7b04226.

[2] P.E. Sudol, K.M. Pierce, S.E. Prebihalo, K.J. Skogerboe, B.W. Wright, R.E. Synovec, Development of gas chromatographic pattern recognition and classification tools for compliance and forensic analyses of fuels: a review, Anal. Chim. Acta 1132 (2020) 157–186, doi: 10.1016/j.aca.2020.07.027.

[3] F. Stilo, C. Bicchi, A.M. Jimenez-Carvelo, L. Cuadros-Rodriguez, S.E. Reichenbach, C. Cordero, Chromatographic fingerprinting by comprehensive two-dimensional chromatography: fundamentals and tools, TrAC Trends Anal. Chem. 134 (2021) 116133, doi: 10.1016/j.trac.2020.116133.

[4] F. Stilo, C. Bicchi, A. Robbat, S.E. Reichenbach, C. Cordero, Untargeted approaches in food-omics: the potential of comprehensive two-dimensional gas chromatography/mass spectrometry, TrAC Trends Anal. Chem. 135 (2021) 116162, doi: 10.1016/j.trac.2020.116162.

[5] L.T. Vaz-Freire, M.D.R.G. da Silva, A.M.C. Freitas, Comprehensive two-dimensional gas chromatography for fingerprint pattern recognition in olive oils produced by two different techniques in Portuguese olive varieties Galega Vulgar, Cobrançosa e Carrasquenha, Anal. Chim. Acta 633 (2009) 263–270, doi: 10.1016/j.aca.2008.11.057.

[6] E.M. Humston, J.D. Knowles, A. McShea, R.E. Synovec, Quantitative assessment of moisture damage for cacao bean quality using two-dimensional gas chromatography combined with time-of-flight mass spectrometry and chemometrics, J. Chromatogr. A 1217 (2010) 1963–1970, doi: 10.1016/j.chroma.2010.01.069.

[7] J.E. Welke, M. Zanus, M. Lazzarotto, F.H. Pulgati, C.A. Zini, Main differences between volatiles of sparkling and base wines accessed through comprehensive two dimensional gas chromatography with time-of-flight mass spectrometric detection and chemometric tools, Food Chem 164 (2014) 427–437, doi: 10.1016/j.foodchem.2014.05.025.

[8] R. Costa, C. Fanali, G. Pennazza, L. Tedone, L. Dugo, M. Santonico, D. Sciarrone, F. Cacciola, L. Cucchiarini, M. Dachà, L. Mondello, Screening of volatile

compounds composition of white truffle during storage by GCxGC-(FID/MS) and gas sensor array analyses, LWT - Food Sci. Technol. 60 (2015) 905–913, doi: 10.1016/j.lwt.2014.09.054.

[9] S. Carlin, U. Vrhovsek, P. Franceschi, C. Lotti, L. Bontempo, F. Camin, D. Toubiana, F. Zottele, G. Toller, A. Fait, F. Mattivi, Regional features of northern Italian sparkling wines, identified using solid-phase micro extraction and comprehensive two-dimensional gas chromatography coupled with time-of-flight mass spectrometry, Food Chem 208 (2016) 68–80, doi: 10.1016/j. foodchem.2016.03.112.

[10] P.-.H. Stefanuto, K.A. Perrault, L.M. Dubois, B. L'Homme, C. Allen, C. Loughnane, N. Ochiai, J.-.F. Focant, Advanced method optimization for volatile aroma pro- filing of beer using two-dimensional gas chromatography time-of-flight mass spectrometry, J. Chromatogr. A 1507 (2017) 45–52, doi: 10.1016/j.chroma.2017. 05.064.

[11] J.M. Muñoz-Redondo, M.J. Ruiz-Moreno, B. Puertas, E. Cantos-Villar, J.M. Moreno-Rojas, Multivariate optimization of headspace solid-phase microextraction coupled to gas chromatography-mass spectrometry for the analysis of terpenoids in sparkling wines, Talanta 208 (2020) 120483, doi: 10.1016/j.talanta.2019.120483.

[12] F. Stilo, M. del, P. Segura borrego, C. Bicchi, S. Battaglino, R.M. Callejón fernadez, M.L. Morales, S.E. Reichenbach, J. Mccurry, D. Peroni, C. Cordero, Delineating the extra-virgin olive oil aroma blueprint by multiple headspace solid phase microextraction and differential-flow modulated comprehensive two-dimensional gas chromatography, J. Chromatogr. A 1650 (2021) 462232, doi: 10.1016/j.chroma.2021.462232.

[13] F. Stilo, E. Liberto, N. Spigolon, G. Genova, G. Rosso, M. Fontana, S.E. Reichenbach, C. Bicchi, C. Cordero, An effective chromatographic fingerprinting work- flow based on comprehensive two-dimensional gas chromatography –Mass spectrometry to establish volatiles patterns discriminative of spoiled hazelnuts (Corylus avellana L, Food Chem 340 (2021) 128135, doi: 10.1016/j.foodchem. 2020.128135.

[14] B. Mendes, J. Gonçalves, J.S. Câmara, Effectiveness of high-throughput miniaturized sorbent- and solid phase microextraction techniques combined with gas chromatography–mass spectrometry analysis for a rapid screening of volatile and semi-volatile composition of wines—A comparative study, Talanta 88 (2012) 79–94, doi: 10.1016/j.talanta.2011.10.010.

[15] T. Ilc, D. Werck-Reichhart, N. Navrot, Meta-analysis of the core aroma components of grape and wine aroma, Front. Plant Sci. 7 (2016) 1472, doi: 10.3389/ fpls.2016.01472.

[16] J.V. Seeley, N.E. Schimmel, S.K. Seeley, The multi-mode modulator: a versa- tile fluidic device for two-dimensional gas chromatography, J. Chromatogr. A (2017), doi: 10.1016/j.chroma.2017.06.030.

[17] B.C. Reaser, B.W. Wright, R.E. Synovec, Using receiver operating characteristic curves to optimize discovery-based software with comprehensive two-dimensional gas chromatography with Time-of-flight mass spectrometry, Anal. Chem. 89 (2017) 3606–3612, doi: 10.1021/acs.analchem.6b04991.

[18] L.C. Marney, W. Christopher Siegler, B.A. Parsons, J.C. Hoggard, B.W. Wright, R.E. Synovec, Tile-based Fisher-ratio software for improved feature selection analysis of comprehensive two-dimensional gas chromatography–time- of- flight mass spectrometry data, Talanta 115 (2013) 887–895, doi: 10.1016/j. talanta.2013.06.038. [19] B.A. Parsons, L.C. Marney, W.C. Siegler, J.C. Hoggard, B.W. Wright, R.E. Synovec, Tile-Based Fisher Ratio Analysis of Comprehensive Two-Dimensional Gas Chromatography Time-of-Flight Mass Spectrometry (GC ×GC–TOFMS) data using a null distribution approach, anal. chem. 87 (2015) 3812– 3819, doi: 10.1021/ ac504472s.

[20] N.E. Watson, B.A. Parsons, R.E. Synovec, Performance evaluation of tile-based Fisher Ratio analysis using a benchmark yeast metabolome dataset, J. Chromatogr. A 1459 (2016) 101–111, doi: 10.1016/j.chroma.2016.06.067.

[21] G.S. Ochoa, S.E. Prebihalo, B.C. Reaser, L.C. Marney, R.E. Synovec, Statistical inference of mass channel purity from Fisher ratio analysis using comprehensive

two-dimensional gas chromatography with time of flight mass spectrometry data, J. Chromatogr. A 1627 (2020) 461401, doi: 10.1016/j.chroma.2020. 461401.

[22] S.E. Prebihalo, G.S. Ochoa, K.L. Berrier, K.J. Skogerboe, K.L. Cameron, J.R. Trump, S.J. Svoboda, J.K. Wickiser, R.E. Synovec, Control-normalized fisher ratio analysis of comprehensive two-dimensional gas chromatography time-of-flight mass spectrometry data for enhanced biomarker discovery in a metabolomic study of orthopedic Knee-Ligament injury, Anal. Chem. 92 (2020) 15526–15533, doi: 10.1021/acs.analchem.0c03456.

[23] P.E. Sudol, G.S. Ochoa, R.E. Synovec, Investigation of the limit of discovery using tile-based Fisher ratio analysis with comprehensive two-dimensional gas chromatography time-of-flight mass spectrometry, J. Chromatogr. A 1644 (2021) 462092, doi: 10.1016/j.chroma.2021.462092.

[24] C.N. Cain, P.E. Sudol, K.L. Berrier, R.E. Synovec, Development of variance rank initiated-unsupervised sample indexing for gas chromatography-mass spectrometry analysis, Talanta 233 (2021) 122495, doi: 10.1016/j.talanta.2021. 122495.

[25] R.M. Heiberger, E. Neuwirth, R Through Excel, Springer New York, New York, NY, 2009, doi: 10.1007/978- 1- 4419- 0052- 4.

[26] C.D. Brown, H.T. Davis, Receiver operating characteristics curves and related decision measures: a tutorial, Chemom. Intell. Lab. Syst. 80 (2006) 24–38, doi: 10.1016/j.chemolab.20 05.05.0 04.

[27] J. Yin, J. Xie, X. Guo, L. Ju, Y. Li, Y. Zhang, Plasma metabolic profiling analysis of cyclophosphamide-induced cardiotoxicity using metabolomics coupled with UPLC/Q-TOF-MS and ROC curve, J. Chromatogr. B 1033–1034 (2016) 428–435, doi: 10.1016/j.jchromb.2016.08.042.

[28] I. Ruisánchez, A.M. Jiménez-Carvelo, M.P. Callao, ROC curves for the optimization of one-class model parameters. A case study: authenticating extra virgin olive oil from a Catalan protected designation of origin, Talanta 222 (2021) 121564, doi: 10.1016/j.talanta.2020.121564.

[29] G. Ivosev, L. Burton, R. Bonner, Dimensionality reduction and visualization in principal component analysis, Anal. Chem. 80 (2008) 4 933–4 944, doi: 10.1021/ ac800110w.

[30] R.A. van den, H.C. Berg, J.A. Hoefsloot, A.K. Westerhuis, M.J. Smilde, van der Werf, Centering, scaling, and transformations: improving the biological information content of metabolomics data, BMC Genomics 7 (2006) 142, doi: 10. 1186/1471-2164-7-142.

[31] I. Aloisi, B. Giocastro, A. Ferracane, T.M.G. Salerno, M. Zoccali, P.Q. Tranchida, L. Mondello, Preliminary observations on the use of a novel low duty cycle flow modulator for comprehensive two-dimensional gas chromatography, J. Chromatogr. A 1643 (2021) 462076, doi: 10.1016/j.chroma.2021.462076.

[32] S. Schöneich, T.J. Trinklein, C.G. Warren, R.E. Synovec, A systematic investigation of comprehensive two-dimensional gas chromatography time-of-flight mass spectrometry with dynamic pressure gradient modulation for high peak capacity separations, Anal. Chim. Acta 1134 (2020) 115–124, doi: 10.1016/j.aca. 2020.08.023.

[33] M.S. Klee, J. Cochran, M. Merrick, L.M. Blumberg, Evaluation of conditions of comprehensive two-dimensional gas chromatography that yield a near- theoretical maximum in peak capacity gain, J. Chromatogr. A 1383 (2015) 151–159, doi: 10.1016/j.chroma.2015.01.031.

[34] The Good Scents Company - Flavor, Fragrance, Food and Cosmetics Ingredients information, Good Scents Co. (n.d.) (2021) http://www.thegoodscentscompany.com/(accessed August 23.

[35] E. Paula Barros, N. Moreira, G. Elias Pereira, S.G.F. Leite, C. Moraes Rezende, P. Guedes de Pinho, Development and validation of automatic HS-SPME with a gas chromatography-ion trap/mass spectrometry method for analysis of volatiles in wines, Talanta 101 (2012) 177–186, doi: 10.1016/j.talanta.2012.08. 028.

[36] E. Campo, V. Ferreira, A. Escudero, J. Cacho, Prediction of the wine sensory properties related to grape variety from dynamic-headspace gas chromatography

−olfactometry data, J. Agric. Food Chem. 53 (2005) 5682–5690, doi: 10.1021/jf047870a.

[37] S.-.T. Chin, G.T. Eyres, P.J. Marriott, Identification of potent odourants in wine and brewed coffee using gas chromatography-olfactometry and comprehensive two-dimensional gas chromatography, J. Chromatogr. A 1218 (2011) 7487–7498, doi: 10.1016/j.chroma.2011.06.039.

[38] J.E. Welke, M. Zanus, M. Lazzarotto, C. Alcaraz Zini, Quantitative analysis of headspace volatile compounds using comprehensive two-dimensional gas chromatography and their contribution to the aroma of Chardonnay wine, Food Res. Int. 59 (2014) 85–99, doi: 10.1016/j.foodres.2014.02.002.

[39] A.L. Robinson, P.K. Boss, H. Heymann, P.S. Solomon, R.D. Trengove, Development of a sensitive non-targeted method for characterizing the wine volatile profile using headspace solid-phase microextraction comprehensive two-dimensional gas chromatography time-of-flight mass spectrometry, J. Chromatogr. A 1218 (2011) 504–517, doi: 10.1016/j.chroma.2010.11.008.

[40] G. Dugo, F.A. Franchina, M.R. Scandinaro, I. Bonaccorsi, N. Cicero, P.Q. Tranchida, L. Mondello, Elucidation of the volatile composition of Marsala wines by using comprehensive two-dimensional gas chromatography, Food Chem 142 (2014) 262–268, doi: 10.1016/j.foodchem.2013.07.061.

[41] K.P. Nicolli, A.C.T. Biasoto, É.A. Souza-Silva, C.C. Guerra, H.P. dos Santos, J.E. Welke, C.A. Zini, Sensory, olfactometry and comprehensive two- dimensional gas chromatography analyses as appropriate tools to characterize the effects of vine management on wine aroma, Food Chem 243 (2018) 103–117, doi: 10.1016/j.foodchem.2017.09.078.

[42] B.T. Weldegergis, A. de Villiers, C. McNeish, S. Seethapathy, A. Mostafa, T. Górecki, A.M. Crouch, Characterisation of volatile components of Pinotage wines using comprehensive two-dimensional gas chromatography coupled to time-of-flight

mass spectrometry (GC ×GC–TOFMS), Food Chem 129 (2011) 188–199, doi: 10.1016/j.foodchem.2010.11.157.

[43] K. Furdíková, L. Bajnociová, F. Malík, I. Špánik , Investigation of volatile profile of varietal Gewürztraminer wines using two-dimensional gas chromatography, J. Food Nutr. Res. 56 (2017) 73–85.

[44] M. Salinas, A. Zalacain, F. Pardo, G.L. Alonso, Stir Bar Sorptive extraction applied to volatile constituents evolution during Vitis vinifera ripening, J. Agric. Food Chem. 52 (2004) 4 821–4 827, doi: 10.1021/jf040040c.

[45] R. López, M. Aznar, J. Cacho, V. Ferreira, Determination of minor and trace volatile compounds in wine by solid-phase extraction and gas chromatography with mass spectrometric detection, J. Chromatogr. A 966 (2002) 167–177, doi: 10.1016/S0 021-9673(02)0 0696-9.

[46] J.E. Welke, V. Manfroi, M. Zanus, M. Lazzarotto, C. Alcaraz Zini, Differentiation of wines according to grape variety using multivariate analysis of comprehensive two-dimensional gas chromatography with time-of-flight mass spectrometric detection data, Food Chem 141 (2013) 3897–3905, doi: 10.1016/j. foodchem.2013.06.100.

[47] M. Del Carlo, A. Pepe, G. Sacchetti, D. Compagnone, D. Mastrocola, A. Cichelli, Determination of phthalate esters in wine using solid-phase extraction and gas chromatography–mass spectrometry, Food Chem 111 (2008) 771–777, doi: 10. 1016/j.foodchem.2008.04.065.

[48] H. Chen, H. Gao, X. Fang, L. Ye, Y. Zhou, H. Yang, Effects of allyl isothiocyanate treatment on postharvest quality and the activities of antioxidant enzymes of mulberry fruit, Postharvest Biol. Technol. 108 (2015) 61–67, doi: 10.1016/j. postharvbio.2015.05.011.

[49] B. Yang, L. Li, H. Geng, C. Zhang, G. Wang, S. Yang, S. Gao, Y. Zhao, F. Xing, Inhibitory effect of allyl and benzyl isothiocyanates on ochratoxin a producing fungi in grape and maize, Food Microbiol 100 (2021) 103865, doi: 10.1016/j.fm. 2021.103865.

[50] B. Lantz, The large sample size fallacy, Scand. J. Caring Sci. 27 (2013) 487–492, doi: 10.1111/j.1471-6712.2012. 01052.x.

[51] J.W. Tukey, The philosophy of multiple comparisons, Stat. Sci. 6 (1991) 100–116 https://www.jstor.org/stable/2245714 (accessed August 6, 2021).

[52] L. Held, M. Ott, How the maximal evidence of P-Values against point null hypotheses depends on sample size, Am. Stat. 70 (2016) 335–341, doi: 10.1080/00031305.2016.1209128

[53] R.G. Brereton, P values and multivariate distributions: non-orthogonal terms in regression models, Chemom. Intell. Lab. Syst. 210 (2021) 104264, doi: 10.1016/j.chemolab.2021.104264 .

[54] B. Xiao, Y. Li, B. Sun, C. Yang, K. Huang, H. Zhu, Decentralized PCA modeling based on relevance and redundancy variable selection and its application to large-scale dynamic process monitoring, Process Saf. Environ. Prot. 151 (2021) 85–100, doi: 10.1016/j.psep.2021.04.043.

[55] V.E. de Almeida, D.D. de Sousa Fernandes, P.H.G.D. Diniz, A. de Araújo Gomes, G. Véras, R.K.H. Galvão, M.C.U. Araujo, Scores selection via Fisher's discriminant power in PCA-LDA to improve the classification of food data, Food Chem 363 (2021) 130296, doi: 10.1016/j.foodchem.2021.130296.

[56] H. Yamamoto, H. Yamaji, Y. Abe, K. Harada, D. Waluyo, E. Fukusaki, A. Kondo, H. Ohno, H. Fukuda, Dimensionality reduction for metabolome data using PCA, PL S, OPL S, and RFDA with differential penalties to latent variables, Chemom. Intell. Lab. Syst. 98 (2009) 136–142, doi: 10.1016/j.chemolab.2009.05.006.

Chapter 6
Flow-modulated comprehensive two-dimensional gas chromatography combined with time-of-flight mass spectrometry: use of hydrogen as a more sustainable alternative to helium[*]

The present research is focused on the use and evaluation of hydrogen, as a more sustainable alternative to helium, within the context of fast flow-modulation comprehensive two-dimensional gas chromatography-time-of-flight mass spectrometry. All experiments were carried out by using the following column set: low polarity with dimensions 10 m × 0.25 mm ID × 0.25 μm d_f and medium polarity with dimensions 2 m × 0.10 mm ID × 0.10 μm d_f. Fundamental gas chromatography parameters were measured under different experimental conditions, using the two carrier gases. Efficiency was measured in both the first and second dimensions, using a probe compound under isothermal conditions; after defining the optimum carrier gas conditions, a mixture containing 20 pesticides was analysed to measure resolution, again in the first and second dimension, using a temperature program. It was found that a similar chromatography performance can be attained when using hydrogen, albeit with a circa 25% reduction in analysis time. Signal-to-noise ratios of the pesticides were calculated, using both carrier gases, with such values generally reduced (on average by 14%) when using hydrogen. Finally, a comparison was made between mass spectral profiles obtained analysing the pesticides and fatty acid methyl esters using the two mobile phases. Even though mass spectral differences were observed, the ion profiles can be considered as generally similar.

6.1 Introduction

Fast gas chromatography (GC) analyses provide clear advantages compared to conventional GC analyses, such as decreased operational costs and an enhanced laboratory throughput [1]. The use of H_2 as carrier gas offers important advantages over He, in particular in terms of speed. In fact, under optimum gas flow conditions, H_2 GC can provide an altogether similar chromatography performance compared to He GC, in a shorter time [2].

Helium is the most popular carrier gas due to its safety, inertness, and purity; however, in recent years, the natural availability of He has decreased. Apart from GC separation speed, a further advantage of H_2 consists in a lower economical cost due to the possibility to use generators [3,4]; therefore, there is no necessity to transport gas cylinders. Such factors are certainly positive, in relation to a reduced environmental impact.

In the field of GC combined with mass spectrometry (GC-MS), the use of H_2 as carrier gas, instead of He, has been investigated. For example, H_2 GC-MS was used by Muñoz-Guerra *et al.* for the analysis of steroids: increased resolution, in a reduced analysis time, was observed [3]. However, a reduction of the vacuum level, an increase in the background noise, and a modification of the spectral profiles were also observed. In a further study, Nnaji *et al.* used H_2 GC-MS for the analysis of illicit drugs and explosives [4]. In this case, the authors showed that H_2 was an effective replacement for He as carrier gas, considering the similarity of the spectral profiles attained.

In the field of comprehensive two-dimensional gas chromatography, combined with mass spectrometry (GC×GC-MS), no in-depth studies involving the use of H_2 have been. On the other hand, when using GC×GC combined with a flame ionization detector, the use of H_2 as carrier gas has been historically the prime choice, due to the inherent characteristics of the second-dimension separations (usually very fast, on 1-2 m segments of a 0.1 mm ID column) [5,6].

A "fast" FM GC×GC-time-of-flight mass spectrometry (ToFMS) method, using He as carrier gas, was developed to increase the modulator duty cycle. In the present research, the same low-duty-cycle FM was employed, under fast GC×GC-ToFMS conditions, using He and H_2 as carrier gases. Fundamental GC parameters were

measured in both dimensions under different experimental conditions, obtaining detailed information related to method optimization. Additionally, a comparison was made between signal-to-noise ratios (*S/N*), measured after analyzing a mixture of pesticides. Finally, He and H_2 mass spectral databases involving pesticide and fatty acid methyl ester (FAME) mixtures were constructed, and He experimental spectra were searched against H_2 database ones, and *vice versa*.

6.2 Experimental

Chemicals and sample preparation

The C_{12} *n*-alkane, naphthalene, C37 fatty acid methyl ester mixture and solvents (*n*-hexane and acetonitrile) were kindly provided by Merck Life Science (Merck KGaA, Darmstadt, Germany). A solution of C_{12} *n*-alkane was prepared in *n*-hexane at the 10 μg mL^{-1} level. The naphthalene solution was prepared in acetonitrile at a concentration level of 100 μg mL^{-1}. The FAMEs solution was injected neat; the FAME concentrations were in the following range: 200-600 μg mL^{-1}. GC Multiresidue Pesticide Standard #2 was acquired from Restek Corporation (Bellefonte, USA), to obtain a solution containing 20 pesticides at a concentration level of 20 μg mL^{-1}.

Instrumentation

The GC×GC-ToFMS applications were performed on a Pegasus® BT 4D GC×GC-ToFMS system equipped with a flow modulation system Flux™ (LECO, Mönchengladbach, Germany). The GC×GC column set was: an SLB-5ms [silphenylene polymer with similar polarity to poly(5% diphenyl/95% dimethyl siloxane)] with dimensions 10 m × 0.25 mm ID × 0.25 μm d_f was employed as ^{1}D column, while the ^{2}D column was an SLB-35ms [silphenylene polymer with similar polarity to poly(35% diphenyl/65% dimethyl siloxane)] with dimensions 2 m × 0.10 mm ID × 0.10 μm d_f (with 0.3 m located inside the MS transfer line). All columns were provided by Merck Life Science. All the applications were performed by using both He and H_2 as carrier gas. The C_{12} *n*-alkane applications were carried out under isothermal conditions (90°C) using the system in the mono-dimensional (1D) mode. The injection volume was 1 μL, using a split ratio of 1:20. A positive offset of 70°C

was applied to the ^{2}D column. The naphthalene applications were carried out at a ^{1}D column temperature of 95°C. The injection volume was 1 μL, using a split ratio of 1:20. A positive offset of 5°C was applied to the ^{2}D column; the modulation period (P_M) was 6.0 s, with a re-injection period of 0.08 s. The pesticide mixture was analyzed under the following conditions. In the 1D mode, the injection volume was 1 μL, using a split ratio of 1:20. The analysis performed with He as carrier gas was carried out using the following GC temperature program: 100°C to 290°C at 9°C min^{-1}. The GC temperature program using H$_2$ as a carrier gas was as follows: 100°C to 290°C at 12°C min^{-1}; the ^{2}D temperature for both methods: positive offset of 70°C. In the GC×GC mode, the injection volume was 1.2 μL using a split ratio of 1:5. The GC temperature programs were the same as in 1D mode, except for the ^{2}D temperature where the offset was +5°C. The P_M was set at 2 s, with a re-injection period of 0.08 s in both cases. The auxiliary pressure unit (EPC) provided a constant flow of 3.5 mL min^{-1} to the modulator. With regard to the MS conditions, the samples were analyzed using a mass range of 45-400 *m/z* (electron ionization was performed at 70 eV), with a spectral generation frequency of 5 Hz in the 1D mode, and 150 Hz in the GC×GC one. Transfer line and ion source temperatures were 250°C and 280°C, respectively. The vacuum pressure values were evaluated: $3.33×10^{-7}$ and $6.73×10^{-7}$ mbar were the observed values using He (flow: 0.60 mL min^{-1}) an H$_2$ (flow: 0.65 mL min^{-1}), respectively. In all cases, the vacuum levels were within the operational requirements. The mass spectral databases used were the Pesticides Library (Chromaleont s.r.l., Italy), and NIST/EPA/NIH Mass Spectral Library (NIST 17). An autotuning process was performed every time the gas flow conditions were modified. The only instrumental modification required to work with H$_2$ as carrier gas is the installation of a kit (provided by the instrumental company) consisting of a connection tube, seal gasket, and ferrules, between the caliper solution and the ion source.

6.3 Results and discussion

The main object of the research work was an in-depth evaluation of the GC×GC-ToFMS performances using two different carrier gases, namely He and H$_2$, with the latter being a more sustainable alternative. It is well known that an increase in the

analyte-gas diffusion coefficient will lead to an increase in the optimum column gas velocity [2]. In such a respect, H_2 is characterized by a higher analyte-gas diffusion coefficient compared to He. Moreover, under optimum gas velocity conditions both He and H_2 will provide the same/similar efficiency (in terms of minimum plate height). So, H_2-based GC analyses can be performed in a shorter time, while generating the same sort of chromatographic separation. In the following sections, the ^1D and ^2D average gas linear velocity values reported are those provided by the instrumental software.

First dimension results

Helium and hydrogen Golay curves, in relation to the low-polarity ^1D column, were constructed by analyzing C_{12} alkane (an apolar compound) at a ^1D temperature of 90°C (Figure 6.1 a-b).
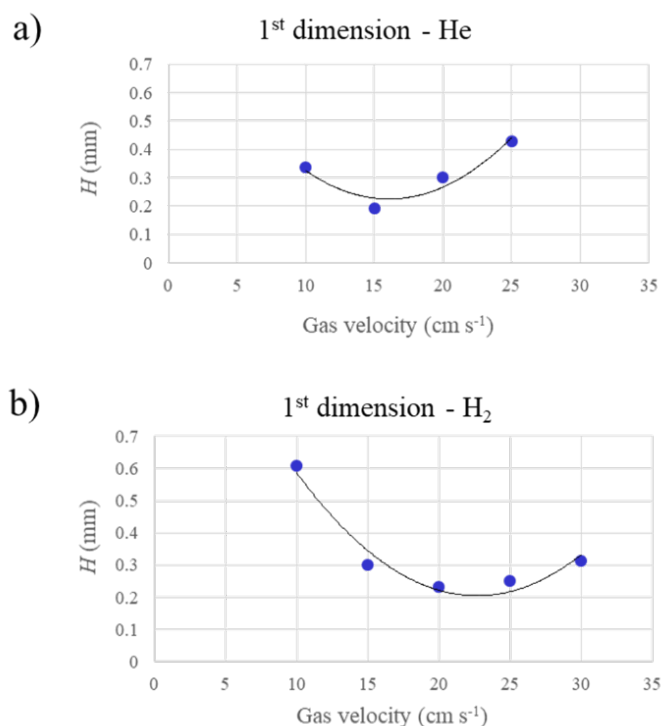
Figure 6.1. *He and H_2 Golay curves, in relation to the ^1D column.*

The retention factor (*k*) was approx. 7 (a value between 5 and 10 is herein considered as appropriate for this type of evaluation). The ^2D temperature was set rather high (160°C) to minimize the interaction of the probe analyte with the ^2D stationary phase. Three consecutive analyses were performed at each value of average linear

velocity. The He applications were performed at 10, 15, 20 and 25 cm s^{-1} (or column flows of 0.60, 1.35, 2.45 and 3.85 mL min^{-1}, respectively). The average plate height (*H*) and plate number (*N*) values are reported in Table 6.1: as can be readily seen, the lowest *H* value (0.209 mm) was attained at a gas velocity of 15 cm s^{-1} (dead time: 66.7 s), leading to an overall efficiency of just over 48,000 *N* [the peak width at half height (*w*$_h$) was 6.3 s].

As reported in previous research, the high ^{1}D pressure conditions (the main pressure drop occurs in the second column - pressure at mid-point was 285.44 kPa at the beginning of the analysis) will reduce the analyte-gas diffusion coefficient, and hence, optimum velocities are lower than in single-column GC [7].

Table 6.1. Theoretical average linear velocity (ALV) along with plate height (H), peak width at half height (w$_h$) and plate number (N), calculated by using both helium and hydrogen in the 1D mode (n = 3).

1D							
Helium				Hydrogen			
ALV (cm s^{-1})	*H* (mm)	*N*	*w*$_h$ (s)	ALV (cm s^{-1})	*H* (mm)	*N*	*w*$_h$ (s)
10	0.305	32946	12.2	10	0.612	16338	19.2
15	0.209	48165	6.3	15	0.278	36553	7.5
20	0.303	33024	5.5	20	0.231	43357	4.8
25	0.425	23550	5.3	25	0.249	40258	4.0
				30	0.317	31562	3.7

With regard to the H$_2$ applications, these were carried out at 10, 15, 20, 25 and 30 cm s^{-1} (or column flows of 0.30, 0.65, 1.20, 1.80 and 2.60 mL min^{-1}, respectively). The *H* and *N* values are listed in Table 6.1: as can be observed, the lowest *H* value (0.231 mm) was attained at a gas velocity of 20 cm s^{-1} (dead time: 50 s), leading to an overall efficiency of approx. 43,400 *N*. The *w*$_h$ value was 4.8 s. In consideration of the results obtained, it can be concluded that it is possible to shorten the ^{1}D analysis time when using H$_2$ by 25%, while maintaining a similar (albeit slightly lower) column efficiency.

Second dimension results

Helium and hydrogen Golay curves, in relation to the medium-polarity ^{2}D column, were constructed by analyzing naphthalene (a medium-polarity compound) at a ^{2}D

temperature of 100°C (Figure 6.2 a-b). The k value was approx. 6.5. The ^{1}D column temperature was 95°C.
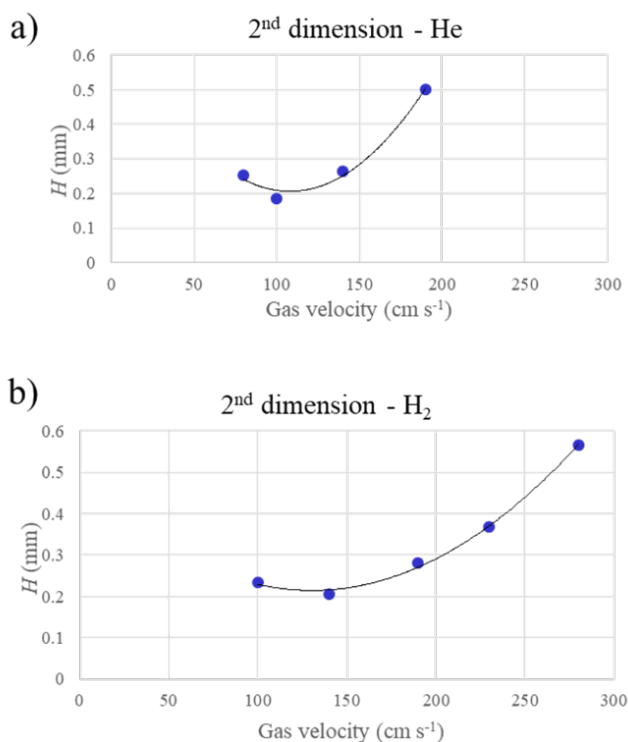
Figure 6.2. He and H$_2$ Golay curves, in relation to the ^{2}D column.

Three consecutive analyses were performed at each value of average linear velocity. The He applications were performed at 80, 100, 140 and 190 cm s^{-1} (or column flows of 0.48, 0.74, 1.46 and 2.70 mL min^{-1}, respectively). The average H and N values are reported in Table 6.2: the lowest H value (0.182 mm) was attained at a gas velocity of 100 cm s^{-1}, leading to an overall efficiency of approx. 11,000 N. The average w_h value was 204 ms.

With regard to the H$_2$ applications, these were carried out at 100, 140, 190, 230 and 280 cm s^{-1} (or column flows of 0.34, 0.66, 1.22, 1.79 and 2.65 mL min^{-1}, respectively). The H and N values are listed in Table 6.2: as can be observed, the lowest H value (0.193 mm) was attained at a gas velocity of 140 cm s^{-1}, leading to an overall efficiency of approx. 10,400 N. The average w_h value was 148 ms.

Table 6.2. *Theoretical average linear velocity along with plate height, peak width at half height and plate number, calculated by using both helium and hydrogen in the GC×GC mode (n = 3).*

2D							
Helium				Hydrogen			
ALV (cm s^{-1})	H (mm)	N	w_h (s)	ALV (cm s^{-1})	H (mm)	N	w_h (s)
80	0.236	8799	0.237	100	0.233	8569	0.226
100	0.182	10968	0.204	140	0.193	10379	0.149
140	0.266	7511	0.177	190	0.267	7499	0.130
190	0.493	4059	0.179	230	0.364	5498	0.125
				280	0.556	3600	0.128

Considering the 2 m × 0.10 μm d_f × 0.10 μm d_f ^{2}D column, minimum H values were higher than expected (≈ 0.100 mm). It can be speculated that there is some additional contribution towards band broadening during the modulation process.

Again, and in consideration of the results obtained, it can be concluded that it is possible to shorten the overall analysis time when using H_2, while maintaining a similar (albeit slightly lower) column efficiency.

GC×GC results and mass spectral profiles

At this point, temperature-programmed (unmodulated and GC×GC) analyses were performed on a mixture of 20 pesticides, by using He and H_2. The initial ^{1}D average gas velocities were optimum in each application (the instrument can be operated only under constant flow conditions): when using He, the initial gas velocity was 15 cm s^{-1} (100°C), while the end one was 17 cm s^{-1} (290°C); with regard to H_2, the initial gas velocity was 20 cm s^{-1}, while the end one was 22 cm s^{-1}. When a specific ^{1}D column flow is selected, considering the specific combination of columns, then the pressure at the modulator will be automatically set by the instrumental software, to enable proper modulation processes. The ^{2}D column flow is the same as the ^{1}D one. The only restriction related to the ^{1}D column flow is that it cannot exceed 3.5 mL min^{-1}. The temperature programs were normalized (10°C/^{1}D void time, considering the initial analysis conditions), to enable the same/similar analyte elution temperatures [8].

Unmodulated chromatograms, using He and H_2, are illustrated in Figure 6.3 a-b. A ^{2}D temperature offset of +70°C was used, to minimize the interactions of the pesticides with the ^{2}D stationary phase. If one considers the peak pairs 1/2, 3/4, and 5/6 (identities are reported in the figure legend), then average resolution values (n = 3) are 2.8, 4.0, and 1.8, respectively, in the He analysis, and 2.9, 4.2, and 2.5, respectively, in the H_2 analysis. Consequently, resolution was in general better in the H_2 chromatogram, especially in its later parts. The reason for such a performance can be related to the range of ^{1}D average gas velocities, nearer to the optimum value (Figure 6.1 a-b) in the H_2 (20-22 cm s^{-1}) analysis (the H_2 Golay curve rises less rapidly), with respect to the He one (15-17 cm s^{-1}).
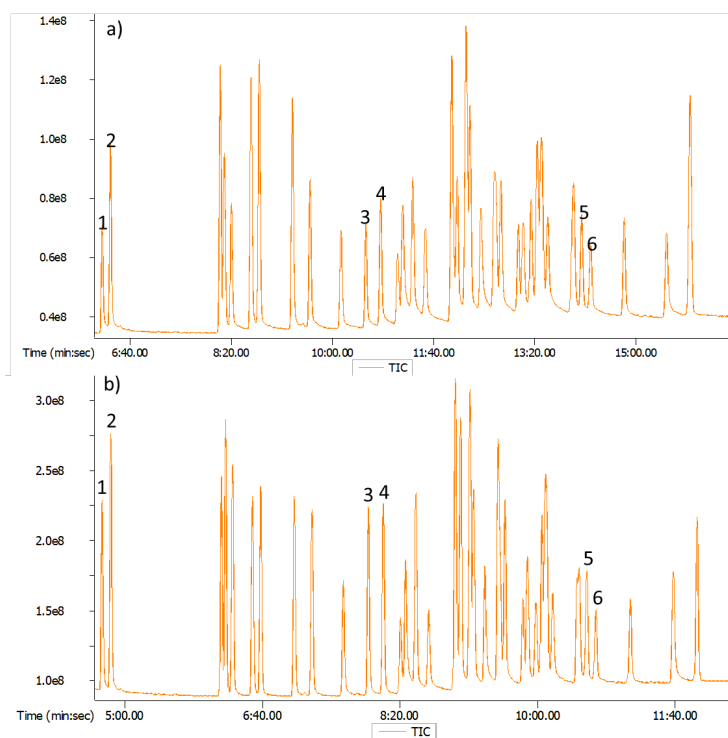
Figure 6.3. *Unmodulated GC×GC-ToFMS chromatograms on a mixture of 20 pesticides, using He (a) and H_2 (b) as carrier gas. Peak identification: 1. chloroneb; 2. pentachlorobenzene; 3. pentachlorothioanisole; 4. aldrin; 5. 4,4'-DDT; 6. Methoxychlor.*

It is noteworthy that the (total ion current) peak profiles are, in places across the chromatograms, dissimilar (e.g., see the three peaks eluting after compound 2). This, presumably due to different ionization efficiencies of specific pesticides when using the two carrier gases.

The GC×GC chromatograms related to the He and H_2 analyses, are illustrated in Figure 6.4. With regard to the ^2D average gas velocities (the ^1D average gas velocities are those reported above), when using He, the initial gas velocity was 122 cm s^{-1} (105°C - a +5°C offset was applied), while the end one was 147 cm s^{-1} (295°C); with regard to H_2, the initial gas velocity was 164 cm s^{-1}, while the end one was 198 cm s^{-1}. Consequently, in both cases the ^2D gas velocities were always higher than the optimum values.
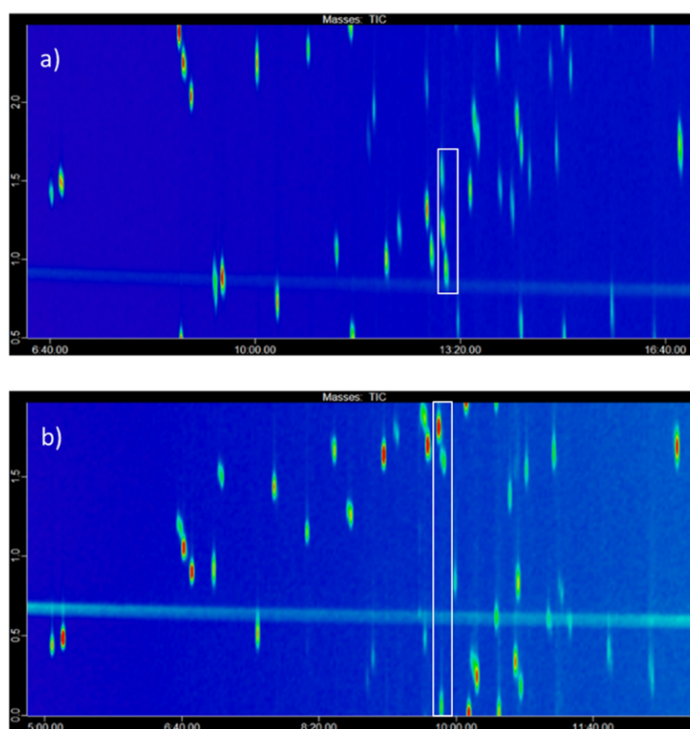
Figure 6.4. *Total-ion-current GC×GC-ToFMS chromatograms related to the He (a) and H_2 analyses.*

To make a direct comparison between the two chromatography performances was not a straightforward task. However, a triple ^1D co-elution (resolved on the second column) occurred at around 13 min in the He analysis, involving *tr*-nonachlor (peak 1), *cis*-chlorane (peak 2) and endosulfan (peak 3). Considering a single analysis in the second dimension (at approx. 217°C), involving the three analytes, this occurred at a gas velocity of 139 cm s^{-1}. Considering the ^2D He Golay curve, an average *H* value of 0.267 mm was attained at a gas velocity of 140 cm s^{-1} (Table 6.2). With regard to the GC×GC H_2 analysis, the three compounds were analyzed on the ^2D compound at a temperature again of approx. 217°C, and at a gas velocity of 187 cm

s^{-1}. Considering the ^{2}D H_2 Golay curve, again an average H value of 0.267 mm was attained, this time at a gas velocity of 190 cm s^{-1} (Table 6.2).

So, in principle, the same/similar chromatography performances should be attained on the ^{2}D column. In such a respect, resolution values between peaks 1-2, 1-3, and 2-3 were 1.0, 2.3, and 1.4 (respectively) in the He analysis, and 0.9, 2.1, and 1.3 in the H_2 one (Figure 6.5).
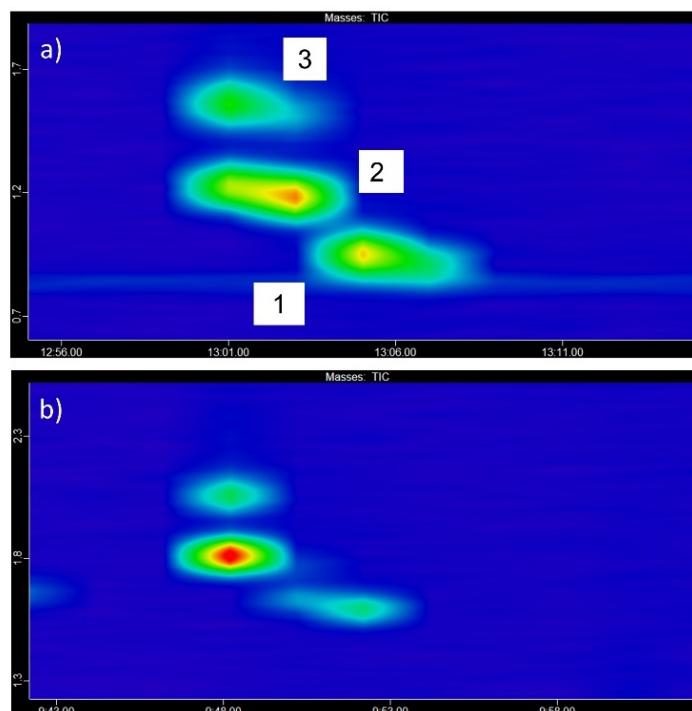
Figure 6.5. *GC×GC-ToFMS chromatogram expansions related to the analysis of a mixture of 20 pesticides, using He (a) and H_2 (b) as carrier gas. Peak identification: 1. trans-nonachlor; 2. cis-chlorane; 3. endosulfan.*

A comparison between the GC×GC-ToFMS responses of the pesticides, when using the two carrier gases, was made by considering the *S/N* values of each analyte when extracting the quantifier ion. As can be seen for the absolute *S/N* values listed in Table 6.3, these were generally lower (in 15 cases) when using H_2, with an overall % difference of -14% considering the average S/N values using the two mobile phases. In such a respect, when using H_2 Muñoz-Guerra *et al.* observed a general decrease of the ion signals (especially the more compound-specific ones) and an increase of the background noise [3].

Mass spectral profile differences were evaluated in a preliminary manner, on 20 pesticides and 13 FAMEs (from no to six double bonds), by using databases

constructed by analyzing the mixtures using He and H_2 as carrier gas. The He GC×GC mass spectra were searched against those present in the H_2 database, and *vice versa* (forward match values were searched). Considering the pesticides, as expected the mass spectral results (experimental spectra *vs.* database) were in general altogether similar (Table 6.3). The biggest difference (14 points) was found for fenthion, while the overall average mass spectral similarity value was the same in both cases (904).

Table 6.3. *Results for He GC×GC mass spectra searched against those present in the H_2 database (and vice versa), along with extracted-ion-chromatogram S/N values using the quantifier ion (± 500 ppm), and % difference when using H_2 as carrier gas (n = 3).*

Compound	He spectra *vs* H_2 database	H_2 spectra *vs* He database	Quant. ion	He - S/N	H_2 - S/N	H_2 % difference
Sulfotep	907	907	64.99	379	200	-47
Phorate	902	912	75.03	401	323	-19
Hexachlorobenzene	952	952	283.81	4864	4746	-2
Diazinon	887	886	137.07	456	252	-45
Lindane	933	934	180.94	922	511	-45
Fonofos	925	925	108.99	1196	866	-28
Disulfoton	913	913	88.03	476	318	-33
Endosulfan ether	955	955	69.04	494	511	3
Chlorpyrifos methyl	867	865	124.98	464	285	-38
Fenthion	851	837	278.02	685	222	-68
Aldrin	939	939	66.05	401	432	7
4,4'-Dichlorobenzophenone	930	930	138.99	812	375	-54
Fenson	908	908	77.04	365	173	-53
Bromophos methyl	903	911	93.01	287	379	24
Bromophos ethyl	890	890	96.95	238	158	-34
Chlorbensid	837	837	125.01	643	435	-32
Chlorfenson	903	903	111.00	460	282	-39
Pentachlorothioanisole	925	925	295.84	2716	3418	21
Isodrin	919	921	66.05	305	317	4
Prothiofos	886	884	112.92	270	246	-9
Average	*904*	*904*	*-*	*842*	*722 (-14%)*	

The FAMEs results are reported in Table 6.4; also in this case the mass spectral results were similar, with the biggest difference being only 2 units observed for

palmitic acid methyl ester, while the overall average mass spectral similarity value was again the same in both cases (893).

Table 6.4. *Results for He GC×GC mass spectra searched against those present in the H_2 database, and vice versa. Components listed in the table were analyzed as methyl ester derivatives.*

Compound	He spectra *vs* H_2 database	H_2 spectra *vs* He database
Myristic acid (C14:0)	944	944
Myristoleic acid (C14:1ω5)	895	895
Pentadecanoic acid (C15:0)	811	811
Pentadecenoic acid (C15:1ω5)	890	890
Palmitic acid (C16:0)	862	860
Palmitoleic acid (C16:1ω7)	957	956
Heptadecanoic acid (C17:0)	945	945
Heptadecenoic acid (C17:1ω7)	922	922
Linoleic acid (C18:2ω6)	921	921
γ-Linolenic acid (C18:3ω6)	808	808
Arachidonic acid (C20:4ω6)	893	893
Eicosapentaenoic acid (C20:5ω3)	893	893
Docosaesaenoic acid (C22:6ω3)	872	872
Average	*893*	*893*

The He and H_2 mass spectral profiles of the analyzed pesticides and FAMEs present general similarity (even though to various degrees). Considering the worst-case pesticide (in terms of spectral similarity), namely chlorbensid with a similarity of 837 in both cases (Figure 6.6), the most significant difference is given by a fragment at *m/z* 91, present only in the H_2 spectrum (15% intensity). Evident differences were also present in the spectra of fenthion (Figure 6.7): *e.g.*, a fragment at *m/z* 78 was present only in the He spectrum (20% intensity). Regarding the FAME spectra, considering the worst-case match, namely γ-linolenic acid (C18:3ω6) with an MS similarity of 808 in both cases, the differences become evident after a brief observation (Figure 6.8).
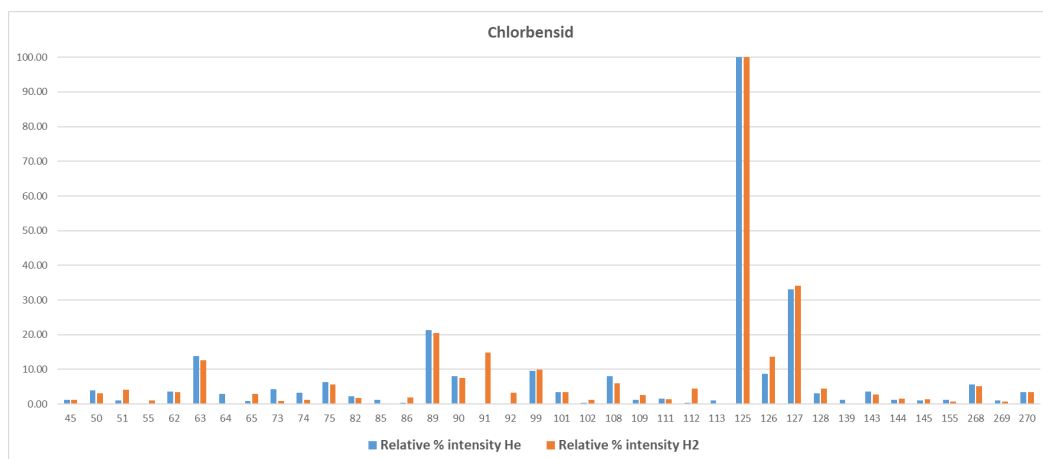
Figure 6.6. *Comparison of the mass spectral ion profiles (expressed as relative percentage intensity) of chlorbensid obtained using He and H₂.*
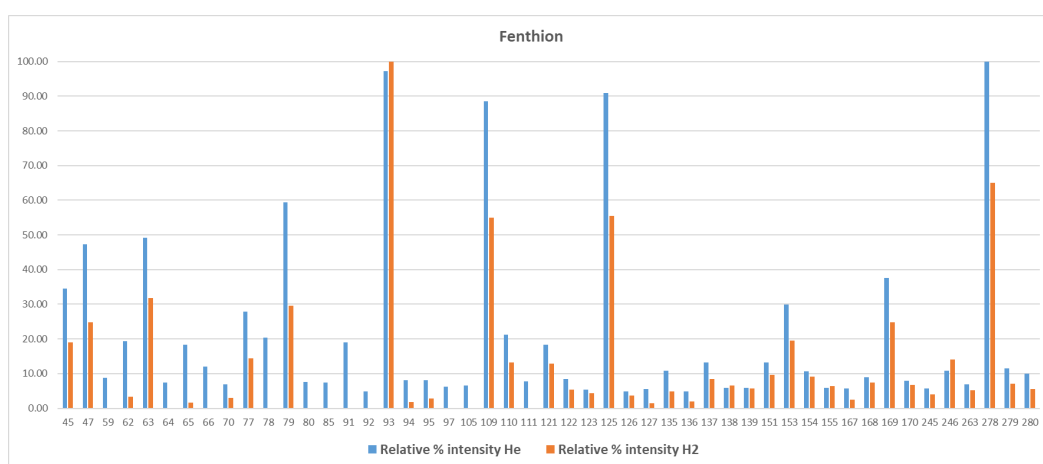
Figure 6.7. *Comparison of the mass spectral ion profiles (expressed as relative percentage intensity) of fenthion obtained using He and H₂.*
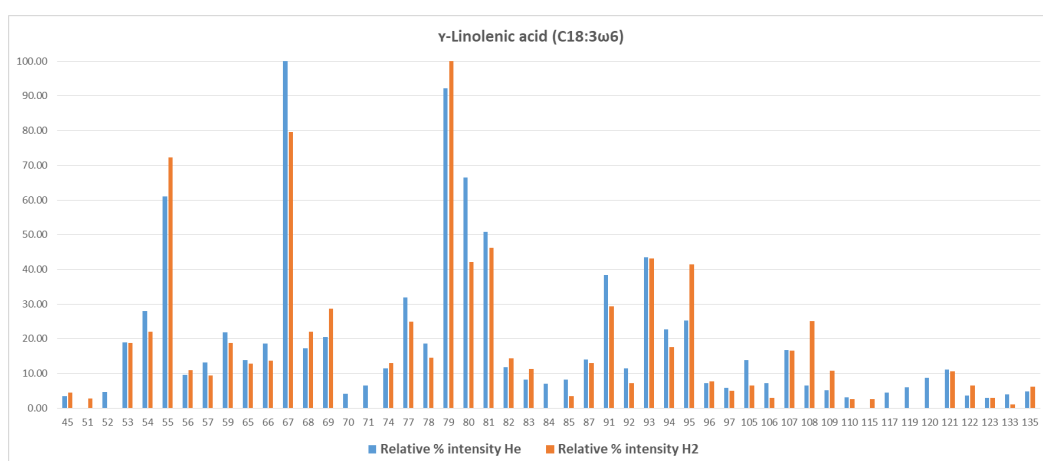
Figure 6.8. *Comparison of the mass spectral ion profiles (expressed as relative percentage intensity) of γ-linolenic acid (C18:3ω6) obtained using He and H₂.*

6.4 Conclusions

The main novelty of the present research consists in the use and evaluation of hydrogen as carrier gas, within the context of FM GC×GC-ToFMS analysis, as a more sustainable alternative to helium. In fact, as the cost of helium increases, hydrogen is an effective alternative because it can be produced using generators, which are safer and more cost-effective than gas cylinders.

The results herein reported on the use of hydrogen and helium were obviously expected: it is possible to obtain an altogether similar optimized separation result (in terms of resolution) in a shorter time (about 25% less) when using hydrogen.

In terms of mass spectral profiles, limited (though not negligible) differences were observed when using hydrogen and helium, and they were compound-specific. However, since the fragmentation patterns observed were generally comparable, available commercial databases can be most probably employed for MS spectra searching. Even so, further investigation on this specific issue is required. About *S/N* values (a quantifier ion was used), relative to the mixture of pesticides, these were generally lower when using hydrogen, with a minimum value of -68% (for fenthion). The impact of such a decrease in S/N values can only be evaluated in specific applicational research, where low limits of quantification must be reached (e.g., pesticides in food products).

References

[1] M. Dömötörová, M. Kirchner, E. Matisová, J. De Zeeuw, Possibilities and limitations of fast GC with narrow-bore columns, J. Sep. Sci. 29 (2006) 1051-1063, doi: 10.1002/jssc.200500472

[2] L.S. Ettre, J.V. Hinshaw, Basic relationships of gas chromatography, Cleveland: Advanstar Communications Inc; 1993.

[3] J.A. Muñoz-Guerra, P. Prado, S.V. García-Tenorio, Use of hydrogen as a carrier gas for the analysis of steroids with anabolic activity by gas chromatography-mass spectrometry, J. Chromatogr. A 1218 (2011) 7365-7370, doi: 10.1016/j.chroma.2011.08.009.

[4] C.N. Nnaji, K.C. Williams, J.M Bishop, G.F. Verbeck, Hydrogen as a GC/MS carrier and buffer gas for use in forensic laboratories, Sci. Justice 55 (2015) 162-167, doi: 10.1016/j.scijus.2015.01.003.

[5] Z. Liu, J.B. Phillips, Comprehensive two-dimensional gas chromatography using an on-column thermal modulator interface, J. Chromatogr. Sci. 29 (1991) 227-231, doi: 10.1093/chromsci/29.6.227.

[6] R.B. Gaines, E.B. Ledford, J.D. Stuart, Analysis of water samples for trace levels of oxygenate and aromatic compounds using headspace solid-phase microextraction and comprehensive two-dimensional gas chromatography, J. Microcolumn Sep. 10 (1998) 597-604, doi: 10.1002/(SICI)1520-667X(1998)10:7<597::AID-MCS6>3.0.CO;2-B.

[7] J. Beens, H.G. Janssen, M. Adahchour, U.A.Th. Brinkman, Flow regime at ambient outlet pressure and its influence in comprehensive two-dimensional gas chromatography, J. Chromatogr. A 1086 (2005) 141-150, doi: 10.1016/j.chroma.2005.05.086.

[8] L.M. Blumberg, F. David, M.S. Klee, P. Sandra, Comparison of one-dimensional and comprehensive two-dimensional separations by gas chromatography, J. Chromatogr. A 1188 (2008) 2-16, doi: 10.1016/j.chroma.2008.02.044.

Chapter 7
A green and sustainable method for Capsicum volatilome investigation by means of headspace solid-phase microextraction combined with flow-modulated two-dimensional gas chromatography-mass spectrometry using hydrogen as carrier gas[*]

The present research is focused on the development of a green and sustainable analytical method, based on the use of headspace solid-phase microextraction (HS SPME), and hydrogen as carrier gas, within the context of fast flow-modulation comprehensive two-dimensional gas chromatography-time-of-flight mass spectrometry (FM GC×GC-ToFMS), for the investigation of the volatile composition of Capsicum peppers. In such a respect, three different species were analysed: Annuum, Baccatum, and Chinense. Following HS SPME FM GC×GC-ToFMS analysis, a tile-based Fisher-ratio software was used to easily determine compounds that varied the most within the same variety of Capsicum samples. Particular emphasis was also devoted to the aroma profile of the thirty most sample-distinguishing compounds.

7.1 Introduction

Peppers of the genus *Capsicum* are among the spices most consumed worldwide; due to their attributes of color, aroma, flavour and pungency they find numerous uses in the food, pharmaceutical, and cosmetic industries [1]. Among the species of the genus *Capsicum*, five are widely cultivated and consumed: *Capsicum Annuum*, *Capsicum Baccatum*, *Capsicum Chinense*, *Capsicum Frutescens* and *Capsicum Pubescens* [2].

The characterization of the food volatilome is important in the food industry, not only to achieve the desired flavor profile during food production, but also to distinguish different products. An ideal "green" technique for the extraction of food volatiles is (headspace - HS) solid-phase microextraction (SPME).

The volatile fraction of different varieties of *Capsicum* peppers has been thoroughly investigated in the last decade, to provide information regarding authenticity, quality, and origin [3-6]. More than 300 individual compounds have been identified: many esters providing fruity notes, terpenes providing woody, floral, fruity, and spicy notes, followed by other minor compounds such as alcohols (high odour threshold), aldehydes (green, pungent, and herbaceous notes), aromatic and aliphatic hydrocarbons, ketones, and pyrazines conferring a powerful and robust aroma [3-6].

In the present investigation, HS SPME FM GC×GC-ToFMS was used to perform a detailed comparison of the volatile compounds released from sixteen fresh chili peppers, belonging to three varieties of *Capsicum*, namely *Annuum, Baccatum, and Chinense*. The acquired raw data were compared through a tile-based Fisher-ratio software, to easily determine compounds that vary the most within the same variety of *Capsicum* [7,8]. Particular emphasis was devoted to the aromatic characteristics of the thirty most sample-distinguishing compounds.

7.2 Experimental

Chemicals and sample preparation

Sixteen fresh chili peppers, belonging to the genus *Capsicum*, were kindly provided by «Azienda Agricola Rita Salvadori» (Livorno, Italy). Specifically, two varieties of *C. Baccatum* (Aji, Erotico), three varieties of *C. Annuum* (Banana, Caienna Impala, Jalapeño), and eleven varieties of *C. Chinense* (Madame Janette, Bhut Jolokia,

Moruga Rosso Ter. Selection, Moruga Red Car. Selection, Trinidad Scorpion Moruga Yellow, Naga Morich, Carolina Reaper Red, Carolina Reaper Green, Habanero Fatali, Habanero Red Savina, Habanero Chocolate) were investigated. The *n*-hexane and butylhydroxytoluene (BHT), used as internal standard (IS), were purchased from Merck Life Science (Merck KGaA, Darmstad, Germany). The IS was solubilized in *n*-hexane and was added to *C. Annuum* and *C. Baccatum* peppers at a concentration level of 10 μg mL^{-1}, and at a concentration level of 100 μg mL^{-1} in *C. Chinense* peppers. A C$_7$-C$_{30}$ *n*-alkane (10 μg mL^{-1}) series was purchased from Merck Life Science for the calculation of the linear retention index (LRI) values.

Instrumentation

The HS SPME process was performed automatically by using an L-PAL3 GC Autosampler (LECO, Mönchengladbach, Germany). The extraction procedure was based on a previous published paper [5].

A 50/30 μm divinylbenzene/carboxen/polydimethylsiloxane (DVB/CAR/PDMS) SPME fiber was conditioned according to the manufacturer's guidelines. One gram of the sample was introduced into a 20 mL headspace vial, along with 10 μL of IS. The samples were incubated for 5 min at 50 °C, followed by 50 min of extraction at the same temperature. The agitation speed was 250 rpm. After extraction, the analytes were desorbed for 1 min at 250 °C in the splitless mode for *C. Annuum* and *C. Baccatum* peppers, and in the split mode (40:1) for *C. Chinense* peppers. After each extraction and desorption procedure, the fiber was reconditioned for 15 min at 250 °C, to eliminate analyte carryover between extractions. Three replicates for each sample were carried out.

The FM GC×GC-ToFMS applications were performed on a Pegasus® BT 4D GC×GC-ToFMS system equipped with a Flux™ modulator (LECO). The GC×GC column set was: an SLB-5ms [silphenylene polymer with similar polarity to poly(5% diphenyl/95% dimethyl siloxane)] with dimensions 10 m × 0.25 mm ID × 0.25 μm d$_f$ employed as ^{1}D column, while the ^{2}D column was an SLB-35ms (silphenylene polymer with similar polarity to poly(35% diphenyl/65% dimethyl siloxane) with dimensions 2 m × 0.10 mm ID × 0.10 μm d$_f$ and with 0.3 m located inside the MS transfer line (250°C). All columns were provided by Merck Life Science.

The carrier gas used was H_2, delivered at a constant flow of 1.1 ml min^{-1}. The initial ^{1}D average linear velocity (ALV) was approx. 20 cm s^{-1}, while the initial ^{2}D ALV was approx. 165 cm s^{-1}. The main GC oven was held at 40 °C for 1 min, then ramped up to 195 °C at 12 °C min^{-1}, with a secondary oven temperature offset of +5°C. The modulation period (P_M) was set at 2 s, with a re-injection period of 80 ms. The auxiliary pressure unit (EPC) provided a constant flow of 3.5 ml min^{-1}. The MS parameters were as follows: acquisition delay was 180 s; acquisition rate was 150 spectra s^{-1}; electron ionization was performed at 70 eV, while mass spectra were acquired in the mass channel range *m/z* 40–400. Data were acquired and processed by using the ChromaTOF software v. 5.50.55.0.63466 (LECO) and ChromaTOF Tile v.1.01 (LECO). The mass spectral databases used were the Flavour and Fragrance Natural and Synthetic Compounds (FFNSC) v. 4.0 (Chromaleont s.r.l. Messina, Italy), and Lipids (Chromaleont s.r.l.).

Data processing

All data were imported to the ChromaTOF Tile v.1.01 software for tile-based Fisher ratio analysis. The sample files were divided according to *Capsicum* pepper varieties, with three replicates per class. Specifically, there were two classes for *C. Baccatum*, three for *C. Annuum*, and eleven for *C. Chinense*. One-point normalization was performed prior to data analysis using the BHT IS peak signal (^{1}t$_R$ = 595.323 s, ^{2}t$_R$ = 0.23 s) at *m/z* 205. Tile sizes of 4 modulations for the ^{1}D separation and 52 spectra for the ^{2}D one were selected for *C. Baccatum* and *C. Annuum* peppers, while the same tile size for the ^{1}D separation and 101 spectra for the ^{2}D one were chosen for *C. Chinense* peppers. A minimum of 3 samples were required to exceed the *S/N* threshold of 10, as this was the number of samples per class. No F-ratio threshold was set herein. The spectrum used for the spectral search is based on the difference between the most differentiated class and the other classes, with the resulting average spectrum then background subtracted. Such a procedure removes both background noise and some of the interfering *m/z* values. All the heat map were carried out by Excel v.2204.

7.3 Results and discussion

The goal of the present research was the development of a green and sustainable method to perform a detailed comparison of sixteen fresh chili peppers belonging to three different *Capsicum* species namely *Annuum*, *Baccatum*, and *Chinense*. For such a purpose, the volatiles were extracted by using HS SPME in a solvent-free manner, while separation and identification were carried out by using fast FM GC×GC-ToFMS (no cryogenic fluids involved) with H_2 (produced by a generator) as carrier gas. After, a dedicated software was exploited to compare the acquired raw data. Briefly, the software algorithm works by creating four grids (composed of tiles) offset from each other, where the tile dimensions should be properly selected to fit the analysed compounds.

The four stacked grids are able to detect the targeted compound in each analysis, even in case of slight misalignment eliminating the need for GC×GC chromatogram alignment. The area of the targeted analytes present in the tile was calculated by summing all the signals at the most discriminating *m/z* value [9]. Compound tentative identification was carried out through the combined use of MS database spectral searching and LRI information (comparison between the MS database and experimental LRI values) considering a similarity match value $\geq$ 800 and an experimental LRI value within a $\pm$ 20 LRI tolerance window. Hits that had noisy spectra and redundant analytes were manually removed from the hit list.

The differences within the same species of *Capsicum* were calculated considering the normalized average area of each analyte ($n = 3$): results were expressed as area ratios, normalizing the higher average area value to 1. In this manner, quantification differences for the same compound between different samples become immediately evident. The 30 compounds with the greatest differences are reported, along with % areas. The present Authors are aware that MS % areas do not faithfully reflect the relative composition of the detected compounds; however, such an approach is herein employed to provide an indicative idea.

Capsicum Baccatum

Two varieties of *C. Baccatum* were investigated, respectively Aji and Erotico: the 30 compounds with the greatest differences are reported in Table 7.1 along with their

chemical class, MS similarity, Δ LRI, sensory profile, flavour dilution factor (FDF) when found in the literature, normalized area ratio, and % area (reported in brackets).
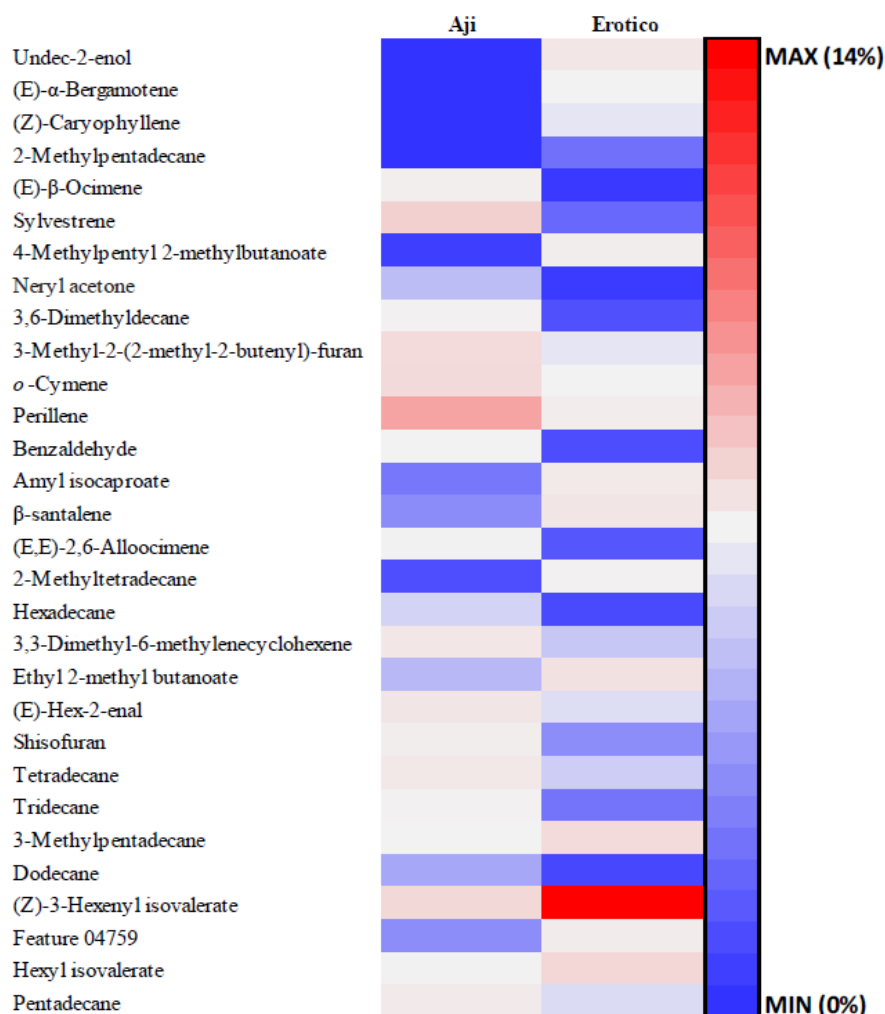
Figure 7.1. *Heat map constructed by using the data reported in Table 7.1, relative to Capsicum Baccatum samples.*

Among the 30 compounds with the greatest differences, there were: 1 alcohol, 2 aldehydes, 5 esters, 1 ether, 10 hydrocarbons, and 10 terpenes (1 compound was not tentatively-identified). Of these 17 were more abundant in the Aji variety and 13 in the Erotico one. Considering the Aji variety, the % values were in the "not detected" - 4.893% range summing to a total of *circa* 18%, whereas for the Erotico variety the % values were in the 0.006 - 14.591%, summing to a total of *circa* 25%. The presence of all esters (except amyl isocaproate, to the best of the present Authors' knowledge), all hydrocarbons (except 3,6-dimethyldecane and 3,3-dimethyl-6-methylenecyclohexene, to the best of the present Authors' knowledge), and several

terpenes, namely (E)-α-bergamotene, (E)-β-ocimene, neryl acetone, *o*-cymene, (E,E)-2,6-allocimene, (Z)-caryophyllene, have been previously reported in the literature [5,6]. The heat map of the two varieties of *C. Baccatum* is shown in Figure 7.1, where the greater relative abundance of (Z)-3-hexenyl isovalerate (14.591 %) in the Erotico variety and perillene (4.893 %) in the Aji one is immediately noticeable; the former confers a green, fruity, floreal, and tropical flavour, while the latter a woody one.

Table 7.1. *Compounds of the two varieties of C. Baccatum along with their chemical class, MS spectral similarity, Δ LRI values, sensory profile, flavour dilution factor (FDF), normalized abundance, and % area (nd = not detected).*

Compound #	Compound	Chemical class	MS similarity	Δ LRI	Sensory Profile[a]	FDF	Aji	Erotico
1	Undec-2-enol	Alcohol	805	12	Floral	-	nd	1.00 (0.921)
2	(E)-α-Bergamotene	Terpene	938	1	Woody	-	nd	1.00 (0.221)
3	(Z)-Caryophyllene	Terpene	957	-10	Sweet, spicy, woody	1[b]	nd	1.00 (0.152)
4	2-Methylpentadecane	Hydrocarbon	927	4	-	-	0.01 (trace)	1.00 (0.052)
5	(E)-β-Ocimene	Terpene	886	-1	Sweet, herbal	27[c]	1.00 (0.431)	0.01 (0.006)
6	Sylvestrene	Terpene	828	14	-	-	1.00 (2.199)	0.01 (0.046)
7	4-Methylpentyl 2-methylbutanoate	Ester	831	0	-	-	0.02 (0.010)	1.00 (0.463)
8	Neryl acetone	Terpene	824	-6	Fatty	-	1.00 (0.118)	0.05 (0.007)
9	3,6-Dimethyldecane	Hydrocarbon	820	3	-	-	1.00 (0.301)	0.07 (0.025)
10	3-Methyl-2-(2-methyl-2-butenyl)-furan	Heterocycle	865	1	Caramel, green, minty	-	1.00 (1.589)	0.08 (0.152)
11	*o*-Cymene	Terpene	861	-11	-	-	1.00 (1.600)	0.09 (0.172)
12	Perillene	Terpene	895	-2	Woody	-	1.00 (4.893)	0.09 (0.536)
13	Benzaldehyde	Aldehyde	901	6	Fruity, cherry, woody, tropical	512[e]	1.00 (0.205)	0.09 (0.023)
14	Amyl isocaproate	Ester	815	-4	-	-	0.09 (0.058)	1.00 (0.755)
15	β-santalene	Terpene	860	0	Woody	-	0.09 (0.075)	1.00 (0.980)

16	(E,E)-2,6-Alloocimene	Terpene	869	-6	Sweet, floral	-	1.00 (0.254)	0.10 (0.030)
17	2-Methyltetradecane	Hydrocarbon	939	-4	-	-	0.10 (0.023)	1.00 (0.293)
18	Hexadecane	Hydrocarbon	825	20	Fusel-like, fruity, sweet	-	1.00 (0.136)	0.11 (0.019)
19	3,3-Dimethyl-6-methylenecyclohexene	Hydrocarbon	849	-5	-	-	1.00 (0.889)	0.11 (0.126)
20	Ethyl 2-methyl butanoate	Ester	909	-13	Fruity, sweet, green, apple	128[d]	0.12 (0.113)	1.00 (1.183)
21	(E)-Hex-2-enal	Aldehyde	871	-15	Fruity, sweet, almond, apple, green	64[f]	1.00 (0.968)	0.12 (0.145)
22	Shisofuran	Terpene	912	-6	-	-	1.00 (0.486)	0.13 (0.077)
23	Tetradecane	Hydrocarbon	801	13	Mild, waxy	81[g]	1.00 (0.798)	0.13 (0.131)
24	Tridecane	Hydrocarbon	815	-18	Fuel-like	-	1.00 (0.320)	0.14 (0.055)
25	3-Methylpentadecane	Hydrocarbon	921	-3	-	-	0.14 (0.185)	1.00 (1.588)
26	Dodecane	Hydrocarbon	865	7	Skunk cooked meat	-	1.00 (0.099)	0.14 (0.018)
27	(Z)-3-Hexenyl isovalerate	Ester	835	-4	Green, fruity, floral, tropical	-	0.15 (1.714)	1.00 (14.591)
28	Feature 04759	-	-	-	-	-	0.15 (0.077)	1.00 (0.628)
29	Hexyl isovalerate	Ester	821	-5	Sweet, green, fruity, waxy	-	0.16 (0.246)	1.00 (1.861)
30	Pentadecane	Hydrocarbon	810	1	Waxy	81[g]	1.00 (0.658)	0.18 (0.143)
Average			864					

The sensory profile for 19 compounds is reported in Table 7.1 [10]; furthermore, the (literature) FDF values of 7 out of the 30 volatile compounds was found and were within the range 1-512. The most aroma-active compound is benzaldehyde with an FDF of 512 and a fruity, cherry, woody, tropical flavour. The Aji sample was characterized by a benzaldehyde % area value ten times higher with respect to the Erotico one [5]. With regard to the MS similarity, an average value of 864 was calculated, ranging between 801 and 957.

Capsicum Annuum

Three varieties of *C. Annuum* were analysed namely Banana, Caienna Impala, and Red Jalapeño; the 30 compounds with the greatest differences are reported in Table 7.2. Among the 30 compounds, there were: 2 alcohols, 9 esters, 4 hydrocarbons (2 aromatic), 1 ketone, 1 pyrazine, 9 terpenes, while 4 compounds were not tentatively identified. Interestingly, all the 30 components were present in higher concentrations in the Banana variety. Considering this variety, the % areas were in the 0.058 - 12.175 % range, summing to a total of *circa* 45%, whereas for the Caienna Impala variety the % areas were in the "not detected" - 2.047 % range, summing to a total of *circa* 7%; finally, for the Red Jalapeño variety, the % areas were in the 0.004 % - 1.069 % range, summing to a total of *circa* 6%. The bi-dimensional chromatogram of C. Annuum Banana sample, is shown in Figure 7.2. As can be seen, the 30 most sample-distinguishing compounds eluted in a ^{1}D separation window from 192 to 527 s.
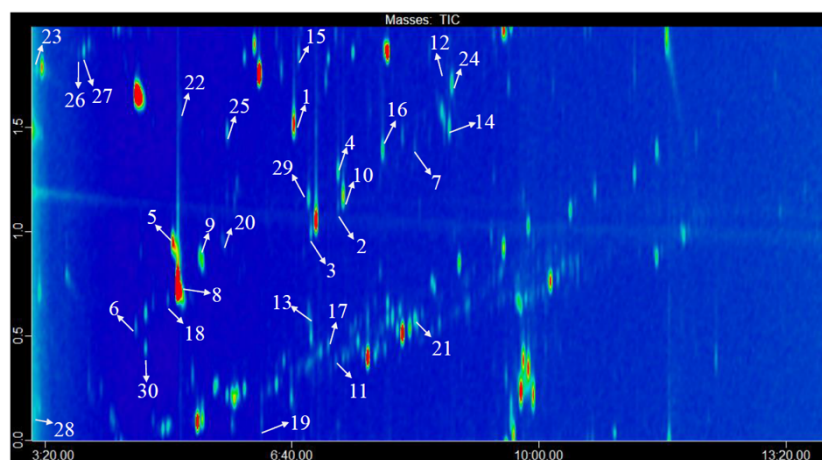
Figure 7.2. *Bi-dimensional total ion current chromatogram of the analysed C. Annuum Banana sample (refer to Table 7.2 for peak identity)*

Table 7.2. *Compounds of the three varieties of C. Annuum along with their chemical class, MS spectral similarity, Δ LRI values, sensory profile, FDF, normalized abundance, and % area.*

Compound #	Compound	Chemical class	MS similarity	Δ LRI	Sensory Profile	FDF	Caienna Impala	Red Jalapeño	Banana
1	2-Isobutyl-3-methoxypyrazine	Pyrazine	950	20	Green, galbanum	-	< 0.01 (0.002)	< 0.01 (0.006)	1.00 (0.370)
2	3-Methylpentyl butyrate	Ester	857	18	-	-	0.01 (0.113)	0.01 (0.175)	1.00 (4.178)
3	4-Methylpentyl 2-methylbutanoate	Ester	894	-7	-	-	0.01 (0.305)	0.01 (0.661)	1.00 (12.175)
4	cis-3-Hexenyl isovalerate	Ester	851	-4	Green, fruity, floral	-	0.02 (0.210)	0.01 (0.251)	1.00 (4.339)
5	Sylvestrene	Terpene	829	0	-	-	0.02 (0.172)	0.03 (0.466)	1.00 (3.334)
6	β-Pinene	Terpene	885	2	Herbal, woody, minty	27[b]	< 0.01 (0.003)	0.05 (0.059)	1.00 (0.297)
7	4-Methylhexyl 2-methylbutanoate	Ester	864	20	-	-	0.05 (0.026)	0.01 (0.004)	1.00 (0.172)
8	Limonene	Terpene	901	1	Citrus	243[b]	0.02 (0.148)	0.03 (0.385)	1.00 (2.579)
9	γ-Terpinene	Terpene	861	-1	Sweet, citrus, woody	243[b]	nd	0.07 (0.083)	1.00 (0.296)
10	3-Methyl-hexyl butanoate	Ester	890	-6	Green, fruity, apple, sweet	-	0.02 (0.091)	0.05 (0.223)	1.00 (1.155)
11	Feature 05042	-	-	-	-	-	0.06 (0.068)	0.02 (0.030)	1.00 (0.345)
12	Phenylbenzene	Aromatic hydrocarbon	893	-1	Green, floral, geranium, bergamot	-	0.04 (0.056)	0.05 (0.087)	1.00 (0.397)
13	Methyl salicylate	Ester	868	0	Sweet, minty	1[h]	0.04 (0.091)	0.06 (0.199)	1.00 (0.765)
14	Feature 01047	-	-	-	-	-	nd	0.10 (0.048)	1.00 (0.107)

#	Compound	Class	RI		Odor	Threshold			
15	Thujyl alcohol	Alcohol	800	12	Minty, camphhoreous	-	0.05 (0.047)	0.06 (0.078)	1.00 (0.313)
16	Ethyl nonanoate	Ester	898	-8	Waxy, soapy, cognac, fruity, tropical, grape	-	0.08 (0.018)	0.03 (0.010)	1.00 (0.073)
17	Feature 03626	-	-	-	-	-	0.08 (0.031)	0.03 (0.015)	1.00 (0.116)
18	α-Terpinene	Terpene	857	1	Woody, herbal	27[b]	0.03 (0.120)	0.09 (0.464)	1.00 (1.229)
19	Limona ketone	Ketone	800	0	-	-	0.06 (0.043)	0.06 (0.055)	1.00 (0.209)
20	Terpinolene	Terpene	890	-2	Woody, sweet, lemon	243[b]	0.07 (0.092)	0.06 (0.102)	1.00 (0.384)
21	Feature 02115	-	-	-	-	-	0.11 (0.021)	0.03 (0.008)	1.00 (0.058)
22	1,4-Dichlorobenzene	Aromatic hydrocarbon	816	17	-	-	0.09 (0.094)	0.07 (0.105)	1.00 (0.330)
23	2-Methyl-1-pentanol	Alcohol	800	-4	-	-	0.14 (1.831)	0.04 (0.632)	1.00 (4.121)
24	β-Elemene	Terpene	941	-4	Herbal, citrous, sour	81[c]	0.08 (0.036)	0.13 (0.076)	1.00 (0.141)
25	p-Cymene	Terpene	892	-3	Woody,citrus, spicy	243[b]	0.08 (0.096)	0.13 (0.204)	1.00 (0.375)
26	2,6-dimethyl octane	Hydrocarbon	847	-18	-	-	0.15 (2.047)	0.06 (1.069)	1.00 (4.183)
27	Nonane	Hydrocarbon	812	18	Gasoline	-	0.15 (0.653)	0.07 (0.403)	1.00 (1.394)
28	Ethyl 2-methylbutanoate	Ester	820	-14	Fruity, sweet, green, apple	128[d]	0.11 (0.188)	0.11 (0.258)	1.00 (0.544)
29	Ethyl octanoate	Ester	907	-10	Waxy, fruity, creamy, fatty, sweet	64[d]	0.16 (0.234)	0.06 (0.107)	1.00 (0.449)
30	Myrcene	Terpene	876	1	Woody, tropical, citrus, fruity	256[d]	0.04 (0.018)	0.22 (0.149)	1.00 (0.159)
Average			865						

The bi-dimensional chromatograms of C. Annuum Caienna Impala and Red Jalapeño samples (Figures 7.3 A-B) are very similar, making it difficult to determine variations between them. For example, 4-methylpentyl 2-methylbutanoate (analyte 3) and cis-3-hexenyl isovalerate (analyte 4), are present in a similar amount in the Caienna Impala and Red Jalapeño varieties and in a higher amount the in Banana variety. The latter compound confers a green, fruity, and floral aroma [10]. It is noteworthy that 2-isobutyl-3-methoxypyrazine (analyte 1) provides a characteristic green bell pepper odour in *C. Annuum* and is present in much higher amounts in the Banana variety [11].
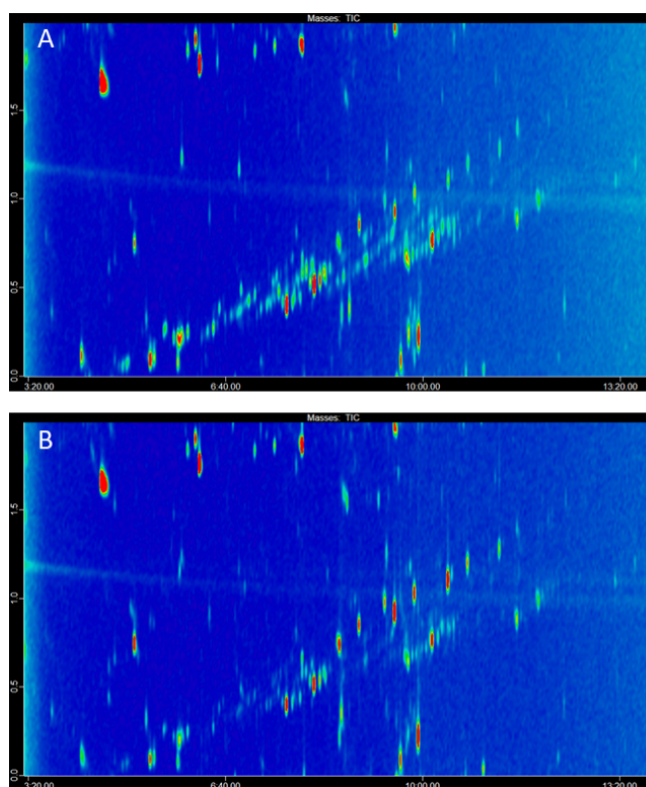
Figure 7.3. *Bi-dimensional total ion current chromatogram of A) C. Annuum Caienna Impala, B) C. Annuum Red Jalapeño.*

The heat map of the three varieties of C. *Annuum* is shown in Figure 7.4. Furthermore, and in relation to literature data on the *C. Annuum* variety, the presence of different esters such as 4-methylpentyl 2-methylbutanoate, 4-methylhexyl 2-methylbutanoate, 3-methyl-hexyl butanoate, methyl salicylate, ethyl 2-methylbutanoate, and terpenes such as limonene, γ-terpinene, β-elemene, *p*-cymene, and myrcene has already been reported [3,5].

The sensory profile for 18 compounds can be found in Table 7.2, along with FDF values for eleven of these, ranging from 1 to 256. The highest FDF was determined for myrcene with woody, tropical, citrus, fruity sensory attributes, contained in the Banana variety in the highest amount. Furthermore, four compounds with an FDF of 243 were detected namely: limonene (citrus note), γ-terpinene (citrus, sweet and woody note), terpinolene (lemon, sweet and woody note), and *p*-cymene (citrus, woody note); these components, also, were present in greater amounts in the Banana variety. Information related to retention times in both dimensions, normalized average areas, coefficients of variation (CV%) values (in the range 1-18 %) regarding the Banana variety, are reported in Table 7.3. Finally, considering mass spectral similarity, the average value was 865, with a range between 800 and 950.
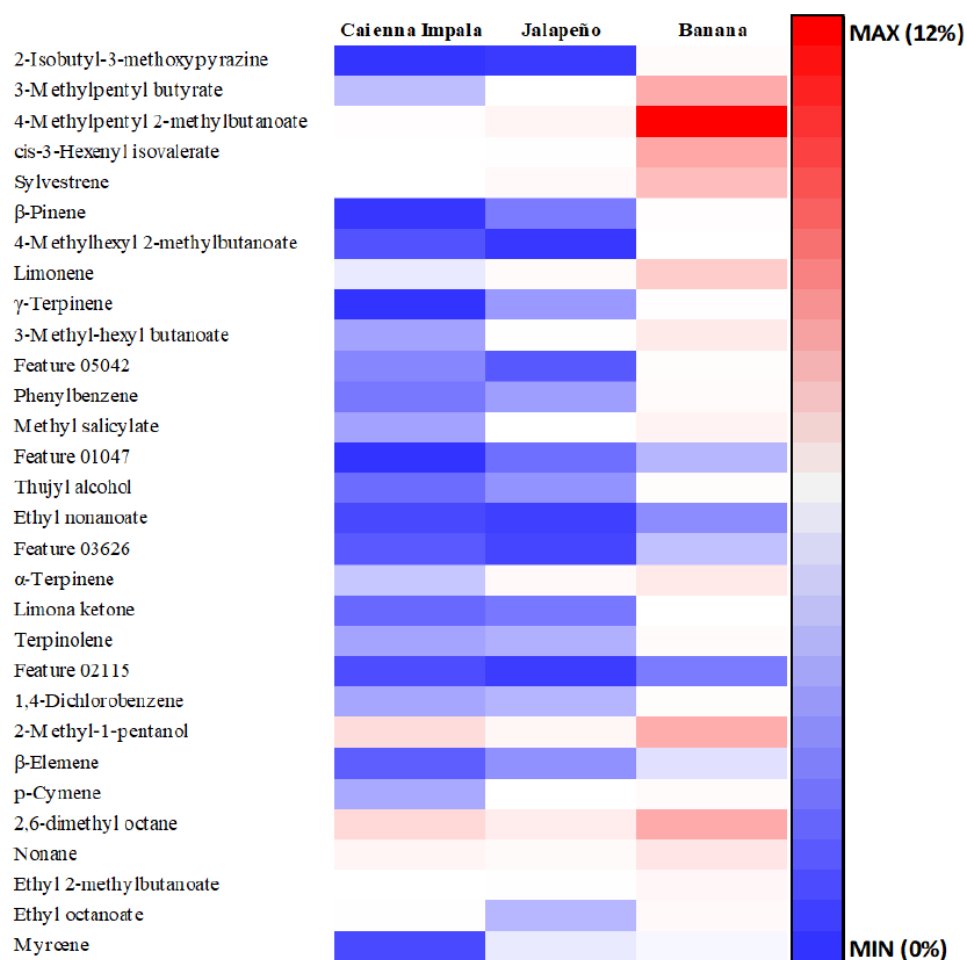
Figure 7.4. *Heat map constructed by using the data reported in Table 7.2 relative to C. Annuum samples.*

***Table** 7.3. Compounds of the C. Annuum Banana sample along with first and second dimension retention times (t_R), average area (n = 3), and CV% values.*

Compound #	Compound	^{1}D t_R (s)	^{2}D t_R (s)	Average area	CV%
1	2-Isobutyl-3-methoxypyrazine	401.6	1.5	0.15	10
2	3-Methylpentyl butyrate	437.6	1.1	2.08	10
3	4-Methylpentyl 2-methylbutanoate	415.6	1.0	6.09	11
4	cis-3-Hexenyl isovalerate	437.6	1.3	2.16	13
5	Sylvestrene	307.7	0.8	1.37	7
6	β-Pinene	273.8	0.6	0.13	11
7	4-Methylhexyl 2-methylbutanoate	499.5	1.4	0.09	1
8	Limonene	307.8	0.8	1.09	8
9	γ-Terpinene	325.8	0.9	0.13	4
10	3-Methyl-hexyl butanoate	441.6	1.2	0.55	9
11	Feature 05042	429.6	0.4	0.15	11
12	Phenylbenzene	525.2	1.8	0.18	6
13	Methyl salicylate	413.6	0.6	0.36	13
14	Feature 01047	527.4	1.5	0.04	12
15	Thujyl alcohol	405.6	1.9	0.14	12
16	Ethyl nonanoate	473.5	1.4	0.04	8
17	Feature 03626	429.6	0.9	0.06	8
18	α-Terpinene	299.8	0.7	0.54	13
19	Limona ketone	375.7	0.1	0.09	14
20	Terpinolene	343.7	1.0	0.17	15
21	Feature 02115	499.4	0.5	0.03	14
22	1,4-Dichlorobenzene	309.8	1.6	0.14	12
23	2-Methyl-1-pentanol	194	1.8	2.18	12
24	β-Elemene	529.4	1.7	0.06	18
25	p-Cymene	347.7	1.5	0.16	12
26	2,6-dimethyl octane	227.9	1.9	1.96	8
27	Nonane	231.9	1.9	0.69	8
28	Ethyl 2-methylbutanoate	192	0.1	0.28	14
29	Ethyl octanoate	413.6	1.2	0.16	8
30	Myrcene	281.8	0.5	0.07	6

Capsicum Chinense

Eleven varieties of *C. Chinense* were investigated: namely Madame Janette, Bhut Jolokia, Moruga Red Ter. Selection, Moruga Red Car. Selection, Trinidad Scorpion Moruga Yellow, Naga Morich, Carolina Reaper Red, Carolina Reaper Green, Habanero Fatali, Habanero Red Savina, and Habanero Chocolate. The 30 compounds that differentiate the samples most are reported in Tables 7.4 and 7.5 and belong to the following chemical classes: 5 alcohols, 1 aldehyde, 7 esters, 6 hydrocarbons, 9 terpenes, and 2 compounds were not tentatively identified.
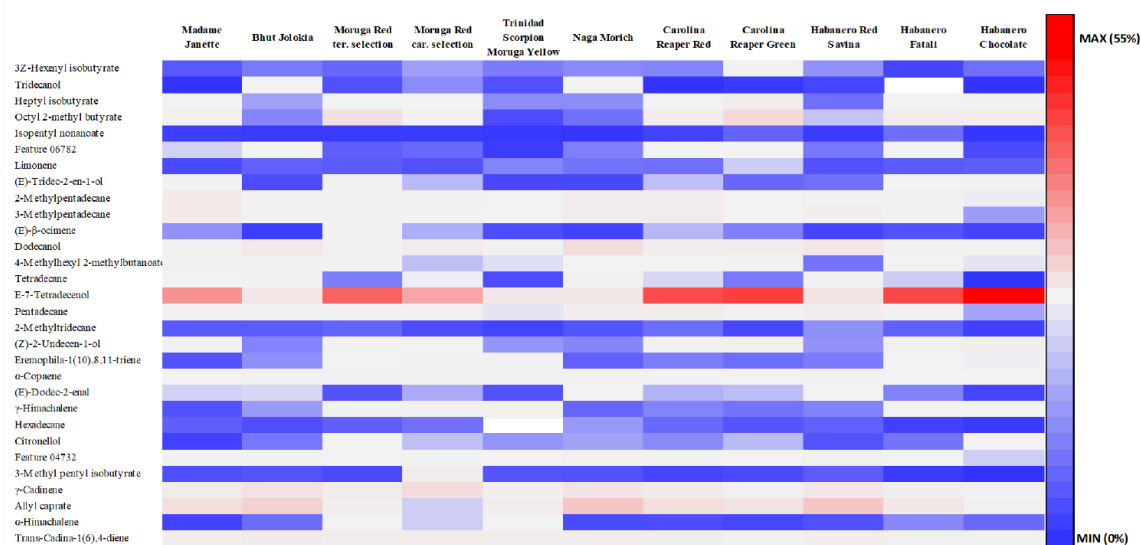
Figure 7.5 *Heat map constructed by using the data reported in Table 7.4 and 7.5 relative to C. Chinense samples.*

Of the 30 compounds with the greatest differences, 11 were more abundant in the Carolina Reaper Green variety, 7 in the Carolina Reaper Red variety, 5 in the Naga Morich variety, 4 in the Trinidad Scorpion Moruga Yellow variety, 2 in the Habanero Chocolate variety, and one in the Moruga Red Ter. Selection. The % areas were in the "not detected" - 22.168 % range in the Madame Janette variety (total sum was *circa* 42 %), in the 0.010 - 7.887 % range in the Bhut Jolokia variety (total sum was *circa* 26 %), in the 0.009 - 32.986 % range in the Moruga Red Ter. Selection variety (total sum was *circa* 51 %), in the 0.009 - 17.517 % range in the Moruga Red Car. Selection variety (total sum was *circa* 36 %), in the "not detected" - 3.061 % range in the Trinidad Scorpion Moruga Yellow variety (total sum was *circa* 13 %), in the 0.004 - 10.236 % range in the Naga Morich variety (total sum was *circa* 33 %), in the 0.001 - 38.229 % range in the Carolina Reaper Red variety (total sum was

circa 59 %), in the 0.007 - 41.063 % range in the Carolina Reaper Green variety (total sum was *circa* 60 %), in the 0.021 - 10.519 % range in the Habanero Red Savina variety (total sum was *circa* 30 %), in the "not detected" - 39.265 % range in the Habanero Fatali variety (total sum was *circa* 52 %), in the 0.001 - 55.082 % range in the Habanero Chocolate variety (total sum was *circa* 64 %). The between-sample differences can be observed in the heat map reported in Figure 7.5, where the high amount of E-7-tetradecenol (55.082 %) in the Habanero Chocolate and allyl caprate (10.236 %) in the Naga Morich variety is evident. The latter provides fatty and fruity notes. Furthermore, the presence of octyl 2-methyl butyrate (6.051 %) in Carolina Reaper Verde and dodecanol (5.206 %) in Naga Morich are immediately evident; the first confers a green, fruity, creamy, and waxy flavour, while the latter a soapy and fatty one. Previously, the presence of all the hydrocarbons, all the terpenes [except eremophila-1(10),8,11-triene, to the best of the present Authors' knowledge], all the esters [except (Z)-3-hexenyl isobutyrate, isopentyl nonanoate, and allyl caprate, and one alcohol [(E)-2-tridecen-1-ol] has been reported in literature [3,5,6].

A sensory profile is provided for eighteen compounds [10], with FDF values found for six of these, ranging from 27 to 243. The highest reported FDF value was 243 for limonene (citrus) and α-copaene (woody), followed by tetradecane (fuel-like), pentadecane (waxy), citronellol (citrus, floral, green, sweet) with an FDF of 81 An average value of 860 was found for the mass spectral similarity, with a range between 800 and 953.

Table 7.4. *Compounds of five varieties of C. Chinense along with their chemical class, MS spectral similarity, Δ LRI values, sensory profile, FDF, normalized abundance, and % area.*

Compound #	Compound	Chemical class	Match	Δ LRI	Sensory Profile[a]	FDF	Madame Janette	Bhut Jolokia	Moruga Red ter. selection	Moruga Red car. selection	Trinidad Scorpion Moruga Yellow
1	(Z)-3-Hexenyl isobutyrate	Ester	832	-4	Fruity, sweet, green, apple	-	0.01 (0.042)	0.01 (0.079)	0.03 (0.059)	0.07 (0.120)	0.05 (0.081)
2	Tridecanol	Alcohol	857	3	Musty	-	nd	0.16 (0.263)	0.05 (0.033)	0.21 (0.099)	0.07 (0.033)
3	Heptyl isobutyrate	Ester	800	-4	Green, fruity, tropical, sweet	-	0.01 (0.225)	0.01 (0.122)	0.05 (0.259)	0.09 (0.352)	0.02 (0.099)
4	Octyl 2-methyl butyrate	Ester	810	-20	Waxy, fruity, creamy, green, musty	-	0.01 (1.036)	0.01 (0.091)	0.18 (4.290)	0.04 (0.644)	0.01 (0.028)
5	Isopentyl nonanoate	Ester	801	9	Fruity, oily, apricot, floral, winey	-	0.01 (0.013)	0.02 (0.010)	0.04 (0.009)	0.05 (0.009)	0.03 (0.006)
6	Feature 06782	-	-	-	-	-	0.02 (0.177)	0.06 (0.237)	0.03 (0.050)	0.05 (0.061)	0.01 (0.011)
7	Limonene	Terpene	893	1	Citrus	243[b]	0.01 (0.026)	0.03 (0.052)	0.07 (0.045)	0.07 (0.036)	0.17 (0.091)
8	(E)-2-Tridecen-1-ol	Alcohol	800	11	Waxy	-	0.08 (0.665)	0.01 (0.029)	0.35 (0.475)	0.14 (0.151)	0.02 (0.023)
9	2-Methylpentadecane	Hydrocarbon	927	-1	-	-	0.08 (2.480)	0.05 (0.700)	0.12 (0.685)	0.21 (0.897)	0.07 (0.310)
10	3-Methylpentadecane	Hydrocarbon	932	-1	-	-	0.07 (2.312)	0.04 (0.624)	0.11 (0.631)	0.20 (0.886)	0.08 (0.379)
11	(E)-β-ocimene	Terpene	861	4	Sweet, herbal	27[c]	0.03 (0.107)	0.01 (0.012)	1.00 (0.656)	0.28 (0.139)	0.05 (0.028)
12	Dodecanol	Alcohol	807	-19	Waxy, soapy, fatty	-	0.02 (0.911)	0.10 (2.501)	0.07 (0.651)	0.27 (1.910)	0.08 (0.615)
13	4-Methylhexyl 2-methylbutanoate	Ester	883	-12	-	-	0.06 (0.626)	0.11 (0.537)	0.39 (0.707)	0.11 (0.157)	0.13 (0.192)

14	Tetradecane	Hydrocarbon	940	-2	Fuel-like	81[g]	0.04 (0.231)	0.33 (0.881)	0.09 (0.084)	0.28 (0.209)	0.04 (0.028)
15	(E)-7-Tetradecenol	Alcohol	800	14	-	-	0.02 (22.168)	0.01 (3.288)	0.20 (32.986)	0.14 (17.517)	0.02 (3.061)
16	Pentadecane	Hydrocarbon	813	-1	Waxy	81[g]	0.04 (0.980)	0.07 (0.831)	0.12 (0.520)	0.30 (1.020)	0.05 (0.198)
17	2-Methyltridecane	Hydrocarbon	915	-2	-	-	0.04 (0.043)	0.08 (0.044)	0.27 (0.055)	0.18 (0.028)	0.15 (0.024)
18	(Z)-2-Undecen-1-ol	Alcohol	825	8	-	-	0.02 (0.535)	0.01 (0.091)	0.20 (0.774)	0.14 (0.414)	0.04 (0.110)
19	Eremophila-1(10),8,11-triene	Terpene	859	-18	-	-	0.01 (0.036)	0.04 (0.103)	0.41 (0.429)	0.67 (0.530)	1.00 (0.842)
20	α-Copaene	Terpene	801	-4	Woody	243[c]	0.02 (0.323)	0.09 (0.686)	0.16 (0.771)	0.29 (0.552)	0.17 (0.550)
21	(E)-Dodec-2-enal	Aldehyde	845	0	Citrus, waxy, fatty	-	0.05 (0.177)	0.11 (0.184)	0.06 (0.036)	0.28 (0.134)	0.07 (0.034)
22	γ-Himachalene	Terpene	828	9	-	-	0.01 (0.036)	0.04 (0.116)	0.44 (0.487)	0.70 (0.591)	1.00 (0.900)
23	Hexadecane	Hydrocarbon	934	2	Fusel-like, fruity, sweet	-	0.04 (0.050)	0.06 (0.031)	0.25 (0.050)	0.46 (0.070)	nd
24	Citronellol	Terpene	861	-10	Floral, green, sweet, citrus	81[c]	0.01 (0.016)	0.04 (0.077)	0.55 (0.357)	0.32 (0.158)	0.20 (0.108)
25	Feature 04732	-	-	-	-	-	0.04 (0.450)	0.16 (0.860)	0.12 (0.236)	0.30 (0.473)	0.22 (0.359)
26	3-Methyl pentyl isobutyrate	Ester	828	-4	-	-	0.05 (0.031)	0.13 (0.038)	0.25 (0.027)	0.56 (1.992)	0.44 (0.038)
27	γ-Cadinene	Terpene	950	4	Woody	-	0.05 (1.976)	0.20 (3.673)	0.27 (1.804)	0.38 (5.240)	0.24 (1.307)
28	Allyl caprate	Ester	815	-12	Fatty, fruity	-	0.01 (5.185)	0.08 (7.887)	0.71 (1.512)	0.75 (0.174)	1.00 (1.732)
29	α-Himachalene	Terpene	953	1	Woody	-	0.01 (0.016)	0.08 (0.064)	0.71 (0.217)	0.75 (0.174)	1.00 (0.246)
30	Trans-Cadina-1(6),4-diene	Terpene	903	17	-	-	0.005 (1.124)	0.20 (2.104)	0.30 (1.665)	0.39 (1.849)	0.24 (1.747)
Average			860								

Table 7.5. *Compounds of six varieties of C. Chinense along with their normalized abundance, and % area.*

Compound #	Compound	Naga Morich	Carolina Reaper Red	Carolina Reaper Green	Habanero Red Savina	Habanero Fatali	Habanero Chocolate
1	3Z-Hexenyl isobutyrate	0.08 (0.097)	0.13 (0.091)	1.00 (0.555)	0.04 (0.106)	0.01 (0.021)	0.08 (0.068)
2	Tridecanol	1.00 (0.340)	0.01 (0.001)	0.05 (0.007)	0.03 (0.022)	nd	0.01 (0.001)
3	Heptyl isobutyrate	0.03 (0.101)	0.19 (0.341)	1.00 (1.373)	0.01 (0.068)	0.06 (0.277)	0.22 (0.457)
4	Octyl 2-methyl butyrate	0.01 (0.069)	0.21 (1.610)	1.00 (6.051)	0.01 (0.161)	0.09 (1.778)	0.19 (1.749)
5	Isopentyl nonanoate	0.04 (0.004)	0.25 (0.018)	1.00 (0.054)	0.04 (0.010)	0.40 (0.067)	0.05 (0.004)
6	Feature 06782	0.10 (0.085)	0.51 (0.261)	1.00 (0.400)	0.04 (0.077)	0.28 (0.351)	0.04 (0.026)
7	Limonene	0.19 (0.071)	0.31 (0.068)	1.00 (0.172)	0.04 (0.034)	0.08 (0.044)	0.19 (0.049)
8	(E)-Tridec-2-en-1-ol	0.03 (0.024)	0.35 (0.157)	0.17 (0.059)	0.04 (0.068)	0.36 (0.392)	1.00 (0.523)
9	2-Methylpentadecane	0.49 (1.578)	1.00 (1.854)	0.24 (0.350)	0.15 (1.105)	0.10 (0.453)	0.10 (0.206)
10	3-Methylpentadecane	0.50 (1.607)	1.00 (1.858)	0.29 (0.422)	0.15 (1.136)	0.11 (0.505)	0.05 (0.117)
11	(E)-β-ocimene	0.05 (0.017)	0.69 (0.148)	0.52 (0.087)	0.04 (0.021)	0.07 (0.035)	0.11 (0.018)
12	Dodecanol	1.00 (5.206)	0.49 (1.475)	0.54 (1.266)	0.24 (2.945)	0.08 (0.591)	0.14 (0.498)
13	4-Methylhexyl 2-methylbutanoate	0.43 (0.436)	0.46 (0.270)	1.00 (0.463)	0.03 (0.072)	0.16 (0.227)	0.29 (0.199)
14	Tetradecane	1.00 (0.552)	0.58 (0.184)	0.32 (0.079)	0.47 (0.615)	0.22 (0.172)	0.01 (0.002)
15	E-7-Tetradecenol	0.03 (2.873)	0.73 (38.229)	1.00 (41.063)	0.02 (3.686)	0.31 (39.265)	0.90 (55.082)

16	Pentadecane	0.74 (1.872)	1.00 (1.470)	0.56 (0.643)	0.30 (1.786)	0.14 (0.496)	0.07 (0.128)
17	2-Methyltridecane	0.33 (0.037)	1.00 (0.065)	0.45 (0.023)	0.39 (0.103)	0.32 (0.051)	0.20 (0.015)
18	(Z)-2-Undecen-1-ol	0.04 (0.092)	0.74 (0.930)	1.00 (0.985)	0.02 (0.107)	0.32 (0.968)	0.89 (1.311)
19	Eeremophila-1(10),8,11-triene	0.09 (0.051)	0.24 (0.083)	0.25 (0.065)	0.06 (0.081)	0.37 (0.301)	0.53 (0.210)
20	α-Copaene	0.53 (0.798)	0.62 (0.521)	1.00 (0.358)	0.29 (0.599)	0.30 (0.416)	0.21 (0.278)
21	(E)-Dodec-2-enal	1.00 (0.357)	0.69 (0.142)	0.95 (0.154)	0.29 (0.240)	0.18 (0.089)	0.08 (0.020)
22	γ-Himachalene	0.09 (0.058)	0.25 (0.091)	0.25 (0.072)	0.06 (0.089)	0.38 (0.336)	0.55 (0.232)
23	Hexadecane	1.00 (0.113)	0.92 (0.060)	0.77 (0.039)	0.20 (0.052)	0.10 (0.016)	0.12 (0.009)
24	Citronellol	0.34 (0.124)	0.45 (0.097)	0.91 (0.151)	0.04 (0.038)	0.14 (0.072)	1.00 (0.249)
25	Feature 04732	0.85 (0.970)	1.00 (0.662)	0.55 (0.285)	0.35 (0.933)	0.22 (0.352)	0.23 (0.175)
26	3-Methyl pentyl isobutyrate	0.59 (0.035)	0.61 (0.021)	1.00 (0.027)	0.32 (0.046)	0.12 (0.010)	0.001 (0.001)
27	γ-Cadinene	0.91 (3.463)	1.00 (2.208)	0.41 (0.702)	0.34 (3.054)	0.21 (1.134)	0.18 (0.454)
28	Allyl caprate	0.16 (10.236)	0.29 (4.935)	0.28 (3.715)	0.08 (10.519)	0.40 (2.813)	0.53 (1.086)
29	α-Himachalene	0.16 (0.027)	0.29 (0.028)	0.28 (0.022)	0.08 (0.033)	0.40 (0.096)	0.53 (0.061)
30	Trans-Cadina-1(6),4-diene	0.88 (1.952)	1.00 (1.357)	0.50 (0.449)	0.38 (1.770)	0.26 (1.014)	0.24 (0.454)

7.3 Conclusions

A green and sustainable analytical approach based on the use of HS SPME (no solvents were used), coupled with FM GC×GC-ToFMS and H_2 as carrier gas (a greener alternative to helium), was developed for the investigation of the volatile composition of *Capsicum* peppers. The sample complexity observed did justify the use of a high-resolution GC approach, such as GC×GC, to create sample-specific fingerprints. Moreover, the software used enabled a fine differentiation between peppers of the same variety. Such an analytical workflow could obviously be applied to other types of foods and beverages of high commercial importance - an HS SPME FM GC×GC-ToFMS method has been developed for the differentiation of white wines [17] - to pinpoint the most sample-distinguishing volatile compounds and relate these to between-sample aroma differences.

References

[1] E.T. Sousa, F.M. Rodrigues, C.C. Martins, F.S. Oliveira, P.A.P. Pereira, J.B. Andrade, Multivariate optimization and HS-SPME/GC-MS analysis of VOCs in red, yellow and purple varieties of capsicum chinense sp. peppers, Microchem. J. 82 (2006) 142-149, doi: 10.1016/j.microc.2006.01.01.

[2] J.S. Pruthi, Spices and condiments: chemistry, microbiology, technology, Academic Press, New York, 1980.

[3] A. Rodrĺguez-Burruezo, H. Kollmannsberger, M.C. González-Mas, S. Nitz, F. Nuez, HS-SPME comparative analysis of genotypic diversity in the volatile fraction and aroma-contributing compounds of capsicum fruits from the annuum-chinense-frutescens complex, J. Agric. Food Chem. (2010) 4388–4400, doi: 10.1021/jf903931t.

[4] S. Bogusz Junior, A. Tavares Melo, J. T. Filho, C.A. Zini, H.T. Godoy, Analysis of the volatile compounds of Brazilian chilli peppers (Capsicum spp.) at two stages of maturity by solid phase micro-extraction and gas chromatography-mass spectrometry, Food Res. Int. (2012) 98–107, doi: 10.1016/j.foodres.2012.02.005.

[5] E. Trovato, F. Vento, D. Creti, P. Dugo, L. Mondello, Elucidation of analytical–compositional fingerprinting of three different species of chili pepper by using headspace solid-phase microextraction coupled with gas chromatography–mass spectrometry analysis, and sensory profile evaluation, Molecules, 27 (2022) 2355, doi: 10.3390/molecules27072355.

[6] S. Bogusz Junior, P.H. Março, P. Valderrama, F.C. Damasceno, M.S. Aranda, C.A. Zini, E.B. Caramão, A.M. Tavares Melo, J.T. Filho, H.T. Godoy, Analysis of volatile compounds in Capsicum spp. by headspace solid-phase microextraction and GC×GC-TOFMS, Anal. Methods (2015) 521-529, doi: 10.1039/c4ay01455c.

[7] S.E. Prebihalo, K.L. Berrier, C.E. Freye, H.D. Bahaghighat, N.R. Moore, D.K. Pinkerton, R.E. Synovec, Multidimensional gas chromatography: advances in instrumentation, chemometrics, and applications, Anal. Chem. 90 (2017) 505-532, doi: 10.1021/acs.analchem.7b04226.

[8] P.E. Sudol, M. Galletta, P.Q. Tranchida, M. Zoccali, L. Mondello, R.E. Synovec, Untargeted profiling and differentiation of geographical variants of wine samples using headspace solid-phase microextraction flow-modulated comprehensive two-dimensional gas chromatography with the support of tile-based Fisher ratio analysis. J. Chromatogr. A 1662 (2022) 462735, doi: 10.1016/j.chroma.2021.462735.

[9] L.C. Marney, W. Christopher Siegler, B.A. Parsons, J.C. Hoggard, B.W. Wright, R.E. Synovec, Tile-based Fisher-ratio software for improved feature selection analysis of comprehensive two-dimensional gas chromatography–time-of-flight mass spectrometry data, Talanta, 115 (2013) 887-895, doi: 10.1016/j.talanta.2013.06.038.

[10] The Good Scents Company - Flavor, Fragrance, Food and Cosmetics Ingredients information, Good Scents Co. (n.d) (2021). https://www.thegoodscentscompany.com /index.html.

[11] P.A Luning, T. de Rijk, H.J. Wichers, J.P Roozen, Gas chromatography, mass spectrometry, and sniffing port analyses of volatile compounds of fresh bell peppers (Capsicum annuum) at different ripening stages. J. Agric. Food Chem. (1994) 4977–983, doi: 10.1021/jf00040a027.

Chapter 8
Use of headspace SPME coupled with flow-modulated comprehensive two-dimensional gas chromatography (enantio×polar) with time-of-flight mass spectrometry to determine chiral lactones and characterize the volatilome of Marsala wines[*]

The present research is focused on the proposal of use of flow-modulation comprehensive two-dimensional enantio-gas chromatography (FM eGC×GC) as a valid, flexible, and possibly superior alternative to heart-cutting multidimensional enantio-GC (eMDGC). The latter is used specifically for the targeted separation of chiral compounds, whereas FM eGC×GC can produce both targeted and high-resolution untargeted information in a single run. It is clearly possible to use eMDGC for untargeted analysis, often with a flame ionization detector (stand-by analysis), to monitor a first-dimension (^{1}D) separation, of much lower peak capacity compared to FM eGC×GC. If eMDGC is used with mass spectrometry (MS), it is normally exploited to monitor the second-dimension (^{2}D) separation. The analytical instrument consisted of automated solid-phase microextraction, and a low duty-cycle FM eGC×GC system (with time-of-flight MS), equipped with an enantioselective ^{1}D column (2,3-di-O-methyl-6-t-butyl silyl β-cyclodextrin derivative) and a ^{2}D polyethylene glycol one. Ten Marsala wines were subjected to analysis, for the determination of chiral lactones and for general analyte profiling. Then, statistical analysis (ANOVA-simultaneous component analysis and partial least squares discriminant analysis) is used for sample differentiation.

8.1 Introduction

Heart-cutting enantioselective multidimensional gas chromatography (eMDGC) is a technique of established utility for the targeted analysis of specific chiral compounds, often contained in food samples [1]. Commonly, a Deans switch is used as transfer device, with an achiral separation performed in the first dimension (^{1}D) and a chiral one in the second dimension (^{2}D). Additionally, an initial "stand-by" ^{1}D analysis is performed to monitor the whole sample chromatogram, and to enable the selection of the heart-cut time windows. After, a "cut" analysis is carried out, during which the target chiral compounds are separated on the ^{2}D column. A flame ionization detector (FID) is often used for the "stand-by" analysis, while mass spectrometry, or in alternative a FID, are used for the "cut" analysis. In this way, enantiomer ratios can be determined in a reliable manner, greatly reducing the occurrence of chromatographic interferences, often observed in eGC [2]. Though variations do exist, the aforedescribed instrumental configuration is the most popular among eMDGC analysts [3]. Enantioselective comprehensive two-dimensional gas chromatography (eGC×GC) has been previously reported, with both cryogenic and flow modulation (CM/FM) [4-5]. With regard to CM, experiences with ^{1}D and ^{2}D enantioselective columns have been made [6-8]; the choice of an enantioselective ^{1}D column is the best choice, due to a much higher separation power compared to a short ^{2}D one. Proceeding onto FM, then it appears to be a better choice (compared to CM) for three reasons: 1) the increase of signal-to-noise ratio (s/n) values provided by CM is not necessary in enantioselective analyses; 2) FM systems have a lower economical cost; 3) if required, brief ($<$ 500 ms) modulation periods (P_M) can be applied, which becomes an important factor for closely-eluting enantiomers.

The present investigation involves the targeted and untargeted headspace analysis of Marsala wine. Marsala wine (or "Marsala") is one of the four most important fortified aged wines [9], with classification related to aging, colour, and sugar [10]. Considering aging, Marsala can be distinguished in "Fine" (min. 1 year), "Superiore" (min. 2 years), "Superiore Riserva" (min. 4 years.), "Vergine" (min. 5 years) and "Stravecchio" (min. 10 years). The beverage is available in three different colours namely gold, amber, and ruby, and is also classified as dry, semi-dry, and sweet according to the sugar content [11]. Finally, Marsala wines are classified as Marsala
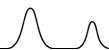
Vergine (Marsala Vergine and Stravecchio) and Marsala Conciati (Fine, Superiore and Superiore Riserva) based on the production process. Aging is carried out using oak and/or cherry barrels [12]. The study of wine aroma is an important factor in quality control. In particular, γ- and δ-lactones are important constituents of beverage aromas, especially barrel-aged ones [13]. These compounds are often potent and pleasant odorants, that contribute to a variety of aromas, including "coconut", "fatty" and "sweet fruit" [14]. Almost all lactones are chiral, and the abundance of the single enantiomers varies significantly, although the (*R*)-enantiomer is dominant [15,16]. Furthermore, lactones can be exploited as markers for beverages aged in wood barrels, and for possible cases of adulteration [17]. The use of oak wood aging and specific fermentation methods cause different changes in the beverage chemical composition and overall sensory properties [17]. Among the compounds found in oak wood, *cis*- and *trans*-β-methyl-γ-octalactones (commonly known as whisky lactones) are key compounds that significantly contribute to the final aroma, with their concentration increasing proportionally to the aging time. Specifically, whiskey lactones can exist in the form of four stereoisomers - two enantiomeric pairs of two diastereomers. Each isomer has its own characteristic coconut-based odor (*cis*-, with additional earthy, hay-like notes, while *trans*- with celery-like ones) and specific odor thresholds; furthermore, the *cis* isomer is a stronger odorant than the *trans* one [18,19]. It should be noted that in nature, oak wood contains only *trans*-(+)-(3S,3R) and *cis*-(−)-(3S,4S) whisky lactone isomers [20].

The present research is based on the use of (low duty-cycle) FM eGC×GC, as a valid (and potentially superior alternative) to eMDGC. Ten Marsala wine samples were subjected to headspace solid-phase microextraction (HS SPME), while detection was carried out by using time-of-flight mass spectrometry (ToFMS) - hydrogen was used as carrier gas [21,22]. Fifteen target chiral lactones were determined, with 14 existing as enantiomers. The lactones were quantified by constructing matrix-matched calibration curves; moreover, instrumental detection limits (IDL) were calculated. The developed method was also exploited to investigate the Marsala volatilomes, highlighting their highly complex nature, with over 300 compounds tentatively-identified. The samples were differentiated through statistical analysis specifically by means of ANOVA-simultaneous component analysis (ASCA) and Partial Least

Squares Discriminant Analysis (PLS-DA). It is noteworthy, that the Marsala volatilome has been previously investigated by using HS SPME cryogenic-modulation GC×GC-MS [9]; that research, however, was based only on untargeted profiling using achiral columns.

8.2 Experimental

Samples and chemicals

Ten Marsala wines were obtained directly from commercial activities located in Messina. The bottles were stored at ambient temperature prior to analysis. They belonged to three different types of Marsala: six Fine, three Superiore and one Stravecchio.

The following lactones, available as standard compounds, were investigated: γ-valerolactone (purity ≥ 99%), γ- and δ-hexalactone (purity ≥ 98%), γ-heptalactone (purity ≥ 98%), γ- and δ-octalactone (purity ≥ 97%), γ- and δ-nonalactone (purity ≥ 98%), γ- and δ-decalactone (purity ≥ 98%), γ- and δ-undecalactone (purity ≥ 98%), γ- and δ-dodecalactone (purity ≥ 97%), *cis*- and *trans*-whisky lactone (purity ≥ 98%). The standards, sodium chloride, ethanol, and 3-octanol, used as internal standard (IS), were purchased from Merck Life Science (Merck KGaA, Darmstadt, Germany). The IS was solubilized in ethanol and was added to each sample at a concentration of 170 μg L^{-1}. Individual stock standard solutions were prepared in ethanol, for all the lactones.

Instrumentation

The HS SPME extractions were performed automatically by using an L-PAL3 GC Autosampler (LECO, Mönchengladbach, Germany). The extraction procedure was based on a previously published paper [18]. Briefly, 5 mL of each sample were place in a 20 mL headspace vial, along with 0.5 g of NaCl and 5 μL of IS. A 50/30 μm divinylbenzene/carboxen/polydimethylsiloxane (DVB/CAR/PDMS) SPME fiber was conditioned according to the manufacturer's guidelines. The samples were incubated for 30 min at 60 °C, followed by 30 min of extraction at the same temperature. The agitation speed was 500 rpm. After extraction, the analytes were desorbed for 2 min at 220 °C, in the splitless mode. After each extraction and desorption procedure, the

fiber was reconditioned for 5 min at 220 °C, to avoid analyte carryover between following extractions. Three replicates for each sample were carried out.

The FM eGC×GC-ToFMS applications were performed on a Pegasus® BT 4D GC×GC-ToFMS system equipped with a Flux™ modulator (LECO). The GC×GC column set was: Astec CHIRAL DEX B-DM [2,3-di-O-methyl-6-t-butyl silyl derivative of β-cyclodextrin phase] with dimensions 30 m × 0.25 mm ID × 0.12 μm d_f employed as ^{1}D column, while the ^{2}D column was a Supelcowax 10 [polyethylene glycol] with dimensions 1.30 m × 0.10 mm ID × 0.10 μm d_f and with 0.3 m located inside the MS transfer line (220°C). All columns were provided by Merck Life Science. The carrier gas used was H_2, delivered at a constant flow of 0.8 ml min^{-1}. The main GC oven was held at 50 °C for 2 min, then ramped up to 220 °C at 2 °C min^{-1}, with a secondary oven temperature offset of +10°C. The modulation period (P_M) was set at 4 s, with a re-injection period of 80 ms. The auxiliary pressure unit (EPC) provided a constant flow of 3.5 ml min^{-1}. The MS parameters were as follows: acquisition delay was 240 s; acquisition rate was 150 spectra s^{-1}; electron ionization was performed at 70 eV, while mass spectra were acquired in the mass channel range m/z 40–400. Data were acquired and processed by using the ChromaTOF software v. 5.50.55.0.63466 (LECO). The mass spectral databases used were the Flavour and Fragrance Natural and Synthetic Compounds (FFNSC) v. 4.0 (Chromaleont s.r.l. Messina, Italy) and the mainlib (NIST).

Data analysis

For "hit" recognition the LECO ChromaTOF Tile-computed v.1.01 (LECO Corporation, St. Joseph, MI) software was used. Normalization was performed using the 3-octanol IS peak signal (^{1}t$_R$ = 1594.03 s, ^{2}t$_R$ = 1.6881 s), extracted at m/z 59. Tile sizes of 3 modulations for the ^{1}D separation and 23 spectra for the ^{2}D were selected, to encompass the average peak widths along both dimensions. A s/n threshold of 10 was applied to exclude low signal hits from the hitlist [23]. No F-ratio threshold was set herein, the entire m/z range was included for tile-based F-ratio analysis.

After hit list generation, compound tentative identification was performed using the FFNSC and the mainlib (NIST) databases. The sample files were labeled according

to Marsala type, resulting in ten classes for F-ratio analysis, with three replicates per class.

ANOVA simultaneous component analysis - ASCA

ASCA performs a multivariate analysis of variance (ANOVA) - even when the number of measured variables is higher than the available samples - by applying principal component analysis (PCA) to each of the factors under study [24,25]. Such an approach allows to determine if a given factor is significant relative to the residual error. ASCA models show if the factor under study has a significant role in explaining the variance structure of the experimental data. Cases in which more than one factor is involved can also be studied. For significance estimation, the *p*-value is calculated for each factor based on a test consisting in repeated random permutation of the factor levels. ASCA tests a null hypothesis H_0 of no experimental effect of the factor of interest against the alternative hypothesis (H_1) of an experimental effect, at a preselected significance level of *p*.

In the present study the factor considered is the type of Marsala wine, encoded at three levels: Fine, Superiore, Stravecchio. Descriptor variables are the FM eGC×GC data.

Data processing was performed by means of PLS_Toolbox® (Version 9.2, Eigenvector Research Inc.) that allows the calculation of ASCA+ models [26], suitable also for cases in which unbalanced classes (different number of samples in each level of the factor) are considered.

Partial least squares discriminant analysis - PLS-DA

PLS is a widespread linear classification technique particularly useful in cases in which the number of samples is lower than the number of measured variables. The method applies PLS regression using a dummy index (*e.g.*, encoded by 0 and 1) as the response variable [27]. When more than two classes are involved, it is necessary to apply a PLS-2 algorithm, which allows to predict one matrix of response variables, with as many columns as classes.

PLS-DA can be used for building predictive models, which can be applied to determine class membership of new samples, and/or to assess the importance of

descriptor variables in characterizing the different classes under study. This latter aim can be achieved by computing the VIP (variable importance in projection) scores, a value computed for each descriptor variable in each class [28]. A VIP score higher than one indicates that the corresponding variable is important in the model obtained for the characterization of the specific class.

8.3 Results and Discussion

The aim of the present investigation was the development of an HS SPME FM eGC×GC-ToFMS method for the simultaneous determination of fifteen target chiral lactones and of the volatile fraction of Marsala wines. Hence, the instrumental approach is of a both untargeted and targeted nature, and is herein proposed as a valid, if not better alternative to eMDGC.

The HS SPME method used has been previously published [18], while the FM eGC×GC-ToFMS one was optimized to avoid the loss of ^{1}D resolution, potentially leading to an incorrect measurement of enantiomeric ratios. Moreover, lactones are generally present at the µg L^{-1} concentration levels, thus attention was also devoted to the instrumental detection limits (IDLs), considering that a low duty-cycle modulator was used. A P_M of 4 s was applied with a re-injection pulse of 80 ms, leading to a theoretical duty cycle of 0.02 (*circa* 2% of the ^{1}D effluent reaches the detector). The resolution between all the enantiomers was satisfactory, as can be seen in Fig. 8.1; it is noteworthy that δ-hexalactone (peak 3) is present as a single enantiomer. Table 8.1 reports IDLs, coefficient of variation (CV%) values, full widths at half maximum, tailing factors and ^{1}D resolution values ($n = 3$) calculated without performing the modulation process.

The IDLs were calculated by multiplying the standard deviation of the analyte area at the lowest concentration level (1 µL liquid injection, in the splitless mode) by the statistical confidence factor *t*. The confidence factor *t* is determined using Student's t-distribution with a 99 % confidence level and *n*-1 degrees of freedom. For each pair of enantiomers, the average IDLs are reported. The average IDL values ranged from 0.02 ng for δ-undecalactone, δ-dodecalactone, and *cis*-whisky lactone to 0.17 ng for δ-hexalactone. The tailing factor values ranged from 1.3 to 1.7. With regard

enantiomeric resolution, values ranged from 1.4 for δ-decalactone and δ-dodecalactone to 12.0 for *trans*-whisky lactone.

Particular attention was devoted to determining the enantiomeric ratios of the target chiral lactones. Indeed, the enantiomeric ratio values, calculated by performing an unmodulated analysis of the standard components, were compared with those obtained through eGC×GC. The values obtained in both modes were in agreement with each other, demonstrating that the modulation process had no influence on the calculation of the enantiomeric ratios.

The quantification of all the target compounds was carried out by using the multiple standard addition method, with each sample spiked at five different concentration levels, according to the initial amount of lactones present in the sample.
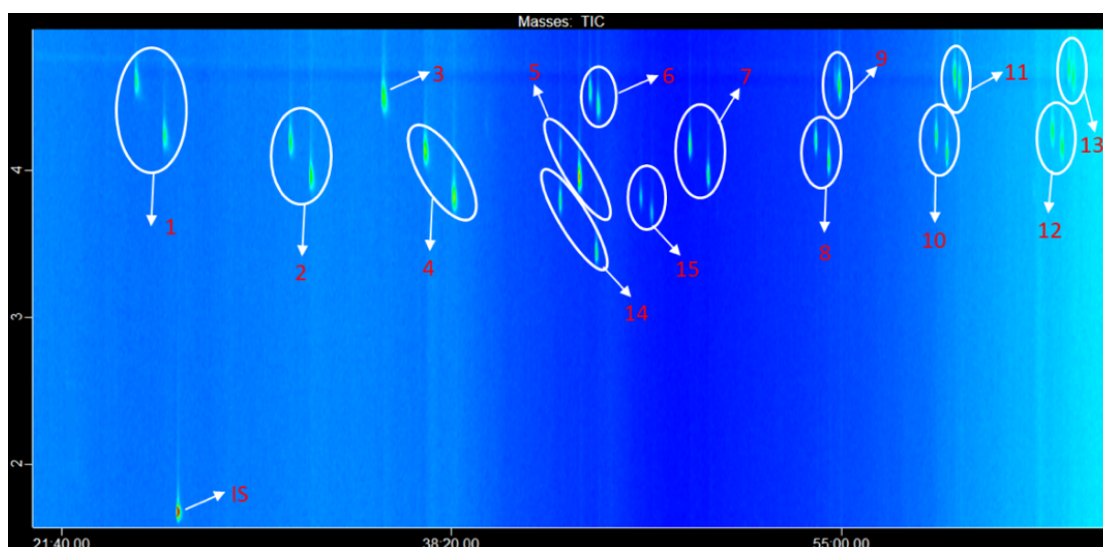
Figure 8.1. *FM GC × GC-ToFMS chromatogram of a mixture of 14 chiral and the IS.*

Peak identification: 1. γ-valerolactone; 2. γ-hexalactone; 3. δ-hexalactone; 4. γ-heptalactone; 5. γ-octalactone; 6. δ-octalactone; 7. γ-nonalactone; 8. γ-decalactone; 9. δ-decalactone; 10. γ-undecalactone; 11. δ-undecalactone; 12. γ-dodecalactone; 13. δ-dodecalactone; 14. trans whisky lactone trans; 15. cis whisky lactone.

Table 8.1. *List of the analyzed lactones with concentration range, average instrumental detection limit values (IDL), coefficient of variation CV% values, full width half maximum (FWHM), tailing factors (TF) and ^1D resolution (R_S) (n = 3).*

Compound	Concentration range (ng)	IDL (ng)	CV%	FWHM (s)	TF	R_S	Enantiomeric ratio
γ-valerolactone: 1	0.24-5.02	0.03	12.1	0.142	1.4	6.4	50/50
γ-valerolactone: 2	0.26-4.98		14.8	0.132	1.5		
γ-hexalactone: 1	0.25-4.92	0.05	11.9	0.129	1.5	5.7	50/50
γ-hexalactone: 2	0.25-5.08		8.3	0.123	1.5		
δ-hexalactone	0.50-10.0	0.17	14.9	0.136	1.5	-	-
γ-heptalactone: 1	0.25-5.09	0.14	15.0	0.125	1.5	8.5	50/50
γ-heptalactone: 2	0.25-4.91		14.9	0.118	1.5		
γ-octalactone: 1	0.04-1.09	0.13	14.3	0.124	1.5	6.1	10/90
γ-octalactone: 2	0.46-8.91		12.3	0.122	1.5		
δ-octalactone: 1	0.23-5.36	0.03	14.9	0.130	1.4	2.6	44/56
δ-octalactone: 2	0.27-4.64		15.0	0.129	1.4		
γ-nonalactone: 1	0.24-5.15	0.08	13.8	0.125	1.5	5.8	50/50
γ-nonalactone: 2	0.26-4.85		13.0	0.118	1.5		
γ-decalactone: 1	0.26-5.01	0.05	13.1	0.123	1.4	4.4	49/51
γ-decalactone: 2	0.24-4.99		12.4	0.118	1.4		
δ-decalactone: 1	0.08-1.54	0.03	11.1	0.135	1.3	1.4	15/85
δ-decalactone: 2	0.42-8.46		11.1	0.132	1.3		
γ-undecalactone: 1	0.24-4.96	0.03	9.2	0.121	1.4	3.7	50/50
γ-undecalactone: 2	0.26-5.04		11.6	0.119	1.4		
δ-undecalactone: 1	0.25-5.06	0.02	10.2	0.131	1.2	1.6	48/52
δ-undecalactone: 2	0.25-4.94		9.0	0.129	1.2		
γ-dodecalactone: 1	0.24-5.02	0.04	14.6	0.120	1.3	3.1	48/52
γ-dodecalactone: 2	0.26-4.98		13.9	0.117	1.3		
δ-dodecalactone: 1	0.24-4.98	0.02	14.4	0.128	1.2	1.4	48/52
δ-dodecalactone: 2	0.26-5.02		13.9	0.129	1.2		
trans-whisky lactone: 1	0.25-5.04	0.03	12.9	0.118	1.5	12.0	51/49
trans-whisky lactone: 2	0.25-4.96		12.2	0.109	1.5		
cis-whisky lactone: 1	0.24-5.08	0.02	14.5	0.120	1.6	3.6	50/50
cis-whisky lactone: 2	0.26-4.92		12.1	0.114	1.5		

Target analyses

Ten Marsala wines were then analyzed, for the determination of the chiral lactones. All the investigated Marsala samples were amber in color, while the Marsala Superiore, Stravecchio, and Fine 6 were dry, and the other Marsala Fine samples were semi-dry. Table 8.2 reports the chiral lactone amounts ($n = 3$), involving a total of six different compounds. The absolute quantities of each compound are reported, along with the % values of each enantiomer, with these showing a great variability. The CV% values are satisfactory, always lower than 15%. Whisky lactones have the highest concentration among the investigated lactones. In particular, the *trans* isomer ranged from 0.33 to 145.75 µg L^{-1} (Marsala Superiore 2 and Marsala Stravecchio, respectively), while the *cis* isomer ranged from 8.50 to 496.00 µg L^{-1} (Marsala Fine 5 and Marsala Stravecchio, respectively). Whisky lactones are the most important volatile compounds present in oak wood, because they contribute to the final aroma of the product, and they are considered as oak markers [8]. No whisky lactones were found in Marsala Fine 1 and 2, while only the *cis* isomer was determined in Marsala Fine 5 and 6. Different factors, such as the wood structure, toasting technique, and aging time, affect the whisky lactone amount in the product. The first (eluting) γ-nonalactone enantiomer of (ranging from 3.00 to 6.00 µg L^{-1}) was always present in excess with respect to the second one (ranging from 0.03 to 3.18 µg L^{-1}), with this below its IDL in Marsala Fine 6. In Marsala Fine 3, Fine 4, and Superiore 1, the γ-nonalactone enantiomers were not determined. Both γ-decalactone enantiomers were observed in five samples, mainly those with more aging (Marsala Superiore 2 and 3, Stravecchio), apart from Marsala Fine 1 and 2. Low concentrations of both γ-undedecalactone isomers were observed in Marsala Superiore 2 and 3, and Stravecchio 1 (0.15-1.29 and 0.04 to 1.09 µg L^{-1}, for enantiomers 1 and 2, respectively). Only two aged samples (Marsala Superiore 2 and 3) contained both γ-dodecalactone isomers. The results indicate a steady, albeit slightly irregular increase in lactones with aging. Moreover, enantiomer 1 was always present in higher amounts, apart for γ-decalactone and γ-dodecalactone in Marsala Superiore 2. According to previously published papers [15,16], the first eluting enantiomer can be tentatively-identified as the (R)-enantiomer form. Enantiomer % values varied

greatly - *e.g.*, the γ-nonalactone enantiomers were determined in six samples, with the first present in the range 55-99%.

Untargeted analysis

The method developed enabled also an in-depth study of the volatile composition of the ten Marsala wine samples. To illustrate the high complexity of Marsala wines, the chromatogram of the Stravecchio sample is shown in Figure 8.2, in which the eight lactones determined are indicated; variations in analyte retention times between the standard solution and the beverage are due to the different injection procedures. Overall, 325 compounds were tentatively identified.
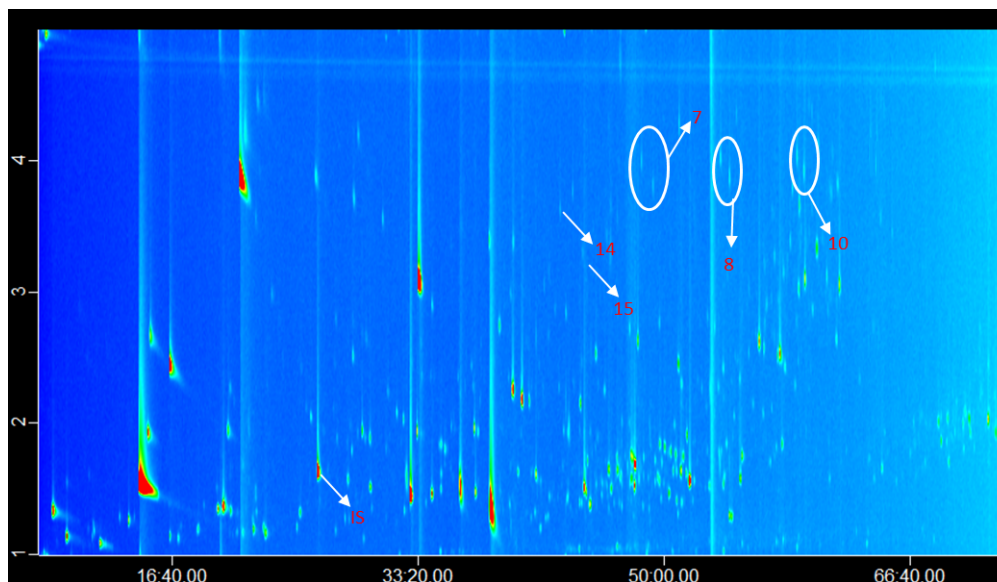
Figure 8.2. *FM GC × GC-ToFMS chromatogram of the Marsala "Stravecchio" headspace.*

Absolute quantification was not performed, it being outside the scope of the present investigation; however, MS % areas can be exploited to evaluate concentration trends of the same compound in the different samples. In general, enantiomer ratios can be determined through MS peak areas. Among the tentatively-identified compounds, fatty acid esters comprise a significant group of compounds in Marsala wines. The most abundant esters were ethyl octanoate and diethyl succinate, that confer fruity and tropical notes; specifically, their amounts increased from the youngest to the oldest sample. Also, ethyl acetate (ethereal, fruity, sweet, weedy, green odour) exhibited the highest amount in Marsala Stravecchio and the lowest in

the youngest wine (Marsala Fine 2). Other esters found in the investigated samples were isoamyl acetate, ethyl butyrate, ethyl hexanoate, ethyl decanoate and ethyl lactate. The first compound showed the highest amount in Marsala Fine 1 and Marsala Stravecchio 1, ethyl butyrate in Marsala Fine 5 and Superiore 2, ethyl hexanoate in Marsala Fine 5, and ethyl decanoate in Marsala Superiore 1. Finally, ethyl lactate - an important compound which contributes to the broader, fuller taste of wine - showed the highest amount in Marsala Superiore 3 [29]. The most abundant alcohol (excluding ethanol) was isopentyl alcohol, providing chemical notes, detected in comparable amounts in all samples except for Marsala Fine 4, where its level was the lowest [2]. Isobutyl alcohol was found in similarity quantities in all the investigated samples. A wide range of aldehydes with diverse odour notes were also found. Increasing values of furfural that confers sweet, woody and roasty notes were found from Marsala Fine 1 (2.95) to Marsala Superiore 1 (66.62) [29]. Untargeted enantiomers were also detected: phenethyl alcohol enantiomers were separated, with the first enantiomer in higher amounts it being characterized by a floral odour [9].

.

Table 8.2. *Analyzed samples along with lactone concentrations, enantiomeric ratios (%) reported in parenthesis, and CV% values.*

Sample	*trans*-whisky lactone		*cis*-whisky lactone		γ-nonalactone: 1		γ-nonalactone: 2		γ-decalactone: 1		γ-decalactone: 2		γ-undecalactone: 1		γ-undecalactone: 2		γ-dodecalactone: 1		γ-dodecalactone: 2	
	ppb	CV%	ppb	CV%	ppb	CV%	ppb	CV%	ppb	CV%	ppb	CV%	ppb	CV%	ppb	CV%	ppb	CV%	ppb	CV%
Marsala Fine 1	-	-	-	-	3.91 (55)	7.1	3.18 (45)	3.1	3.89 (54)	8.0	3.28 (46)	10.9	-	-	-	-	-	-	-	-
Marsala Fine 2	-	-	-	-	6.00 (96)	5.5	0.25 (4)	8.6	0.35 (68)	14.3	0.17 (32)	14.1	-	-	-	-	-	-	-	-
Marsala Fine 3	10.00	14.9	66.50	14.3	-	-	-	-	-	-	-	-	-	-	-	-	-	-	-	-
Marsala Fine 4	39.50	9.2	227.00	14.5	-	-	-	-	-	-	-	-	-	-	-	-	-	-	-	-
Marsala Fine 5	-	-	8.50	14.7	3.23 (78)	0.5	0.93 (22)	14.2	-	-	-	-	-	-	-	-	-	-	-	-
Marsala Fine 6	-	-	-	-	5.91 (73)	13.3	2.15(27)	5.6	-	-	-	-	-	-	-	-	-	-	-	-
Marsala Superiore 1	52.71	9.9	154.00	10.7	-	-	-	-	-	-	-	-	-	-	-	-	-	-	-	-
Marsala Superiore 2	0.33	14.5	12.00	14.0	3.00 (99)	7.5	0.03 (1)	5.3	0.68 (42)	13.1	0.94 (58)	14.4	1.29 (54)	10.4	1.09 (46)	14.4	0.90 (45)	14.5	1.12 (55)	11.7
Marsala Superiore 3	16.20	5.8	136.28	1.7	4.55 (70)	13.2	1.91 (30)	14.4	0.79 (92)	11.1	0.07 (8)	12.5	1.36 (82)	11.3	0.31 (18)	13.5	0.73 (95)	4.8	0.04 (5)	14.7
Marsala Stravecchio	145.75	2.4	496.00	7.1	4.77 (81)	2.3	1.14 (19)	8.4	0.67 (79)	14.3	0.18 (21)	8.4	0.15 (79)	12.4	0.04 (21)	11.7	-	-	-	-

Multivariate data processing

The multivariate data processing performed in the present study is aimed at evaluating, from an exploratory point of view, the possibility of differentiating Marsala wine samples according to three different types (Fine, Superiore and Stravecchio) and to identify which compounds, among the ones tentatively-identified, are the most informative for such a profiling. The chemometric methods applied (ASCA and PLS-DA) were limited to the exploratory domain and were not aimed at building predictive models, also considering the reduced sample size. ASCA was applied considering as the data matrix the FM eGC×GC data and, as the factor under study, the class membership at three possible levels: Fine, Superiore and Stravecchio. The effect of the factor "Marsala type" contributes to the overall sum of squares of the data matrix with a 22.73% of explained variance. This indicates that this information is not predominant in the dataset, but significant and useful for sample differentiation at a 5% significance level (*p-value* = 0.02).

The figure 8.3 shows that the different Marsala types are characterized by a different average score value on PC1 of ASCA decomposition. In more detail, Fine samples are described by the lowest average score value, at around -1. Superiore samples present again a negative average score value, but higher (around -0.5). Stravecchio wine, in turn, is characterized by positive score value (on average about 1.25).
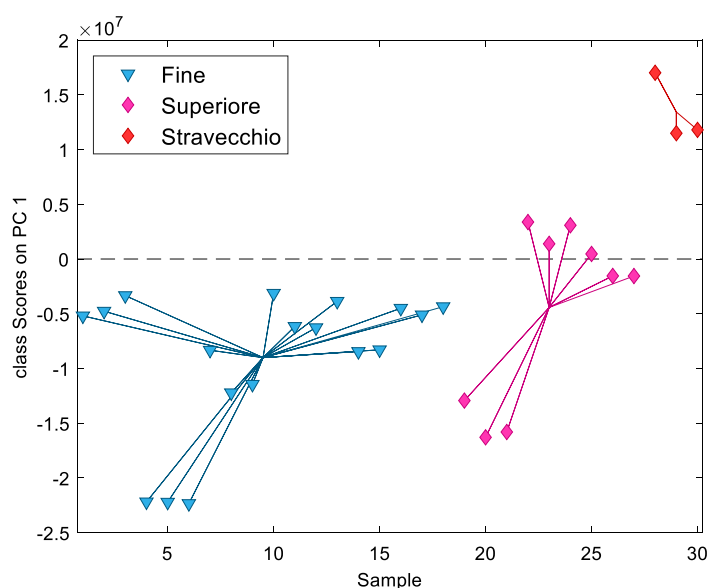

Figure 8.3. *Scores on PC1 of ASCA decomposition for the factor "Marsala type".*

In particular, among the 1186 variables analysed, only the ones with an associated loading absolute value higher than 0.1 are represented (for the sake of clarity). The same variables are also listed in Table 8.3, reporting the variable number, the compound identity and the associated numerical loading value. It must be highlighted that the higher the absolute value of the loading, the more important is the contribution of the corresponding variable for the differentiation of the Marsala type.

Table 8.3 *Variables with loading value on PC1 higher than 0.1 (absolute value).*

Variable number	Compound	PC1 loading value
53	2,5-dimethyl-5-hexen-3-ol	0.1130
129	**2-oxopentanedioic acid**	**0.1897**
157	**Octan-3-ol**	**0.2878**
171	Whiskey lactone cis	0.1172
202	**Ethyl benzoate**	**0.4277**
206	Cyclobutane-1,1-dimethyl-2-octyl	0.1127
249	**Ethyl 2-furoate**	**0.2261**
267	Whiskey lactone trans	0.1038
347	**Diethyl malate**	**0.2427**
401	**Ethyl phenylacetate**	**0.4790**
513	2-phenylethyl formate	0.1823
562	**Phenethyl alcohol**	**-0.3889**
812	14-methyl-8*E*-hexadecenal	-0.1095
1178	3-Butyn-1-ol	0.1406

Moreover, from a joint interpretation of ASCA scores and loadings, it can be concluded that compounds with a negative loading value present a higher concentration in Marsala types with negative scores: Fine and Superiore. Conversely, Stravecchio Marsala wine (with positive scores) is characterized by a higher concentration of compounds with positive loadings. To verify the consistency of the chemical characterization performed by means of ASCA decomposition, PLS-DA was carried out considering the three Marsala types as three classes to be modelled. Afterwards, a variable evaluation was performed by analysing the VIP profiles and selecting the most informative analytical descriptors for discrimination of the three classes. The selection criterion was defined as VIP value higher than 4 for all the three classes. In this way, twelve descriptors were selected; they are listed in Table 8.4, indicating the detail of the VIP score value for each of the three classes.

Table 8.4. *Variables with VIP score values higher than 4 for all the three classes.*

Variable number	Compound	VIP scores for class one Fine	VIP scores for class two Superiore	VIP scores for class three Stravecchio
15	Pent-4-enophenone	4.82	5.69	5.59
19	α-terpineol	4.80	6.46	6.65
129	**2-oxopentanedioic acid**	**5.83**	**4.15**	**4.93**
157	**Octan-3-ol**	**9.02**	**7.29**	**7.23**
202	**Ethyl benzoate**	**10.37**	**8.08**	**10.39**
246	Delta cadinene	5.84	6.99	7.11
249	**Ethyl 2-furoate**	**5.78**	**4.39**	**5.67**
296	1,4,4-trimethyl-3,5-dimethylidenecyclopentene	9.31	11.68	8.49
347	**Diethyl malate**	**7.09**	**6.38**	**6.53**
401	**Ethyl phenylacetate**	**10.08**	**10.43**	**12.62**
477	2-phenethyl acetate	6.83	7.02	4.61
562	**Phenethyl alcohol**	**10.88**	**6.46**	**9.46**

Variables selected by both of the approaches (ASCA and PLS-DA) are highlighted in bold, confirming a good consistency between the two outcomes. It is also noticeable that the commonly selected variables are the ones with the highest absolute value of the ASCA loadings and of the PLS-DA VIP scores. These can be, therefore, considered as the most important compounds for the characterization and differentiation of the three Marsala wines.

The normalised areas of the five most informative compounds defined both statistical approaches are shown in Figure 8.4. The Stravecchio sample is the one with the higher amounts of ethyl benzoate, ethyl 2-furoate, and ethyl phenylacetate. The first gives a pleasant fruity odour, the second has a balsamic smell, while the third has a honey-like aroma. Malate diethyl is present in similar quantities in the Stravecchio and Superiore 2 samples, with caramel and fruity notes. Phenethyl alcohol, which gives a floral (rose) odour, is present in higher quantities in all Fine samples (except Fine 1) and the Superiore 1 and 2 samples.
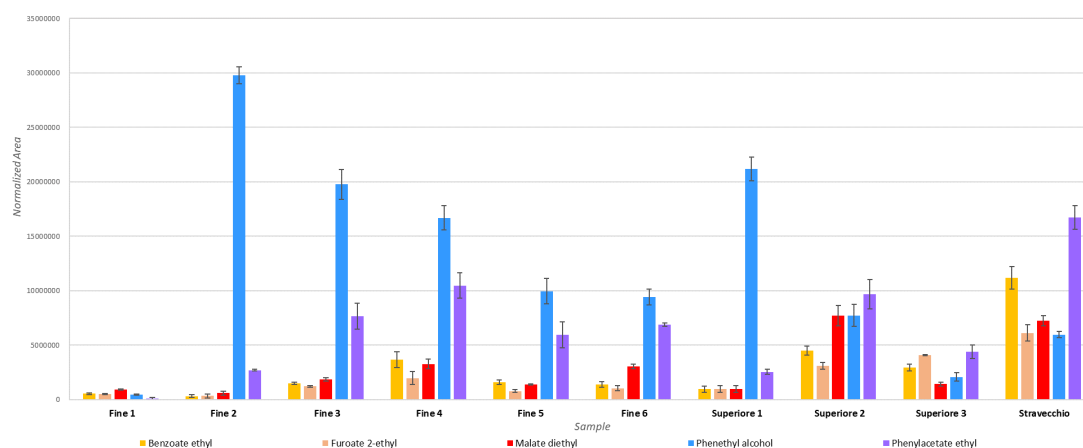
Figure 8.4. *Bar chart reporting the normalized areas of the five most informative compounds of the investigated Marsala wines.*

8.4 Conclusions

The scope of the present research is to propose the use of FM eGC×GC as a prime choice for the determination of both chiral and untargeted volatile compounds. For such a demonstrative objective, Marsala wine was subjected to analysis. In such a respect, the results attained confirm the high usefulness of the analytical platform employed, inasmuch that two types of information can be produced in a single run. Even though a low duty cycle modulator was used, inevitably causing a great reduction of the analyte amounts reaching the MS system, the chiral lactones were detected at the low ppb level. Moreover, the headspace chromatogram profiles were of high complexity and detail. Even though a reduced number of samples was subjected to investigation, statistical analysis enabled a clear differentiation between Marsala types, and the highlighting of five compounds which differed most. The superiority of FM eGC×GC over classical eMDGC, in untargeted analysis, is clear. Future research will be devoted to a side-by-side comparison between FM eGC×GC and eMDGC in the chiral-only analysis of well-known food samples, such as Citrus essential oils.

References

[1] A.A. Elbashir, H.Y. Aboul-Enein, Multidimensional gas chromatography for chiral analysis, Crit. Rev. Anal. Chem. 48 (2018) 416-427, doi: 10.1080/10408347.2018.1444465.

[2] Y. Nolvachai, C. Kulsing, P.J. Marriott, Multidimensional gas chromatography in food analysis, Trac-Trend. Anal. Chem. 96 (2017) 124-137, doi: 10.1016/j.trac.2017.05.001.

[3] Basic multidimensional gas chromatography (chapter 2) 2020 edited by N.H Snow.

[4] O. Vyviurska, N. Koljančić, A. A. Gomes, I. Špánik, Optimization of enantiomer separation in flow-modulated comprehensive two-dimensional gas chromatography by response surface methodology coupled to artificial neural networks: wine analysis case study, J. Chromatogr. A 1675 (2022) 463189, doi: 10.1016/j.chroma.2022.463189.

[5] M. Junge, H. Huegel, P.J. Marriott, Enantiomeric analysis of amino acids by using comprehensive two-dimensional gas chromatography, chirality (2207) 228-234, doi:10.1002/chir.20371.

[6] R. Shellie, P.J. Marriott, Comprehensive two-dimensional gas chromatography with fast enantioseparation, Anal. Chem. 74 (2002) 5426-5430, doi: 10.1021/ac025803e.

[7] C. Legrum, P. Slabizki, H.-G. Schmarr, Enantiodifferentiation of 3-sec-butyl-2-methoxypyrazine in different species using multidimensional and comprehensive two-dimensional gas chromatographic approaches, Anal. Bioanal. Chem. 407 (2015) 253–263, doi: 10.1007/s00216-014-8061-8.

[8] S. Krögera, Y.F. Wong, S.-T. Chin, J. Grant, D. Lupton, P. J. Marriott, Evaluation of reversible interconversion in comprehensive two-dimensional gas chromatography using enantioselective columns in first and second dimensions. J. Chromatogr. A 1404 (2015) 104–114, doi: 10.1016/j.chroma.2015.05.049.

[9] G. Dugo, L. La Pera, T.M. Pellicanò, G. Di Bella, M. D'Imperio, Determination of some inorganic anions and heavy metals in D.O.C. golden and amber marsala wines: statistical study of the influence of ageing period, colour and sugar content, Food Chem. 91 (2005) 355–363, doi: 10.1016/j.foodchem.2004.09.001.

[10] G. Dugo, F.A. Franchina, M.R. Scandinaro, I. Bonaccorsi, N. Cicero, P.Q. Tranchida, L. Mondello, Elucidation of the volatile composition of Marsala wines by using comprehensive two-dimensional gas chromatography, Food Chem. 142 (2014) 262–268, doi: 10.1016/j.foodchem.2021.130029.

[11] G.L. La Torre, L. La Pera, R. Rando, V. Lo Turco, G. Di Bella, M. Saitta, G. Dugo, Classification of Marsala wines according to their polyphenol, carbohydrateand heavy metal levels using canonical discriminant analysis, Food Chem. 110 (2008) 729–734, doi: 10.1016/j.foodchem.2008.02.071.

[12] C. Condurso, F. Cincotta, G. Tripodi, A. Verzera, Characterization and ageing monitoring of Marsala dessert wines by a rapid FTIR-ATR method coupled with multivariate analysis, Eur. Food Res. Technol. (2018), doi:10.1007/s00217-017-3025-9.

[13] G.C. Miller, L.I. Pilkington, D.Barker, R.C. Deed, Saturated Linear Aliphatic γ- and δ-Lactones in wine: A review, J. Agric. Food Chem. 70 (2022) 15325–15346, doi:10.1021/acs.jafc.2c04527.

[14] X. Qian, Y. Lan, S. Han, N. Liang, B. Zhu, Y. Shi, C. Duan, Comprehensive investigation of lactones and furanones in icewines and dry wines using gas chromatography-triple quadrupole mass spectrometry, Food Res. Int. 137 (2020) 109650, doi: 10.1016/j.foodres.2020.109650.

[15] P. Stamatopoulos, E. Brohan, C. Prevost, T. E. Siebert, M.Herderich, P. Darriet, Influence of chirality of lactones on the perception of some typical fruity notes through perceptual interaction phenomena in bordeaux dessert wines, J. Agric. Food Chem. 64 (2016) 8160−8167, doi: 10.1021/acs.jafc.6b03117.

[16] R.C. Cooke, K.A. van Leeuwen, D.L. Capone, R. Gawel, G.M. Elsey, M.A. Sefton, Odor detection thresholds and enantiomeric distributions of several 4-alkyl substituted γ-lactones in australian red wine, J. Agric. Food Chem. 57 (2009) 2462-2467, doi: 10.1021/jf802866f.

[17] G.-D. Dumitriu (Gabur), C.Teodosiu, I. Gabur, V.V. Cotea, R. A. Peinado, N. López de Lerma, In-depth search focused on furans, lactones, volatile phenols, and acetals as potential age markers of madeira wines by comprehensive two-dimensional gas chromatography with time-of-flight mass spectrometry combined with solid phase microextraction, Foods 8 (2019) 662, doi:10.3390/foods8120662.

[18] L. Khvalbota, A. a Machyňáková, J. Čuchorová, K. Furdíková, I. Špánika, Enantiomer composition of chiral compounds present in traditional slovak tokaj wines, J. Food Compost. Anal. 96 (2021) 103719, doi: 10.1016/j.jfca.2020.103719.

[19] S. J. Pérez-Olivero, M. L. Pérez-Pont, J. E. Conde, J. P. Pérez-Trujillo, Determination of lactones in wines by headspace solid-phase microextraction and gas chromatography

coupled with mass spectrometry, J. Anal. Methods Chem. (2014) 1–10. doi:10.1155/2014/863019.

[20] O. Vyviurska, N. Koljančić, H.A.Thai, R. Gorovenko, I. Špánik, Classification of botrytized wines based on producing technology using flow-modulated comprehensive two-dimensional gas chromatography, Foods 10 (2021) 876. doi: 10.3390/foods10040876

[21] M. Galletta, M. Zoccali, N. Jones, L. Mondello, P.Q. Tranchida, Flow-modulated comprehensive two-dimensional gas chromatography combined with time-of-flight mass spectrometry: use of hydrogen as a more sustainable alternative to helium, Anal. Bioanal. Chem. 414 (2022) 6371–6378, doi:10.1007/s00216-022-04086-4.

[22] M. Galletta, M. Zoccali, D. Creti, L. Mondello, P.Q. Tranchida, A green and sustainable method for Capsicum volatilome investigation by means of headspace solid-phase microextraction combined with flow-modulated two-dimensional gas chromatography-mass spectrometry using hydrogen as carrier gas, Green Anal. Chem. 4 (2023) 100050, doi: 10.1016/j.greeac.2023.100050.

[23] P.E. Sudol, M. Galletta, P.Q. Tranchida, M. Zoccali, L. Mondello, R.E. Synovec, Untargeted profiling and differentiation of geographical variants of wine samples using headspace solid-phase microextraction flow-modulated comprehensive two-dimensional gas chromatography with the support of tile-based fisher ratio analysis, J. Chromatogr. A 1662 (2022) 462735, https://doi.org/10.1016/j.chroma.2021.462735.

[24] A.K. Smilde, J.J. Jansen, H.C.J. Hoefsloot, R.-J. A. N. Lamers, J. van der Greef, M. E. Timmerman, ANOVA–simultaneous component analysis (ASCA): a new tool for analyzing designed metabolomics data, Bioinformatics 21 (2005) 3043-3048, doi: 10.1093/bioinformatics/bti476.

[25] G. Zwanenburg, H.C.J. Hoefsloot, J.A. Westerhuis, J. J. Jansen, A.K. Smilde, ANOVA-principal component analysis and ANOVA-simultaneous component analysis: a comparison, J. Chemometr. 25 (2011) 561-567, doi: 10.1002/cem.1400.

[26] M. Thiel, B. Féraud, B. Govaerts, ASCA+ and APCA+: extensions of ASCA and APCA in the analysis of unbalanced multifactorial designs, J. Chemometr. 31 (2017) e2895, doi: 10.1002/cem.2895

[27] M. Barker, W. Rayens, Partial least squares for discrimination, J. Chemometr. 17 (2003) 166-173, doi: 10.1002/cem.785.

[28] S. Wold, E. Johansson, M. Cocchi, PLS: partial least squares projections to latent structures, Stampa (1993) 523-550.

[29] The good scents company - flavor, fragrance, food and cosmetics ingredients information, good scents co. (n.d) (2021). https://www.thegoodscentscompany.com /index.html.

Chapter 9
Development of innovative oligonucleotide-based supports for the selective extraction of zearalenone and its metabolites from urine samples*

The aim of this research is the development of a novel, powerful, and selective solid-phase extraction strategy based on molecular recognition using aptamers immobilized on a solid support for the extraction of the mycotoxin zearalenone and its two metabolites: alpha-zearalenol and beta-zearelenol.

Three oligonucleotide sequences reported in literature as specific to zearalenone were covalently grafted on activated Sepharose, and once the supports packed in cartridges, a thorough study of the elution conditions favoring zearalenone retention was performed, demonstrating the importance of the nature of this medium. The high selectivity was obtained when applying the optimal conditions as a recovery of 88% was obtained using the sorbent functionalized with one of the specific aptamers. The extraction procedure was then applied to a urine sample.

9.1 Introduction

Mycotoxins are a large group of secondary metabolites generated by various filamentous fungi that contaminate food and feed products. Mycotoxins may cause many different adverse health effects such as induction of cancer and mutagenicity, as well as estrogenic, immunologic, gastrointestinal and kidney disorders. Their presence in food and feed ingredients is therefore considered a critical food safety issue, particularly in economically developing regions, and can pose a significant risk to human and animal health if consumed in high quantities [1-3].

Common mycotoxins include aflatoxins (AFT), ochratoxin A (OTA), fumonisins (FB), tricothecenes, zearalenone and others. Contamination can occur during the growth, harvest and storage of crops such as cereals, nuts and spices under conditions favourable to fungal growth. Proper monitoring and control measures are essential to reduce the health risks associated with mycotoxin contamination. Zearalenone (ZEA) and its major metabolites, α-zearalenol (α-ZEL) and β-zearalenol (β-ZEL), are produced by numerous species of *Fusarium* fungi (F. graminearum, F. culmorum, F. equiseti and F. crookwellense), which frequently contaminate agricultural crops such as maize (corn) and its products, wheat, barley, oats, rice and vegetable oils [4-5]. ZEA is known to have estrogenic activity due to its structural similarity to 17β-estradiol, causing reproductive problems such as reduced fertility and abnormal estrous cycles [6]. Most of the mycotoxins are present in the final product due to their stability to processing. Considering the increase level of contamination, the European Union (EU) has formulated specific regulations for ZEA in food products, considering consumer health risks. According to the EU legislation, the maximum allowable limits for ZEA are defined as follows: 20-400 μg kg^{-1} in foodstuffs as reported in the Commission Regulation (CE) 1881/2006. Specifically, the European Food Safety Authority (EFSA) defines that the maximum permissible limits for ZEA should be 100-200 μg kg^{-1} in unprocessed cereals, 75 μg kg^{-1} for processed cereals, 20 μg kg^{-1} in processed cereal foods and 50 μg kg^{-1} in cereal snacks [7]. Therefore, the development of reliable, accurate, faster, and highly sensitive analytical methods for the detection and quantification of mycotoxins is important for the identification and detection of these compounds. In this context, the most widely adopted methods are based on traditional chromatographic techniques, including high performance

liquid chromatography (HPLC) coupled with fluorescence or mass spectrometric detection [8,9], gas chromatography-mass spectrometry (GC-MS) [10].

In addition, antibody-based immunoassays such as radiolabelled immunoassays (RIA), enzyme immunoassays (EIA), enzyme-linked immunosorbent assays (ELISA) and biosensors have been developed to overcome some of the limitations of previous methods. Solid-phase extraction (SPE) is widely considered as a powerful method for sample preparation with different sorbents available to improve selectivity and affinity [11,12]. In this context, an approach for molecular recognition consists in using aptamers immobilized on a solid support to form an oligosorbent (OS) dedicated to the target compound. Aptamers are single-stranded DNA or RNA molecules with a short length (20–60 nucleotides), created utilizing the SELEX process [13]. Aptamers can fold into unique three-dimensional conformations that allow for selective and strong interactions with a specific target molecule with high affinity and specificity. Due to their large surface area, the interactions between the aptamers and the target molecule are enhanced, preventing binding at the smallest possible differences. Most of the isolated sequences are directed towards large molecules such as peptides, proteins or nucleic acids. Nevertheless, a considerable number of aptamers have been developed for small molecules [14,15]. In addition, aptamers have many advantages over the use of an antibody, including equal or superior affinity and specificity for the target, smaller size, easier modification and immobilisation, better stability at ambient and high temperatures, and higher repeatability.

Urine is usually the biological matrix of choice to measure mycotoxin exposure due to its easiness and large amounts collected. Thus, this study allows to demonstrate the very high affinity of the aptamer towards ZEA and its two main metabolites. After the development of a selective extraction procedure for oligosorbents, their capacity and their binding efficiency were determined. An optimised procedure involving the use of the oligosorbent based on the covalent binding was applied to the determination of ZEA in urine sample. To the best of our knowledge, the use of an OS for the selective extraction of ZEA from urine has never been exploited. Compared to plasma or serum, urine samples have the advantage of being easy to

collect non-invasively, less dangerous to handle, and provide the analyst with a cleaner biological matrix for analysis.

9.2 Experimental

Chemicals and reagents

Zearalenone, α-zearalenol, β-zearalenol, calcium cloride ($CaCl_2$), magnesium chloride ($MgCl_2$), trizma hydrochloride (Tris-HCl), sodium chloride (NaCl), potassium chloride (KCl), di-sodium hydrogenophosporate (Na_2HPO_4), sodium acetate (CH_3COONa), acetic acid (CH_3COOH), triethylammine and CNBr activated Sepharose (4B, 90 μm) were purchased from Sigma Aldrich (Saint Quentin Fallavier, France). HPLC grade acetonitrile (ACN), methanol (MeOH) and formic acid (HCOOH) were from Carlo Erba (Val de Reuil, France). High-purity water was obtained using a Milli-Q purification system (Millipore, Saint-Quentin en Yvelines, France). Sodium hydroxide (NaOH) and hydrocloric acid (HCl) were purchased ftom Fluka (Saint Quentin Fallavier, France). Three 5'-amino-modified with C12 spacer arm DNA nucleotides: 8Z31N (5'-ATGGTACATTACTATCTGTAATGTGATAT), 8Z31(5'-TCATCTATCTATGGTACATTACTATCTGTAATGTGATAT-G), and 5Z28 (5'-CCTATAGTG-GCC-GCATATCTTTTTGCGGTCGC-TTGCC) were synthesized and purified by HPLC by Eurogentec (Angers, France). The selection buffer (SB) used during the SELEX procedure consisted of Tris–HCl (20 mM), NaCl (100 mM), KCl (5 mM), $MgCl_2$ and $CaCl_2$ (1 mM) at pH 7.4 This buffer was always stored and used at 4 °C.

Apparatus and analytical conditions

An Agilent 1200 series (Agilent Technology, Massy, France) LC system equipped with a binary pump, an autosampler and coupled to quadrupole time-of-flight (Q-ToF) MS was used for the characterization of the target compounds and oligosorbents. Target compounds were separated on a Waters Atlantis dC18 column (150 mm × 2.1 mm, i.d.; particle size: 3 μm, Waters, Saint Quentin en Yvelines, France) maintained at 35 °C. The mobile phase used for the separation in the isocratic mode were first blended and consisted of a mixture of acetonitrile and water (55:45; *v/v*) at a flow rate of 0.2 ml min^{-1}, and the injected volume was 5 μL.

Calibration curves over the concentration range of 0.05 to 5 μg ml^{-1} showed a good linearity.

HPLC-UV aptamer analysis

This method was adapted from previous studies realized by our group [14]. Grafting yields were determined by analysing aptamer content in the solutions recovered after the grafting procedure, by ion pair RP-HPLC-UV (reverse-phase high performance liquid chromatography) using an Agilent 1200 series HPLC system equipped with an 1100 series autosampler and a 1200 series UV detector. The aptamers were monitored at 260 nm. The separation was achieved on a Kinetex core shell C18 column (100 × 3 mm i.d., 5 μm, 100 Å) from Phenomenex (Le Pecq, France) at 30 °C. The column was connected to a precolumn filter (0.5 μm frit, 2.39 × 1.65 mm, Upchurch Scientific, Oak Harbor, WA, USA). The mobile phase was composed of water with 0.1 M triethylammonium acetate (TEAA, prepared with TEA and acetic acid) pH 7 and acetonitrile (85/15; *v/v*). The gradient applied was as follows: 0 min, 0% B; 10 min, 100%B; 12 min, 100%B; 13 min, 0%B; 23 min, 0%B. The flow rate was set at 0.5 ml min^{-1} and the injected volume was 25 μL. Before sample injection, a calibration process for each aptamer sequence was performed from 1 to 10 μg mL^{-1} and showed a good linearity for all aptamers (the equations for the linear regression were y = 79,164x + 10,335, R²=0,9951; y=86,348x-61,092, R²=0,9863 and y=69,487x-8,7262, R² = 0,9969, respectively for 8Z31N, 8Z31 and 5Z28). The limit of detection was 0.51, 0.15 and 0.02 μg ml^{-1} for 8Z31N, 8Z31 and 5Z28, respectively, while the limit of quantification was 1.70, 0.51 and 0.05 μg ml^{-1} for 8Z31N, 8Z31 and 5Z28, respectively.

Oligosorbents synthesis

The procedure used to immobilize aptamers on CNBr-activated Sepharose has been previously described by our group to develop OS [14-15]. Briefly, prior to immobilization, the dried aptamers were dissolved at 1 g L^{-1} in a buffer (200 mM Na$_2$HPO$_4$ and 5 mM MgCl$_2$, pH 8) and denatured by heating at 75 °C for 5 min. Then, the solution was left at room temperature for 30 min. 35 mg of dry CNBr-activated Sepharose was weighed and washed six times with 1 mL of HCl (1 mM).

The gel was then rinsed with 1 mL of deionised water and with 175 µL of 200 mM Na$_2$HPO$_4$ (pH 8), 5 mM MgCl$_2$. Then, 150 µL of aptamer solution was mixed with the gel and left overnight at room temperature. The resulting oligosorbent was packed between two PTFE frits (Sigma Aldrich) in a 1 mL SPE cartridge. Three washing steps with 1 mL of 200 mM Na$_2$HPO$_4$ (pH 8) were performed to remove any impurities. These washing solutions were recovered and diluted in 200 mM Na$_2$HPO$_4$ and 5 mM MgCl$_2$ to measure their content in non-grafted aptamers and then to calculate the grafting yield for each support. Remaining active cyanate ester groups were blocked by a 0.1 M Tris-HCl 100 mM (pH 8) for 2 h at room temperature. Finally, the OS was washed three times alternately with 2 mL of an acetate buffer (0.1M acetate + 0.5MNaCl, pH 4) and 2 mL of a Trizma buffer (0.1M+ 0.5 M NaCl, pH 8). The same experiment was carried out in parallel on a blank support sorbent prepared using the same protocol.

Extraction procedure in pure media

Before each extraction, the OSs were conditioned with 1 mL of binding buffer (BB). The percolation solution consists of 1 mL of the tested buffer spiked at 60 µg L^{-1} with the selected mycotoxins to study the specificity. The sorbent was further washed with 500 µL of BB. Finally, elution is performed with 2 x 250 µL of H$_2$O/ACN (60/40, *v/v*). All steps were performed at 4 °C and the pH of BB was set at 5. Each SPE fraction (percolation, washing and elution) was then diluted 1/100 or 1/10 in BB for HPLC-MS analyses. The capacity of the most promising OS was determined using the same protocol described above but by percolating 1 mL containing increasing amounts of ZEA from 60 to 2000 ng on the OS. The elution fractions were then diluted with a dilution factor adapted to the introduced amount of ZEA to be in the calibration curve range.

Urine samples

The optimised oligoextraction protocol was applied to 1 mL of treated urine sample. Specifically, the loading step was performed by using 1 mL mixture of (urine spiked at 3 concentration levels: 60.0, 6.0 and 0.6 ng mL^1) loading 0.5 mL equivalent urine. After oligoextraction, the elution fractions were analysed by HPLC-MS; in fact, the

analytes are present only in the first elution fraction. The determination of mycotoxin concentrations was performed by means of a calibration curve. Three replicates were performed for each spiking level.

9.3 Results and discussion

Oligosorbent synthesis and grafting yields

Among the anti-zearalenone aptamers identified by Chen *et al.* [16], two aptamers (5Z28 and 8Z31) were selected for their good affinity (respectively Kd of 29 ± 5 and 41 ± 5 nM) and their selectivity for ZEA and were used to synthesize two oligosorbents (respectively named OS-5Z28 and OS-8Z31 according to the aptamers grafted). For the covalent grafting of aptamers, CNBr-activated Sepharose was chosen because it is a hydrophilic support preventing the development of non-specific interactions with ZEA that could occur because of the hydrophobicity of ZEA (log P = 3.04). In addition, in order to maximize the capacity of the OS, both aptamers were 5'-amino-modified with a C12 spacer arm and immobilized on CNBr-activated Sepharose following a procedure already described by our group for the grafting of aptamers with target cocaine and another mycotoxin, ochratoxin A (OTA) [14-18]. As described in the experimental section, the solution containing the unbound aptamers during the grafting procedure were analyzed by HPLC-UV and allowed to determine a grafting yield of 32.0%, 29.0% and 30.0% for OS-5Z28, OS-8Z31N and OS-8Z31, respectively. Such grafting yields were consistent with those described previously for aptamers for other target compounds but grafted with the same procedure on CNBr-activated Sepharose (grafting yield of 19.3% and of 33%, for anti-cocaine [15] and for anti-OTA aptamers, respectively [18]).

Assuming one molecule of ZEA is retained by one aptamer, a theoretical binding efficiency can be calculated. The grafting of 47.68 µg, 45.68 µg and of 45.00 µg, *i.e.,* 3.8 nmol, 5.0 nmol, and 3.6 nmol of 5Z28, 8Z31N and 8Z31 aptamers, respectively, on 35 mg of the Sepharose-based OSs, corresponds to a capacity of 1222 ng, 1580 ng and 1114 ng of ZEA. According to this difference of theorical capacity between the OSs, and to be certain not to overload the support, the quantity of ZEA percolated on each OS during the optimization of the extraction procedure was defined to be around 10 times lower than the capacity values.

Optimization of the oligo-extraction procedure in pure media

As for conventional SPE extraction procedure, an oligo-extraction procedure is composed of four steps: (i) the conditioning step aims to equilibrate the OS with the buffer which will then be used for the percolation of the sample; (ii) the loading of the aqueous sample on the OS, in order to favor the interaction between the OS and the target analyte, leading to a strong and selective retention of the analyte; (iii) the washing with a buffer or a solvent, used to disrupt the low non-specific interactions that may occur between the OS and the matrix component; (iv) the elution of the target analyte with a solvent mixture able to denaturate the aptamer and dissociate the complex analyte-aptamer. The extraction recovery corresponds to the percentage of percolated ZEA found in the elution fraction.

The pH and the composition in salts of the buffer used during percolation and washing steps have therefore an important impact on the 3D structure of the aptamer, thus conditioning the formation of the complex between the aptamer and the ZEA. Usually, a medium favoring a high affinity used during the selection of the aptamer during the SELEX procedure was used as binding buffer. Then, the first experiments of this study were carried out on the basis of the oligo-extraction procedure already described for others targets analytes [14,17], except for the percolation step that was performed in SB at pH=8 in order to obtain a strong analyte/aptamer complex. Briefly, after the percolation of 1 mL of SB at pH=8, spiked with ZEA on the three OSs, these were washed with 500 µL of BB, while elution was performed with 250 µL of a water/acetonitrile mixture (60/40, *v/v*). This experiment led to a significant loss of ZEA during percolation and washing on the 3 synthesized oligosorbents (data not shown). In order to highlight the effects of pH on the retention of ZEA, the salt composition of the BB was maintained, and the PH was adjusted to 5. The decrease in pH from 8 to 5 led to the total retention of ZEA during the percolation step for the three OSs. In this context, the elution profile was similar on three OSs: a total retention during percolation step, a low loss during the washing step and a high recovery yield in the elution fraction of 88% and 91% and 72%, for OS-5Z28, OS-8Z31 and OS-8Z31N, respectively (Table 9.1). However, the aptamers trap the metabolites (particularly β-zearalenol) much less efficiently, leading to a drastic decrease in extraction yields.

Table 9.1. *Extraction recovery in %(n=3) with standard deviation for zearalenone, α-zearalenol, β-zearalenol and propazine in the elution fraction after percolation of BB1 spiked at 60 ng mL^{-1} on OS 5Z28, 8Z31, 8Z31N.*

	5Z28	**8Z31**	**8Z31N**
Zearalenone	88 ± 9	91 ± 3	72 ± 10
Propazine	3 ± 1	2 ± 1	3 ± 1
β-zearalenol	45 ± 12	35 ± 4	42 ± 6
α-zearalenol	77 ± 15	74 ± 9	77 ± 6

As the salt composition of BBs is one of the key factors in the ability of aptamers to recognize target molecules, tests were carried out by removing certain salts from the BBs. The results showed that removing one salt ($CaCl_2$ or $MgCl_2$) or of a combination of two ($CaCl_2$ and $MgCl_2$), three ($CaCl_2$, $MgCl_2$ and KCl), and finally no salts (BB was only constituted of TrisHCl) did not affect the extraction recovery. In fact, the good retention for ZEA was maintained but did not appear to increase the retention of β-zearalenol. Lastly, small differences could also be linked to experimental variability. It was therefore decided to use the selected buffer (BB1 at pH=5) for the extraction procedure. The performance comparison of the 3 OSs led us to select the one with the highest extraction recovery for the 3 targeted analytes: 5Z28. In addition, OS-8Z31N, which gave a similar yield, resulted in higher variability. In order to evaluate the repeatability of the synthesis procedure, a second cartridge also containing the 5Z28 aptamer was obtained (39% grafting yield) and the previous extraction procedure was applied. The extraction profiles obtained on the 2 cartridges were compared and led to similar extraction recovery (Figure 9.1).
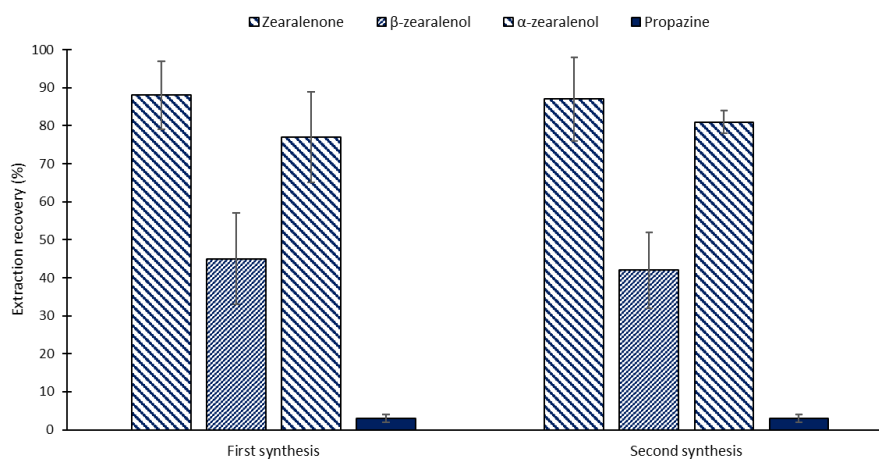
Figure 9.1. *Extraction recovery in % (n=3) for zearalenone, α-zearalenol, β-zearalenol and propazine in the elution fraction after percolation of BB1 spiked at 60 ng mL^{-1} on OS-5Z28 obtained in two independent synthesis.*

Determination of the oligosorbent capacity

The capacity of an OS corresponds to the maximum amount of ZEA that can be retained by specific interactions. This capacity was directly linked to the number of active aptamers covalently grafted on the support. For such a determination, increasing amounts of ZEA (from 100 to 2000 ng) were percolated through OS-5Z28. The ZEA amounts found in the elution fraction for the different amounts percolated are illustrated in Figure 9.2. At low dose of ZEA, the amount found in elution fraction increased proportionally with the amount percolated, that corresponds to the extraction recovery obtained with the optimized extraction procedure in pure media. Then the curve reached a plateau, corresponding to the retention of ZEA on OS-5Z28 by non-specific interactions. Thus, it appears that saturation occurs at about 800 ng, while up until that point the sorbent retains about 65% of the amount percolated.
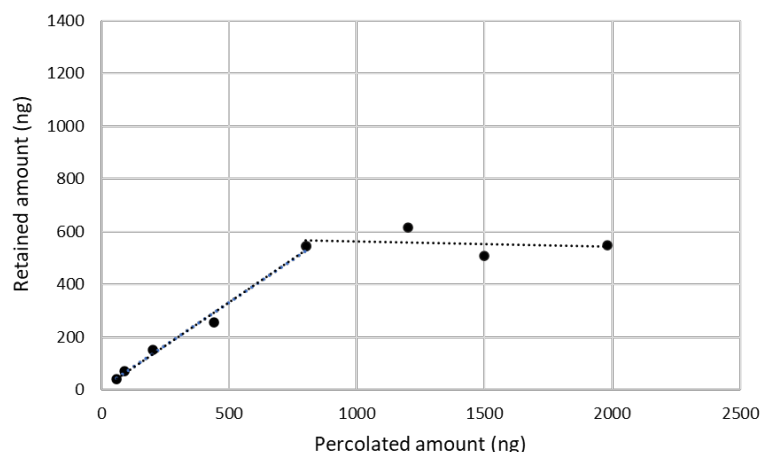
Figure 9.2. *Capacity of the OS-5Z28 to retain ng amounts of ZEA, in function of the amount percolated.*

Once the performance of OS-5Z28 evaluated, the extraction procedure was applied to human urine samples. The extraction procedure was the same as that related to Table 9.1, except that 1 mL of urine spiked with 0.6, 6 or 60 ng of ZEA (n = 3 for each concentration level) and diluted (1/1, *v/v*) with BB1 2x (salts concentration is doubled) was percolated, instead of BB1. Results are reported in Table 9.2. The extraction recovery was maintained for α-zearalenol and ZEA, compared to the pure media. A decrease in extraction recovery (30 to 17%) was also observed for β-zearalenol, but as α-zearalenol and ZEA are more abundant in urine, this was not a major concern.

Table 9.2. *Extraction recovery in % with standard deviation for zearalenone, α-zearalenol, β-zearalenol in the elution fraction after percolation of spiked urine samples on OS-5Z28;(nd = not detected).*

Concentration in urine (ng mL^{-1})	β-zearalenol	α-zearalenol	Zearalenone
60	17 ± 5	88 ± 9	72 ± 10
6	11 ± 3	88 ± 5	72 ± 6
0,6	nd	83 ± 9	78 ± 8

These results confirm the high potential of oligoextraction as an extraction method of ZEA from a biological sample. It is also important to notice that all extraction procedures in pure medium over a period of 6 months were carried out and no loss of

retention was observed. Chromatograms corresponding to the elution fractions resulting from the use of OS-5Z28 for urine spiked at 0. 6 ng mL^{-1} (blue line) and of the same spiked urine sample after only the filtration step (red line) are presented in Figure 9.3. These results indicate that the interfering components were removed during the washing step and that the oligosorbent efficiency was not affected by a matrix effect. Furthermore, the improvement of the clean-up by the oligosorbent proves its great potential for the selective extraction of ZEA from complex matrices.
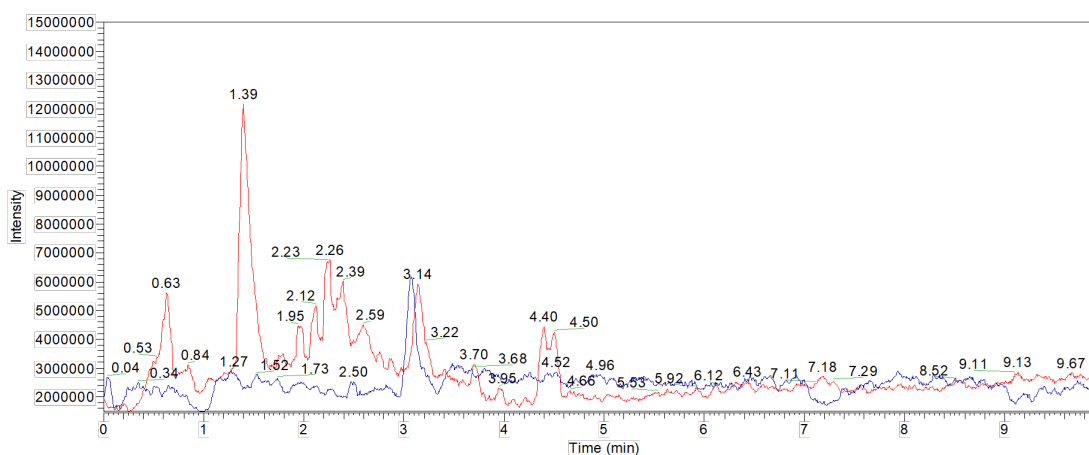

Figure 9.3. *HPLC-MS chromatograms (scan mode, m/z 100–600) of the eluate obtained after application of the oligoextraction method on 5Z28 for urine spiked at the 0,6 ng mL^{-1} level (blue line) and of the same spiked urine sample after only the filtration step (red line).*

9.3 Conclusions

The objective of this study was to develop for the first time a selective and specific extraction sorbent based on aptamers to extract ZEA from a urine sample. After identifying three promising sequences in literature, they were grafted on CNBr-activated Sepharose. This study finally showed that once the procedure was optimized, its application to a real-world sample led to performances like those obtained in pure media.

References

[1] Y.G. Lijalem, M.A. Gab-Allah, K. Choi, B. Kim, Development of isotope dilution-liquid chromatography/tandem mass spectrometry for the accurate determination of zearalenone and its metabolites in corn, Food Chem. 384 (2022) 132483. doi: 10.1016/j.foodchem.2022.132483.

[2] F. Al-Taher, J. Cappozzo, J. Zweigenbaum, H.J. Lee, L. Jackson, D. Ryu, Detection and quantitation of mycotoxins in infant cereals in the US market by LC-MS/MS using a stable isotope dilution assay, Food Control 72 (2017) 27–35. doi: 10.1016/j.foodcont.2016.07.027.

[3] M. Eskola, G.Kos, C. T. Elliott, J. Hajšlová, S. Mayar, R. Krska, Worldwide contamination of food-crops with mycotoxins: Validity of the widely cited 'FAO estimate' of 25%, , Crit. Rev. Food Sci. (2019) 1–17. doi: 10.1080/10408398.2019.1658570.

[4] M. Zhou, L.J. Yang, W.R. Yang, L.B. Huang, X.M. Zhou, S.Z. Jiang, Z.B. Yang, Effects of zearalenone on the localization and expression of the growth hormone receptor gene in the uteri of post-weaning piglets, Asian-Australasian J. Anim. Sci. 31 (2018) 32 - 39. doi: 10.5713/ajas.17.0526.

[5] A. Rai, M. Das, A. Tripathi, Occurrence and toxicity of a fusarium mycotoxin, zearalenone, Crit. Rev. Food Sci. (2020) 2710-2729. doi: 10.1080/10408398.2019.1655388

[6] N. Nuryono, C.T. Noviandi, J. Bohm J, E. Razzazi-Fazeli, A limited survey of zearalenone in Indonesian maize-based food and feed by ELISA and high performance liquid chromatography, Food Control (2005) 65–71. doi: 10.1016/j.foodcont.2003.11.009.

[7] EFSA. 2011. Scientific opinion on the risks for public health related to the presence of zearalenone in food (by EFSA panel on contaminants in the food chain), EFSA J. 9 (2):2197.

[8] S.J. Macdonald, S. Anderson, P. Brereton, R. Wood, A. Damant, M. Aletrari, P. Welsh, Determination of zearalenone in barley, maize and wheat flour, polenta, and maize-based baby food by immunoaffinity column cleanup with liquid

chromatography: Interlaboratory study, J. AOAC Int 88 (2005) 1733-40. doi: 10.1021/jf0479315

[9] F. Berthiller, R. Schuhmacher, G. Buttinger, R. Krska, Rapid simultaneous determination of major type A- and B-trichothecenes as well as zearalenone in maize by high performance liquid chromatography-tandem mass spectrometry, J. Chromatogr. A 106 (2005) 209–216. doi: 10.1016/j.chroma.2004.11.011

[10] Y. Rodríguez-Carrasco, H. Berrada, G. Font, J. Mañes, Multi-mycotoxin analysis in wheat semolina using an acetonitrile-based extraction procedure and gas chromatography-tandem mass spectrometry, J. Chromatogr. A 1270 (2012) 28-40. doi: 10.1016/j.chroma.2012.10.061

[11] C. Zhang, H. Xing, L. Yang, P. Fei, H. Liu, Development trend and prospect of solid phase extraction technology, Chin. J. Chem. Eng. 42 (2022) 245–255. doi: 10.1016/j.cjche.2021.05.031.

[12] A.B. Kanu, Recent developments in sample preparation techniques combined with high-performance liquid chromatography: a critical review, J. Chromatogr., A 1654 (2021), 462444. doi: 10.1016/j.chroma.2021.462444.

[13] V. Pichon, F. Brothier, A. Combès, Aptamer-based-sorbents for sample treatment-a review, Anal. Bioanal. Chem. 407 (2015) 681–698. doi: 10.1007/s00216-014-8129-5.

[14] C.L.A. Hamula, J.W. Guthrie, H. Zhang, X.-F. Li, X.C. Le, Selection and analytical applications of aptamers. TrAC-Trend. Anal. Chem 25 (2006) 681-691. doi: 10.1016/j.trac.2006.05.007.

[15] E. Peyrin, Nucleic acid aptamer molecular recognition principles and application in liquid chromatography and capillary electrophoresis. J. Sep. Sci. 32 (2009) 1531–1536. doi: 10.1002/jssc.200900061.

[14] B. Madru, F. Chapuis-Hugon, E. Peyrin, V. Pichon, Determination of Cocaine in Human Plasma by Selective Solid-Phase Extraction Using an Aptamer-Based Sorbent. Anal. Chem. 81 (2009) 7081–7086. doi: 10.1021/ac9006667.

[15] B. Madru, F. Chapuis-Hugon, E. Peyrin, V. Pichon, Novel extraction supports based on immobilised aptamers: Evaluation for the selective extraction of cocaine. Talanta (2011) 616-624. doi: 10.1016/j.talanta.2011.04.016.

[16] X. Chen, Y. Huang, N. Duan, S. Wu, X. Ma, Y. Xia, C. Zhu, Y.Jiang, Z. Wang, Selection and identification of ssDNA aptamers recognizing zearalenone, Anal. Bional. Chem. 405 (2013) 6573-6581. doi: 10.1007/s00216-013-7085-9.

[17] F. Chapuis-Hugon, A. du Boisbaudry, B. Madru, V. Pichon, New extraction sorbent based on apatmers for the determination of ochratoxin A in red wine, Anal. Bional. Chem. 400 (2011) 1199-1207. doi: 10.1007/s00216-010-4574-y.

[18] W.H. Ali, V. Pichon, Characterization of oligosorbents and application to the purification of ochratoxin A from wheat extracts, Anal. Bional. Chem. 406 (2014) 1233-1240. doi: 10.1007/s00216-013-7509-6.